
S. B. DAWES
PH.

THS
090
106
PH. D

THS
090
106

PH. D.

THESIS

LIBRARY
Michigan State
University

This is to certify that the

dissertation entitled

STRUCTURAL AND MAGNETIC PROPERTIES OF THE ELECTRIDES OF CESIUM COMPLEXED BY 15-CROWN-5 AND 18-CROWN-6

presented by

Steven B. Dawes

has been accepted towards fulfillment
of the requirements for

Ph.D. degree in Chemistry

James L. Dye
Major professor

Date June 4, 1986

MSU is an Affirmative Action/Equal Opportunity Institution

O-12771



RETURNING MATERIALS:
Place in book drop to remove this checkout from your record. FINES will be charged if book is returned after the date stamped below.

OCT 0051 2003

STRUCTURAL AND MAGNETIC PROPERTIES OF THE ELECTRIDES OF CESIUM COMPLEXED BY 15-CROWN-5 AND 18-CROWN-6

45-7443-71

By

Steven B. Dawes

A DISSERTATION

Submitted to
Michigan State University
in partial fulfillment of the requirements
for the degree of

DOCTOR OF PHILOSOPHY

Department of Chemistry

1986

ABSTRACT

The nature of the trapped electron in two compounds, the newly synthesized $Cs^+(15C5)_2 \cdot e^-$ and $Cs^+(18C6)_2 \cdot e^-$, were explored by structural, magnetic, optical, and thermal techniques. The first crystal structure of an electride, $Cs^+(18C6)_2 \cdot e^-$, was determined. The unit cell is monoclinic, C2/c, with $\underline{a}$ = 13.075 Å, $\underline{b}$ = 15.840 Å, $\underline{c}$ = 17.359 Å, β = 92.30°, and $\underline{z}$ = 4. The electride is isostructural to $Cs^+(18C6)_2 \cdot Na^-$ except that the anionic sites contain less than 0.07 e^- $Å^{-3}$. The monoclinic (C2/c) cell of $Cs^+(18C6)_2 \cdot Na^-$ has $\underline{a}$ = 13.581 Å, $\underline{b}$ = 15.684 Å, $\underline{c}$ = 17.429 Å, β = 93.16°, and $\underline{z}$ = 4. The structure of $Cs^+(15C5)_2 \cdot I^-$ was solved. The tetragonal (I4) unit cell has $\underline{a}$ = 13.173 Å, $\underline{c}$ = 16.645 Å, and $\underline{z}$ = 4. Both electrides are paramagnetic and obey the Curie-Weiss law. $Cs^+(15C5)_2 \cdot e^-$, when slowly cooled from a phase transition at 238 K, displays antiferromagnetism (T_N = 4.2 K). The interacting electrons appear to couple via direct exchange in spite of a long interelectronic distance (~8.7 Å). The spin lattices are weakly affected by crystalline anisotropy; at 1.6 K a spin-flop occurs at 1.5 kG. The cation in both electrides displays a temperature dependent Knight shift in the ^{133}Cs MAS-NMR spectrum, that is proportional to the paramagnetic electron density at the nucleus, $\langle\{(\psi(0))^2\}\rangle$ = 6.2 × 10^{24} e^- cm^{-3} and 2.1 × 10^{25} e^- cm^{-3} for

$Cs^+(18C6)_2 \cdot e^-$ and $Cs^+(15C5)_2 \cdot e^-$, respectively. The paramagnetic Ramsey shift of "inclusive" complexed Cs^+ in diamagnetic salts from the value of $Cs^+_{(g)}$ is larger for complexes with shorter Cs-O distances, and is largely independent of the counter-ion. The static powder and single crystal NMR spectra of $Cs^+(18C6)_2 \cdot I^-$ and $Cs^+(15C5)_2 \cdot I^-$ are broadened by first order quadrupole, and chemical shift anisotropy effects, e^2qQ/h = 89.6 KHz and 427 KHz, and σ = 32 ppm and 52 ppm respectively. Thermal motion of the complexants in some salts is rapid enough to partially average the ^1H contribution to the dipolar linewidth in cations and anions. The chemical shift of Cs^- in $Cs^+(18C6)_2 \cdot Cs^-$ is downfield from the calculated value of $Cs^-_{(g)}$ by 140 ppm, and is sensitive to changes in the local environment. A compound of mixed anionic stoichiometry, $Cs^+(18C6)_2 \cdot Na^-_{0.125}e^-_{0.875}$, gave a five line NMR spectrum. The data fit a model in which each successive diamagnetic peak corresponds to a sequential substitution of Na^- for electrons in the nearest anion shell about a complexed cation.

TO MY PARENTS

ACKNOWLEDGEMENTS

I am grateful to many people, who over the course of this thesis work have contributed their time and friendship to my efforts. In particular, I am indebted to Professor James L. Dye, who taught, guided and supported me throughout this research. I appreciate the efforts and advice of my guidance committee, Dr. R.H. Schwendeman, Dr. H.A. Eick, and especially Dr. J.A. Cowen.

I am grateful to Dr. Donald L. Ward whose efforts were vital to the crystal structure determinations in this work. I thank the technical staff for their excellent work, electronics designer Marty Rabb glassblowers, Keki Mistry, Manfred Langer and Scott Bankroff machinists Deak Watters, Russ Geyer, and Dick Menke and NMR specialist Kermit Johnson. I appreciate the efforts and the patience of Margy Lynch, Carol Zink, Naomi Hack and Bill Draper who helped in the production of this manuscript.

Finally, I acknowledge the tremendous support, help and friendship of the solid state research group, Drs. D. Issa, B. Van Eck, L.D. Le, A. Ellaboudy, M. Faber, and M. Tinkham, and O. Fussá, J. Papaioannou, R. Huang, Z. Li, F. Tientega, J. Skowyra, L. Hill, J. Kim, M. Kuchenmeister, and again Dr. J. Dye.

I acknowledge research support from the National Science Foundation Grants DMR 84-14154 and DMR 79-21979.

TABLE OF CONTENTS

CHAPTER		PAGE
TABLE OF CONTENTS		v
LIST OF TABLES		x
LIST OF FIGURES		xiii
I.	Introduction	1
I.A	Trapped Electrons in the Solid State	2
I.A.1	Color Centers	2
I.A.2	Electrons Trapped in Glassy Matrices	6
I.A.3	Lithium Tetraamine - Expanded Metals	15
I.B	Solutions of Alkali Metals	20
I.B.1	Metal Ammonia Solutions	20
I.B.2	Alkali Metal Complexation	27
I.C	Alkalides and Electrides	35
I.C.1	Alkalides	35
I.C.2	Electrides	42
I.D	Objectives of this Work	45
II.	Experimental Details	48
II.A	Synthetic and General Handling Techniques	48
II.A.1	Alkali Metals	48
II.A.2	Complexants	48
II.A.3	Solvents	49
II.A.4	Synthesis of Alkalides and Electrides	50
II.B	General Handling Techniques	52

CHAPTER		PAGE
II.C	Recrystallization Methods for Single Crystal X-ray Diffraction Studies.	.54
II.D	Instrumental and Experimental Description.	.58
II.D.1	X-ray Crystallography	
II.D.1.a	Mounting of Crystals of $Cs^+(18C6)_2 \cdot Na^-$.	.58
II.D.1.b	X-ray Data Collection for $Cs^+(18C6)_2 \cdot Na^-$.	.60
II.D.1.c	X-ray Data Collection for $Cs^+(18C6)_2 \cdot e^-$.	63
II.D.1.d	Mounting of a crystal of $Cs^+(15C5)_2 \cdot I^-$.	66
II.D.1.e	X-ray Data Collection for $Cs^+(15C5)_2 \cdot I^-$.	66
II.D.2	Magnetic Susceptibility.	68
II.D.3	Optical Spectroscopy.	.70
II.D.4	Electron Paramagnetic Resonance. .	.70
II.D.5	Differential Scanning Calorimetry.	71
II.D.6	Nuclear Magnetic Resonance.	.72
III.	Crystal Structures of $Cs^+(18C6)_2 \cdot Na^-$, $Cs^+(18C6)_2 \cdot e^-$ and $Cs^+(15C5)_2 \cdot I^-$.	73
III.A.	Background.	.73
III.A.1	Previous Work.	73
III.A.2	Fundamental Methods for Solving Structures.	.76
III.B.	Structure Solution and Refinement for $Cs^+(18C6)_2 \cdot Na^-$ and $Cs^+(18C6)_2 \cdot e^-$.	83
III.B.1	General Approach.	.83
III.B.2	Results of the Structure Determination of $Cs^+(18C6)_2 \cdot Na^-$ at 213 K.	84
III.B.3	Results of the Structure Determination of $Cs^+(18C6)_2 \cdot e^-$ at 216 K.	.100

CHAPTER PAGE

III.C. Structure Solution and Refinement of $Cs^+(15C5)_2 \cdot I^-$ 116
III.C.1 General Approach. 116
III.C.2 Results of the Structure Determination of $Cs^+(15C5)_2 \cdot I^-$ 117

IV. Thermal Characteristics of the Iodides and Electrides of $Cs^+(18C6)_2$ and $Cs^+(15C5)_2$ Complexed Cations. 126

IV.A Differential Scanning Calorimetry. 127
IV.A.1 DSC of $Cs^+(15C5)_2 \cdot I^-$ and $Cs^+(18C6)_2 \cdot I^-$. 127
IV.A.2 DSC of $Cs^+(15C5)_2 \cdot e^-$ and $Cs^+(18C6)_2 \cdot e^-$. 129

IV.B Optical Spectroscopy of $Cs^+(15C5)_2 \cdot e^-$. 134

V. The Nuclear Magnetic Resonance of ^{133}Cs in Salts that Contain Complexed Cesium Cations and/or Cesium Anions. 139

V.A Cs -- 133 Nuclear Magnetic Resonance Studies of Crystalline Salts With and Without Complexation by Crown Ethers and a Cryptand. 140
V.A.1 Introduction. 140
V.A.1.a ^{133}Cs NMR Spectra. 140
V.A.2 Lineshape Functions for Static NMR Spectra of Powders and Single Crystals. 143
V.A.2.a Dipolar Broadening. 143
V.A.2.b Chemical Shift Anisotropy. 143
V.A.2.c Quadrupolar Broadening. 146
V.A.3 Experimental. 148
V.A.4 Results and Discussion. 149
V.A.4.a MAS-NMR of Simple Salts and Complexed Salts. 149
V.A.4.b Static Spectra of Simple Salts and Complexed Salts. 154
V.A.4.b.i Cs_2SO_4. 154

CHAPTER		PAGE
V.A.4.b.ii	Static Spectra of $Cs^+(18C6)_2 \cdot I^-$ and $Cs^+(15C5)_2 \cdot I^-$	156
V.A.5	Conclusions.	168
V.A.6	Acknowledgement.	169
V.A.7	References.	169
V.B	Cesium-133 Nuclear Magnetic Resonance Spectroscopy of Alkalides and Electrides.	171
V.B.1	Introduction.	171
V.B.2	Experimental.	173
V.B.3	Results and Discussion.	174
V.B.3.a	^{133}Cs MAS-NMR of Alkalides.	174
V.B.3.b	^{133}Cs MAS-NMR of $Cs^+C222 \cdot e^-$	179
V.B.3.c	^{133}Cs MAS-NMR of $Cs^+(18C6)_2 \cdot e^-$	181
V.B.3.d	^{133}Cs MAS-NMR of Mixed Alkalide-Electride Salts.	188
V.B.4	Conclusions.	197
V.B.5	Acknowledgement.	198
V.B.6	References.	199
V.C	MAS-NMR of $Cs^+(15C5)_2 \cdot e^-$	201
VI.	Magnetic Susceptibility of $Cs^+(18C6)_2 \cdot e^-$ and $Cs^+(15C5)_2 \cdot e^-$	207
VI.A	Background.	208
VI.A.1	Metallic Paramagnetism.	208
VI.A.2	Diamagnetism.	213
VI.A.3	Curie Law Paramagnetism.	216
VI.A.4	Magnetic Ordering and the Curie-Weiss Law.	219
VI.B	The Magnetic Susceptibility of Electrides.	224
VI.B.1	Magnetic Susceptibility of $Cs^+(18C6)_2 \cdot e^-$	226
VI.B.2	Magnetic Susceptibility of $Cs^+(15C5)_2 \cdot e^-$	229
VI.C	Electron Paramagnetic Resonance of $Cs^+(15C5)_2 \cdot e^-$	246
VII.	Conclusions and Suggestions for Future Work.	257
VII.A	Conclusions.	257

CHAPTER PAGE

VII.B Suggestions for Future Work. . . .263

REFERENCES. 267

LIST OF TABLES

TABLE		PAGE
1	Values of log K_{eq} for the Complexation of Alkali Metal Cations with Crown Ethers and Cryptands in Methanol [45].	.30
2	Results of Analyses for $Cs^+(15C5)_2 \cdot e^-$ and $Cs^+(18C6)_2 \cdot Na^-_x \cdot e^-_{1-x}$.	53
3	Table of Experimental Details for the Structure Determination of $Cs^+(18C6)_2 \cdot Na^-$.	.62
4	Table of Experimental Details for the Structure Determination of $Cs^+(18C6)_2 \cdot e^-$. . . .	.65
5	Table of Experimental Details for Structure Solution and Refinement of $Cs^+(18C6)_2 \cdot Na^-$ and $Cs^+(18C6)_2 \cdot e^-$.	85
6	Table of Positional Parameters in Fractional Unit Cell Coordinates and Their Estimated Standard Deviations for Cesium $(18\text{-Crown-}6)_2$ Sodide at 213 K.	86
7	Table of General Displacement Parameter Expressions -- U's (in $Å^2$) for Cesium $(18\text{-Crown-}6)_2$ Sodide.	.88
8	Table of Least Squares Planes for Cesium $(18\text{-Crown-}6)_2$ Sodide.	.93
9	Table of Bond Distances (in Ångstroms) for Cesium $(18\text{-Crown-}6)_2$ Sodide at 213 K and Cesium $(18\text{-Crown-}6)_2$ Electride at 216 K. . . .	95

TABLE PAGE

10 Table of Selected Torsional Angles (in Degrees) for Cesium (18-Crown-6)$_2$ Sodide at 213 K and Cesium (18-Crown-6)$_2$ Electride at 216 K. 97

11 Table of Closest Anionic Contact Distances for Cesium (18-Crown-6)$_2$ Sodide of 213 K, Cesium (18-Crown-6)$_2$ Electride at 216 K, and Cesium (15-Crown-5)$_2$ Iodide at 291 K. . . .99

12 Table of Positional Parameters in Fractional Unit Cell Coordinates and Their Estimated Standard Deviations for Cesium (18-Crown-6)$_2$ Electride at 216 K. 101

13 Table of General Displacement Parameter Expressions -- U's (in Å^2) for Cesium (18-Crown-6)$_2$ Electride. 103

14 A Comparison of Lattice Constants and Interanionic Distances in Cesium (18C6)$_2$ Sodide, Cesium (18C6)$_2$ Electride, and Cesium (15C5)$_2$ Iodide. 106

15 Table of Least-Squares Planes for Cesium (18-Crown-6)$_2$ Electride. 109

16 Table of Positional Parameters and Their Estimated Standard Deviations in Fractional Coordinates for Cesium (15C5)$_2$ Iodide at 291 K. 118

17 Table of General Displacement Parameters Expressions -- U's (in Å^2) for Cesium (15-Crown-5)$_2$ Iodide at 291 K. 119

18 Table of Bond Distances (in Ångstroms) for Cs^+(15-Crown-5)$_2$·I^- at 291 K. 121

19 Table of Least Squares Planes for Cesium (15-Crown-5)$_2$ Iodide at 291 K. 123

20 Summary of DSC Results for the Iodides and Electrides of Cs^+(18C6)$_2$ and Cs^+(15C5)$_2$. . . .131

TABLE		PAGE
21	Chemical Shifts and Linewidths of Simple Cesium Salts With and Without Complexed Cations.	.150
22	Parameters of Anisotropic Interactions in the NMR of Single Crystals of $Cs^+(15C5)_2 \cdot I^-$ at 23.62 MHz.	166
23	Chemical Shifts and Linewidths of ^{133}Cs MAS-NMR Lines in Alkalides and Electrides. . .	.175
24	Summary of Calculated and Representative Observed Chemical Shifts of Alkali Metal Anions.	178
25	Fractional Atomic Character of Some $Cs \cdots e^-$ Solutions and Solids.	.187
26	Table of Least-Squares Best-Fit Parameters for the Temperature Dependence of the Knight Shift of Peaks in $Cs^+(18C6)_2 \cdot Na_x \cdot e_{1-x}$.	.196
27	Table of Parameters and Their Estimated Standard Deviations for the Modified Curie-Weiss Law for $Cs^+(15C5)_2 \cdot e^-$.	.232

LIST OF FIGURES

IGURE		PAGE
1	The geometric structure about the trapped electron in glasses of a) 10 M NaOH, and b) ethanol [9-11].	10
2	The semicontinuum model for the trapped electron. r_v is the void radius, r_s is the effective spherical radius of a first shell solvent molecule, the dipolar interaction radius is r_d and R is the distance from the center of the cavity to the dielectric continuum [12].	12
3	Molecular structures of a) 18-Crown-6, b) 15-Crown-5, and c) Cryptand-222.	28
4	Ortep stereoviews of the complexed cations in a) $K^+(18C6)\cdot SCN^-$ [51], b) $Cs^+(18C6)\cdot SCN^-$ [51], and c) $Na^+(12C4)_2\cdot OH^-\cdot 8H_2O$ [52].	34
5	A schematic packing diagram of the cations and anions in $Na^+(C222)\cdot Na^-$ [60]	38
6	The ^{23}Na NMR spectra of $Na^+C222\cdot Na^-$ in a) methylamine, and b) in the solid state [56,63].	40
7	Apparatus for the recrystallization of alkalides and electrides.	55
8	Packing diagram of the cesium cations, represented by solid circles, and the sodium anions, represented by open circles, in $Cs^+(18C6)_2\cdot Na^-$. Dotted lines represent cation-cation distances, dashed lines represent anion-anion distances, and the weak	

solid lines represent cation anion distances about one cation. 90

9 The structure of the complexed cation, $Cs^+(18C6)_2$ in $Cs^+(18C6)_2 \cdot Na^-$. 94

0 A stereoview of a unit cell in $Cs^+(18C6)_2 \cdot e^-$. The center of the anionic cavity is noted by the symbol ⊙. 104

1 A surface contour representation of an anionic cavity in $Cs^+(18C6)_2 \cdot e^-$, as viewed down the c axis at a = $^1/_2$, b = 0, c = $^1/_2$. The cavity is shown at its maximum size in the a-b plane; channels to neighboring cavities at 1, $^1/_2$, $^1/_2$, and 0, $^{-1}/_2$, $^1/_2$ are indicated by arrows. 112

2 A surface contour representation of the packing of complexed cations and anionic cavities in an a-c plane at b = 0 in $Cs^+(18C6)_2 \cdot e^-$. The oblong shape cavities and the channel structure in the c direction are apparent. 113

3 A surface contour representation of the packing of complexed cations in $Cs^+(18C6)_2 \cdot e^-$ as viewed down the 1,1,0 direction. The interstitial open spaces are channels to cavities behind the "wall" of complexed cations. 114

4 DSC trace of a polycrystalline sample of $Cs^+(18C6)_2 \cdot I^-$. 128

5 DSC trace of a polycrystalline sample of $Cs^+(15C5)_2 \cdot e^-$. 130

6 DSC trace of a polycrystalline sample of $Cs^+(18C6)_2 \cdot e^-$. 133

Normalized optical absorption spectrum of $Cs^+(15C5)_2 \cdot e^-$ at -100 C. 135

Normalized optical absorption spectrum of $Cs^+(15C5)_2 \cdot e^-$ at -35°C and -1°C. 137

FIGURE		PAGE
19	^{133}Cs static NMR spectra, comparing linewidths of Cs_2SO_4 at 52.48 MHz and 23.62 MHz. . .	.155
20a	Static ^{133}Cs NMR spectra of $Cs^+(18C6)_2 \cdot I^-$ at 52.48 MHz. The dashed lines are calculated spectra from equation 16 for ν_Q = 6.5 KHz, δ = 32 ppm and η = 0..	.157
20b	Static ^{133}Cs NMR spectra of $Cs^+(18C6)_2 \cdot I^-$ at 23.62 MHz. The dashed lines are calculated spectra from equation 16 for ν_Q = 6.5 KHz, δ = 32 ppm and η = 0..	.157
21	Static ^{133}Cs NMR spectrum of $Cs^+(15C5)_2 \cdot I^+$ at 23.62 MHz. The dashed line is the calculated spectrum from equation 16 for ν_Q = 30.5 KHz, δ = 52 ppm and η = 0.	.160
22	Static ^{23}Na NMR of $Cs^+(18C6)_2 \cdot Na^-$ at two temperatures, T $\leq$ 210 and 250 K.	.163
23	Single crystal ^{133}Cs NMR spectra of $Cs^+(15C5)_2 \cdot I^-$ at two random orientations. Lines labelled A and B are central $-1/2$ <--> $1/2$ transitions for two $Cs^+(15C5)_2$ orientations. Lines labelled a and b represent corresponding non-central quadrupolar transitions.	.164
24	Single crystal ^{133}Cs NMR spectrum of $Cs^+(18C6)_2 \cdot I^-$ at a random orientation. The sharp spike is apparently due to residual solution.	.167
25	^{133}Cs MAS-NMR spectrum of $Cs^+C222 \cdot e^-$, showing inclusive and exclusive complexed cations, prepared from solutions that contained excess quantities of a) cesium and b) C222. Other lines are spinning sidebands.	.180
26	The chemical shift versus T^{-1} for $Cs^+(18C6)_2 \cdot e^-$. The temperatures of points marked by x were calibrated by comparison with the dipolar splitting of protons in methanol. Other points were constrained to lie on the best-fit line through	

the four calibrated points. 184

27 ^{133}Cs MAS-NMR spectrum of the product obtained from initial stoichiometry $Cs^+(18C6)_3$. Peaks at −50 ppm and −230 ppm are $Cs^+(18C6)_2$ resonances, the peak at 77 ppm is a $Cs^+(18C6)_2 \cdot e^-$ resonance. Other features are spinning sidebands. 190

28 ^{133}Cs MAS-NMR spectra of compounds formed from initial stoichiometry $Cs^+(18C6)_2 \cdot Na_x \cdot e_{1-x}$ for a) $x = 0.2$ and b) $x = 0.8$. Peaks at 73, 57, 42 and 25 ppm are from a mixed compound with $x = 0.1$–0.2; the peak at −61 ppm is from excess $Cs^+(18C6)_2 \cdot Na^-$. Other features are spinning sidebands. 191

29 An anionic packing diagram showing a postulated mixed sodide/electride structure that could account for the observed mixed electride-sodide ^{133}Cs NMR spectra. Open circles are trapped electron sites, solid circles are sodium anions. 194

30 The chemical shift versus T^{-1} for $Cs^+(15C5)_2 \cdot e^-$. The temperatures of points marked by x were calibrated by comparison with the dipolar splitting of methanol. The temperatures of other points were calibrated by simultaneous measurement of the Knight shift of $Cs^+(18C6)_2 \cdot e^-$. 202

31 The density of states with spin up (↑) and spin down (↓) in a metal as a function of energy, E, a) at equilibrium in the absence of an external magnetic field, b) prior to equilibrium upon application of a field, H, and c) at equilibrium in the presence of the applied field [94]. 210

32 The susceptibility of an antiferromagnet as a function of temperature, normalized to the values at T_N; a) for a single crystal with easy axis $\parallel$ to the applied field, H, b) for a single crystal with easy axis $\perp$ to H and the powder average. 223

FIGURE PAGE

33 The reciprocal molar electronic susceptibility of $Cs^+(18C6)_2 \cdot e^-$ as a function of temperature [71]. 227

34 The reciprocal molar electronic susceptibility of a quenched sample of $Cs^+(15C5)_2 \cdot e^-$ as a function of temperature. 231

35 The reciprocal molar electronic susceptibility of an annealed sample of $Cs^+(15C5)_2 \cdot e^-$ as a function of temperature. 233

36 The temperature dependence of the molar electronic susceptibility an annealed sample of $Cs^+(15C5)_2 \cdot e^-$ as a function of the applied field. 235

37 The molar electronic susceptibility of an annealed sample of $Cs^+(15C5)_2 \cdot e^-$ as a function of the applied field at 1.6 K. 236

38 EPR spectra of $Cs^+(15C5)_2 \cdot e^-$, sample 1, at 2.0 K, 48 K, 200 K, 80 K, 14 K, and 5 K. 249

39 EPR spectra of $Cs^+(15C5)_2 \cdot e^-$, sample 2, at 2.8 K, 19 K, 10 K and 2.5 K 250

40a EPR spectra of $Cs^+(15C5)_2 \cdot e^-$, sample 3, at 2.5 K, 6 K, 158 K, and 2.6 K. 251

40b EPR spectra of $Cs^+(15C5)_2 \cdot e^-$, sample 3, at 7.5 K, 19 K, 50 K, and 2.6 K. 252

41 ΔH_{p-p} as a function of temperature for sample 1 of $Cs^+(15C5)_2 \cdot e^-$. 253

CHAPTER 1

INTRODUCTION

Alkalides and electrides are compounds that consist of complexed alkali metal cations countered by alkali metal anions and trapped electrons respectively. This thesis concerns the physical characterization of the unique anions in these materials, with an emphasis on the trapped electron in the electrides. The primary techniques used to characterize the compounds are structural analysis, magnetic susceptibility and magnetic resonance. This chapter will explore the background information about trapped electrons in the solid state, first in the low electron density regime of F-centers and localized electrons in glasses, and then in the high electron density regime of metal ammonia compounds. The description of these systems will emphasize their structure and the magnetic properties of the electrons.

Studies of trapped electrons originated with investigations of metal solutions in ammonia, amines, and ethers. The electron density can be varied easily in these solvents and the association of the solvated electron with other ions in the high concentration limit (and as a

function of the dielectric constant of the solvent) to form various paramagnetic and diamagnetic species will be discussed. Indeed, electrons show similar types of aggregate ion formation in the solid state, which may strongly affect the physical properties of the material. The complexation chemistry of alkali metals with crown ethers and cryptands allowed metal solutions to be studied at higher concentrations in less polar media; these complexes permitted more complete characterization of the associated ionic species. It was this development which led directly to the isolation of alkalide and electride salts by removal of the solvent. The fundamental properties of the alkalides and of some previously synthesized but incompletely characterized electrides will be reviewed. Finally the issues involved in the characterization of electrides will be presented in order to put the present work in perspective.

I.A Trapped Electrons in the Solid State

I.A.1 Color Centers

The first example of electrons trapped in solids was reported 70 years ago when it was noticed that alkali

halide salts that had been exposed to high energy radiation became colored [1]. The radiation interacts with the salt to form excitons, mobile excited state species which consist of an electron bound to a hole. The exciton can dissociate in the vicinity of an anionic vacancy to give a localized electron and a localized hole species. The F-center is an electron trapped at an anionic vacancy. Several variables are pertinent to the stable formation of the localized electron state including the energy of the radiation, the pressure, and the temperature, each of which can affect the mechanism of the excitation and thus the nature of the excitonic species [2]. For example, color centers may be produced in alkali halides by irradiation with ultraviolet light which strips the valence electron from the anion. The electron is initially loosely bound to the halogen atom at an energy just below the conduction band. The electron may be trapped at a pre-existing vacancy to form the F-center. Harder radiation is capable of creating the anionic vacancy by ejecting an anion from its lattice site; the electron may be trapped at the vacant site while the hole forms some other defect center. Regardless of the mechanism of its formation, the nature of the color center remains constant. Color centers can be formed at concentrations up to 10^{18} electrons/cm^3. At high concentrations there is a tendency for F-centers to

aggregate and form more complex crystalline defects.

The optical absorption spectrum of these colored salts was found to have a bell-shaped band with an energy at the maximum absorbance that was inversely related to the nearest neighbor separation a in Ångstroms. An empirical relationship due to Mollwo and Ivey gives $E = 17.7\ a^{-1.84}$ [3] for the energy in electron volts of the absorption maximum. The breadth of the band increases with increasing temperature, while the oscillator strength remains constant. The Mollwo-Ivey relation roughly accounts for this phenomenon since the interionic separation, a, will have a larger range of values for increased thermal vibration in the lattice [4].

The nature of the wave function of the electron at the ionic defect has been treated at various levels of sophistication. At its simplest, it can be approximated as a particle in a cubical box of edge-length 2 a. More complex potential wells which vary periodically similar to the Madelung Energy, with an average decrease proportional to 1/r have been used. The idea that the electron might interact with more than one shell of nearest neighbors is substantiated by EPR and ENDOR studies. Hyperfine coupling due to ions as far away as the eighth nearest neighbor shell has been detected for color centers in KBr [5]. These experiments indicate that, while the electron has

long range interactions with the ionic lattice, the bulk of the electron density (63%) lies inside the vacancy, and 99% of the electron density is found within the first two shells of ionic neighbors.

Electrons that behave much like the color centers can be formed in the molten alkali halides by addition of pure alkali metal to the melt. The concentration of electrons can be varied by varying the amount of metal, which dissociates in the fluid to M^+ and e^-. It has been shown that molten salt color centers follow a Mollwo-Ivey type relation [6]. Although the concentration of metal can be raised to beyond the non-metal to metal transition, the concentration of color centers does not get large. Trapped electrons in high concentrations ($>10^{18}$ electrons/cm^3) tend to form aggregates with other ions, resulting in metal clusters of low charge.

Even in this simplest of trapped electron systems some themes that will recur in similar trapped electron materials arise. The localized electron is highly polarizable; it can have a significant density away from the electron trap. The trapped electron tends to associate with other ionic species at high concentrations to form more complex ionic aggregates. The local structure of the color center is known since the electron is trapped at an anionic vacancy in a simple salt structure. Even so, it is

apparent that to fully understand the localized electron its interaction with the local environment must be probed.

I.A.2 Electrons Trapped in Glassy Matrices

Ionizing radiation has been used to generate electrons in non-polar systems such as amines and ethers, and glasses of alcohols and H_2O. Electrons trapped in fluids will be discussed in section B of this chapter. The study of electrons trapped in glasses has been especially fruitful for describing the general solvated electron structure. In contrast to the electrons trapped in ionic vacancies in a crystalline lattice, which were surrounded by attractive and repulsive charges that stablize the trapped electron, electrons localized in non-polar media often are not stable with respect to reduction of surrounding molecules. An electron injected into water has a half-life of about 1 millisecond with respect to reduction of the solvent [7]. The localization itself is not an obvious process. There are no vacant lattice sites, and no coulombic attractions to charged species with which to interact; instead, the electron interacts with the dipole moments of the solvent.

The work that will be discussed here involves injection of electrons into glasses at temperatures between 4 and 77 K. The lifetime of trapped electrons is greatly

enhanced over that in fluid systems due to the reduced thermal motion of the medium. The mechanism for solvation of the electron has been studied both in fluids and in glasses, primarily by rapid spectroscopic methods. After complete solvation, the trapped electron is assumed to have an average equilibrium structure which can be determined in glasses by electron spin echo modulation spectroscopy. The geometric structure of the cavity about an electron in a glassy matrix might be expected to be similar to the average structure in solutions. The theoretical ideas concerning the localization of electrons should be applicable to both glasses and solutions. A brief outline of the most universally accepted model for the trapped electron will be presented.

An injected electron is trapped in a glass or solvent by a two stage mechanism, in which the first step accounts for the localization of the itinerant electron at a pre-existing trap, and the second step is the equilibration of the trap into the lowest energy configuration. The first step is rapid, typically on the order of 10 picoseconds in H_2O and 40 nanoseconds in glasses. The amorphous structure of the glass has a large number of sites arising from fortuitous random molecular orientation of the dipoles which serve as initial traps for the electron. The time-scales of localization into pre-existing traps were

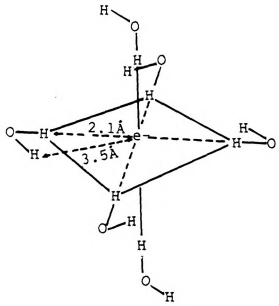
determined by picosecond pulse radiolysis experiments [8]; the optical absorption maximum tends to occur at ~1500 nm in most solvent systems. As the trap relaxes to an equilibrium structure, the low energy peak decays and an absorption at ~600 nm arises which is stable for the lifetime of the species.

The structure of the equilibrium solvation shell of an electron trapped in a glassy matrix has been deduced by electron spin resonance techniques. The hyperfine interaction of magnetic nuclei surrounding a paramagnetic electron is very informative in terms of the strength (distance) of the coupling and the nuclear species involved. Traditional methods for determining hyperfine coupling failed in the glasses because broad resonance lines obscured the weak couplings. Kevan [9] employed a multipulse electron resonance technque known as electron spin echo modulation to probe the hyperfine interactions of the trapped electron. Several pulse sequences may be used to measure the modulation function. The most common experiment was a two pulse EPR sequence in an applied field, $\underline{H}$, oriented along the z axis. The pulse sequence must be short relative to the relaxation time of the electron spin. The physical description of the pulse sequence is as follows. A 90° pulse is applied perpendicular to the applied field, which flips the electron spins

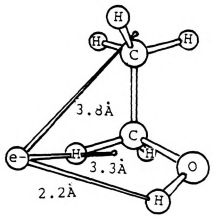
into the x-y plane. The spins are allowed to precess for a time, τ, during which they dephase in the x-y plane due to various hyperfine contacts. A second pulse is applied which flips the spins 180° and keeps them in the x-y plane. The dephasing which had occurred during time τ rephases after another period of τ, releasing a burst of microwave energy whose intensity is measured as a function of τ. Two factors influence the strength of the microwave emission; first, the relaxation of the spins causes an exponential decay of the power with time, and second a modulation function arises from the dephasing influence of the dipolar hyperfine contact with neighboring nuclei [10]. The modulation function can be fit with an equation which has three parameters: the number of neighbors, the hyperfine coupling constant, and the distance between the electron and the interacting nucleus. In order to get unique neighbor information, selective deuteration of equivalent protons was used. Since the magnetic moment of deuterium is much smaller than that of the proton, the hyperfine contact with only the substituted deuterons could be measured. Thus, added information about the orientation of solvent molecules around the trapped electron could be obtained.

The average geometric structure of the solvated electron in glasses made from 10 M NaOH in water and in pure ethanol glasses is shown in Figure 1 [11,12]. The

a)



b)



igure 1. The geometric structure about the trapped electron
n glasses of a) 10 M NaOH, and b) ethanol [9-11].

structure of the aqueous glass was found to be independent of the ions in solution; thus, the only hyperfine interactions of the trapped electrons were with protons on H_2O. The best fit to the modulation function gave two proton distances at 2.1 Å and 3.5 Å for six nearest neighbor molecules. Studies with enriched $H_2{}^{17}O$ verified the coordination number. A geometry with an octahedral arrangement of the six water molecules oriented with an O-H bond directed toward the center of the electron cavity agreed with all of the data. The electronic character at the first shell molecules from hyperfine constants was only 4%, so that 96% of the trapped electron density resides in an s-type wave function centered at the cavity.

The geometric structure of a trapped electron in ethanol required selective deuteration methods to determine the orientation of the solvent molecules. The results indicated that four ethanol molecules arranged tetrahedrally form the electron cavity. The distances to neighboring protons are 2.2 Å to the hydroxyl proton, 3.3 Å to the β-proton and 3.8 Å to the α-proton. The only geometry that coincides with these data is one which orients the molecular dipole moment of the ethanol towards the center of the cavity, rather than the O-H bond as was seen in H_2O. The trap has remarkably similar dimensions to the cavity formed in H_2O.

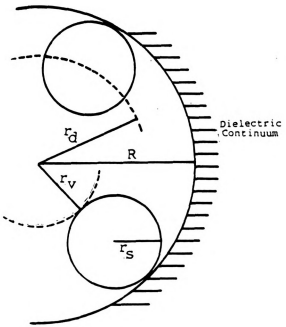


Figure 2. The semicontinuum model for the trapped electron. r_v is the void radius, r_s is the effective spherical radius of a first shell solvent molecule, the dipolar interaction radius is r_d and R is the distance from the center of the cavity to the dieletric continuum [12].

The results of electron spin echo modulation experi-
nts concurred with a theoretical model known as the semi-
ntinuum model, which was independently proposed in 1970
two groups [13,14]. The semi-continuum model gives only
mi-quantitative agreement to observed electrical, optical
d magnetic data, but is still regarded as the best model
r the trapped electron.

The semi-continuum model, depicted in Figure 2, assumes
at the excess electron is trapped in a spherical cavity
radius r_v created by a finite number, z, of solvent
lecules. The z first shell molecules are treated as
eal point dipoles in their electrostatic interactions
th the electron, but are assigned a real spatial radius
. Solvent beyond the spherical volume of radius R =
r_s of the cavity and first solvent shell is treated as a
electric continuum. The energy of the trapped electron
determined by long range interactions with the continuum
screened coulombic polarization, and by short range
eractions with the first solvation shell. The model
n has three parameters, the coordination number z, the
ity radius r_v and the free (itinerant) electron energy.
agreement with the structures implied from electron
n echo experiments is good. Typical values for the
ameters are z = 4-8 and r_v = 1.7-2.2 Å. The semi-
tinuum model is an extension of Jortner's [15] earlier

tinuum model which treated the electron cavity immersed
the dielectric continuum without accounting for any
licit short range forces. The major improvements of the
l-continuum model are that the energy required to orient
first solvation sphere is accounted for and the
ngest dipole attractions of the electron with the first
ation shell are explicitly included. The ground state
he electron is a 1s type wavefunction, and various
odsethods have been used to calculate the energy of the
ped electron. The agreement with experimental data
s not to be quantitative; however, the model does
ict trends with variation of temperature, pressure, and
ents. It reproduces the optical absorption maxima, but
not properly account for the shape of the band.
Two types of solids which are able to localize
trons into stable traps at cavities in the medium in
concentrations have been reviewed. The predominant
e that stabilizes the F-center is clearly the reduction
ne coulombic repulsions of the cations bordering the
ncy. It is remarkable that non-ionic systems are able
calize an electron at energies that are 1-2 electron
below the conduction band by primarily long and short
polarization of dipolar molecules.

A.3. Lithium Tetraamine -- Expanded Metals

Lithium (as well as other alkali metals) dissociates in quid ammonia to form the solvated cation and electronic ecies which vary in nature depending on the concentration the metal. At a concentration of one lithium to four monia molecules there is a deep eutectic in the phase agram. The solution has a low vapor pressure and a large othermic heat of solution at the eutectic, which is ique to lithium in the alkali series; this indicates that $(NH_3)_4$ forms a compound rather than being an immiscible tem. The conductivity of the solid phase was measured; results were not those of a eutectic mixture of Li and monia, but of a compound [16]. Several of the alkaline ths form similar compounds of stoichiometry $M(NH_3)_6$ for Ca, Sr, or Ba. The properties of only the lithium raamine will be discussed here, as it has the lowest ctron density and thus most nearly approximates ctrides. The solution freezes at 89 K to form a gold id that retains many of the nearly free electron perties of the solution. The electron density in the id is approximately 5×10^{21} electrons/cm^3, much greater n the electron densities in either the color centers or irradiated glasses.

X-ray and neutron powder diffraction patterns have been analyzed as a function of temperature for this compound [17,18]. The compound $Li(NH_3)_4$ crystallizes into a body centered cubic lattice with 16 formula units per unit cell. The lattice parameter a is 14.98 Å between 89 and 82 K; at 82 K there is a phase transition below which the lattice parameter is only 14.93 Å. Interestingly, the fully deuterated ammonia compound does not have a different high temperature crystalline phase; it forms only the low temperature phase upon crystallization at 89 K. As the temperature is lowered still further to 25 K neutron diffraction shows a transition to an antiferromagnetic phase as indicated by a doubling of the magnetic lattice parameter.

The magnetic susceptibility of this material has been measured over the entire temperature range of 4 to 300 K [19,20]. The magnetic susceptibility is, in this case, a sensitive probe of electronic interactions with other paramagnetic electrons. Above 82 K in $Li(NH_3)_4$ the susceptibility is Pauli paramagnetic, indicative of a nearly free electron metal. The phase transition at 82 K causes the system, which is still metallic by conductivity and Hall measurements, to show an inverse temperature dependence in susceptibility following the Curie Weiss law. The strongly correlated electron gas arises from the larger

-Li distances (or the low electron density) such that the
ectron density is found to partially occupy cavity
ates, so that the electron gas is not fully degenerate.

The picture that is generally drawn for the lithium
traammine system is that of an "expanded metal" [21];
at is, a $Li(NH_3)_4^+$ ion enclosed in a spherical Li 3s
ectron orbital. The Li 2s and 2p orbitals are hybridized
a set of sp^3 orbitals which interact with the lone pairs
the ammonia. There is no evidence that anionic electron
ps away from the nuclear species exist in this system;
more strongly corresponds to a metallic structure
ilar to that of pure lithium, a closest packed lattice
cationic cores bound by the electron gas.

Compounds which have stoichiometry Li (methylamine)$_4$
e also been isolated. Preliminary studies of the
netic susceptibility, ESR and conductivity of the
erial indicate that this system is also a highly
related metal [22].

The solid state materials that have been discussed
ve show trends and characteristics that must be
sidered when discussing electrides. The low electron
sity glasses or alkali halides have electrons that are
pped in otherwise void space. The electron has a
dency to "leak" into its surroundings, spreading its
sity over its nearest neighbors. Highly polar ionic

lts enable electron density to spread into distant ionic
ells more easily than do the relatively non-polar
lutions. The trapped electrons in alkali halides and
asses are present at such low concentrations that there
no interaction with other trapped electrons, and, in the
e of the glasses, with any ionic species. There is also
dence in these systems that, as the electron density
reases, there is a tendency for much more complex
cies to form, which involve more than one electron
/or cation in direct association.

Certainly, in the metal ammonia compounds the electron-
ctron interaction is strong enough to form the band type
rgy levels characteristic of metals. Mott described the
dency of materials to go through a transition from a
allic state to a non-metallic state in terms of two
meters; the effective Bohr radius (a^*) of the outermost
ctron and the electron density ρ. The Mott criterion
es that a material should go metallic when $\rho^{1/3}a^* > 0.25$
. The idea is that in a given medium a valence
tron will have some volume which can be represented in
s of a spherical Bohr radius a^*. The electron is
acted to a positive charge with a potential energy
ortional to $-1/r$. As the dielectric constant of the
um is increased there is a decrease in the attraction
he electron to neighboring charges, thus increasing a^*.

As the concentration of valence electrons is increased, the overlap of electrons increases the screening between an electron and positive charges. The combined effect of increasing both a^* and the electron density, ρ, is to reduce the energy required to remove an electron from one positive charge and place it on another. When the electron is free to move it is considered to be metallic [24]. The electron density in $Li(NH_3)_4$ can be calculated from the structure and is 4.8×10^{21} e^-/cm^3. The effective Bohr radius is $a^* = 2.76$ Å. The Mott criterion for metallic character is satisfied, $\rho^{1/3}a^* = 0.47$ which is greater than .25. If it is assumed that the electron density in $Li(NH_2CH_3)_4$ is one-half that seen in the tetraammine, then the Mott criterion is satisfied for $a^* > 1.87$ Å. The dielectric constant in methylamine is smaller than that of ammonia so the radius a^* would be reduced, and the material is expected to be just at the metallic- nonmetallic borderline.

The metal ammonia compounds are very near the metal-nonmetal transition. It is unfortunate that other compounds such as $Na(NH_3)_6$ or $Li(NH_2C_2H_5)_4$ do not exist, for the reduction of electron density or dielectric constant could push these compounds to the nonmetallic regime. It would be interesting in these cases to see whether the nonmetallic compounds would have the electron

localized in excited s-orbitals or whether trap states would have a lower energy.

It might be expected that electrides are within an order of magnitude in electron density of the expanded metals. Since dielectric constant and electron densities of electrides might be expected to vary from one compound to another the study of their electron-electron interactions might provide valuable insights into the nature of the metal-nonmetal transition.

I.B Solutions of Alkali Metals

I.B.1 Metal Ammonia Solutions

Most of the scientific attention to the properties of trapped electrons has been in the area of metal solutions in ammonia, amines, and ethers, rather than in the solid state materials described above. Indeed, metal ammonia compounds, electrons in glasses, and alkalides and electrides have evolved from research initiated in the metal solution area. There are advantages and disadvantages to studying solutions rather than the solid state. The greatest advantage is the ability to increase continuously the electron concentration in solution by increasing the metal concentration and/or to change the

lectric constant of the medium by varying the solvent. major disadvantage is that ions in solution are able to rate easily and rapidly; this makes the structures of ionic species and their interactions with other ions ficult to measure.

The published observations of Weyl [25] in the 1860's he physical nature of solutions of alkali metals in id ammonia were the starting point for what was to me an enormously popular field of research in the ical sciences. Davy's notebooks of 1808 [26] indicate he had observed "fine blue solution films" upon mixing ssium and ammonia. It wasn't until 100 years later Kraus began to make progress in the understanding of l ammonia solutions by measuring physical properties as the vapor pressure above the solution [27] and the uctivity as a function of metal composition and concen- ion [28]. The experimental and theoretical work in field is comprehensively reviewed in Thompson's book, *ctrons in Liquid Ammonia"* [29], and in the *Procedings olloque Weyl IV* [30], *V* [31], and *VI* [32]. The ssion here will focus on those aspects of metal ions that concern the structure of the solvated ions heir interionic interactions. This may aid in the pretation of results obtained in solid state studies kalides and electrides.

The alkali metals (Li, Na, K, Rb, and Cs), some
aline earths (Ca, Sr, Ba), and some rare earths (Eu and
dissociate in liquid ammonia according to the
ilibrium

$$M + NH_3 \rightleftharpoons M_s^+ + e_s^- \qquad (1a)$$

$$M + NH_3 \rightleftharpoons M_s^{++} + 2e_s^- \qquad (1b)$$

re the nature of the ionic species can be complex
ending on the metal concentration. Similar solutions of
als in solvents with lower dielectric constant may form
in general the total metal concentration in solution is
ll. Very dilute metal solutions in ammonia [below 10^{-4}
percent metal (MPM)] consist of essentially non-
racting solvated ions. The magnetic susceptibility has
general limiting result that the number of paramagnetic
ies is equal to the metal concentration [33,34]. The
ty in which the electron is trapped is considered to be
lar to that described by the semi-continuum model [12].
optical absorption, electrical conductance, excess
me of solution of the metal and magnetic properties
elate well with the model of a solvated electron. As
concentration of the metal is increased (or as the
ectric constant of the solution is decreased) the ionic

ecies tend to interact more strongly with one another
5]. Electron-cation interactions result from the
tractive coulomb potential between the ions, drawing them
to an associated ion pair species of stoichiometry M_{solv}.
e structure of the ion paired species can vary between
o extremes; the solvent-shared ion pair and the solvated
al atom. The ions in the solvent-shared species retain
ir respective traps, but one or more of the solvent
ecules may form part of each ion's solvation sphere.
solvent-shared ion pair seems to be the most accurate
cription of this species in metal-ammonia solutions, in
ch optical absorption and NMR Knight shift data indicate
t the electron trap retains its integrity. The
lectric constant and donor number of the medium are
ortant in determining the extent and type of ionic
eraction. Higher dielectric media favor less associa-
n of ionic species. The contact ion-pair- solvated ion-
r equilibrium in this case has been driven to the left
he media's inability to solvate the ions. The
ngest evidence of atom-like associated species comes
magnetic resonance detection of hyperfine contact of
excess electron to the cationic nucleus [36]. EPR
riments in the less polar solvents show hyperfine
tting patterns from which the extent of atomic
acter can be calculated. In more polar solvents, rapid

hange between the associated species M and ionic species
rows the EPR line so that hyperfine information is lost.
studies of the cations permit detection of a
magnetic shift due to the hyperfine contact in all
ents [37]. The general trend in these experiments is
the ion-pair is of smaller atomic character as the
rity of the solvent is increased, and the solvent-
ed species is favored. As the dielectric constant of
medium is decreased, the associated ion pair tends
rds the "solvated metal monomer". The hyperfine
tant was measured for K solutions in NH_3, $MeNH_2$, $EtNH_2$,
THF, and the density of the trapped electron at the
eus corresponded to 0.5, 3.0, 12, and 36% atomic
acter respectively. Edwards and Catterall [38] found
Cs in frozen HMPA solutions gave solvated species with
atomic character.

In addition to the paramagnetic ion pairs, even more
ex diamagnetic species form as the metal concentration
creased in ammonia or as the dielectric constant is
ased. Magnetic susceptibility results indicate that
e metal concentration in NH_3 approaches 1 MPM, the
ntration of paramagnetic species is an order of magni-
smaller, so that most of the electrons are interacting
each other strongly enough to couple their spin
ar momenta.

The nature of the spin-paired species is more difficult
etermine than that of the paramagnetic species because
agnetic probes such as EPR and magnetic susceptibility
ot useful. NMR techniques are also unable to
tain the nature of the associated species in polar
nts, because rapid exchange broadens the resonance to
the information, while non-polar solvents support only
low solubilities of the ionic species. Theoretical
derations of a doubly occupied electron cavity
ate that $e_2^=$ could be stable with respect to dissocia-
into two solvated electrons [39], but if this were a
species the volume of the solution would be expected
crease with spin-pairing, and the equilibrium would
to shift to the spin-paired state with increased
ure; neither effect is seen in any solvent. Other
gnetic species which could form are the dimer M_2, the
riple $e^- \cdot M^+ \cdot e^-$, and the alkali metal anion M^- [35].
irst species could consist of dimers of any of the
aired paramagnetic species discussed previously. The
ture of the ion triple may vary between the solvent-
d species and the contact ion species. The three ions
solvent shared ion triple share one or more solvent
ules, but retain their respective traps. The contact
riple includes direct interaction of the three
ted ions. Ammonia solutions almost surely have

nt shared types of electron-electron coupling. Beyond iamagnetism of the solution there is no evidence of hanges in the properties of the solution that would ate a trap greatly different from that seen at low ntration. The limiting case of the contact ion-triple at in which the two electrons occupy the s orbital of lkali metal, giving the third species M_s^-. This es has not been observed in ammonia solutions although odynamic arguments have been constructed that predict M^- should exist in ammonia solutions [40]. Optical ra were obtained in solvents such as ethylenediamine, show a metal dependent peak attributable to the M^- es [41], which followed the trends predicted by charge fer to solvent theory [42]. There was, however, no evidence that pointed to the presence of alkali anions with filled s-orbitals as the proper descrip- f this species. Other spin-paired species could also t for the absorption. Again the diamagnetism of the s and the low solubilities of the alkali metals in w dielectric solvents (where stronger ionic ation is favored) prevented direct determination of ructure of the spin-paired species.

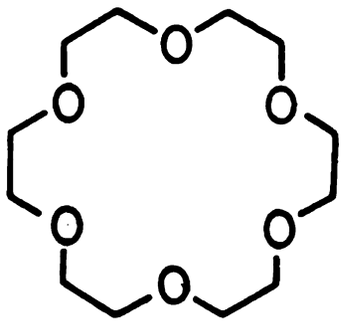
hancement of the metal solubility in non-polar ts became possible in the late 1960's with the pment of a new alkali metal complexation chemistry.

evelopment was crucial in the determination of the
of the anionic species in low dielectric media.

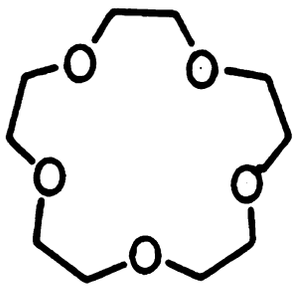
Alkali Metal Complexation

chemistry of alkali metals prior to the 1960's had
nfined to the hard sphere ionic nature shown in the
nce state. With growing recognition of the
nce of Na^+ and K^+ in biological systems, researchers
interested in the chemistry of ionic transport.
n and Moore [43] discovered that the antibiotic
ycin could act by specifically binding alkali
this became a challenge to organic syntheticists
oduce such complexation by smaller molecules.
[44] in 1967 succeeded by synthesizing a class of
ls known as crown ethers.
generic crown ether m-Crown-n (or mCn) consists of
ethoxy groups forming a carbon and oxygen ring
atoms, and n oxygens. Figures 3a and 3b show the
15C5 molecules. Side groups such as benzo- or
ano groups can be attached to the ring. These
crown ethers interact with alkali cations via a
harge attraction in a very selective way. The
ring of the crown ether formed by the oxygens, is
rized by a hole radius r_H which is on the order of

a)



b)



c)

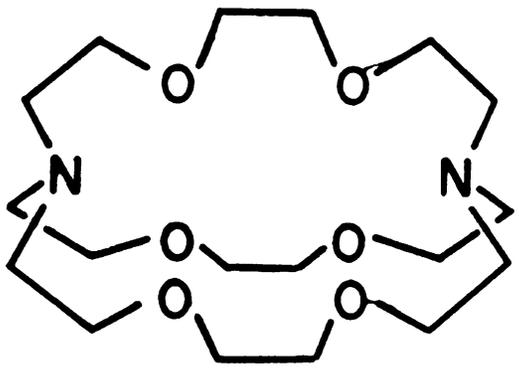


Figure 3. Molecular structures of a) 18-Crown-6, b) 15-Crown-5, and c) Cryptand-222.

e ionic radii of the alkali cations. A 1:1 complex tends
form when the cation interacts strongly with the oxygen
ne pairs that line the hole. The stability of the
plex depends on the "fit" of the ion into the hole; if
ion is too small the mean contact distance lengthens,
it is too large the ion cannot fit into the center of
ring.

Lehn and coworkers in 1969 synthesized yet another
portant class of compounds known as cryptands [46].
ptands are three dimensional bicyclic polyethers
sisting of two nitrogens tying down 3 strands of m, n,
o ethoxy groups, respectively, for CmnO. Cryptand 222
22) is drawn in Figure 3c. The three dimensional nature
the polyether cavity puts a more stringent constraint on
size selectivity of cryptands than the crown ethers.
general result is that cryptands tend to have larger
ilibrium constants for the complexation reaction than do
wn ethers. In addition cryptands are more selective for
ions based on size effects [47].

Tab

===

C

Ho

Cat

L
N

R
C

===

co

is

di

li

th

Na

di

Rb

Values of log K_{eq} for the Complexation of Alkali Metal Cations with Crown Ethers and Cryptands in Methanol [45].

exant	15C5	18C6	21C7	C222
adius	0.85 Å	1.38 Å	1.70 Å	
Radius				
0.74				~1.7
1.02	3.3	4.4	1.7	7.2
1.38	3.7	6.1	4.2	9.6
1.49	3.3	5.3	4.5	8.3
1.70	2.0	4.6	5.0	3.4

e 1 shows the equilibrium constant for 1:1
tion reactions in methanol. The equilibrium here

$$M_s^+ + C_s \rightleftharpoons M^+C_s \qquad (2)$$

an be seen that several trends arise that are
related to the size effects of the ion and the
The series of 18C6 with the various cations shows
C6, which is a perfect fit, is more stable than
nd Cs^+18C6 (each of which have ionic radii ~0.3 Å
than K^+) by nearly two orders of magnitude. Even
a is only 0.1 Å larger than K^+, has a K_{eq} nearly

ten

comp

is s

equa

cons

the

cryp

its

fit

grea

valu

equi

18C6

acc

eas

the

par

str

of

2.0

equ

dev

dis

smaller. 15C5 does not form such strong
with any of the cations, because its hole radius
r than the ionic radius of Na^+. 15C5 is nearly
ble to complex Na^+, K^+, Rb^+; the Cs^+ equilibrium
is an order of magnitude smaller. The trend in
dimensional cryptands is even more dramatic. The
molecule is quite flexible and is able to change
rmation to better complex small cations. The best
222 is K^+, the equilibrium constant is ~1000
han the for complexation of K^+ with 18C6. The
K_{eq} for Na^+ and Rb^+ are similarly increased. The
um constant for Cs^+ is smaller for C222 than for
cavity in the cryptand is too small to readily
te Cs^+, whereas the two-dimensional 18C6 can
plex the large cation.

mplexation equilibrium has a strong dependence on
t as well as on ionic radii. The more able any
solvent is to solvate the bare cation, the more
t is able to compete with the ligand. The value
$_q$) for complexation of K^+ with 18C6 in water is
orders of magnitude smaller than the same
in ethanol [45].

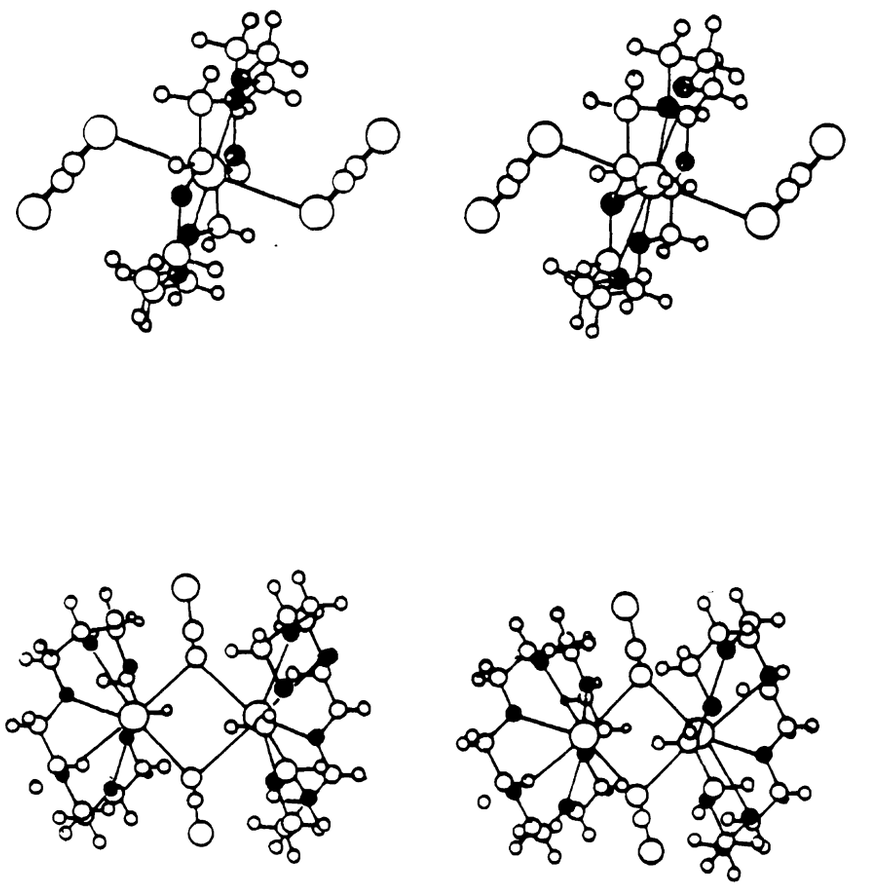
cryptands were very important in the historical
of alkalides and electrides, and will be
ater in this context, the present work is almost

vely based on crown ethers and further discussion
limited to their properties. The complexation of
metals by crown ethers is not just as simple as the
mistry that has been discussed so far [48]. The
ing is quite flexible so that many conformations of
may exist. For cations which fit into the plane of
gens, 1:1 complexes are the most stable [49].
cations that are too large for the hole most sit on
g and may be complexed in a 1:2 ratio (the cation
ched" by two crown ethers) or in a 2:3 ratio (a
andwich" structure). Large crown ethers which have
times larger than the size of the cation may assume
rmation in which the cation is surrounded by the
ther in much the same way that the cork center of a
l is surrounded by it's seam (i.e. Na^+ and 24C8)
Structures have been determined for several crown
mplexes with alkali metal cations including the 1:1
s of $M^+18C6{\cdot}SCN^-$ for $M^+ = Na^+$, K^+, Rb^+, and Cs^+
the sandwiched 1:2 complex of $Na^+(12C4)_2{\cdot}OH^-{\cdot}8H_2O$
hese structures indicate how the conformation of
tively flexible crown ether changes to best complex
on. For example, in the thiocyanate series, K^+18C6
arly planar arrangement of the six ether oxygens
e equator of the cation, whereas the smaller Na^+ is
l by a plane of 5 of the 6 oxygens, the sixth is

above the plane to make closer contact to the small
Rb^- sits 0.94 Å (and Cs^+ sits 1.44 Å) above the mean
of the ether oxygens [51]. The Rb^+ and Cs^+
ures are also characterized by the formation of
; two cations sit above their respective rings facing
ther. The structure is stabilized by two anions,
are each coordinated to the two cations. Figure 4
structures of the complexed cations in the K^+18C6
the $Cs^+18C6 \cdot SCN^-$ and the $Na^+(12C4)_2 \cdot OH^- \cdot 8H_2O$ salts to
rate the variety of complexes that can form. It is
hat the structure of the complexed cation could
y affect the interactions of the cation with its
nvironment.

enhancement of metal solubility by alkali complexa-
low dielectric media allowed the study of ionic
to be carried out at higher concentrations by
magnetic resonance methods [53]. The nature of
ine and metal-ether solutions was explored by Dye
workers in the early 1970's.

itions of sodium and Cryptand 222 in ethylenediamine
idied by ^{23}Na NMR [54], and the two-peak spectrum
ulted provided the first positive identification of
li metal anion. The first peak was shifted by
relative to the chemical shift of Na^+ at infinite
in water, the same peak position was observed in a



4. Ortep stereoviews of the complexed cations in
18C6)·SCN⁻ [51], b) Cs^+(18C6)·SCN⁻ [51], and c)
C4)$_2$·OH⁻·8H$_2$O [52].

222 salt solution; thus, the peak is due to a
ed $Na^+ \cdot C222$. The NMR of complexed cations will be
ed in Chapter V. The second peak was a narrow line
ppm, at exactly the position calculated for gaseous
]. Thus in low dielectric constant media the
M^- exists as a true alkali metal anion with two
s filling the 3s orbital, essentially unperturbed
as-like state. As the dielectric constant of the
is reduced, the tendency to form the alkali metal
increased, the chemical shift of Na^- in $MeNH_2$,
nd THF were correspondingly found at -61 ppm [56].
major diamagnetic anionic constituent in solvents
olarity has been determined, but the problem still
in ammonia; there is no direct identification of
-paired species.

Alkalides and Electrides

Alkalides

olutions of alkali metals with C222 were found to
resting properties when the solvent was removed.
f the recombination of the ionic species to form
ing materials as is seen in the pure metal
, the residue was a gold colored crystalline

soli

222

cla

can

ani

met

the

yie

spe

Na

so

so

bo

st

no

an

ab

th

c

g

c

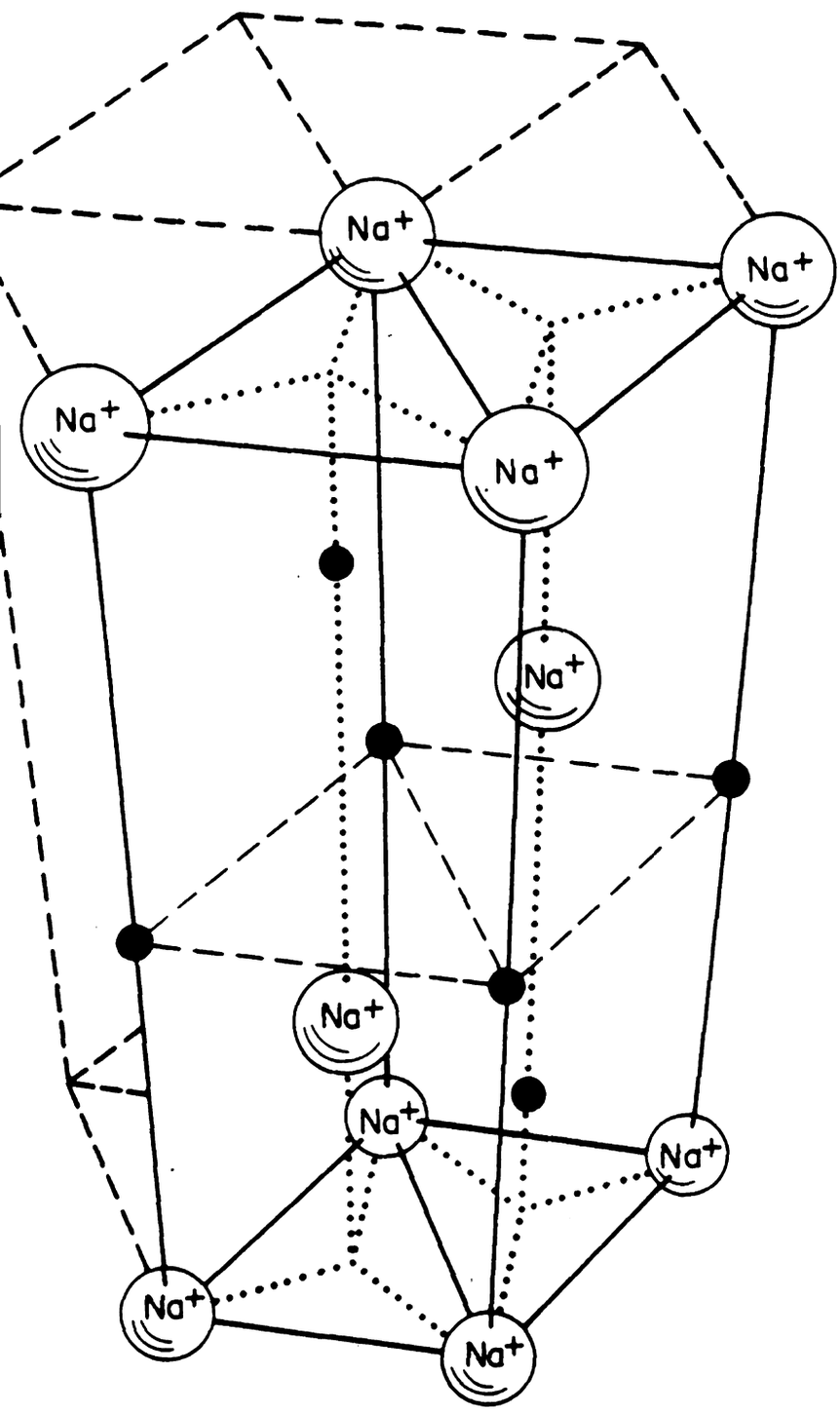
i

h

The material that was isolated from sodium cryptate
tions was found to be the first example of a new
compounds now known as alkalides [57]. Alkalides
escribed as ionic solids that contain alkali metal
The -1 valence state for a member of the alkali
as very unusual, but a full characterization proved
gnment.

optical spectrum of a thin film of $Na^+C222 \cdot Na^-$
a broad absorption with a maximum at 650 nm. This
was nearly identical to that seen for solutions of
hylenediamine [58]. This absorption band in
had been attributed to a charge-transfer-to-
band for the alkali metal anion. A similar bound-
.e. 3s→3p) transition is postulated for the solid
ion. In solution however the nature of M^- could
scribed necessarily to the pure centrosymmetric $3s^2$
nce various ion pairs could account for the 650 nm
on. Likewise the optical absorption of a film of
le was not definite proof of the alkali anion.
$Na^+C222 \cdot Na^-$ appears to be metallic with a gold
nductivity measurements indicate that it is not a
uctor. The material behaves as an intrinsic semi-
with a band gap of ~2.4 eV. Recent measurements
that the conduction that occurs in this material
nificant ionic contribution. It appears that a

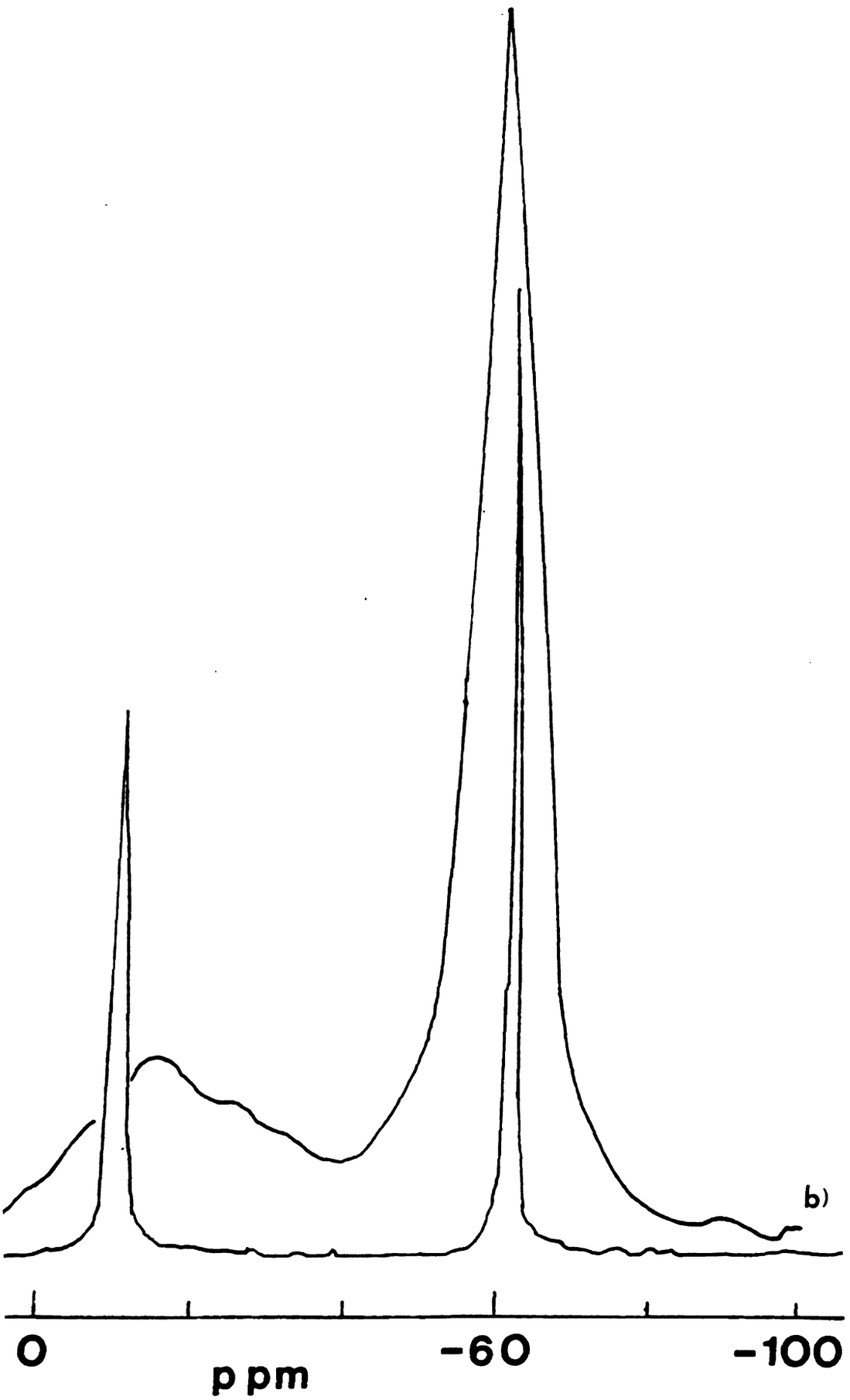
ble migration of Na^+ to the cathode occurs [59].
proof that the material was a true sodide was
d when Tehan, Barnett and Dye [60] solved the
structure of the material. Figure 5 shows the
of anions about a complexed cation of $Na^+C222 \cdot Na^-$.
ucture consists of closest packed cryptated cations
e sodium anions filling the octahedral holes. The
ed cation consists of a sodium cation in a nearly
ral arrangement of cryptand oxygens, with the Na-O
e the proper sums of the van der Waals radii of Na^+
gen. The anionic radius, estimated from van der
ontact with the nearest cryptate protons to the
is ~2.2-2.4 Å. The Na^- radius is slightly larger
e I^- radius (2.2 Å), and corresponds well to the
pproximation that for monovalent ions the sum of the
adii equals the sum of the atomic radii.
or the determination of the crystal structure of
Na^- it became a prototype for the development of
niques used to characterize other alkalides and
es. The thermodynamics of its formation from the
d complexant were experimentally determined by
high precision β alumina electrode [61]. The Gibbs
rgy of formation was found to be -7.1 +/- 0.6 KJ
at 298 K. The photoemission spectrum of
a^- has been measured [62]. The spectrum consists



re 5. A schematic packing diagram of the
ns and anions in $Na^+(C222)\cdot Na^-$ [60].

eak at 370 nm due to photoemission from Na^- and one
nm due to photoemission from electrons trapped in
ttice.

id state Magic Angle Sample Spinning (MAS) NMR
ques have become very important in the characteriza-
f alkalide salts. Figure 6 shows the ^{23}Na MAS NMR
m of $Na^+C222 \cdot Na^-$ along with the spectrum of the same
l dissolved in methylamine [56,63]. The similarity
two spectra strengthens the assertion that the
in low dielectric solutions are alkali metal anions.
plexed cation resonance occurs downfield from the
amagnetic anion resonance, and can usually be
ced in other complexed salts such as $Na^+C222 \cdot I^-$.
e, the Na^- resonance occurs at the value (-61 ppm)
ed for Na^-_g by theoretical calculations [55]. MAS
capable of detecting complexed ^7Li, ^{23}Na and ^{133}Cs
as well as ^{23}Na, ^{39}K, ^{87}Rb and ^{133}Cs anions, and
me a powerful technique for identifying the
metry of various alkalide salts.
e the synthesis of the first alkalide in 1973, more
others have been isolated, including cations of
the stable alkali metals, and anions of each except
e complexants include the cryptands C222 and C211
the crown ethers 12C4 [65], 15C5 [66], and 18C6



The ^{23}Na NMR spectra of $Na^{+}C222 \cdot Na^{-}$ in a) methylamine, he solid state [56,63].

optical spectroscopy of thin films of alkalides
o follow the charge-transfer-to-solvent order of the
of maximum absorbance: larger anions absorb at
nergies [68,69]. Red or blue shifts may occur for
anion, depending on the band structure for that
lar salt. Conductivities tend to be those of
ic semiconductors, with band gaps typically in the
f 0.6 to 1.5 eV [70]. These low apparent band gaps
ecause, in general, significant populations of
electrons tend to reside in the crystal. The
electron population allows an EPR signal to be
l in most compounds. Hyperfine structure arising
rapped electron interacting with the cation can be
in $Rb^+(18C6)\cdot Na^-$ [71] and $K^+(18C6)\cdot Na^-$ [72],
the EPR resonances in other salts are typically
featureless. The hyperfine structure consists of
ines for ^{87}Rb and 4 lines each for ^{85}Rb and ^{39}K
dicates that the paramagnetic electron trapped in
s seems to be associated with only one cation
han with several equivalent cations. The bulk
susceptibility is diamagnetic, showing that the
concentrations are very low.

Electrides

the same time that optical spectra of thin films of
es were being determined, the effect of varying the
e concentration of metal-to-complexant was studied.
found that complexant rich solutions left films with
absorptions further into the infrared than had been
h alkalides [69]. In particular, films of Cs and
:1 or 1:2), Na and C222 (1:1), and Cs and C222 (1:1
made from NH_3 solutions gave peaks which had
on maxima between 1300 nm and 2000 nm. These
are similar to the solvated electron spectra seen
e metal ammonia solutions, including the presence
sorption tail at high energies. Films of KC222
d LiC211 (1:1) had spectra which were similar to
ma absorption seen in more concentrated (metallic)
monia solutions, an increasing absorbance from
ith no maxima to 2500 nm. The analogy to the
electrons in metal ammonia solutions led Dye to
se films <u>electrides</u> [68], the first salts that
trapped electrons as the stoichiometric anionic
ent.

ers of $Li^+C211 \cdot e^-$ [73] and $K^+C222 \cdot e^-$ [74] were
, and preliminary characterization showed them to
different from alkalides. The dark blue to black

of the powders contrasted with the gold/bronze/copper
seen in alkalide crystals. In addition to the
spectroscopy referred to above, magnetic suscepti-
es, microwave conductivities, and EPR spectra were
ed. LiC211 showed a temperature dependent spin
both in magnetic susceptibility measurements and
ctra. At high temperatures (>60 K) the material
as a Curie Weiss paramagnet with the susceptibility
off as 1/T, indicative of a weakly interacting set
magnetic (unpaired) electrons. A powder with
= 1.57 showed a maximum in the susceptibility at
th the susceptibility falling to zero as the
ture went to zero. As the lithium concentration was
, the temperature at which the susceptibility
a maximum increased. The general behavior was
ent with a material which has a lattice composed of
packed $Li^{+}C211$ cations with trapped electron holes,
dependence of the magnetic behavior on composition
, and is still not, well understood [75]. A
e explanation for the spin-pairing is that the
undergoes a phase transition which results in
ation so that electrons in two adjacent cavities are
red. Since excess lithium tends to decrease the
ring transition temperatures it is possible that
tial lithium may affect the coupling of the two

The nature of the spin-pairing and the role that
ithium plays in the physical properties of this
are still unclear at this point.
on $K^+C222 \cdot e^-$ indicated a different type of
[74]. This salt, with a plasma optical absorption
ve of electron delocalization was very temperature
e and therefore difficult to handle. The microwave
vity of this material was high, similar to that of
ic sample. The magnetic susceptibility did not
he Curie Weiss law, but could be attributed to
ramagnetism. Again, all of the results correlated
odel of an expanded metal electride, perhaps
in nature to the metal ammonia compounds.
eakthrough came in 1983 when improved synthetic
es [76] were used to isolate a crystalline
$Cs^+(18C6)_2 \cdot e^-$ [77]. This material was
ized by a localized optical absorption peak at
The magnetic susceptibility followed the Curie
; and the EPR spectrum gave a narrow asymmetric
= 2.0023 indicative of a good microwave conductor
e MAS ^{133}NMR spectrum showed a one line spectrum,
paramagnetically shifted by 140 ppm from typical
$_2$ chemical shifts. Again all of the results agree
picture of a salt which has a trapped electron as
.

Objectives of This Work

ch effort has been devoted to defining the properties
ctrons trapped in cavities. The electron trapped at
talline vacancy (the F-center) has been quite
ghly explained, in part because the structure of the
l defines the structure of the cavity. In dipolar
s, solid or solution, there is inevitably some
which hampers the full characterization of the
l electron. The low concentrations of electrons in
ted glasses and in metal solutions in non-polar
s preclude techniques such as NMR from probing the
nteractions of the electron. The average
ical structure of the electron was determined in
; however, these are electrons which are at very low
rations and are not able to interact freely with one
. The complexity of ionic associations in metal
solutions has limited experimenters' abilities to
fully the structure of the species responsible for
sical properties of the solution.
class of compounds known as electrides has
ns in high concentrations in the crystalline state,
ve and below the electron density normally required
allic character. The possibility of defining the

ure of the electron trap, as well as measuring the interactions of the trapped electron with other ons and with cations in the lattice was the impetus s thesis research. Each new synthesis of another de material has generated a new set of properties, ndicates that these crystalline compounds do have a range of fundamental interactions.

objectives of this thesis may be summarized as: 1) l characterization of the electride $Cs^{+}(18C6)_2 \cdot e^{-}$, ad been synthesized and partially characterized o this work [71]; and 2) the synthesis and charac- ion of a new crystalline electride, $Cs^{+}(15C5)_2 \cdot e^{-}$. er compounds were studied to model the complexed or to measure the effect of doping an electride diamagnetic anion; however, the focus of this work he properties of the electrides. Several techniques ed to characterize electrides.

ajor goal of the electride group has been to obtain al structure of an electride salt. In much the same t the proof of the stoichiometry of the first sodide ly established by determination of the structure of Na^{-}, the structure of an electride is required to he structural implications of their properties. rts to determine the structure of the electrides is d in Chapter III.

gic Angle Sample Spinning NMR has been used to
ne the valence state of alkali ions in the solid
it is also an excellent probe of the electron-
interaction by means of the Knight shift. Chapter
ibes ^{133}Cs NMR studies of complexed cations, first
amagnetic anions and then with trapped electrons.
s to dope the electride with alkali metal anions are
scribed.

sensitivity of the paramagnetic trapped electrons
hboring trapped electrons can be measured in certain
y magnetic susceptibility methods. The previously
erized electrides have shown great diversity in
agnetic susceptibilities, ranging from apparent
c Pauli paramagnetism to diamagnetic complete spin
($Cs^+C222 \cdot e^-$). The susceptibility results of the
ject compounds are carefully compared and contrasted
er VI.

implications of these results and suggestions for
ork are presented in Chapter VII.

CHAPTER II

EXPERIMENTAL DETAILS

Synthetic and General Handling Techniques

sful syntheses required high purity metals and
xants and dried solvents free of reducible impuri-

Alkali Metals

dium metal (99.95%) was obtained from Alpha Ventron
ts in 5 gram argon filled glass ampoules. Cesium
(99.95%) was donated by Dow Chemical Company, and was
ed in vacuum sealed Pyrex ampoules. Redistribution
amounts of the metals into small diameter (2-5 mm)
was done under high vacuum (~10^{-5} torr) as described
[79]. Quantified amounts of the metals were
d by sealing off a measured length of metal in a
ube of known diameter.

Complexants

Crown-5 (15C5, 1,4,7,10,13-pentaoxa-cyclopenta-
and 18-Crown-6 (18C6, 1,4,7,10,13,16,hexaoxa-cyclo-

cane) were obtained from P.C.R. Inc. or Parrish
l Co. The solid 18C6 was recrystallized from
trile. Both complexants were vacuum distilled to
impurities [72].

Solvents

ethyl ether (Me_2O, Matheson, Anhydrous), methylamine
theson, Anhydrous), trimethylamine (TMA, Matheson,
us) and diethyl ether (DEE, E.M. Science, 99.95%,
us) were purified by first distilling the solvent
acuum over calcium hydride to remove water. The
was transferred repeatedly into bottles containing
s or NaK_3 alloy, with benzophenone for Me_2O, TMA,
until the blue solution, which is indicative of the
e of solvated electrons or free radicals, was
The solvents were repeatedly frozen in liquid
and pumped to 10^{-5} torr to remove soluble gases.
MA, and MA were transferred to clean stainless steel
or storage; DEE was stored over NaK_3 in glass
[71].

II.

for

cle

rir

cor

us

so

ev

ha

ge

wi

(u

di

ve

d

A

t

C

(

t

T

b

4 Synthesis of Alkalides and Electrides

he synthesis of alkalides and electrides is straight-
rd but rigorous. Glassware (Pyrex or quartz) is
ed by an HF/detergent cleaner followed by a thorough
ng and then is soaked in aqua regia overnight. The
usly rinsed glassware is oven dried at 180°C prior to

ll handling of alkalides and electrides and their
ions is done at temperatures below -20°C after
ating the vessel to ~10^{-5} torr. The synthetic methods
been described in detail elsewhere [71,76]. The
al procedure is first to load an appropriate apparatus
the proper molar ratios of the metal(s) and complexant
ly 1-2 millimoles of the complexant). The metal is
led under vacuum to form a film on the wall of the
. An appropriate solvent is added (Me_2O or MA) to
ve the complexant and then to dissolve the metal.
the materials are dissolved, the solution is concen-
to saturation by removing the volatile solvent.
ls are formed upon addition of a less polar solvent
r DEE) and cooling; further removal of solvent allows
sired compound to completely fall out of solution.
crystals are washed with TMA or DEE, and vacuum dried
being sealed off into storage fingers. The samples

e stored at −75°C indefinitely in the case of
$3C6)_2 \cdot Na^-$ and $Cs^+(18C6)_2 \cdot e^-$ and for weeks in the case
$^+(15C5)_2 \cdot e^-$.

ll compounds have been analyzed for metal and crown
content. The analysis scheme consists of 5 over-
ng experiments. The reducing power of a known mass of
ial is measured by slowly decomposing the alkalide or
ride with water to generate $H_2(g)$. The net reaction
alkalide is

$$M^- + 2H_2O \text{ ---> } M^+ + N^+ + 2C + 2OH^- + H_2(g) \qquad (2.1)$$

r an electride

$$M^- + H_2O \text{ ---> } M^+ + 2C + OH^- + {}^1/_2H_2(g) \ . \qquad (2.2)$$

drogen gas was collected to quantify the number of
of water that had been reduced. The hydroxide that
rmed was titrated for the total number of moles of
Individual metal quantities are found by flame
on spectroscopy of a solution of the residue relative
et of standards of known concentration. Crown ethers
antified by ^1H NMR. The unknown crown is dissolved
with a known amount of sodium acetate. The NMR peak
ities are measured for relative proton content. Full
s of this analysis scheme are given by Van Eck et al.

[64]

Cs^+(

Cs^+(

esta

flan

x, f

forn

II.

MAS

cal

or

Rac

har

ele

by

to

vac

ni-

ne

ta

cl

ex

The results of the analysis for two samples of
$C5)_2 \cdot e^-$ are given in Table 2. The stoichiometry of
$C6)_2 \cdot e^-$ and $Cs^+(18C6)_2 \cdot Na^-$ had been previously
shed by Ellaboudy [71]. Also tabulated are the
mission results and the per cent sodide character,
three mixed alkalide-electride salts of general
$Cs^+(18C6)_2 \cdot Na^-_{1-x} e^-_x$ where $0<x<1$.

General Handling Techniques

ical spectroscopy, recrystallization, analysis, EPR,
, magnetic susceptibility and differential scanning
etry measurements all required the subject alkalide
tride to be transferred to an appropriate vessel.
periment will be described below, but the general
g techniques are the same. As alkalides and
des rapidly decompose by reaction with O_2 or H_2O, or
rnal thermal decomposition, great care must be taken
samples cool and in an inert atmosphere or under
A polyethylene glove bag was purged with dry
gas until the measured relative humidity was
%. A Styrofoam well which held an aluminum cold
as filled with liquid nitrogen. The sample finger,
tools (glass knife, spatula, etc.) and the
ental vessel were admitted to the glove bag and

Table 2. Results of Analyses for $Cs^+(15C5)_2 \cdot e^-$ and $Cs^+(18C6)_2 \cdot Na^-_x \cdot e^-_{(1-x)}$.

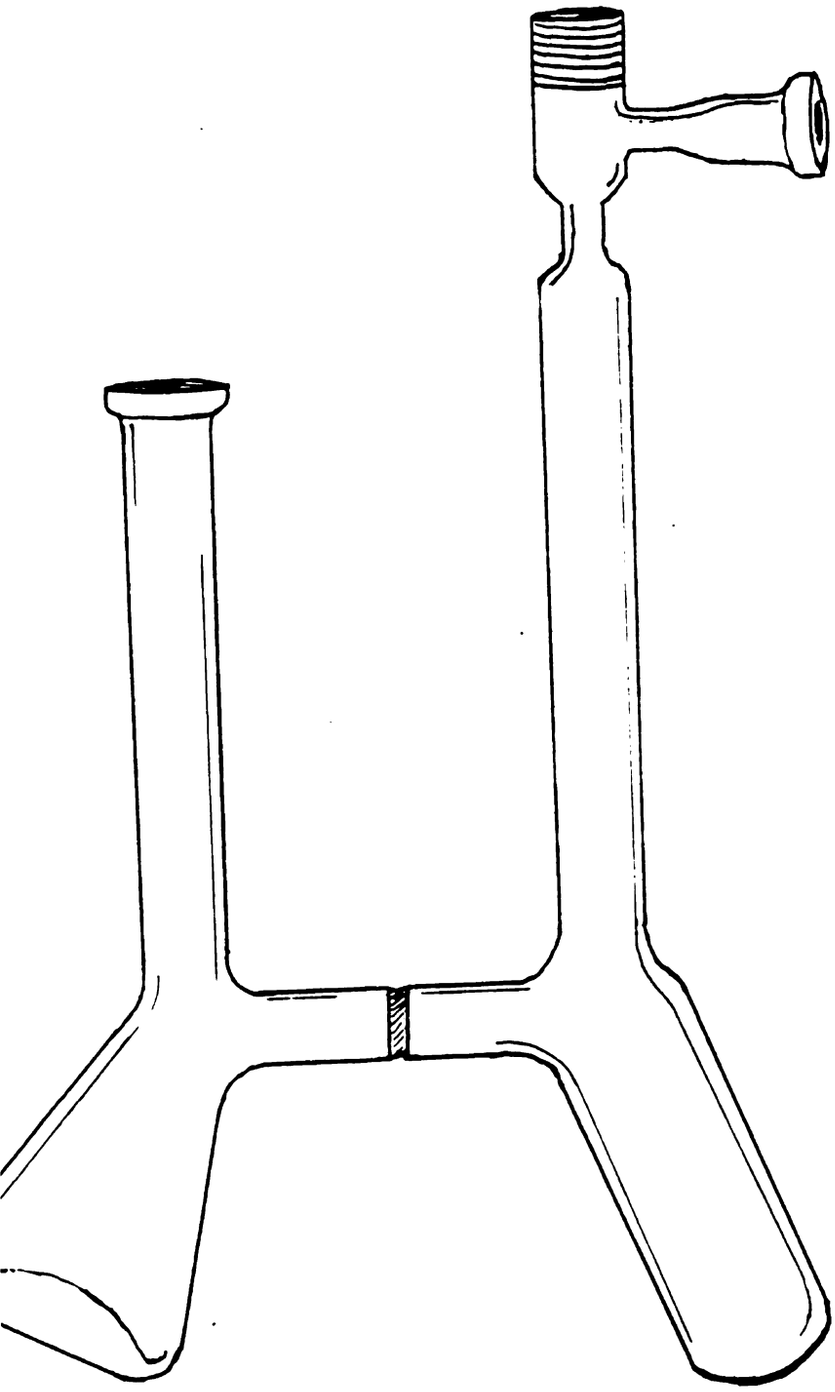
Compound	Mass (# Moles)	Moles H_2 Collected	Moles OH From Titration	Moles M^+ Flame Emission	Moles Crown ^1H NMR
$Cs^+(15C5)_2 \cdot e^-$					
I	61.8 mg (10.8)	a	8.42	8.37	17.4
II	43.0 mg (7.5)	a	7.03	6.98	
$Cs^+(18C6)_2 \cdot Na^-_x \cdot e^-_{(1-x)}$					x
I	138.9 mg (20.4)	10.2	37.7	Cs = 24.4 Na = 20.7	0.84
	10.3 mg			Cs = 2.26 Na = 0.435	0.19

a) No results from hydrogen evolution due to sample decomposition during the experiment.

d in the well or on the cold table. The sample finger
cribed and the material was transferred to the
imental vessel either directly or via a wax coated
ing paper which allowed more control over the
ment of the crystals. In the case of optical
roscopy, EPR, analysis and recrystallization, the
l was a Pyrex or quartz cell, which was sealed off in
love bag with Kontes valves and Fisher Porter unions.
ell was immersed in either liquid nitrogen or a dry
sopropanol bath and transported to a vacuum line where
evacuated for the next step of the experiment. In
ase of magnetic susceptibility, MAS-NMR and DSC the
was loaded and transported directly to the
ment immersed in liquid nitrogen.

Recrystallization Methods for Single Crystal X-Ray Diffraction

ngle crystals of $Cs^{+}(18C6)_2 \cdot Na^{-}$ and $Cs^{+}(18C6)_2 \cdot e^{-}$ for
diffraction studies were grown by careful recrystal-
on of the sodide or electride. A small amount (~100
material was transferred to a recrystallization
tus at -40°C and was evacuated to 10^{-5} torr. The
tallization apparatus, shown in Figure 7, consists of
ambers. The crystallization chamber is made from an
eyer flask with a flat surface to induce crystal



ure 7. Apparatus for the recrystallization of
alides and electrides.

th. The second chamber is separated by a glass frit
s used for removing solvents, and excess mother
or. Long extensions are used to separate the chambers
the entry port and the high vacuum connection. All
are made by Kontes valves or Fisher-Porter o-ring
s. The long extensions are necessary to isolate the
m junctions from cold baths where the o-ring could
e. Dimethyl ether was added to the crystals until
were completely dissolved at -40°C. The solution was
d to -20°C and either diethyl ether or trimethylamine
dded until some crystallization was apparent. More
was added until the solution was just saturated.
als were obtained by two methods from this point.
he first method employed a variable temperature bath
was capable of controlling the temperature in a ramp
or a cycle mode. The solution was cooled until
als began to form at some temperature T_{cryst}. The
rature was then cycled between (T_{cryst} -30°C) and
$_{st}$ +~2°C) at a rate of about 5°C per hour. The
ng was intended to grow crystals as the temperature
ased, and to dissolve small crystals as the tempera-
increased. After 1 to 3 days of cycling, the tempera-
was slowly ramped to -70°C. The mother liquor was
ed off the crystals and the solvent was evacuated
he apparatus. Either DEE or TMA was distilled onto

e crystals to rinse them; the wash solvent was poured off
l the crystals were evacuated until dry. The crystals
re stored at -70°C under vacuum until use.

The second method of growing high quality crystals
quired enough Me_2O to keep the sodide or electride
pletely dissolved at -50°C. The solution in the
stallization chamber was kept at -50°C, while the second
mber was kept ~5°C colder. The temperature gradient
ses a slow distillation of solvent rich in the highly
atile Me_2O from the mother liquor: crystals grew as the
vent mixture became less polar. A cycling effect could
achieved by pouring a small amount of the recondensed
vent back into the solution and continuing the distilla-
n. When the crystals became sufficiently large the
her liquor was decanted off, and the crystals were
hed as in the previous method.

Of the two methods the second produced generally better
ults. Two advantages of the solvent evaporation method
that the crystals are grown at a constant temperature,
ch was matched with the temperature at which the
eriment was to be done, and the time that the solution
t stay stable was reduced from three days to twelve
rs. Several attempts to grow crystals in the low
perature bath ended in decomposed solutions. The
ital that was used for the structure elucidation of

Cs^+

tem

Cs^+

sin

amo

50°

the

sol

wit

upo

wit

li

II

II

II

re

re

at

$Cs^+(18C6)_2 \cdot e^-$ was grown by R. Huang [80] by the variable temperature method.

Single crystals of the salts $Cs^+(15C5)_2 \cdot I^-$ and $Cs^+(18C6)_2 \cdot I^-$ were prepared for crystallography and for single crystal solid state NMR studies. Stoichiometric amounts of CsI and crown ether were dissolved in MeOH at 50°C. A small amount of tert-butanol was added such that the material remained in solution at room temperature. The solution was poured into a Petri dish which was covered with a larger Petri dish and set aside. Crystals formed upon evaporation of the methanol. The crystals were washed with cold t-butanol and oven dried at ~50°.

The same method was used for synthesizing polycrystalline samples of $Cs^+(15C5)_2 \cdot Br^-$ and $Cs^+(15C5)_2 \cdot SCN^-$.

II.D Instrumental and Experimental Description

II.D.1 X-Ray Crystallography

II.D.1.a Mounting of Crystals of $Cs^+(18C6)_2 \cdot Na^-$ and $Cs^+(18C6)_2 \cdot e^-$

The extreme sensitivity of alkalide and electride salts required better methods for mounting single crystals for x-ray diffraction studies then had been used in previous attempts to elucidate structures [79]. These new methods

were based on a suggestion that the crystal might be best protected by immersing it in an inert fluid and mounting the fluid coated crystal in the cold nitrogen gas stream [83]. Octane was chosen because of its temperature characteristics; it freezes at -55°C, it is stable in a reducing atmosphere, and it has a low vapor pressure at temperatures below 0°C. Purum grade n-octane was further purified by distillation onto a sodium film, and successive freeze pumping. The octane was redistilled and stored for use.

Microscopic selection of crystals was done on a cold stage, a microscope slide fitted onto a copper block which was cooled to -40°C by a nitrogen cold stream. The microscope and cold stage were enclosed in a glove bag which was purged with dry nitrogen gas. The crystals, in a sealed tube, were introduced to the glove bag, opened and quickly placed on the cold stage, and immersed in cold octane. Crystals treated in this manner survived for over 4 hours on the microscope stage. When a crystal was chosen for further x-ray investigation it was mounted onto a glass fiber fixed into a standard goniometer pin. The fiber was coated with Celvacene grease which enabled a secure fixture of the crystal onto the pin. The pin was transferred to a portable cold stream for transportation to the diffractometer. The diffractometer was equipped with a customized Nicolet low temperature fixture which cooled the crystal in

a sheath of cold nitrogen gas. Over the course of initial measurements to determine the quality of the crystal, the octane coating appeared to sublime away, leaving the bare crystal exposed only to the cold nitrogen gas. The stability of such a crystal was found to be on the order of a week. Frost accumulated on the crystal in several instances, but there was no reaction at the low temperatures nor any adverse effect on the ability of the crystal to diffract. The crystal remained on the goniometer in the cold stream for the duration of the experiment.

II.D.1.b X-Ray Data Collection for $Cs^{+}(18C6)_2 \cdot Na^{-}$

Preliminary examination of the crystal and subsequent data collection were performed with Mo K_α radiation (λ = 0.71073 Å) on a Nicolet P3F computer-controlled 4-circle diffractometer equipped with a graphite crystal incident beam monochrometer.

The unit cell constants for $Cs^{+}(18C6)_2 \cdot Na^{-}$ and an orientation matrix for data collection were obtained from least squares refinement, using the setting angles of 20 reflections in the range $35<2\theta<40°$. The monoclinic cell parameters and calculated volume are: $\underline{a}$ = 13.581(3), $\underline{b}$ = 15.684(2), $\underline{c}$ = 17.429(4) Å, β = 93.16(2), and V = 3706.8(15) Å^3. For Z = 4 and a formula weight of 684.54

g/mole the calculated density of the sodide is 1.23 g/cm^3. From the systematic absences of reflections satisfying the following relations,

hkl $h + k = 2n + 1$ and h0l $l = 2n + 1$

and from least squares refinement, the space group was determined to be C2/c (#15 in the International Tables [81]).

The data were collected at a temperature of 213(3) K using the theta-2 theta scan technique. Experimental details for the structure determination of $Cs^+(18C6)_2 \cdot Na^-$ are summarized in Table 3. A total of 5150 reflections were collected, of which 2445 were unique and not systematically absent. As a check on crystal and electronic stability three representative reflections were measured every 45 reflections. The intensities of these three reflections remained constant within experimental error throughout the data collection. No decay correction was applied.

Tabl

Ces

For

x-r

Mon

a = 1

V = 3

Ine

Sc

#

Co

Table 3. Table of Experimental Details for the Structure Determination of $Cs^{+}(18C6)_2Na^{-}$.

------ Crystal Data ------

Cesium (18-crown-6)$_2$ sodide $C_{24}H_{48}CsNaO_{12}$
Formula weight = 684.54 F(000) = 1416 T = 213(3)
x-rays = MoK$_\alpha$ (λ = 0.71073 Å) peak width at half height = 0.29°
Monoclinic Space Group C/C C2/c

= 13.581(3) Å b = 15.684(2) Å c = 17.429(4) Å B = 93.16°(4)
= 3706.8(15) Å^3 Z = 4 ρ_{calc} = 1.23 g/cm^3

------ Intensity Measurements ------

Instrument: Nicolet P3F Diffractometer with an incident beam graphite crystal monochrometer
Take off angle: 6.0°
Crystal to detector distance: 19.0 cm

Scan Type: θ-2θ to a maximum 2θ of 45° at 4°/minute in 2θ

# of Reflections Measured: 5150 total, 2445 unique
4096 reflections were averaged
(agreement factor on I = 3.6%)

Corrections: Lorentz Polarization (linear absorption coefficient = 10.5 cm^{-1})
Empirical absorption (Relative transmission coefficients ranged from 0.83 to 1.00 on intensity)

II.D

data
0.71
diff
bean

ori
lea
ref
par
15.
359
g/m
g/c
sat

an
de
[8

us
de

II.D.1.c X-Ray Data Collection for $Cs^+(18C6)_2 \cdot e^-$

Preliminary examination of the crystal and subsequent data collection were performed with Mo K_α radiation (λ = 0.71073 Å) on a Nicolet P3F computer-controlled 4-circle diffractometer equipped with a graphite crystal incident beam monochrometer.

The unit cell constants for $Cs^+(18C6)_2 \cdot e^-$ and an orientation matrix for data collection were obtained from least squares refinement, using the setting angles of 20 reflections in the range $20<2\theta<29°$. The monoclinic cell parameters and calculated volume are: $\underline{a}$ = 13.075(5), $\underline{b}$ = 15.840(7), $\underline{c}$ = 17.359(8) Å, β = 92.30(3), and V = 3592.3(23) $Å^3$. For Z = 4 and a formula weight of 661.55 g/mole the calculated density of the electride is 1.22 g/cm^3. From the systematic absences of reflections satisfying the following relations,

hkl $h + k = 2n + 1$ and h0l $l = 2n + 1$

and from least squares refinement, the space group was determined to be C2/c (#15 in the International Tables [81]).

The data were collected at a temperature of 216(3) K using the Wyckoff omega scan technique. Experimental details for the structure determination of $Cs^+(18C6)_2 \cdot e^-$

are summarized in Table 4. A total of 2661 reflections were collected, of which 2339 were unique and not systematically absent. As a check on crystal and electronic stability three representative reflections were measured every 93 reflections. The intensities of these three reflections remained constant within experimental error throughout the data collection. No decay correction was applied.

Data were collected for a second $Cs^{+}(18C6)_2 \cdot e^{-}$ crystal at 196(5) K, however, the structure could not be solved. The intensities for each reflection were unreliable because of severe problems with the peak to background count ratios which arose from inconsistent peak shapes. The unit cell determined for this crystal differed from that of the crystal whose structure was solved; the cell was tetragonal with $\underline{a}$ = 13.427 Å, $\underline{c}$ = 19.584 Å, and V = 3530 Å. The volume of the tetragonal cell is only two percent smaller than that of the monoclinic cell, but the length of the cell edges are significantly changed. Three possibilities exist to explain the discrepancy of the unit cells. First there may be a phase transition from the high-temperature monoclinic cell to the low-temperature tetragonal cell; second, the electride may crystallize in different morphologies depending on the exact conditions of crystallization; and third, the tetragonal cell may not be real;

Table 4. Table of Experimental Details for the Structure Determination of $Cs^{+}(18C6)_2 \cdot e^{-}$.

------ Crystal Data ------

Cesium (18-crown-6)$_2$ electride $C_{24}H_{48}CsO_{12}$

Formula weight = 661.55 F(000) = 1372 T = 216(3)

x-rays = MoK$_\alpha$ (λ = 0.71073 Å) peak width at half height = 0.50°

Monoclinic Space Group C/C C2/c

a = 13.075(5) Å b = 15.840(7) Å c = 17.359(6) Å B = 92.30°(3)

V = 3592.3(23) Å^3 Z = 4 ρ_{calc} = 1.22 g/cm^3

------ Intensity Measurements ------

Instrument: Nicolet P3F Diffractometer with an incident beam graphite crystal monochrometer
Take off angle: 6.0°
Crystal to detector distance: 19.0 cm

Scan Type: Wyckoff ω scan to a maximum 2θ of 45° at 15°/minute in ω

# of Reflections Measured: 2661 total, 2339 unique
109 reflections were averaged
(agreement factor on I = 7.3%)

Corrections: Lorentz Polarization (linear absorption coefficient = 10.7 cm^{-1})
Empirical absorption (Relative transmission coefficients ranged from 0.68 to 0.99 on intensity)

erroneous cell determination may result from twinning of the crystal. A proper explanation of the multiple morphologies of $Cs^{+}(18C6)_2 \cdot e^{-}$ would require more information than is presently available; a variable temperature powder x-ray study to determine the unit cell could solve the problem.

II.D.1.d Mounting of a Crystal of $Cs^{+}(15C5)_2 \cdot I^{-}$

A single crystal of $Cs^{+}(15C5)_2 \cdot I^{-}$ was loaded into a 0.7 mm quartz capillary tube for x-ray diffraction studies. The crystal was 16-sided with approximate dimensions of 0.6 × 0.4 × 0.3 mm. The tube was sealed off and mounted on the diffractometer.

II.D.1.e X-Ray Data Collection for $Cs^{+}(15C5)_2 \cdot I^{-}$

Preliminary examination of the crystal and subsequent data collection were performed with Mo K_α radiation (λ = 0.71073 Å) on a Picker F.A.C.S.I computer controlled 4-circle diffractometer equipped with a graphite crystal incident beam monochrometer.

The unit cell constants for $Cs^{+}(15C5)_2 \cdot I^{-}$ and an orientation matrix for data collection were obtained from least squares refinement, using the setting angles of 18 reflections in the range $40<2\theta<43°$. The tetragonal cell parameters and calculated volume are: $\underline{a}$ = 13.172(2), $\underline{c}$ = 16.645(3) Å, V = 2888 Å^3. For Z = 4 and a formula weight of 700.34 g/mole the calculated density is 1.61 g/cm^3. As a check on the quality of the crystal, omega scans of several intense reflections were measured; the width at half height was 0.15° with a take-off angle of 6.0°, indicating good crystal quality. From the systematic absences of reflections satisfying the following relation

$$(h,k,l) \qquad h + k + l = 2n + 1$$

and from least squares refinement, the space group was determined to be I4 (#82 in the International Tables [81]).

The data were collected at a temperature of 291(1) K using the theta-2 theta scan technique. The scan rate was 2°/minute (in 2 theta). Data were collected to a maximum 2θ of 80.0°. The ratio of the peak counting time to the background counting time was 2:1.

A total of 4896 reflections were collected, of which 4615 were unique and not systematically absent. As a check on crystal and electronic stability three representative reflections were measured every 47 reflections. The inten-

sities of these three reflections remained constant within experimental error throughout the data collection. No decay correction was applied. Lorentz and polarization corrections were applied to the data. The linear absorption coefficient is 22.3 cm^{-1} for Mo K_{α} radiation. An analytical absorption correction was applied to the data [82]. Relative transmission coefficients ranged from 0.406 to 0.562 with an average value of 0.496. Intensities of equivalent reflections were averaged. The agreement factors for the averaging of 4096 observed and accepted reflections was 3.1% based on intensity and 6.5% based on Fobs.

II.D.2 Magnetic Susceptibility

The magnetic susceptibility of electride salts was measured using an S.H.E. 800 series SQUID magnetometer. This instrument permits computer controlled measurements of the magnetic susceptibility to be made over a temperature range of 1.5 to 300 K, and at magnetic fields of 0 to 9.999 kG. Samples were loaded in inert atmosphere into thin walled Delrin or Kel-F buckets with tight fitting lids. To remove magnetic impurities the buckets were soaked in concentrated Nitric Acid, rinsed and oven dried at 50 °C before use. The loaded bucket was transported to the

instrument under liquid N_2, and was placed in the airlock of the magnetometer. The airlock was typically enclosed in a helium glove bag to avoid accumulation of condensation on the cold bucket. The airlock was purged with helium and the sample was lowered into the SQUID coils. The magnetic moment of the sample and bucket was measured at various desired temperatures and fields. The susceptibility of the sample and bucket, χ_s, was calculated from the average of ten magnetic moment readings, which were computer checked for consistency. The trapped electron contribution to the molar magnetic susceptibility, χ_e, is reported. The calculation of χ_e requires an independent measurement of the decomposed sample and bucket, χ_d, at the same temperatures as the "live" sample. The mass of the sample was typically measured after decomposition. The decomposition product is hygroscopic so care was taken to decompose the sample in a helium atmosphere. χ_e is calculated as

$$\chi_e = \left[\frac{\chi_s - \chi_d}{\text{mass}}\right] \cdot \text{Molecular Weight} \qquad (2.3)$$

This procedure eliminates the diamagnetic contribution to χ_s from the bucket and from the core electrons of the sample.

II.D.3 Optical Spectroscopy

Optical spectra of thin films of $Cs^{+}(15C5)_2 \cdot e^{-}$ were measured with a Beckman DK-2 double beam spectrophotometer. Temperatures between -130 and +25°C could be obtained with a cooled nitrogen gas stream installed in the instrument. Temperatures were recorded with a copper-Constantan thermocouple placed in the cell compartment. Films were made by first dissolving crystals in methylamine in a two chamber optical cell. A small amount of solution was transferred to the chamber fabricated from a quartz optical cell. While vigorously shaking the optical chamber at -78°C the second chamber was placed in liquid N_2, until all of the methylamine was removed from the optical side. The film that resulted was nearly transparent, dark blue, and visually inhomogeneous. The spectrum was recorded from 2400 nm to 500 nm with the reference beam passing through air. Spectra were normalized by subtracting the absorbance of a blank cell and scaling the maximum absorbance to 1.0.

II.D.4 Electron Paramagnetic Resonance

Samples for E.P.R. measurements were loaded into 2-4 mm evacuable quartz tubes, which were sealed off under vacuum. Spectra were recorded on a Bruker 200 X-band spectrometer.

The magnetic fields were measured with a Bruker model ER035M Gaussmeter, frequencies were measured with a Hewlett-Packard 5245L frequency counter with 10 kHz resolution. Temperatures between -150 and +10°C were obtained by flowing cooled nitrogen gas over the sample. Temperatures to 4 K were obtained with an Oxford Instruments (model ESR9) continuous flow helium dewar system.

II.D.5 Differential Scanning Calorimetry

Differential scanning calorimetry (DSC) measurements were obtained on a Dupont 9900 Thermal Analyzer and 910 Differential Scanning Calorimeter equipped with low temperature capabilities. The DSC was loaned to M.S.U. for demonstration purposes. Small amounts (~5 mg) of sample were hermetically sealed in pre-weighed aluminum pans. The cell was cooled to -150°C with an external heat sink. An empty pan served as the reference. The sample was transported to the cell under liquid nitrogen and placed into the cell which had warmed to approximately -130°C. The temperature was ramped at 10°C/minute to +100°C. The heat flow to the pan was measured in milliwatts. The decomposed sample and pan were weighed to get a sample weight. However, all of the pans leaked a small amount of decomposition product so that the masses are only approxi-

mate. The results are reported as heat flow as a function of the temperature.

II.D.6 Nuclear Magnetic Resonance

The experimental details for nuclear magnetic resonance experiments are included in Chapter V.

CHAPTER III

CRYSTAL STRUCTURES OF $Cs^+(18C6)_2 \cdot Na^-$, $Cs^+(18C6)_2 \cdot e^-$, and $Cs^+(15C5)_2 \cdot I^-$

III.A Background

III.A.1 Previous Work

Since the first synthesis of an alkalide and its subsequent characterization, many new alkalides and electrides have been synthesized. However, until this work, the structure of only $Na^+C222 \cdot Na^-$ had been determined. Since knowledge of the crystal structure is invaluable in interpreting solid state properties, the elucidation of the structure of these crystalline compounds has been a major goal of the research group.

Several investigators have attempted to determine crystal structures of alkalides, but problems with synthesis and handling of good single crystals, coupled with instrumentation that was insufficiently equipped to handle the extremely sensitive compounds, were barriers that could not be overcome. Issa [79] reported the unit cell parameters for what was believed to be $Cs^+(18C6) \cdot Na^-$.

The compound was later found to be $Cs^{+}(18C6)_2 \cdot Na^{-}$ whose structure was solved and is reported below. The unit cell parameters were relatively close to those determined in this work, but poor crystal quality prohibited determination of the structure.

In the absence of direct x-ray crystal structure determination, an Extended X-ray Absorption Fine Structure project was initiated [84] to provide short range structural information about the alkali cations and/or anions. EXAFS is a technique which employs a tunable monochromatic x-ray source to scan the energy region near the energy required to remove a 1s electron from a specific atom in the solid. The experiment is typically set up in either the absorption or fluorescence mode. In the absorption experiment the absorption edge rises at the ionization energy and slowly decays with increasing photon energy. The region between 50 and 1000 eV above the edge is characterized by a fine structure which results from modulation of the final state probabilities of the ejected electron by interaction with neighboring atoms. The distances of the neighboring atoms from the central atom may be elucidated from the Fourier transformation of the energy modulation function. The experiment is most useful when similar compounds of known structure can serve as models for the unknown structure. EXAFS provides

relatively low resolution data and is sensitive to neighbors only within 4-5 Å from the excited atom. Some success with the local structures about Rb^+ and Rb^- was realized in alkalides and electrides, and these methods proved very useful in deducing stoichiometry from the intensity of the bound-bound state transitions, however no strong structural detail could be shown.

The structure of an electride is as vital to the development of this class of materials as the $Na^+C222 \cdot Na^-$ structure was to alkalides. The concept of the stoichiometric anionic trapped electron is somewhat contrary to established ideas of the nature of electrons. The direct determination of the structures of the electrides would allow initiation of theoretical consideration of the localization of the electron.

Three structures were solved and will be discussed in this work. $Cs^+(18C6)_2 \cdot Na^-$ and $Cs^+(18C6)_2 \cdot e^-$ were studied at ~215 K on the new Departmental Nicolet PF3 diffractometer. The structure of $Cs^+(15C5)_2 \cdot I^-$ was solved, the complexed cation $Cs^+(15C5)_2$ is the same as that of the electride studied in this work. The iodide ion is spherical with a radius of 2.2 Å, which is only slightly smaller than Na^- and was therefore thought to best mimic alkalide or electride packing. This conclusion was based on the fact that $Na^+C222 \cdot Na^-$ and $Na^+C222 \cdot I^-$ are iso-

structural [60,85]. The crystal was examined at room temperature on a Picker FACS-I diffractometer.

III.A.2 Fundamental Methods for Solving Structures

A monochromatic beam of x-rays of wavelength, λ, will scatter coherently off of lattice planes (noted by Miller indices (h,k,l)) of electron density separated by a distance d(hkl) in a crystalline material to give discrete spots at angles equal to the angle of incidence when the following relationship holds

$$n\lambda = 2d \sin \theta \qquad (3.1)$$

This Bragg relation is the fundamental equation for x-ray crystallography. Knowledge of the lattice parameters of a crystal and the location of a diffracted beam allows the intensity of the scattered beam as a function of the lattice plane (hkl) to be measured. The intensity information holds the key to the position of the atoms in a crystal lattice. The following discussion of structure solution methods follows the description in Stout and Jensen's text [86].

The intensity of a reflection from a plane (h,k,l) in a crystal lattice is related to the electron density which coherently scatters the incoming radiation. The radiation

scattered more strongly by atoms or ions that have many
ectrons; the scattering factor f_i for atom i is a measure
the scattering power of an atom as a function of the
gle of the diffracted beam from the incident beam. The
attering factor is modified by a damping factor that
counts for the diffuseness of the electron cloud and for
ermal motion of the electron cloud, each of which
creases the intensity of the diffracted radiation so that
$= f_{oi}\, e^{-8\pi U(\sin^2\theta/\lambda^2)}$, where U is a tensor that defines
e mean square thermal displacement of atom i, and f_{oi} is
e scattering power of an equivalent number of electrons
ncentrated at the position of the atomic nucleus. The
tensity of the reflection is proportional to the square
the structure factor F(h,k,l), which is related to the
attering factors and positions of the individual atoms by

$$\text{h,k,l)} = \sum_i f_i e^{-2\pi i(hx_i+ky_i+lz_i)} \qquad (3.2)$$

ere x_i, y_i and z_i represent the coordinates of atom i in
e lattice.

The electron density in a unit cell of the crystal can
calculated by Fourier transformation of the structure
ctors

$$(x,y,z) = \frac{1}{V} \sum_h \sum_k \sum_l F_{(h,k,l)} e^{-2\pi i(hx+ky+lz)} \qquad (3.3)$$

The major problem in x-ray structure determination is hat the intensities measured for each reflection in the iffraction experiment only allow the elucidation of the mplitude of the structure factor $|F_{(h,k,l)}|$ which is elated to $F_{(h,k,l)}$ by

$$|F_{(hkl)}|\exp(\alpha_{(hkl)}) = F_{(hkl)} \qquad (3.4)$$

The loss of information provided by the phase angles $\alpha_{(h,k,l)}$ presents the major obstacle to solving a crystal ructure since calculation of the electron density by urier synthesis requires that the phases of the structure ctors be known.

A common method for breaking the phase problem is to ke use of a Fourier series known as the Patterson nction, which has the $|F_{(h,k,l)}|^2$ as coefficients. The ructures in this study were solved by Patterson map chniques.

Since the Patterson function is constructed from a urier series with coefficients $|F_{(h,k,l)}|^2$ no information required that cannot be directly obtained from the ffraction experiment. The Patterson function is given as

$$u,v,w) = \frac{1}{V} \sum_h \sum_k \sum_l |F_{(hkl)}|^2 \cos\{2\pi(hu+kv+lw)\} \qquad (3.5)$$

ere u, v and w are the x, y, and z components of a vector
tween two atoms in real space. The peaks on a Patterson
p then correspond to the vectors between atoms, one at
e origin of the map, the other displaced at u,v,w; the
tensity of a peak is proportional to the product of the
mber of electrons of the two atoms defining the vector.
nce the 0,0,0 vector contains vectors from every atom to
self, the largest peak on the Patterson map is the origin
ak. To get any information from the Patterson map it is
st to have 1 or 2 heavy atoms in the molecule because
aks arising from vectors between large atoms and small
oms can easily be distinguished from those between small
oms. The Cs-crown ether systems are ideal for extraction
atomic positions from the Patterson map. In general
ly a few of the atoms in the molecule can be found in
is manner but this initial set of atoms allows an esti-
te of the phase of each $F_{(h,k,l)}$ to be made by the
verse Fourier transformation of eqn. (3). The
$^+(18C6)_2 \cdot Na^-$ Patterson map allowed the positions of the
$^+$ and four oxygens to be extracted. The rest of the
ructure was solved by successive least-squares refinement
d difference Fourier analysis until all of the atoms were

nd and fully refined.

The least-squares routine requires an input list of ms and their positions with a value of the calculated se for each reflection h,k,l (i.e. starting positions be obtained from a Patterson map). A structure factor based on these positions may be calculated. The ction that is minimized is

$$\sum_{hkl} w_{hkl}\left[|F_o|-|kF_c|\right]^2 \qquad (3.6)$$

re $|F_o|$ is the observed structure factor from intensity surements, with the same phase angles as calculated for , and the summation is over all reflections (h,k,l); $_{k,l)}$ is the statistical weight of each reflection and k scaling parameter. Minimization of an n parameter tem is achieved by setting dD/dp for each parameter p_n l to zero.

$$_{hkl}\left[|F_o|-|kF_c(p_1,p_2\cdots p_n)|\right]\frac{2\partial|kF_c|}{\partial p_n} = 0 \qquad (3.7)$$

Typical parameters are the three coordinates of each (subject to symmetry imposed constraints), thermal meters (i.e. the mean square thermal displacement, U)

that account for vibrational distortions of the electron density of each atom, and the overall scale factor. The parametrized calculated structure factor may be expressed in a Taylor series with initial estimates of the parameters $p_n = a_n$ as

$$|kF_c(p_1,p_2,\ldots p_n)| = |kF_c(a_1,a_2\ldots a_n)| + \frac{\partial|kF_e|}{\partial p_1}\Delta p_1 + \ldots. + \frac{\partial|kF_c|}{\partial p_n}\Delta p_n \qquad (3.8)$$

A series of n equations with n unknowns (the Δp_n's) can be set up and solved for over the m observed $|F_o|$'s. The Δp_n estimated value of a parameter is updated to $a_n' = a_n + \Delta p_n$. The set of a_n' may be used as initial estimates of p_n in a subsequent cycle until convergence of values for the p_n is obtained.

The refined positions of the atoms located in the Patterson sythesis may be used to establish phase angles (h,k,l) for the structure factors. A difference Fourier synthesis was used to locate the rest of the atoms in the molecule.

The difference Fourier synthesis applies the calculated phases from a limited number of known positions to both the observed and calculated structure factors. The coefficients of the Fourier series for $\Delta\rho_{(x,y,z)}$ are $(F_o - kF_c) =$

(h,k,l). The equation for the calculation of the fference Fourier map is

$$(x,y,z) = \frac{1}{V} \sum_h \sum_k \sum_l \Delta F_{hkl} e^{-2\pi i(hx+ky+lz)} \qquad (3.9)$$

e difference Fourier map effectively subtracts the con- ibution of the located atoms from the density map, and us promotes the remaining atoms to the major peaks in the nthesis. The successive use of difference maps and ast-squares refinement enables all of the non-hydrogen om positions to be found. Additional cycles of least- uares including positional and anisotropic thermal rameters of all of the atoms complete the solution and finement of the structure. The agreement factor R is ed to approximate the quality of the fit and is given by

$$= \sum_{hkl} \left| |F_o| - |F_c| \right| \qquad (3.10)$$

ere the summation is over all reflections. The weighted reement factor R_w is given by

$$= \left[\frac{\sum_{hkl} w_{hkl} (|F_o| - |F_c|)^2}{\sum_{hkl} w_{hkl} F_o^2} \right] \qquad (3.11)$$

where $w_{(h,k,l)}$ is calculated from the standard deviation of the observed structure factor, $\sigma(F_o^2)$, as $w_{(h,k,l)} = 1Fo^2/\sigma(F_o^2)^2$.

II.B Structure Solution and Refinement for $Cs^+(18C6)_2 \cdot Na^-$ and $Cs^+(18C6)_2 \cdot e^-$

II.B.1 General Approach

The structure of $Cs^+(18C6)_2 \cdot Na^-$ was solved by the atterson method as described above. The final least quares refinement included 253 parameters: the positional arameters of all atoms except for six hydrogens on disrdered carbons, isotropic temperature factors for all ydrogen atoms and anisotropic temperature factors for the est of the atoms, and an overall scale factor. Na^- and s^+ occupy special positions in the lattice; thus some of heir positional and thermal parameters were fixed due to ymmetry constraints. The final agreement factors were R = .029 and R_w = 0.033.

The structure of $Cs^+(18C6)_2 \cdot e^-$ was solved by use of the ositional parameters of $Cs^+(18C6)_2 \cdot Na^-$ as initial stimates for least-squares refinement. The space group of he two crystals is the same, and the lattice parameters re similar. The final least-squares refinement included 68 parameters: the positional and anisotropic thermal

ameters of the 18 carbon and oxygen atoms and one posi-
nal and four thermal parameters for Cs^+. All hydrogens
e constrained to ride on the carbons, their positional
thermal parameters were not independently refined. The
al agreement factors were R = 0.058 and R_w = 0.070. The
ution and refinement details for both the sodide and the
ctride are summarized in Table 5.

.B.2 Results of the Structure Determination of $Cs^+(18C6)2 \cdot Na^-$

The positional parameters with their estimated standard
iations and isotropic thermal displacement factors are
en in Table 6 for all atoms in $Cs^+(18C6)_2 \cdot Na^-$. The an-
tropic general thermal displacement parameters for the
-hydrogen atoms in $Cs^+(18C6)_2 \cdot Na^-$ are given in Table 7.
tial refinements assigned unusually large thermal
placement parameters to C15, presumably because of
order in the crown ether. Significant improvement of
h the agreement factor and the shift to error ratio of
C15 parameters was obtained by introducing two
itions for C15 separated by 0.5 Å, each with one/half
upancy, and by constraining the hydrogen atoms on C14
both C15's to ride on the carbon atoms with fixed bond
gths and bond angles.

Table 5. Table of Experimental Details for Structure Solution and Refinement of $Cs^+(18C6)_2 \cdot Na^-$ and $Cs^+(18C6)_2 \cdot e^-$.

	$Cs^+(18C6)_2 \cdot Na^-$	$Cs^+(18C6)_2 \cdot e^-$
Solution	Patterson Method	Isostructural parameters
Hydrogen atoms	Located and Refined Isotropically	Full Matrix Least-Squares
Minimization Function	--- $w(\|F_o\|-\|F_c\|)^2$ ---	
Least-Squares Weights	--- $4F_o^2/\sigma(F_o^2)^2$ ---	
Anomolous Dispersion	--- All Non-Hydrogen Atoms ---	
Reflections Included	2069 with $F_o^2 > \sigma(F_o^2) \cdot 3$	1306 with $F_o^2 > \sigma(F_o^2) \cdot 3$
Parameters included	253	168
R_w	0.029	0.058
R	0.033	0.070
Esd of an observation unit weight	1.35	1.21
Convergence, largest shift	0.68 σ	0.03 σ
High Peak in Final Difference Map	0.29(3)$e^-Å^{-3}$	0.73 $e^-Å^{-3}$
Computer Hardware	--- VAX-11/750 ---	
Computer Software	SDP-PLUS (Enraf-Nonius & B.A. Frenz & Associates)	

ABLE 6.

Table of Positional Parameters in Fractional Unit Cell Coordinates and Their Estimated Standard Deviations for Cesium (18-Crown-6)$_2$ Sodide at 213 K

Atom	x	y	z	B(Å^2)
Cs1	0.000	0.02094(3)	0.250	3.238(7)
Na1	0.000	0.500	0.000	8.5(1)
O1	-0.0980(2)	0.1741(2)	0.3653(2)	4.42(7)
O4	0.1135(2)	0.1611(2)	0.3643(2)	4.48(8)
O7	0.1361(2)	-0.0171(2)	0.4081(2)	4.29(7)
O10	-0.0224(2)	-0.1364(2)	0.3877(2)	4.48(7)
O13	-0.1819(3)	-0.1166(2)	0.2736(2)	5.72(9)
O16	-0.2334(2)	0.0605(2)	0.2861(2)	5.23(8)
C2	-0.0318(4)	0.2434(3)	0.3716(3)	5.1(1)
C3	0.0614(4)	0.2169(4)	0.4118(3)	5.2(1)
C5	0.1979(4)	0.1252(4)	0.4032(3)	5.1(1)
C6	0.1766(4)	0.0506(4)	0.4539(3)	5.0(1)
C8	0.1279(4)	-0.0932(4)	0.4518(3)	5.1(1)
C9	0.0765(4)	-0.1599(4)	0.4054(3)	5.4(1)
C11	-0.0823(5)	-0.2028(3)	0.3564(3)	6.2(1)
C12	-0.1829(4)	-0.1706(4)	0.3369(3)	6.6(1)
C14	-0.2753(4)	-0.0765(5)	0.2481(4)	7.9(2)
C15a	-0.306(1)	0.004(1)	0.275(1)	10.4(4)*
C15b	-0.3011(7)	-0.0103(6)	0.2987(5)	4.2(2)*
C17	-0.2616(4)	0.1299(4)	0.3319(3)	5.8(1)
C18	-0.1878(4)	0.1981(4)	0.3285(3)	5.6(1)

Continued

TABLE 6. (CONTINUED)

Table of Positional Parameters in Fractional Unit Cell Coordinates and Their Estimated Standard Deviations for Cesium (18-Crown-6)$_2$ Sodide at 213 K

Atom	x	y	z	B(Å^2)
H2a	-0.060(3)	0.296(3)	0.397(3)	6(1)*
H2b	-0.024(4)	0.264(3)	0.327(3)	7(1)*
H3a	0.054(3)	0.186(3)	0.450(3)	6(1)*
H3b	0.107(4)	0.268(3)	0.426(3)	7(1)*
H5a	0.230(4)	0.176(3)	0.435(3)	6(1)*
H5b	0.238(3)	0.102(3)	0.368(2)	5(1)*
H6a	0.130(4)	0.068(3)	0.487(3)	8(1)*
H6b	0.241(3)	0.028(3)	0.478(3)	6(1)*
H8a	0.093(3)	-0.080(3)	0.493(3)	5(1)*
H8b	0.198(4)	-0.111(3)	0.468(3)	7(1)*
H9a	0.079(3)	-0.215(3)	0.426(2)	5(1)*
H9b	0.105(3)	-0.166(3)	0.364(2)	4(1)*
H11a	-0.082(3)	-0.250(3)	0.386(2)	5(1)*
H11b	-0.062(4)	-0.223(3)	0.319(3)	6(1)*
H12a	-0.211(4)	-0.134(4)	0.368(3)	8(2)*
H12b	-0.226(4)	-0.217(4)	0.327(3)	8(2)*
H14a	-0.326	-0.117	0.252	8.86
H14b	-0.271	-0.061	0.196	8.86
H15aa	-0.354	0.028	0.239	11.45
H15ab	-0.334	-0.004	0.323	11.45
H15ba	-0.368	0.006	0.289	5.15
H15bb	-0.292	-0.030	0.350	5.15
H17a	-0.267(4)	0.111(3)	0.384(3)	7(1)*
H17b	-0.330(4)	0.148(3)	0.310(3)	7(1)*
H18a	-0.216(4)	0.249(3)	0.351(3)	6(1)*
H18b	-0.180(4)	0.215(3)	0.278(3)	6(1)*

Starred atoms were refined isotropically.
Anisotropically refined atoms are given in the form of the isotropic equivalent thermal parameter defined as:

$$(4/3) * [a^2*B(1,1) + b^2*B(2,2) + c^2*B(3,3) + ab(\cos \text{gamma})*B(1,2) + ac(\cos \text{beta})*B(1,3) + bc(\cos \text{alpha})*B(2,3)]$$

Table 7.

Table of General Displacement Parameter Expressions
U's in ($Å^2$) for Cesium (18-Crown-6)$_2$ Sodide

ame	U(1,1)	U(2,2)	U(3,3)	U(1,2)	U(1,3)	U(2,3)
s1	0.0453(2)	0.0448(2)	0.0331(2)	0	0.0045(2)	0
a1	0.077(2)	0.118(3)	0.129(3)	-0.003(2)	0.023(2)	0.024(2)
1	0.064(2)	0.058(2)	0.046(2)	0.006(2)	0.003(2)	0.003(2)
4	0.068(2)	0.064(2)	0.040(2)	-0.009(2)	0.012(2)	-0.005(2)
7	0.054(2)	0.073(2)	0.036(1)	-0.008(2)	0.005(1)	0.014(2)
10	0.069(2)	0.050(2)	0.053(2)	-0.009(2)	0.015(2)	-0.003(2)
13	0.075(2)	0.070(2)	0.074(2)	-0.013(2)	0.012(2)	-0.005(2)
16	0.051(2)	0.068(2)	0.080(2)	-0.009(2)	0.005(2)	-0.002(2)
2	0.099(4)	0.042(3)	0.054(3)	-0.003(3)	0.017(3)	-0.004(2)
3	0.085(4)	0.065(3)	0.049(3)	-0.016(3)	0.016(3)	-0.011(3)
5	0.059(3)	0.081(4)	0.053(3)	-0.016(3)	0.011(2)	-0.006(3)
6	0.051(3)	0.096(4)	0.043(3)	-0.010(3)	-0.000(2)	0.004(3)
8	0.060(3)	0.084(4)	0.051(3)	0.005(3)	0.008(2)	0.026(3)
9	0.086(3)	0.062(3)	0.059(3)	0.013(3)	0.025(3)	0.023(3)
11	0.144(5)	0.051(3)	0.040(3)	-0.029(3)	0.016(3)	-0.003(2)
12	0.090(4)	0.107(4)	0.055(3)	-0.050(3)	0.017(3)	-0.028(3)
13	0.062(4)	0.122(5)	0.117(5)	-0.027(4)	0.004(4)	-0.034(4)
17	0.063(3)	0.100(4)	0.058(3)	0.026(3)	0.014(3)	-0.013(3)
18	0.082(3)	0.071(3)	0.058(3)	0.031(3)	0.001(3)	-0.007(3)

The form of the anisotropic displacement parameter is:

$$\exp[-2\pi^2\{h^2a^2U(1,1) + k^2b^2U(2,2) + l^2c^2U(3,3) + 2hkabU(1,2) + 2hlacU(1,3) + 2klbcU(2,3)\}]$$ where a, b, and c are reciprocal lattice constants.

The ionic packing in $Cs^+(18C6)_2 \cdot Na^-$ (and $Cs^+(18C6)_2 \cdot e^-$) is schematically drawn in Figure 8. Only the cations, Cs^+, with solid circles, and the anions, Na^- (or e^-), with open circles, are included, and distances are not to scale. Nearest anion-anion distances are represented by dotted lines; and nearest cation-cation distances are represented by dashed lines. Each ion is surrounded by eight counter ions; this is represented (for only one cation) by fine solid lines. Anions and cations lie in alternating planes perpendicular to the c-axis, anions at z = 0, $^1/_2$, etc. and cations at z = $^1/_4$, $^3/_4$, etc. Anions at each level in z are at fractional coordinates $\underline{x}$ = 0, 1 and $\underline{y}$ = $^1/_2$; and x = $^1/_2$ and y = 0, 1. The cations at z = $^1/_4$ are at fractional coordinates: $\underline{x}$ = 0, 1 and $\underline{y}$ = 0.0209, 1.0209; and $\underline{x}$ = 0.5 and $\underline{y}$ = 0.5209. The cations at z = $^3/_4$ are at fractional coordinates: $\underline{x}$ = 0, 1 and $\underline{y}$ = -0.0209, 0.9791; and $\underline{x}$ = 0.5 and $\underline{y}$ = 0.4791. The cations are alternately distorted by + and -0.33 Å from $\underline{y}$ = 0, $^1/_2$ and 1 positions. This is shown in Figure 8 by an exaggerated zig-zag stack for cations along the $\underline{c}$-direction. The anions form linear stacks along the $\underline{c}$-direction.

The distance between Cs^+ ions along the $\underline{c}$ axis is 8.74 Å, which is 0.03 Å longer than the separation of Na^- ions along the $\underline{c}$ axis. In planes perpendicular to the $\underline{c}$ axis both cations and anions are separated by 10.37 Å from

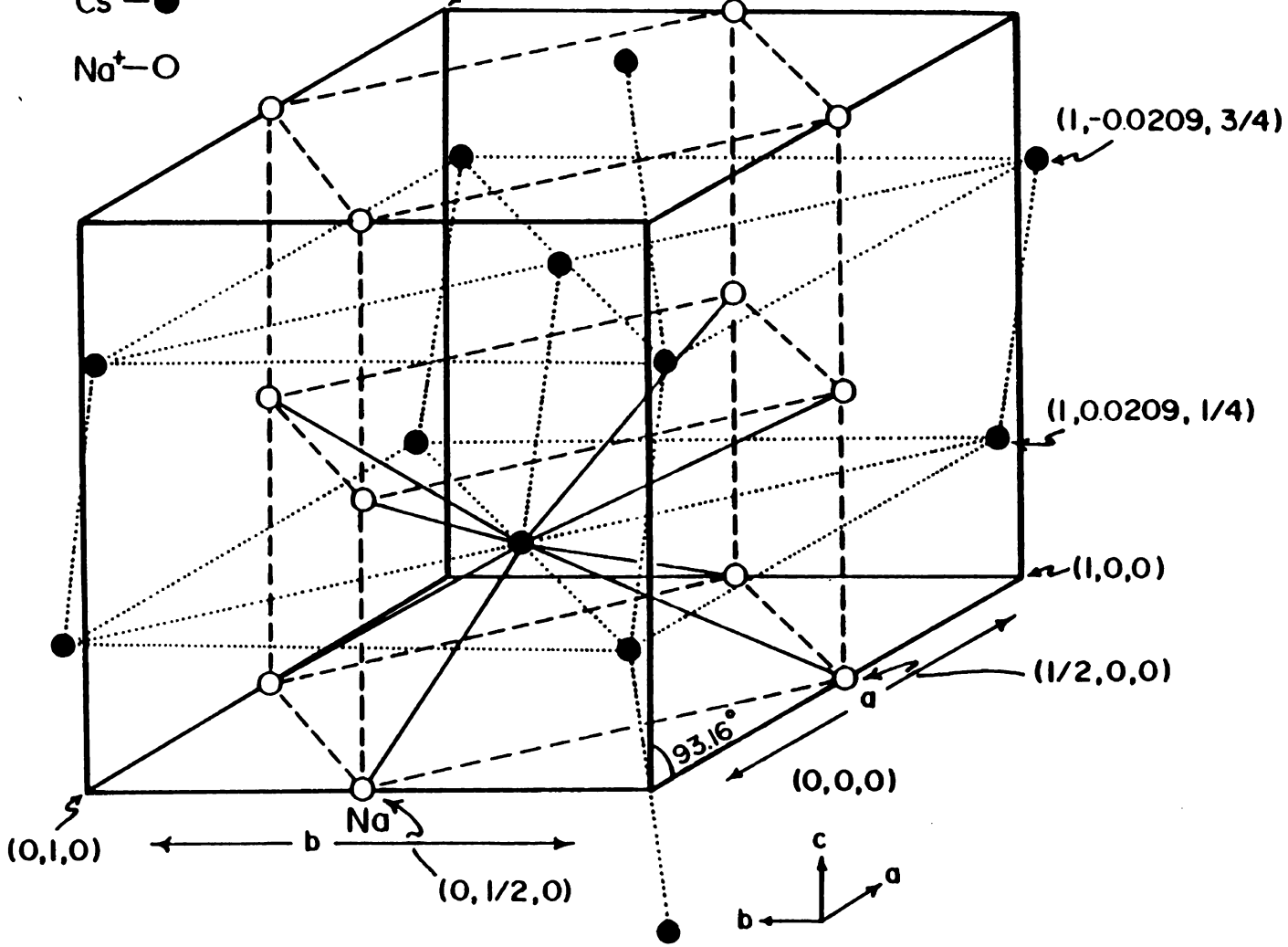


Figure 8. Packing diagram of the cesium cations, represented by solid circles, and the sodium anions, represented by open circles, in $Cs^{+}(18C6)_2 \cdot Na^{-}$. Dotted lines represent cation-cation distances, dashed lines represent anion-anion distances, and the weak solid lines répresent cation anion distances about one cation.

four nearest like-ions.

Each Na^- is coordinated by eight complexed cations. The distance of each inversion related pair of cations from Na^- is different than the others because of the distortion of Cs^+ ions from linear packing along the c axis, and because the Cs^+-Na^- coordination involves a component in the a direction in the a-c plane so that the monoclinic angle, $\beta = 93.16°$ affects the distances. The four unique distances to neighboring Cs^+ ions from an Na^- ion are: 7.87 Å, 8.28 Å, 8.69 Å and 9.26 Å. The two shorter distances are coordinations to Cs^+ ions that lie just off the b-c plane that contains the central Na^-. The two longer distances are coordinations to four Cs^+ ions that lie in the same a-c plane as the Na^-. Thus the coordination of Na^- by cations has only six of the eight first shell anion-cation distances which are shorter than the shortest anion-anion distance.

The crown ether molecules complex the Cs^+ ion by assuming a conformation with the oxygens directed toward the cation. The outer surface of the complexed cation consists almost entirely of the CH_2 groups of the crown ether. Only one of the two crown ethers is unique; the second is generated by two-fold symmetry about the b axis through Cs^+. A least squares plane was fit to the positions of the six oxygens on one crown ether; the results of

this fit are summarized in Table 8. The best fit plane can be described by the equation (in Å units) as

$$5.284x - 0.125y - 16.404z + 5.956 = 0$$

The plane is very nearly parallel to the b axis, and forms an angle when projected onto an a-c plane of ~25° from the a axis toward the c axis. The packing of the crown ethers in the lattice is such that the hole of the crown ether is filled by electron density of carbons and hydrogens of the nearest crown ethers associated with adjacent cations along the c axis.

The structure of one $Cs^+(18C6)_2$ ion is shown in Figure . The distances between the cation and the six crown ether oxygens, as well as bond distances in the crown ether molecule are summarized in Table 9. The mean Cs-O interaction distance is 3.357 Å, with individual contacts ranging from 3.29 Å to 3.47 Å. This mean distance is somewhat longer than that observed in a 1:1 complex of $Cs^+(18C6)\cdot SCN^-$ [51], and is similar to that seen in a Cs^+ dibenzo 18C6) sandwich structure [87] which had Cs-O distances ranging from 3.17 Å to 3.43 Å. The sum of the ionic radius of Cs^+ and the van der Waals radius of oxygen is 3.2 Å. The long distance for the Cs-O interaction in the $Cs^+(18C6)_2$ sandwich indicates that the size of the

Table 8.

Table of Least-Squares Planes
for Cesium (18-Crown-6)$_2$ Sodide

Crystallographic Equation of Plane in Angstroms

5.2844 X + -0.1249 Y + -16.4041 Z - -5.9555 = 0

0.0090 0.0117 0.0252 0.0018

Atom	X(Å)	Y(Å)	Z(Å)	Distance (Angstroms)	Esd
		-----Atoms in Plane -----			
O1	-1.6807	2.7290	6.3567	-0.576	+- 0.003
O4	1.1926	2.5243	6.3404	0.558	+- 0.003
O7	1.4561	-0.2704	7.1018	-0.018	+- 0.003
O10	-0.6771	-2.1416	6.7469	-0.505	+- 0.003
O13	-2.7348	-1.8307	4.7612	0.521	+- 0.004
O16	-3.4443	0.9478	4.9796	0.021	+- 0.004
		----- Other Atoms -----			
Cs1	-0.2399	0.3271	4.3506	1.852	+- 0.000
Na1	0.0045	7.8420	0.0000	5.893	+- 0.000
C2	-0.7869	3.8152	6.4662	-0.338	+- 0.005
C3	0.4399	3.3997	7.1667	-0.503	+- 0.005
C5	2.3013	1.9616	7.0175	0.371	+- 0.005
C6	1.9631	0.7908	7.8997	-0.564	+- 0.005
C8	1.3027	-1.4645	7.8619	-0.768	+- 0.005
C9	0.6482	-2.5101	7.0552	-0.271	+- 0.005
C11	-1.4612	-3.1821	6.2021	-0.300	+- 0.005
C12	-2.8092	-2.6769	5.8628	-0.516	+- 0.005
C14	-3.9780	-1.2017	4.3175	0.440	+- 0.007
C15a	-4.4190	0.0691	4.7793	-0.167	+- 0.017
C15b	-4.3764	-0.1635	5.1987	-0.535	+- 0.009
C17	-3.8706	2.0358	5.7766	-0.888	+- 0.005
C18	-2.8641	3.1053	5.7163	-0.450	+- 0.005

TABLE 9.

Table of Bond Distances (in Angstroms) for Cesium (18-Crown-6)$_2$ Sodide at 213 K and Cesium (18-Crown-6)$_2$ Electride at 216 K

Atom1	Atom2	Sodide Distances	Electride Distances
Cs1	O1	3.445(3)	3.453(8)
Cs1	O4	3.292(3)	3.296(8)
Cs1	O7	3.287(3)	3.305(7)
Cs1	O10	3.468(3)	3.457(8)
Cs1	O13	3.324(4)	3.296(9)
Cs1	O16	3.324(3)	3.304(8)
O1	C2	1.411(6)	1.42(2)
O1	C18	1.397(6)	1.44(2)
O4	C3	1.420(6)	1.42(2)
O4	C5	1.416(6)	1.42(2)
O7	C6	1.421(6)	1.44(1)
O7	C8	1.424(6)	1.39(2)
O10	C9	1.410(6)	1.41(2)
O10	C11	1.412(7)	1.43(2)
O13	C12	1.391(7)	1.39(2)
O13	C14	1.462(7)	1.43(2)
O16	C15a	1.33(2)	1.39(2)
O16	C15b	1.467(10)	
O16	C17	1.414(7)	1.42(2)
C2	C3	1.472(8)	1.47(2)
C5	C6	1.505(8)	1.47(2)
C8	C9	1.474(7)	1.52(2)
C11	C12	1.479(9)	1.50(3)
C14	C15a	1.42(2)	1.51(2)
C14	C15b	1.419(12)	
C15a	C15b	0.48(2)	
C17	C18	1.470(8)	1.47(2)

Numbers in parentheses are estimated standard deviations in the least significant digits.

cationic hole in the complex is not the limiting factor in how closely the two crown ethers may approach each other. The two crown ethers make van der Waals contact with each other before they are fully in contact with the cation. The Cs^+ ion is in a highly enclosed environment; there is very little exposure to species beyond the two complexant molecules.

The disorder on the crown ether is not a surprising result considering the many conformations that are available to the flexible 18 member ring. A summary of selected torsion angles around the backbone of the crown ether is given in Table 10. This conformation has been observed previously in crystalline salts and has no particular internal symmetry [88]. A theoretical consideration of the conformation energy suggests that this structure is not a particularly low energy conformation of the crown ether, but even major conformational changes correspond to only about a 5 Kcal/mole change in the energy [88]. This conformation in $Cs^+(18C6)_2 \cdot Na^-$ is probably stabilized by improved van der Waals attraction of Cs^+ to the ether oxygens, and perhaps by improved lattice packing.

The anion occupies sites in the lattice bounded by eight complexed cations. The cavity in which the sodide ion resides is lined with protons of the crown ethers. The ionic radius of Na^- may be calculated on the assumption

Table 10.

Table of Selected Torsional Angles (in Degrees) for Cesium (18-Crown-6)$_2$ Sodide at 213 K and for Cesium (18-Crown-6)$_2$ Electride at 216 K

Atom 1	Atom 2	Atom 3	Atom 4	Sodide Angle	Electride Angle
C18	O1	C2	C3	178.9	-178.15
C2	O1	C18	C17	-171.6	-170.30
C5	O4	C3	C2	-172.8	-175.94
C3	O4	C5	C6	80.5	75.59
C8	O7	C6	C5	171.6	172.90
C6	O7	C8	C9	174.2	178.24
C11	O10	C9	C8	-168.4	-170.70
C9	O10	C11	C12	-177.6	-178.61
C14	O13	C12	C11	-177.9	179.96
C12	O13	C14	C15a	91.5	78.18
C12	O13	C14	C15b	74.0	
C17	O16	C15a	C14	-163.4	175.45
C17	O16	C15b	C14	176.0	
C15a	O16	C17	C18	-167.5	179.65
C15b	O16	C17	C18	172.7	
O1	C2	C3	O4	70.0	72.84
O4	C5	C6	O7	63.1	63.25
O7	C8	C9	O10	-65.9	-66.20
O10	C11	C12	O13	70.9	73.46
O13	C14	C15a	O16	36.5	62.37
O13	C14	C15b	O16	72.2	
O16	C17	C18	O1	-68.3	-67.19

that the anion is in van der Waals contact with the nearest hydrogens. Table 11 lists the nearest atomic neighbors to Na^-. Na^- can be assumed to be a spherical anion. The ^{23}Na NMR chemical shift of the anion in this and other sodide salts shows no Ramsey shift from the gaseous state anion [63] which indicates that the anion has $3s^2$ configuration. The van der Waals radius of aliphatic hydrogens has been estimated to be 1.2 Å [89], so the Na^- radius can be calculated to be between 2.47 and 2.65 Å. The smaller radius corresponds to the contact with the nearest protons, the larger estimate is from the average contact distance over the six nearest protons. The latter figure is probably a better value because the closest hydrogen is likely to be quite acidic, and thus have a smaller effective radius. This range for the ionic radius of Na^- is in good agreement with the results from the structure determination of $Na^+C222 \cdot Na^-$ [60].

Issa's attempts to isolate crystals of $Cs^+(18C6) \cdot Na^-$ for structure determination yielded lattice constants but the structure could not be solved. The unit cell parameters for cells containing 4 formula units deduced by Issa [79] were $\underline{a}$ = 13.895(11), $\underline{b}$ = 15.501(24) and $\underline{c}$ = 8.939(7) with a monoclinic angle β = 93.25° and cell volume = 1920.7 Å^3. NMR methods later revealed that the compound was in fact $Cs^+(18C6)_2 \cdot Na^-$. The unit cell parameters are

TABLE 11.

Table of closest anionic contact distances for Cesium (18-Crown-6)$_2$ Sodide at 213 K, for Cesium (18-Crown-6)$_2$ Electride at 216 K, and for Cesium (15-Crown-5)$_2$ Iodide at 291 K

Cesium (18-Crown-6)$_2$ Sodide

Contact Pair Atom 1	Atom 2	Van der Waals Contact Distance	Anion Radius
Na^-	H_{6b}	3.67 Å	2.47 Å
Na^-	H_{2a}	3.68 Å	2.48 Å
Na^-	H_{3b}	4.208 Å	3.01 Å
Na^-	H_{5b}	4.509 Å	3.30 Å

Mean Anionic Radius From 6 Nearest Proton Contacts: r_{Na^-} = 2.65 Å

Cesium (18-Crown-6)$_2$ Electride

e^-	H_{6a}	3.292 Å	2.09 Å
e^-	H_{15b}	3.635 Å	2.24 Å
e^-	H_{2a}	3.762 Å	2.56 Å
e^-	H_{17a}	4.085 Å	2.88 Å

Mean Anionic Radius from 6 nearest proton contacts: r_{e^-} = 2.30 Å

Cesium (15-Crown-5)$_2$ Iodide

For I1			
I^-	$H_{9a'}$	3.403 Å	2.20 Å
I^-	H_{3b}	3.456 Å	2.26 Å
I^-	H_{11a}	3.615 Å	2.42 Å
For I2			
I^-	H_{6a}	3.139 Å	2.14 Å
I^-	H_{15b}	3.479 Å	2.28 Å
I^-	H_{11b}	3.795 Å	2.59 Å

Mean Anionic Radius from 12 Nearest Proton Contacts: r_{I1^-} = 2.29 Å, r_{I2^-} = 2.32 Å

very close to those obtained in this study if the c axis length is doubled.

III.B.3 Results of the Structure Determination of $Cs^+(18C6)_2 \cdot e^-$ at 216 K

The refined positional parameters of all of the atoms in $Cs^+(18C6)_2 \cdot e^-$ with their estimated standard deviations and general isotropic thermal displacement parameters are given in Table 12. The general anisotropic thermal displacement parameters of the non-hydrogen atoms are given in Table 13. The positions of the hydrogens were not refined independently, but were constrained to ride on the carbons of the crown ether with a fixed bond length of 0.95 Å and tetrahedral bond angles. There was no indication of disorder in the crown ether ring.

The main features of the crystal structure of $Cs^+(18C6)_2 \cdot e^-$ are nearly identical to those of the $Cs^+(18C6)_2 \cdot Na^-$ structure; the ionic packing shown in Figure 8 is essentially unchanged except for minor changes in distances. The stereographic ORTEP [90] packing diagram is shown in Figure 10. The positions noted with the symbol ⊙ are the positions that were occupied by the anion in the sodide salt. In this case the final Fourier difference map indicated that only noise level electron density existed there. The noise level of the difference map was 0.059

Table 12.

Table of Positional Parameters in Fractional Unit Cell Coordinates and Their Estimated Standard Deviations for Cesium (18-Crown-6)$_2$ Electride at 216 K

Atom	x	y	z	B(Å^2)
Cs1	0.000	0.02650(9)	0.250	2.74(2)
O1	-0.0982(7)	0.1783(5)	0.3693(5)	3.6(2)
O4	0.1224(7)	0.1626(6)	0.3639(5)	3.8(2)
O7	0.1425(6)	-0.0137(6)	0.4073(4)	3.9(2)
O10	-0.0235(6)	-0.1289(5)	0.3879(5)	3.8(2)
O13	-0.1870(7)	-0.1097(6)	0.2728(5)	4.2(2)
O16	-0.2393(6)	0.0642(5)	0.2937(5)	3.8(2)
C2	-0.027(1)	0.2462(8)	0.3765(7)	4.3(3)
C3	0.068(1)	0.2147(9)	0.4150(7)	4.5(4)
C5	0.211(1)	0.1252(9)	0.3984(8)	4.2(3)
C6	0.191(1)	0.0541(8)	0.4499(7)	3.9(3)
C8	0.133(1)	-0.0856(9)	0.4522(8)	4.1(3)
C9	0.078(1)	-0.1543(9)	0.4054(8)	4.6(3)
C11	-0.083(1)	-0.1967(8)	0.3547(8)	4.6(4)
C12	-0.188(1)	-0.1628(9)	0.3367(7)	4.5(4)
C14	-0.283(1)	-0.073(1)	0.2493(8)	4.9(4)
C15	-0.311(1)	0.000(1)	0.2993(9)	6.4(5)
C17	-0.268(1)	0.1366(9)	0.3356(8)	4.5(3)
C18	-0.192(1)	0.2038(9)	0.3299(8)	5.2(4)

Continued.

Table 12 (continued).

Table of Positional Parameters in Fractional Unit Cell Coordinates and Their Estimated Standard Deviations for Cesium (18-Crown-6)$_2$ Electride at 216 K

Atom	x	y	z	B(Å^2)
H2a	-0.056	0.290	0.406	5.4*
H2b	-0.012	0.267	0.327	5.4*
H3a	0.110	0.261	0.431	6.1*
H3b	0.051	0.182	0.459	6.1*
H5a	0.248	0.167	0.427	5.5*
H5b	0.253	0.105	0.359	5.5*
H6a	0.253	0.034	0.474	5.0*
H6b	0.146	0.073	0.488	5.0*
H8a	0.094	-0.073	0.496	5.4*
H8b	0.199	-0.105	0.469	5.4*
H9a	0.113	-0.162	0.359	5.9*
H9b	0.078	-0.206	0.433	5.9*
H11a	-0.084	-0.242	0.390	5.9*
H11b	-0.053	-0.215	0.309	5.9*
H12a	-0.233	-0.209	0.325	6.0*
H12b	-0.211	-0.133	0.380	6.0*
H14a	-0.335	-0.115	0.251	6.3*
H14b	-0.279	-0.053	0.198	6.3*
H15a	-0.377	0.021	0.283	7.5*
H15b	-0.313	-0.018	0.351	7.5*
H17a	-0.274	0.122	0.388	6.0*
H17b	-0.333	0.156	0.316	6.0*
H18a	-0.180	0.214	0.277	6.8*
H18b	-0.216	0.254	0.352	6.8*

Starred atoms were refined isotropically.
Anisotropically refined atoms are given in the form of the isotropic equivalent displacement parameter defined as:
(4/3) * [a^2*B(1,1) + b^2*B(2,2) + c^2*B(3,3)
+ ab(cos gamma)*B(1,2) + ac(cos beta)*B(1,3)
+ bc(cos alpha)*B(2,3)] where a, b, and c are reciprocal lattice vectors.

Table 13.

Table of General Displacement Parameter Expressions
U's (in $Å^2$) for Cesium (18-Crown-6)$_2$ Electride

Name	U(1,1)	U(2,2)	U(3,3)	U(1,2)	U(1,3)	U(2,3)
Cs1	0.0331(5)	0.0441(6)	0.0274(5)	0	0.0065(4)	0
01	0.059(6)	0.040(5)	0.039(5)	0.004(5)	0.005(5)	0.004(4)
04	0.050(5)	0.065(6)	0.029(4)	-0.000(5)	0.011(4)	0.001(5)
07	0.056(5)	0.064(6)	0.028(4)	-0.005(5)	-0.000(4)	0.021(4)
010	0.057(5)	0.044(5)	0.044(5)	-0.004(5)	0.014(4)	-0.002(4)
013	0.057(5)	0.069(6)	0.035(5)	-0.010(5)	0.013(4)	0.008(5)
016	0.046(5)	0.048(5)	0.051(5)	0.000(4)	0.019(4)	-0.006(4)
C2	0.09(1)	0.038(8)	0.039(7)	0.015(8)	0.003(8)	-0.019(6)
C3	0.066(9)	0.07(1)	0.035(7)	-0.008(8)	0.009(7)	-0.004(7)
C5	0.060(8)	0.056(9)	0.046(8)	-0.013(8)	0.017(7)	-0.005(7)
C6	0.038(7)	0.07(1)	0.042(7)	-0.012(7)	-0.003(6)	-0.009(7)
C8	0.041(8)	0.058(9)	0.057(8)	0.009(7)	0.003(7)	0.015(8)
C9	0.050(8)	0.054(9)	0.071(9)	0.027(7)	0.026(7)	0.021(8)
C11	0.10(1)	0.034(8)	0.046(8)	-0.023(8)	0.012(8)	-0.002(7)
C12	0.08(1)	0.054(9)	0.039(8)	-0.024(8)	0.012(8)	-0.005(7)
C14	0.052(9)	0.08(1)	0.056(9)	-0.025(8)	0.002(8)	-0.014(8)
C15	0.059(9)	0.11(2)	0.08(1)	0.002(9)	0.020(8)	-0.029(9)
C17	0.046(8)	0.064(9)	0.062(9)	0.009(8)	0.004(7)	-0.024(7)
C18	0.060(9)	0.07(1)	0.063(9)	0.038(8)	-0.016(8)	0.000(8)

The form of the anisotropic displacement parameter is:
$\exp[-2\pi^2\{h^2a^2U(1,1) + k^2b^2U(2,2) + l^2c^2U(3,3) + 2hkabU(1,2) + 2hlacU(1,3) + 2klbcU(2,3)\}]$ where a, b, and c are reciprocal lattice constants.

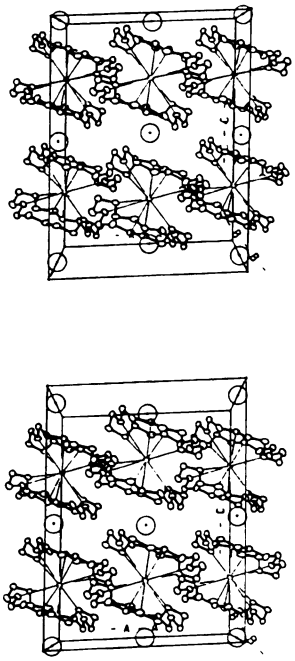


Figure 10. A stereoview of a unit cell in $\overline{Cs^{+}(18C6)_2 \cdot e^{-}}$. The center of the anionic cavity is noted by the symbol 0.

electrons/Å^3; a hydrogen atom with a van der Waals radius of 1.2 Å would have an average electron density of 0.14 e/Å^3 were it localized in the cavity. An electron trapped at this site would not be expected to appear on the final difference Fourier map.

While the gross features of the sodide and electride structures are similar, several different details are notable. Table 14 summarizes the lattice constants and interionic distances of the two compounds. The volume of a unit cell of the electride is 114 Å^3 smaller than that of the sodide, but the cell length in the b-direction is 0.15 Å larger in the electride. The distortion of Cs^+ from linear stacks along the c direction is stronger in the electride than in the sodide. In the sodide, cations lying in planes parallel to the a-c plane at z = $^1/_4$ lie +0.328 Å from y = 0 and y = $^1/_2$ positions; those cations lying in planes perpendicular to z = $^3/_4$ are displaced by -0.328 Å from y = 0 and y = $^1/_2$. The electride has larger displacements, of + and -0.42 Å from y = 0 and y = $^1/_2$ respectively. This displacement does not affect the distances between like ions in planes perpendicular to c, Cs^+-Cs^+ distances and e^--e^- distances are only slightly shorter than those seen in the sodide. The interionic distance in these planes are 10.27 Å in the electride (that is 0.1 Å shorter than in the sodide). Along the c axis the inter-

Table 14.

A Comparison of Lattice Constants and Interionic Distances in Cesium $(18C6)_2$ Sodide, Cesium $(18C6)_2$ Electride, and Cesium $(15C5)_2$ Iodide

Characteristic	$Cs^+(18C6)_2 \cdot Na^-$	$Cs^+(18C6)_2 \cdot e^-$	$Cs^+(15C5)_2 \cdot I^-$
Cell Dimensions			
a (Å)	13.581	13.075	13.172
b (Å)	15.684	15.840	
c (Å)	17.429	17.359	16.645
β (°)	93.16	92.30	
V ($Å^3$)	3706.8	3592.2	2888
z			
Anion-anion Distances (Å)			
along z axis	Two at 8.71	Two at 8.68	8.04 and 8.60
in an x-y plane	Four at 10.37	Four at 10.27	Four at 9.32
Cation-cation Distances (Å)			
Along z axis	Two at 8.74	Two at 8.72	Two at 8.32
In an x-y plane	Four at 10.37	Four at 10.27	Four at 9.32
Anion-cation Distances (Å)			
	Two each at 7.87, 8.28 8.69, 9.26	Two each at 7.71, 8.00 8.67, 9.40	Four at 7.73 Four at 7.86
Cesium-oxygen Distances (Å)			
Range	3.287- 3.468	3.297- 3.457	2.960- 3.219
Mean distance	3.357	3.352	3.108

ionic distance is 8.68 Å for anions and for cations 8.72 Å (only 0.03-0.02 Å shorter than equivalent distances in the sodide). The spread of distances from an anion to its first coordination shell cations is greater than that of the sodide. The electride has Cs^+ ions both 0.15 Å closer than the closest Cs^+ in the sodide, and 0.15 Å longer than the farthest first shell Cs^+ in the sodide.

The structure of the complexed cation is strikingly similar to that of the complexed cation in $Cs^+(18C6)_2 \cdot Na^-$. Table 9 includes the cesium-oxygen distances and bond lengths in the crown ether molecules for the electride. $Cs^+(18C6)_2 \cdot e^-$ has Cs-O distances that range from 3.296 Å to 3.457 Å with a mean distance of 3.352 Å. The sodide, for comparison, has a mean Cs-O interaction distance of 3.357 Å. The crown ether has essentially the same conformation in both structures; the bond distances are generally more nearly ideal and there is no sign of disorder in the crown ethers in the electride structure. The torsion angles are listed with those of the crown ether of the sodide in Table 10, any differences are small. A plane was fit by least-squares methods to the oxygens of one crown ether and has the crystallographic equation, in Ångstroms.

$$4.828\underline{x} + 0.0665\underline{y} + 16.376\underline{z} = 5.944 \text{ Å}$$

The results are listed in Table 15. The plane is nearly parallel to the y axis, and when projected onto the x-z plane the mean oxygen plane makes an angle of ~20° from the x axis toward the z axis. The Cs^+ ion sits 1.852 Å off of the mean plane, exactly as in the sodide.

The environment of the trapped electron in the electride salt is of crucial importance to the interactions of the electron with other electrons, and with the cations in the crystal. The electron cavity, an interstitial void left by the packing of the complexed cations, is bounded essentially entirely by protons. If is is assumed that the hydrogens maintain a van der Waals radius of 1.2 Å then the effective size of a "hard sphere" electron may be estimated. Table 11 includes the closest contacts to the inversion center at the center of the electron cavity. As in the sodide there is one pair of hydrogens that is much closer than the next nearest hydrogens. The estimated "hard-sphere" radius ranges from 2.09 Å for contact with the nearest hydrogens to 2.30 Å for the average contact with the nearest $Cs^+(18C6)_2 \cdot e^-$ hydrogens. Intuitively it is clear that the trapped electron would not be hard sphere-like, but would be polarizable similar to the behavior of electrons in other trapped electron systems. The thermodynamically most stable trap geometry in the electride is not a spherical cavity created by a vacancy in

Table 15.

Table of Least-Squares Planes
for Cesium (18-Crown-6)$_2$ Electride

Crystallographic Equation of Plane 1 in Angstroms

4.8278 X + 0.0665 Y + -16.3764 Z - -5.9440 = 0

0.0216 0.0301 0.0305 0.0042

Atom	X(Å)	Y(Å)	Z(Å)	Distance(Å)	Esd
		--- Atoms in Plane ----			
O1	-1.5406	2.8235	6.4055	-0.566	+- 0.008
O4	1.3469	2.5761	6.3115	0.587	+- 0.008
O7	1.5792	-0.2171	7.0649	-0.039	+- 0.007
O10	-0.5771	-2.0422	6.7287	-0.531	+- 0.008
O13	-2.6348	-1.7373	4.7318	0.566	+- 0.008
O16	-3.3337	1.0170	5.0943	-0.017	+- 0.008
		----- Other Atoms -----			
Cs1	-0.1742	0.4198	4.3363	1.852	+- 0.000
C2	-0.6149	3.8993	6.5304	-0.336	+- 0.013
C3	0.6003	3.4014	7.1990	-0.510	+- 0.013
C5	2.4872	1.9828	6.9111	0.448	+- 0.013
C6	2.1820	0.8575	7.8032	-0.498	+- 0.012
C8	1.4223	-1.3551	7.8431	-0.825	+- 0.013
C9	0.7432	-2.4440	7.0309	-0.326	+- 0.014
C11	-1.3260	-3.1153	6.1529	-0.277	+- 0.014
C12	-2.6936	-2.5781	5.8392	-0.488	+- 0.013
C14	-3.8738	-1.1561	4.3235	0.491	+- 0.014
C15	-4.2765	0.0064	5.1920	-0.460	+- 0.016
C17	-3.7427	2.1639	5.8217	-0.839	+- 0.014
C18	-2.7366	3.2276	5.7216	-0.370	+- 0.014

a cubic lattice, as in an F-center, or a self oriented coordination, as in glasses or solutions, but appears to be simply an interstitial lattice site in the closest-packed cationic system. The radius of the trapped electron cavity is slightly smaller than the radius of Na^-. The effect of putting the larger Na^- anion into the cavity in the $Cs^+(18C6)_2$ system is to push the ions in a-b planes apart; there is little elongation of the distance between anions in the c direction in going from the electride to the sodide. The magnetic properties of these compounds, which will be presented in Chapters V and VI, are used to probe the interactions of the trapped electron with its ionic environment.

To better understand the nature of the anionic cavity the structure of one cavity was studied on an Evans and Sutherland PS300 Graphics system. The surface contour representation of the van der Waals radii of all of the atoms of eight nearest complexed cations to a cavity was constructed on the screen. No thermal displacements of the atoms are accounted for in the van der Waals surface. It was possible to rotate the structure to any crystallographic orientation and to cut into the map to get 3 dimensional cross sections of variable thickness of the molecules and the cavity. The cavity is football shaped, nearly circular in cross sections perpendicular to the c

axis, and is elongated along the c direction. The packing of complexed cations, as shown by the van der Waals radii is very efficient, but does not completely fill the space between the electron cavities so that channels of low electron density connect each cavity to the six nearest cavities in the lattice. Electrons are most likely to interact with other electrons through these channels, rather than through space occupied by high electron density of the complexed cations. The channels are most constricted in the a-b plane that includes four of the six nearest cavities. A view of a cavity from the inversion center along the c axis is shown in Figure 11. The cavity is nearly square shaped at the inversion center with an edge length of ~4.5 Å. Channels that connect the cavity to other cavities in the same a-b planes begin at the corners of the cavity and travel through the packed cations to the next electron traps. In the background of the central trap is an hourglass shaped constriction, which is the interface with the next cavity along the c direction. Cavities along this direction are separated by 8.68 Å. The approximate lateral dimensions of the constriction are 5.0 Å along the b axis by 2.2 Å and 1.0 Å at the widest and narrowest points in the a direction.

The stacked structure of the ions along the c direction is shown in Figures 12 and 13, which were constructed

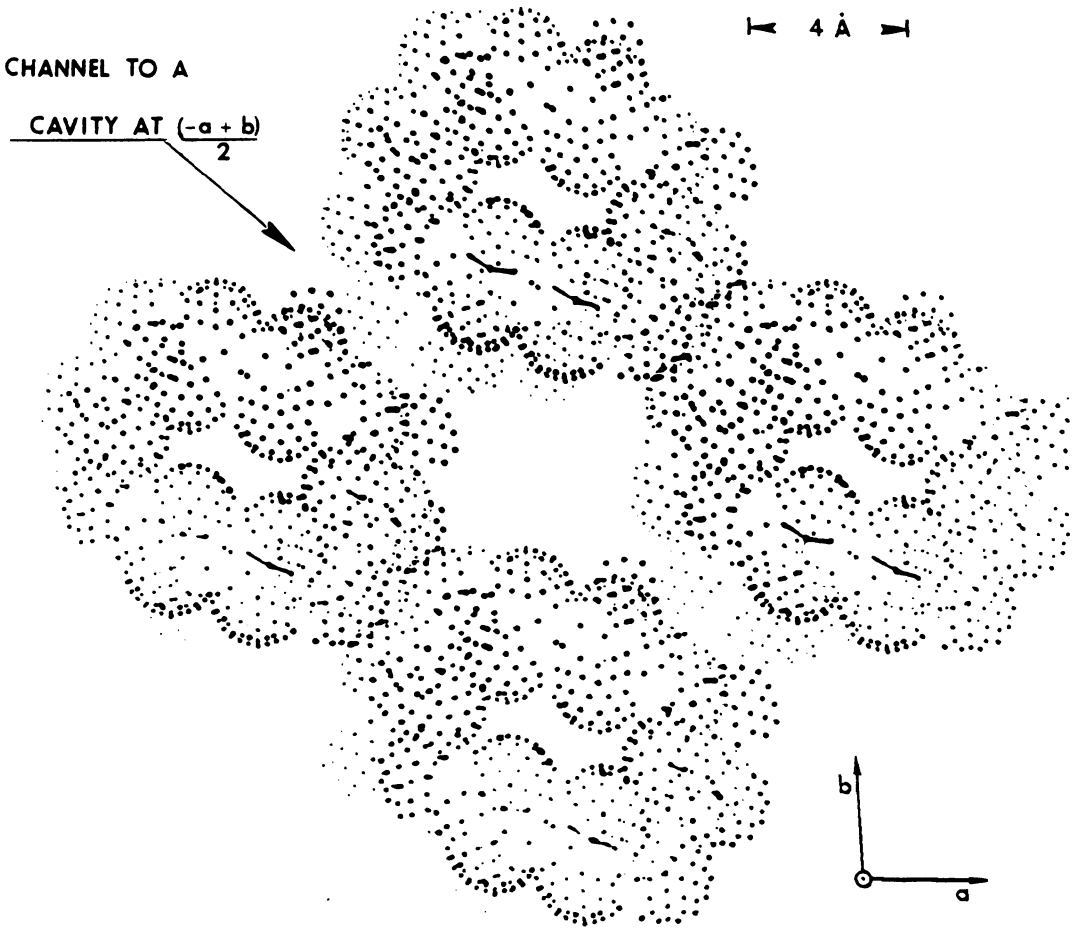


Figure 11. A surface contour representation of an anionic cavity in $Cs^+(18C6)_2 \cdot e^-$, as viewed down the c axis at a = 1/2, b = 0, c = 1/2. The cavity is shown at its maximum size in the a-b plane; channels to neighboring cavities at 1, 1/2, 1/2, and 0, -1/2, 1/2 are indicated by arrows.

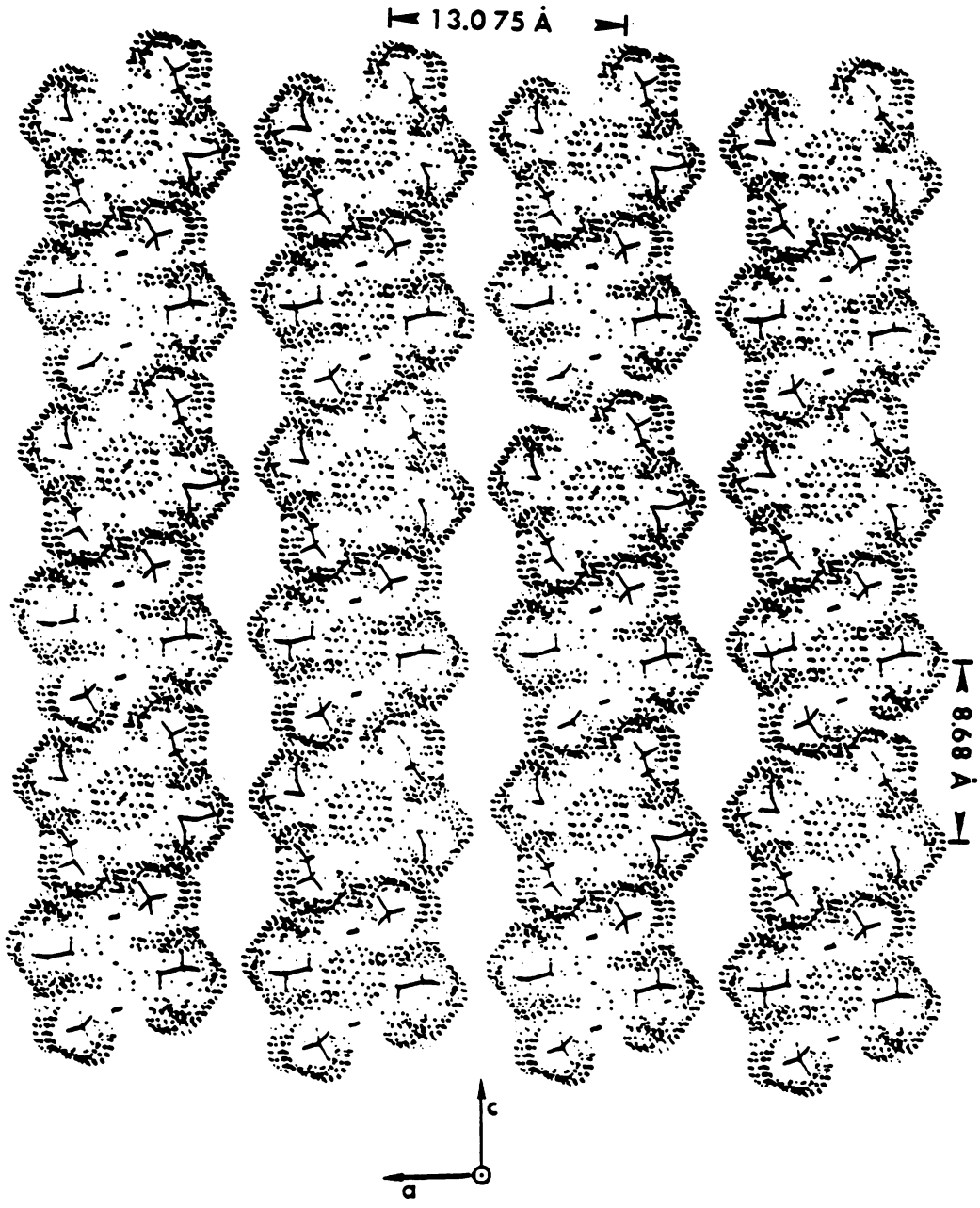


Figure 12. A surface contour representation of the packing of complexed cations and anionic cavities in an a-c plane at b = 0 in $Cs^{+}(18C6)_2 \cdot e^{-}$. The oblong shape cavities and the channel structure in the c direction are apparent.

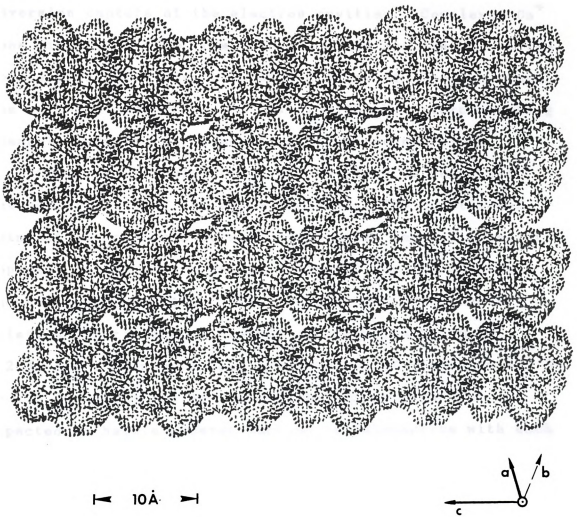


Figure 13. A surface contour representation of the packing of complexed cations in $Cs^{+}(18C6)_2 \cdot e^{-}$ as viewed down the 1,1,0 direction. The interstitial open spaces are channels to cavities behind the "wall" of complexed cations.

by superposition of several identical complexed cation images according to the proper symmetry of the space group. Figure 12 is a view down the b axis of a slice of van der Waals electron density in an a-c plane that includes the inversion centers at the electron cavities. Complexed Cs^+ ions lie only 0.42 Å from this plane and are visible as the boundary in the a direction of the stack of electron traps. The oblong structure of the cavity with the interconnecting channels between the adjacent cavities are notable.

Figure 13 is a view of a (1 1 0) plane of complexed cations with all of the atoms included. The constricted point of the channels between cavities in the a-b plane are apparent in the figure as small gaps in the efficiently packed complexed cation "wall". Two types of channels exist, a bow tie shaped channel of dimension 2.5 Å by 1.2 Å, and a diamond shaped constriction of dimension 2.0 Å by 1.2 Å. Electrons in the same a-b plane might be expected to have a greater barrier to interaction with each other than the electrons along the c direction not only because of the smaller cross sectional area of the channel but also because the constricted channel is 4 Å long between the cavities (see the channels marked by arrows in Figure 11) whereas in the c direction the channel is severely constricted for only ~1.5 Å. Thus an electron trapped in a cavity has a structurally anisotropic environ-

ment in terms of the void space that connects it to other nearby trapped electrons.

III.C. Structure Solution and Refinement for $Cs^+(15C5)_2 \cdot I^-$

III.C.1 General Approach

The crystal structure of $Cs^+(15C5)_2 \cdot I^-$ was solved by the Patterson method. Refinement of 146 parameters required restraint of the positional parameters of the crown ether atoms to maintain a chemically reasonable structure. Least-squares refinement of an unrestrained crown ether resulted in unstable adjustments of the parameters and poor agreement factors. Both Cs^+ and I^- occupy special positions on rotation axes in the lattice; several positional and thermal parameters for these ions were fixed. The final agreement factors obtained in the restrained full matrix least-squares refinement were R = 8.6, and R_w = 11.6.

III.C.2 Results of the Structure Determination of $Cs^+(15C5)_2 \cdot I^-$

The positional and anisotropic thermal parameters are given in Tables 16 and 17, respectively, for all non-hydrogen atoms in $Cs^+(15C5)_2 \cdot I^-$. The positional parameters of the hydrogen atoms were constrained to ride on the carbons of the crown ether, these are included in Table 16. All hydrogens were assigned a constant value of the thermal parameter, U, of 0.216 Å^2; no refinement of the hydrogen thermal parameter was attempted.

The ionic packing in the tetragonal $Cs^+(15C5)_2 \cdot I^-$ is similar to the ionic packing in the 18C6 salts described above. Cations and anions lie in alternating planes perpendicular to the c axis. The cations lie in planes perpendicular to c at z = 0, 1/2, etc.; the positions of the Cs^+ ions on each plane are at the midpoints of the cell edges (i.e. 1/2, 0, z; 0, 1/2, z; etc.). Cations are separated by 8.323 Å along the c direction and by 9.316 Å from four nearest cationic neighbors in the x-y plane. The anions have a small distortion from z coordinates of z = 1/4, 3/4, etc., and lie on four planes perpendicular to the c axis. Two planes consist of anions at the corners of the intersection of the plane with the unit cell at z = 0.24047, and 0.75729. The other half of the anions occupy sites at general positions 1/2, 1/2, z, for z = 0.24729

Table 16.

Table of Positional Parameters and Their Estimated Standard Deviations in Fractional Coordinates for Cesium $(15C5)_2$ Iodide at 291 K

Atom	x	y	z
CS1	0.000	0.500	0.000000
I1	0.000	0.000	0.2405(3)
I2	0.000	0.000	0.7573(3)
O1	0.234(1)	0.496(2)	0.012(2)
C2	0.282(2)	0.428(3)	-0.042(2)
C3	0.243(2)	0.447(2)	-0.125(2)
O4	0.141(1)	0.414(2)	-0.130(2)
C5	0.128(2)	0.308(2)	-0.119(3)
C6	0.022(2)	0.280(3)	-0.140(2)
O7	-0.042(2)	0.300(2)	-0.074(1)
C8	-0.062(2)	0.212(2)	-0.027(1)
O10	-0.067(2)	0.301(3)	0.096(2)
C11	-0.028(2)	0.313(2)	0.175(1)
C12	0.084(2)	0.302(2)	0.172(2)
O13	0.126(2)	0.397(2)	0.143(3)
C14	0.231(2)	0.386(2)	0.124(2)
C15	0.268(2)	0.484(2)	0.092(2)
C9	-0.009(2)	0.227(2)	0.051(1)
C9'	-0.017(2)	0.222(2)	0.054(1)
H2A	0.352(2)	0.453(3)	-0.044(2)
H2B	0.282(2)	0.356(3)	-0.027(2)
H3A	0.245(2)	0.519(2)	-0.140(2)
H3B	0.289(2)	0.408(2)	-0.160(2)
H5A	0.164(2)	0.284(2)	-0.167(3)
H5B	0.158(2)	0.277(2)	-0.071(3)
H6A	0.017(2)	0.207(3)	-0.151(2)
H6B	-0.007(2)	0.318(3)	-0.186(2)
H8A	-0.027(2)	0.153(2)	-0.049(1)
H8B	-0.136(2)	0.202(2)	-0.032(1)
H11A	-0.056(2)	0.267(2)	0.215(1)
H11B	-0.043(2)	0.384(2)	0.192(1)
H12A	0.108(2)	0.285(2)	0.226(2)
H12B	0.101(2)	0.248(2)	0.135(2)
H14A	0.265(2)	0.370(2)	0.175(2)
H14B	0.240(2)	0.330(2)	0.086(2)
H15A	0.248(2)	0.540(2)	0.127(2)
H15B	0.342(2)	0.480(2)	0.091(2)
H9A	0.042(2)	0.203(2)	0.090(1)
H9B	0.024(2)	0.270(2)	0.011(1)
H9'A	-0.021(2)	0.154(2)	0.077(1)
H9'B	-0.039(2)	0.220(2)	-0.002(1)

Table 17.

Table of General Displacement Parameter Expressions
U's in ($Å^2$) for Cesium (15-Crown-5)$_2$ Iodide at 291 K

Name	U(1,1)	U(2,2)	U(3,3)	U(1,2)	U(1,3)	U(2,3)
CS1	0.0599(14)	0.0438(12)	0.092(2)	-0.003(16)	0.0000	0.0000
I1	0.0523(13)	0.0523(13)	0.0630(36)	0.0000	0.0000	0.0000
I2	0.092(2)	0.092(2)	0.083(6)	0.0000	0.0000	0.0000
01	0.108(11)	0.191(14)	0.147(13)	-0.032(14)	0.008(14)	-0.053(11)
C2	0.130(15)	0.261(16)	0.231(16)	0.04(2)	-0.046(15)	-0.038(16)
C3	0.169(15)	0.283(16)	0.119(15)	0.069(15)	0.083(15)	0.059(15)
04	0.149(13)	0.180(13)	0.072(10)	-0.014(11)	0.042(11)	0.032(12)
C5	0.221(16)	0.238(16)	0.266(16)	0.064(16)	-0.078(16)	0.106(15)
C6	0.163(16)	0.138(15)	0.255(16)	-0.057(16)	0.041(16)	0.051(15)
07	0.293(16)	0.101(13)	0.183(14)	-0.069(12)	-0.027(14)	0.024(14)
C8	0.056(12)	0.076(12)	0.204(16)	-0.017(12)	-0.046(12)	0.054(10)
010	0.216(15)	0.265(16)	0.349(17)	-0.004(16)	0.046(16)	0.016(15)
C11	0.290(16)	0.212(16)	0.131(15)	0.089(15)	-0.047(15)	0.016(16)
C12	0.127(14)	0.099(13)	0.078(12)	0.032(11)	0.042(12)	0.048(11)
013	0.226(15)	0.255(15)	0.156(15)	-0.052(15)	0.048(14)	0.013(15)
C14	0.194(15)	0.175(15)	0.184(15)	-0.015(15)	-0.131(14)	0.028(15)
C15	0.115(14)	0.115(14)	0.198(16)	0.019(14)	-0.076(14)	-0.022(13)
C9	0.099(9)	(Refined Isotropically)				
C9′	0.145(13)	(Refined Isotropically)				

Hydrogen U's were not refined, and were set to U(Iso)=0.216 $Å^2$.

The form of the anisotropic displacement parameter is:
$\exp[-2\pi^2\{h^2a^2U(1,1) + k^2b^2U(2,2) + l^2c^2U(3,3) + 2hkabU(1,2) + 2hlacU(1,3) + 2klbcU(2,3)\}]$ where a, b, and c are reciprocal lattice constants.

and 0.74047. The distortion of I^- positions from $\underline{z}$ = $^1/_4$ and $^3/_4$, etc. results in two I^--I^- distances along the $\underline{c}$ direction; a short distance of 8.043 Å and a longer distance of 8.602 Å. The next nearest inter-anionic distances are 9.318 Å between iodides which are nearly planar perpendicular to the $\underline{z}$ axis. Each ion is coordinated by eight counterions, four separated by 7.726 Å and four separated by 7.855 Å.

Both the anions and the cations occupy special positions on rotation axes. The anions are on four-fold rotation axes parallel to the $\underline{z}$ axis, this symmetry generates a square environment about the anion in planes perpendicular to the $\underline{c}$ axis. The cations lie on 4_2 axes aligned parallel to the $\underline{c}$ direction. This symmetry element combines a 90° rotation with a translation of $+^1/_2$ $\underline{z}$, which generates a local two-fold rotation axis. The 4_2 axis, in combination with the four-fold axes at the anions, requires each complexed cation to be rotated by 90° about the $\underline{z}$ axis relative to each of the six nearest neighbor complexed cations. The local two-fold axis at the Cs^+ relates one crown ether to the other, so only one crown ether of each complexed cation is unique.

The crown ether molecule was refined with restrained bond lengths and angles, but was allowed conformational freedom. Table 18 lists cesium-oxygen distances and

Table 18.

Table of Bond Distances (in Angstroms) for $Cs^{+}(15\text{-Crown-5})_2 \cdot I^{-}$ at 291 K

Atom 1	Atom 2	Distance (Angstroms)
CS1	O1	3.092(17)
CS1	O4	3.075(19)
CS1	O7	2.960(18)
CS1	O10	3.194
CS1	O13	3.219
O1	C2	1.418(2)
O1	C15	1.416(2)
C2	C3	1.480(2)
C3	O4	1.418(2)
O4	C5	1.417(3)
C5	C6	1.480(2)
C6	O7	1.417(2)
O7	C8	1.421(2)
C8	C9	1.494(3)
C8	C9′	1.481(2)
O10	C11	1.428(6)
O10	C9	1.445(9)
O10	C9′	1.419(4)
C11	C12	1.485(2)
C12	O13	1.427(6)
O13	C14	1.417(3)
C14	C15	1.480(2)
C9	C9′	0.128

All Carbon-Oxygen Bonds Were Restrained During Refinement.

selected interatomic distances along the crown ether backbone in the $Cs^+(15C5)_2 \cdot I^-$ structure. The mean Cs-O distance in this salt is 3.15 Å, 0.2 Å less than the mean Cs-O distance in the $Cs^+(18C6)_2$ salts. A least-squares plane was fit to the oxygens of one crown ether to describe the orientation of the crown in the structure. The plane fits the crystallographic equation, in Ångstroms, $-7.107\underline{x} + 11.090\underline{y} - 0.081\underline{z} - 3.668 = 0$. The results are given in Table 19. The least-squares plane is nearly parallel to the c axis so that the least-squares planes of adjacent complexed cations along a z axis are perpenduclar.

The anionic radius of I^- has been estimated to be 2.15-2.20 Å [91]. Table 11 lists the nearest proton contact distances to each of the unique iodides. The nearest protons are centered 3.34-3.40 Å away from the I^- centers, which implies a van der Waals radius of 2.14-2.20 Å. The twelve nearest protons give an average radius of 2.3 Å for each of the two I^- ions. The good agreement of the estimated van der Waals radius of I^- from anionic contact distances with established estimates strengthens the validity of the method used to estimate the values of the Na^- and e^- radii.

Since the anionic radius of I^- is similar to that of the trapped electron in $Cs^+(18C6)_2 \cdot e^-$, it might be expected that the structure of $Cs^+(15C5)_2 \cdot e^-$ would be similar to

Table 19.

Table of Least-Squares Planes for
Cesium (15-Crown-5)$_2$ Iodide at 291 K

Crystallographic Equation of Plane in Angstroms

$-7.1070\ X + 11.0900\ Y + -0.0808\ Z - 3.6683 = 0$

Atom	X(Å)	Y(Å)	Z(Å)	Distance(Å)
	----- Atoms in Plane -----			
O1	3.0855	6.5336	0.1949	0.1668
O4	1.8612	5.4493	-2.1673	-0.0741
O7	-0.5530	3.9503	-1.2291	-0.0381
O10	-0.8834	3.9662	1.5998	0.1399
O13	1.6659	5.2074	2.3842	-0.1944
	----- Other Atoms -----			
CS1	0.0000	6.5860	0.0000	1.8767
I1	0.0000	0.0000	4.0026	-3.6878
I2	0.0000	0.0000	12.6051	-3.7295
C2	3.7162	5.6389	-0.7057	-0.9224
C3	3.2069	5.8855	-2.0738	-0.4333
C5	1.6863	4.0558	-1.9774	-1.1539
C6	0.2961	3.6926	-2.3340	-0.7078
C8	-0.8219	2.7942	-0.4487	-0.8702
C11	-0.3670	4.1377	2.9199	-0.0008
C12	1.1090	3.9845	2.8644	-0.9259
C14	3.0425	5.0908	2.0673	-1.0338
C15	3.5288	6.3814	1.5313	-0.2070
C9	-0.1197	2.9918	0.8551	-1.0890
C9′	-0.2204	2.9262	0.8982	-1.0902

that of $Cs^+(15C5)_2 \cdot I^-$. The surface contour representation of the eight complexed cations surrounding an anionic cavity was generated on the Evans and Sutherland PS300 graphics station as a possible model for the electron cavity of $Cs^+(15C5)_2 \cdot e^-$.

The void space left in the crystal structure of $Cs^+(15C5)_2 \cdot I^-$ when the anion, I^-, is removed resembles the cavity and channel structure of $Cs^+(18C6)_2 \cdot e^-$. There is higher symmetry in the 15C5 salt; the four-fold rotation axis along the z axis through the anionic site gives the iodide cavity a more circular shape in planes perpendicular to the c axis. In addition there is less elongation along the c axis in the iodide, so that the three dimensional shape of the cavity is very nearly spherical with a radius of ~2.5 Å.

Adjacent cavities are joined by channels through the complexed cations. The symmetry in the crystal requires the four channels to neighboring anions in a plane perpendicular to the z axis to be identical, thus only two of the six channels are unique. The channel along the c axis is most constricted in those planes perpendicular to c that contain the Cs^+ ions at z = 1/4, 3/4, etc. The constriction in the channel is square shaped, with an edge length of 1.75 Å. The second type of channel connects the set of four neighboring cavities which are nearly in the same a-b

plane as the central anion. The channel is ~4.5 Å long along the c direction and 1-2 Å wide. This channel has a z component since the four anions surrounding the central anion are displaced by 0.559 Å along the z direction; this results in an effective channel size through the lattice that is reduced to only 1 by 3 Å.

If $Cs^+(15C5)_2 \cdot e^-$ crystallizes into a similar structure, based on close packing of the complexed cations, these channels would probably be important to electron-electron interactions. In addition to the more spherical anionic cavity in the $Cs^+(15C5)_2 \cdot I^-$ relative to $Cs^+(18C6)_2 \cdot e^-$, the anion-anion distances are both shorter and more isotropic (see Table 14). The channel structure in the $Cs^+(15C5)_2$ lattice is most notably different from the $Cs^+(18C6)_2 \cdot e^-$ structure in the x-y directions, the channel is significantly larger and shorter. The channels along the c direction are more subtle in their differences; $Cs^+(18C6)_2 \cdot e^-$ has a larger cross-section and a shorter constriction, but $Cs^+(15C5)_2 \cdot e^-$ has a more open channel, the relative effect of these structural features on interactions between anions cannot be easily predicted. Magnetic properties will be used in Chapter VI to probe the electron-electron interaction in the electrides $Cs^+(15C5)_2 \cdot e^-$ and $Cs^+(18C6)_2 \cdot e^-$.

CHAPTER IV

THERMAL CHARACTERISTICS OF THE IODIDES AND ELECTRIDES OF $Cs^+(18C6)_2$ AND $Cs^+(15C5)_2$ COMPLEXED CATIONS

Many of the properties of $Cs^+(15C5)_2 \cdot e^-$ and $Cs^+(18C6)_2 \cdot e^-$ are measured as a function of temperature, and thus may be sensitive to phase transitions, or more subtle changes in the interionic interactions. Differential Scanning Calorimetry (DSC) allows the endothermic and exothermic transitions of a material to be defined in terms of the heat of the transition and the temperature of the transition. Optical spectroscopy, in the case of $Cs^+(15C5)_2 \cdot e^-$, offers information about the temperature dependence of the extent of electronic localization in the cavities of the solid. Information from both of these experiments will be used to interpret the temperature dependence of magnetic data in the following chapters.

IV.A Differential Scanning Calorimetry

IV.A.1 DSC of $Cs^+(15C5)_2 \cdot I^-$ and $Cs^+(18C6)_2 \cdot I^-$

The DSC traces of $Cs^+(15C5)_2 \cdot I^-$ and $Cs^+(18C6)_2 \cdot I^-$ were measured over the temperature range of -120°C (153 K) to 250°C (523 K). The DSC trace of $Cs^+(18C6)_2 \cdot I^-$ is shown in Figure 14. Three features are evident in the trace at -100°C, -35.5°C, and at 185.7°C. The low temperature feature is not a characteristic of the sample, but rather a surge that occurs whenever the instrument begins a sub-ambient temperature scan. The melting point of the $Cs^+(18C6)_2 \cdot I^-$ occurs at 185.7°C and has an approximate ΔH_{melt} = 97.1 J/g. A second endothermic transition occurs at -35.5°C, with a much weaker heat of transition, ΔH_t = 4.7 J/g.

The trace of $Cs^+(15C5)_2 \cdot I^-$ is nearly identical to that of $Cs^+(18C6)_2 \cdot I^-$. Endothermic transitions at -36.3°C, with ΔH_t = 5.4 J/g, and at the melting point, 180.2°C, with ΔH_{melt} = 23.6 J/g are the only transitions in the range of $-100°C<T<250°C$. The discrepancy between ΔH_{melt} of the $Cs^+(15C5)_2 \cdot I^-$ and $Cs^+(18C6)_2 \cdot I^-$ is larger than would be expected; unfortunately the experiments could not be repeated. The result for ΔH_{melt} of $Cs^+(18C6)_2 \cdot I^-$ is probably in error; when translated to a molar heat of

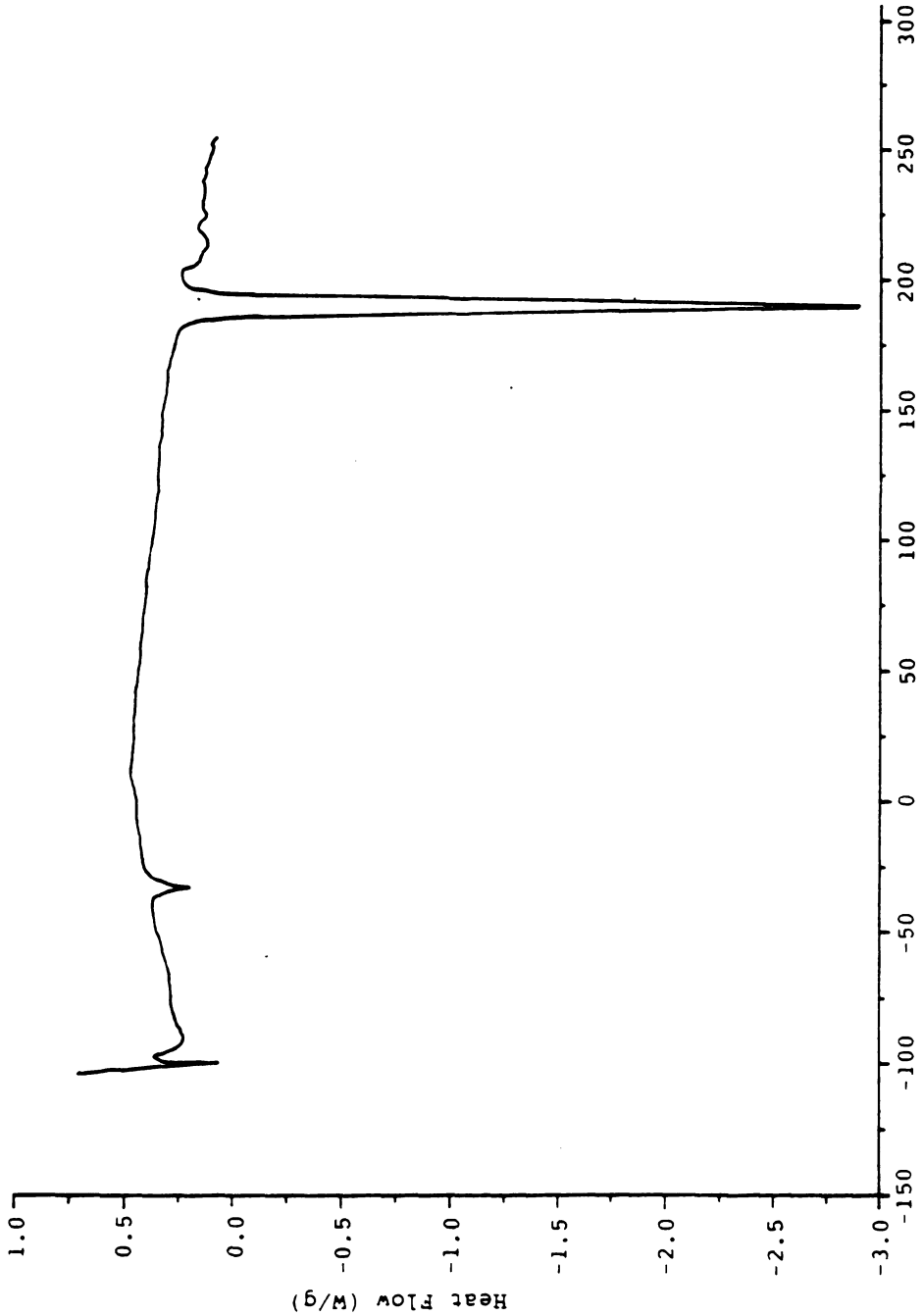


Figure 14. DSC trace of a polycrystalline sample of $Cs^{+}(18C6)_2 \cdot I^{-}$.

melting the ΔH_{melt} of the complexed ΔH exceeds ΔH_{melt} of simple salts by a factor of four. The molar heat of melting for $Cs^{+}(15C5)_2 \cdot I^{-}$ is similar to values of ΔH_{melt}^{molar} of other cesium salts. Clearly these results should be remeasured. The nature of the low temperature transition cannot be deduced from thermal measurements alone, but several possibilities can be ruled out. The melting points of the pure components are: CsI mp = 626°C, 18C6 mp = 39°C, 15C5 mp = -23 to -25°C. Thus the endotherm at ~-35°C cannot be due to excesses of any of the pure components. The fact that similar transitions occur at similar temperatures for the 18C6 and 15C5 salts indicates that the transitions arise from the same type of mechanism in the crystal.

IV.A.2 DSC of $Cs^{+}(15C5)_2 \cdot e^{-}$ and $Cs^{+}(18C6)_2 \cdot e^{-}$

The DSC trace for $Cs^{+}(15C5)_2 \cdot e^{-}$ was run over a temperature range of -140°C to +100°C, well above the decomposition temperature. The DSC trace for $Cs^{+}(15C5)_2 \cdot e^{-}$ is shown in Figure 15. The trace is more complex than that of $Cs^{+}(15C5)_2 \cdot I^{-}$; endotherms occur at -33°C (240 K), with a low temperature shoulder at -38°C (235 K), -6°C (267 K), and at +20°C (293 K). Exothermic decomposition begins

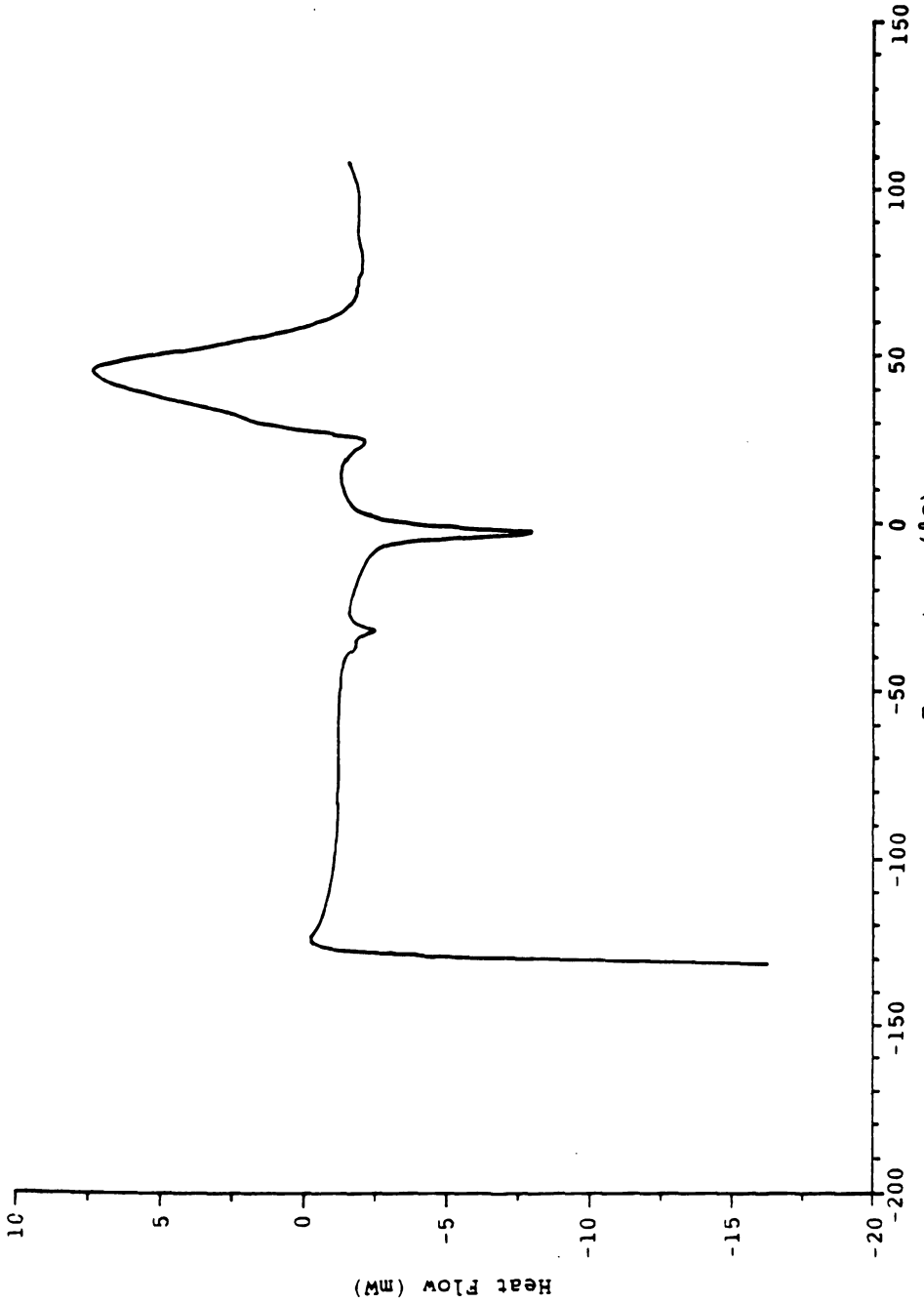


Figure 15. DSC trace of a polycrystalline sample of $Cs^{+}(15C5)_2 \cdot e^{-}$.

Table 20. Summary of DSC Results for the Iodides and Electrides of $Cs^+(18C6)_2$ and $Cs^+(15C5)_2$.

Compound	Transition 1 T (H)	Transition 2 T (H)	Transition 3 T (H)	Melt T (H)	Decomp. T (H)
$Cs^+(15C5)_2 \cdot I^-$	-36.3 C 5.36 J/g			180.2 C 23.6 J/g	
$Cs^+(18C6)_2 \cdot I^-$	-35.5 C 4.81 J/g			181.0 C 97.2 J/g	
$Cs^+(18C6)_2 \cdot e^-$			4.59 C	38.97 C	58.85 C
$Cs^+(15C5)_2 \cdot e^-$					
1	-37.9 C (weak)	-33.9 C 3.7 J/g	-6.5 C 29.1 J/g	17.0 C (overlapping peaks)	25.6 C
2	-37.7 C (weak)	-35.1 C 3.0 J/g	-5.6 C 24.3 J/g	20.0 C (overlapping peaks)	26.6 C

at the melting temperature and continues to 50°C. The approximate heats of each transition are tabulated in Table 20. Approximate values are listed because some sample oozed from the sample pan prior to mass determination. Visual observation of $Cs^+(15C5)_2 \cdot e^-$ indicates that the sample melts with decomposition near room temperature; the DSC trace corroborates this observation. Two other transitions are characteristic of $Cs^+(15C5)_2 \cdot e^-$; the weak pair of endotherms at ~-35°C are similar to the low temperature endotherm in $Cs^+(15C5)_2 \cdot I^-$, the stronger transition at -5°C is unique to the electride.

The DSC traces of three samples of $Cs^+(18C6)_2 \cdot e^-$ were measured with inconsistent results. The melting and decomposition characteristics were consistent for all samples and were in agreement with Dye's results [71]. A typical trace is shown in Figure 16. $Cs^+(18C6)_2 \cdot e^-$ melts at ~39°C, and decomposition starts at immediately higher temperatures with an exothermic peak at 54-58°C. No significance may be attached to the lower temperature transitions as none were reproduced. All three samples were prepared from the same synthesis, and the samples were large enough to expect homogeneous results.

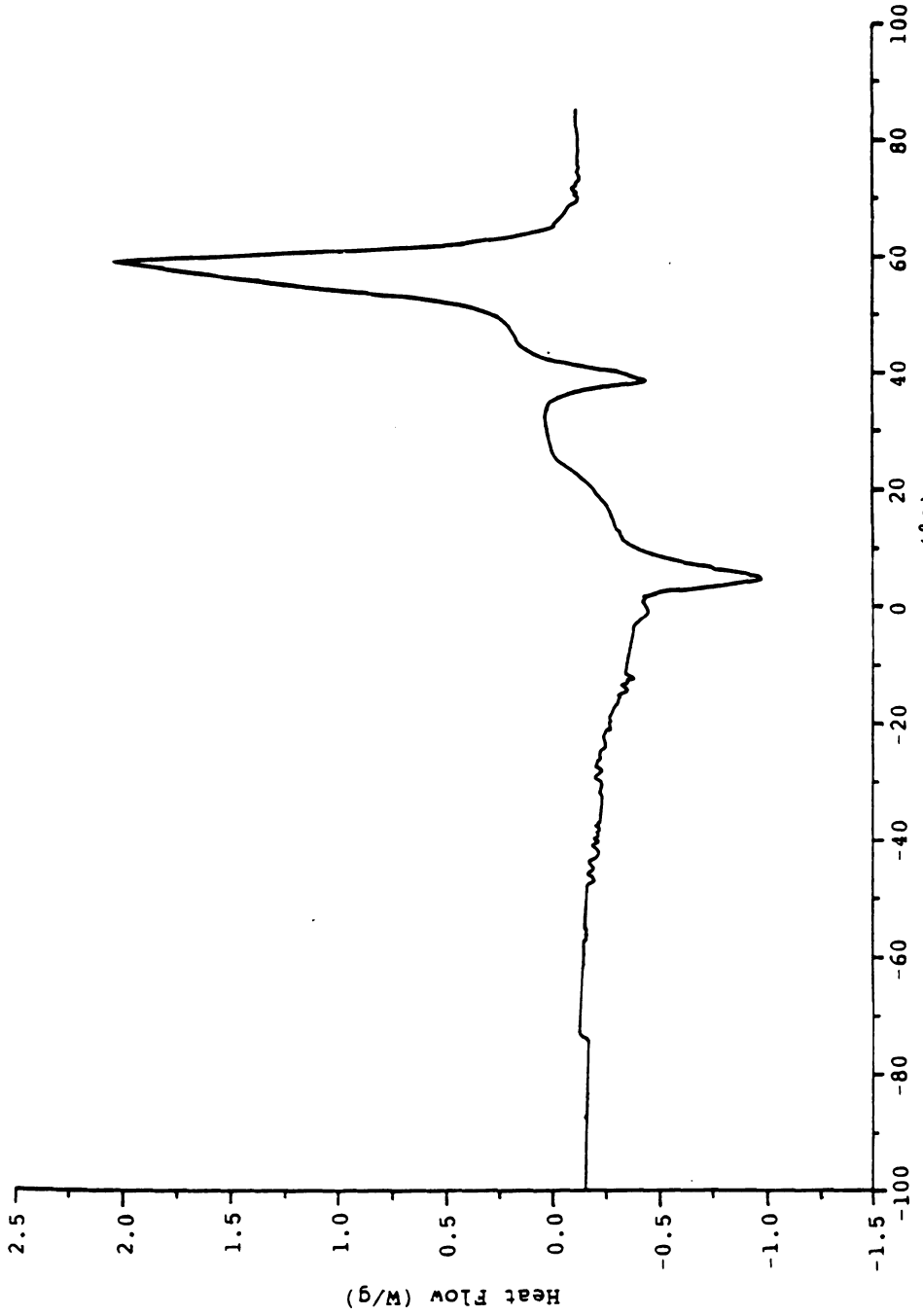


Figure 16. DSC trace of a polycrystalline sample of $Cs^{+}(18C6)_2 \cdot e^{-}$.

IV.B Optical Spectroscopy of $Cs^+(15C5)_2 \cdot e^-$

The optical spectrum of $Cs^+(15C5)_2 \cdot e^-$ has been measured several times with different samples, with only partially reproducible results. The main features of the spectrum are, however, reproducible. There are three maxima in the absorption spectrum which can appear, although any one spectrum may or may not display all of the features. One film was remarkable in its temperature dependence. The spectrum changed reversibly as a function of temperature, showing different spectral features in different temperature regions. Similar results were never reproduced. The method of making films involves several variables which are not controlled, such as the exact temperature of the solution from which the film is made, the rate of film formation, and the thickness and uniformity of the film. These may affect the microcrystallinity of the film and subsequently give variable results.

In all spectra the optical absorption tends to be quite broad, rising from 700 nm to maxima at 900-1000 nm and/or 1250-1350 possibly with a shoulder at 1550 nm and a gradual decay of absorbance to 2500 nm. A typical spectrum, of a film displaying all three features, is shown in Figure 17. The absorption maximum in localized electrides is generally considered to be the excitation energy required to promote

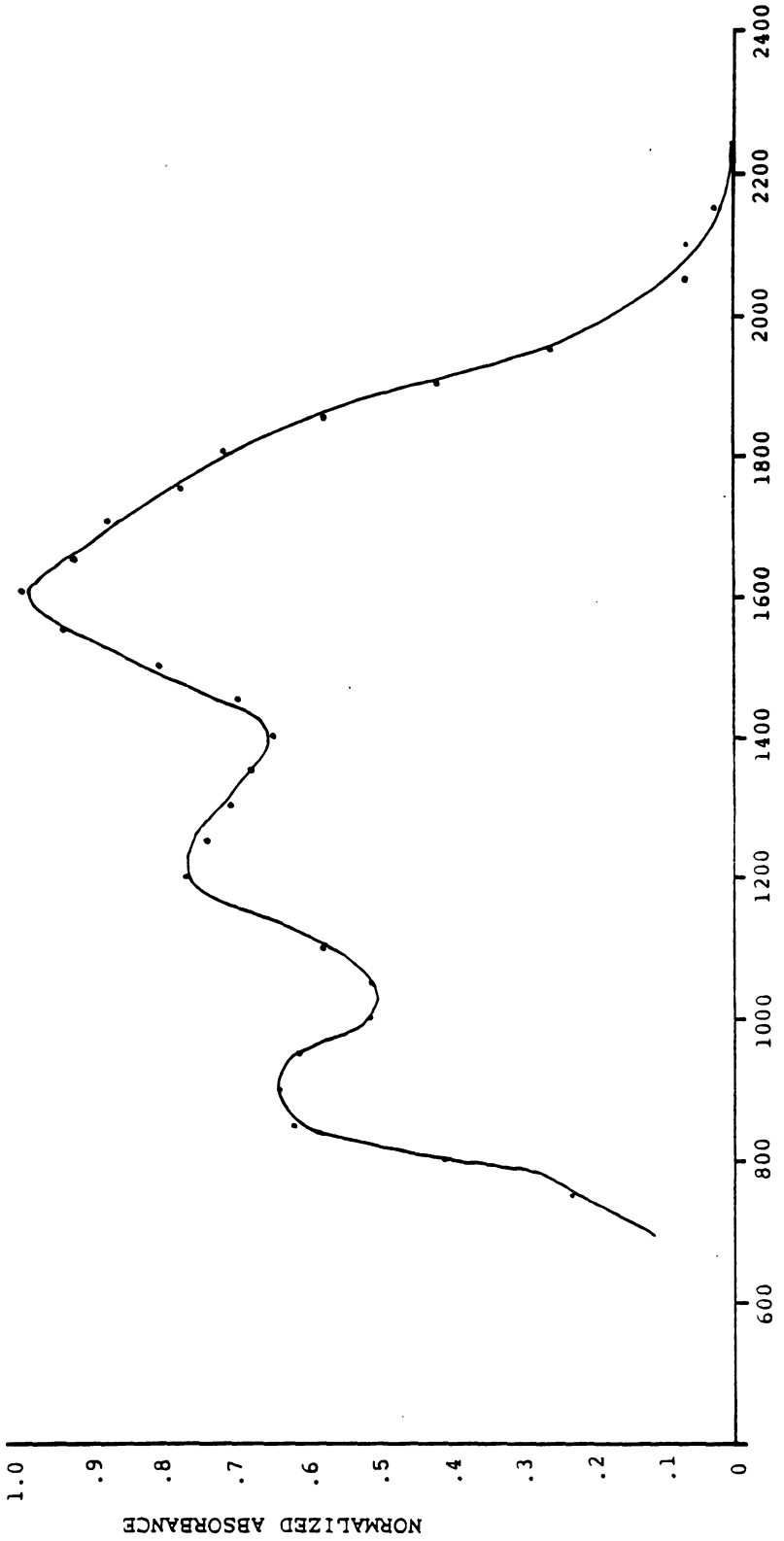


Figure 17. Normalized optical absorption spectrum of $Cs^{+}(15C5)_2 \cdot e^{-}$ at -100°C.

the trapped electron to the conduction band, or to a localized level just below the conduction band. The optical absorption of $Cs^+(18C6)_2 \cdot e^-$ is a one peak spectrum with the maximum absorbance at 1500 nm (.83 eV) [71]. The band gap for this material is 0.9 eV. $Cs^+(15C5)_2 \cdot e^-$ seems to have three different types of traps, all absorbing at higher energies than that of $Cs^+(18C6)_2 \cdot e^-$. Some insight into the nature of the three traps might be gained from the results of one film. Figure 18 shows the temperature dependence of a $Cs^+(15C5)_2 \cdot e^-$ film made from a methylamine solution. The low temperature spectrum (T = -35°C) has contributions from primarily the two lowest energy traps at 1350 and 1550 nm. As the temperature approaches 0°C the 950 nm peak becomes the major feature in the spectrum. The alkali metal anion, Cs^-, absorbs at ~950 nm and could account for the high energy peak; however, the NMR spectrum indicates that Cs^- does not exist in the sample at any temperature. Thus the trapped electron apparently becomes more strongly localized as the temperature is increased. The DSC transition at -5°C has a gradual endothermic slope from -30°C. The transition may be a softening of the lattice with the electron trap no longer a rigid cavity. The electron may be able to re-orient its cavity to create the deeper trap. There is no strong temperature dependence near the -35°C endothermic transition.

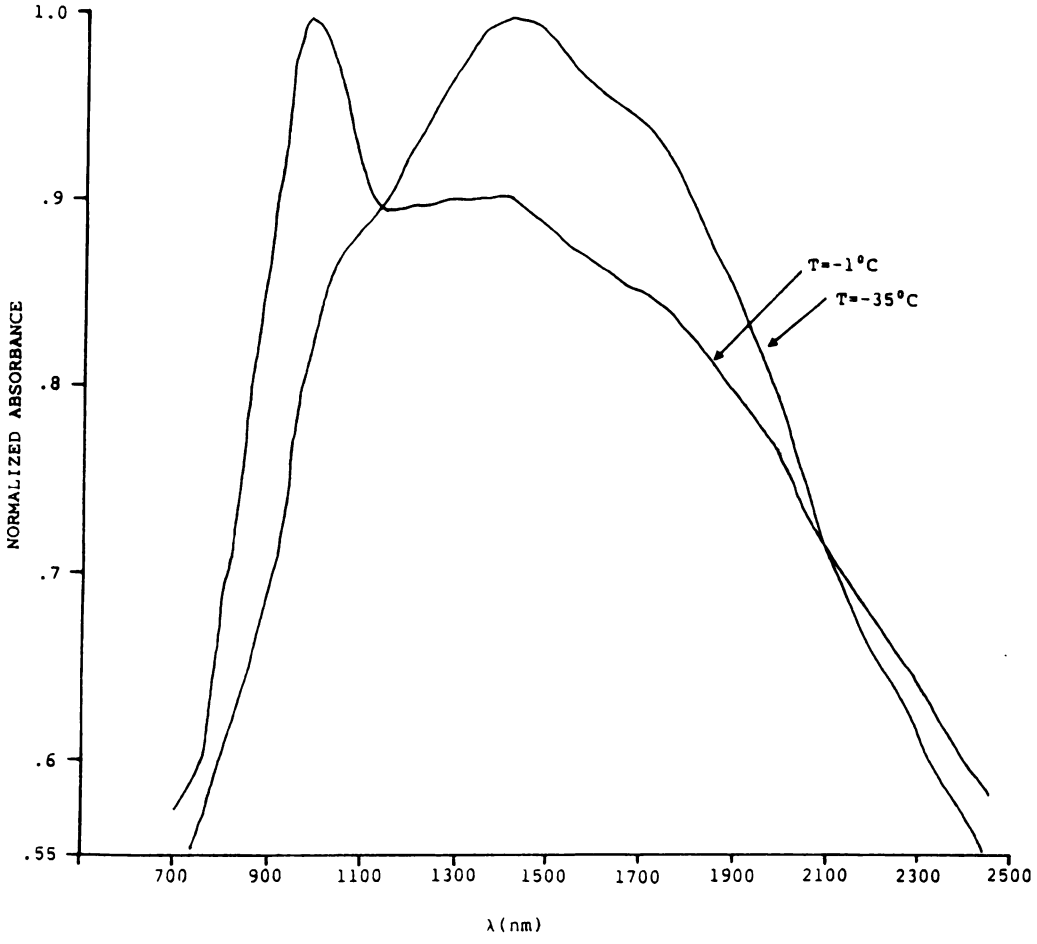


Figure 18. Normalized optical absorption spectrum of $Cs^{+}(15C5)_2 \cdot e^{-}$ at -35°C and -1°C.

The optical spectra indicate that the transition from the ground state to the first excited state in $Cs^{+}(18C6)_2 \cdot e^{-}$ is a lower energy transition than that of $Cs^{+}(15C5)_2 \cdot e^{-}$. The structural characteristics of the anionic cavities can be used to explain this phenomenon; the cavity in $Cs^{+}(15C5)_2 \cdot I^{-}$ is more nearly spherical and accommodates the ground state s-orbital more easily than the excited state p-orbital. The cavity in $Cs^{+}(18C6)_2 \cdot e^{-}$ is somewhat elongated so that p-orbitals are not impeded along the c direction in the crystal and the transition energy is lower than that of $Cs^{+}(15C5)_2 \cdot e^{-}$.

CHAPTER V

THE NUCLEAR MAGNETIC RESONANCE OF ^{133}Cs IN SALTS THAT CONTAIN COMPLEXED CESIUM CATIONS AND/OR CESIUM ANIONS

This chapter consists of three sections, the first two of which are in the form of papers that will be submitted to the Journal of the American Chemical Society, and which are entitled *"Cesium 133 Nuclear Magnetic Resonance Studies of Crystalline Salts With and Without Complexation by Crown Ethers or a Cryptand"* and *"^{133}Cs Solid State Nuclear Magnetic Resonance Spectroscopy of Alkalides and Electrides."* These papers include some original work by Dr. Ahmed Ellaboudy which is detailed in his thesis [71]. References for these sections follow the text in the section. The third section of Chapter V includes a discussion of the ^{133}Cs MAS-NMR of the new compound $Cs^{+}(15C5)_{2}\cdot e^{-}$.

V.A. Cs-133 Nuclear Magnetic Resonance Studies of Crystalline Salts With and Without Complexation by Crown Ethers and a Cryptand

V.A.1. INTRODUCTION

V.A.1.a. ^{133}CS NMR Spectra

Solid-state alkali metal NMR spectroscopy is a powerful tool for the study of crystalline alkalides and electrides, compounds in which the anions are alkali metal anions or trapped electrons.[1-6] While the identification of alkali metal anions is easily made because of their large diamagnetic shifts, the study of the local environments of M^+ and M^- requires a study of the lineshapes at several frequencies.[6] In order to provide information useful in the study of cesium-containing alkalides and electrides, we studied the static and magic angle spinning (MAS) NMR spectra of some simple cesium salts as well as salts in which Cs^+ is complexed by the crown ethers 18-crown-6 (18C6), and 15-crown-5 (15C5) and cryptand (2.2.2), (C222).[7] Such crystalline cesium compounds prove to be ideal testing grounds for lineshape studies because the NMR spectra are sensitive to dipolar, quadrupolar, and chemical shift anisotropy (CSA) effects. By studying static and MAS spectra of powders at several frequencies and the spectra of single crystals, it is possible to separate these effects and hence to determine their individual contributions to the lineshape. The nature of these magnetic interactions is related to the local structure about the Cs^+ ion, specifically the arrangement of the complexant oxygen lone pairs that generate the electronic shielding and electric field gradient, and the arrangement of hydrogen nuclei, which generate a magnetic dipolar field at the ^{133}Cs nucleus.

The sensitivity of ^{133}Cs to each of these interactions should permit even small variations in the local structures to be detectable. The local environment of the cation is important because it, in turn, affects anion-cation interactions.

Solutions of Cs^+ complexed with 18C6[8] or C222[9] in various solvents have been previously studied by ^{133}Cs NMR. In solution, rapid motion on the NMR timescale averages the anisotropic interactions. Then, only the linewidth and the chemical shift become measureable quantities. From the linewidth, the parameters of the quadrupolar interaction or the anisotr py in the chemical shift may be given limits if only one of the interactions is dominant and if a value of the correlation time is known. Most alkali metals have large quadrupole moments so relaxation tends to occur via interaction of the quadrupole moment with electric field gradients. In solutions that contain Cs^+ however, the relaxation mechanism is not so clearly quadrupolar. ^{133}Cs has a very weak quadrupole moment and a large range of chemical shifts, so relaxation may be due to either or both of these mechanisms. The results of solution NMR studies indicate that both the 18C6[8] and C222[9] systems have inclusive and exclusive complexes. In the 18C6 system a 1:1 complex is formed in the limit of large Cs^+ concentrations relative to the 18C6 concentration. This complex is characterized by a chemical shift that is dependent on the solvent and the anion. As the concentration of 18C6 is increased, the chemical shift moves toward a limiting value corresponding to the inclusive $Cs^+(18C6)_2$ complex, whose chemical shift is largely independent of the solvent and the anionic species. Cs^+ forms only 1:1 complexes with C222, but the structure of the complex varies with

temperature. At high temperatures the chemical shift of Cs^+C222 is dependent on the solvent and anion, whereas the low temperature limit finds the resonance downfield and independent of the environment.

The NMR peak in polycrystalline solids is markedly broader than similar lines in solution. This line broadening is primarily due to an orientation dependence of the magnetic field at the nucleus generated by anisotropic interactions. Solid state NMR studies of single crystals remove the orientation averaging seen in polycrystalline samples and have been used to obtain the parameters of these interactions in some materials,[10] but problems with low signal sensitivity and single crystal growth exist. Andrew[11,12] et al. and Lowe[13] developed techniques to remove first order anisotropic broadening in polycrystalline samples. Rapid rotation of the sample about an axis inclined at the 'magic angle' (54.74°) to the magnetic field removes anisotropic contributions to the central line and moves them into sidebands which arise at integral multiples of the spinning frequency from the central line. Thus the isotropic shift may be obtained, but at the expense of information about anisotropies.

Crystals of salts that contain complexed Cs^+ have been isolated,[14,15,16] and several crystal structures are known.[15,17,18] In spite of the favorable NMR characteristics of ^{133}Cs, there has been no systematic study of the solid state NMR spectra of cesium compounds. In this study, MAS NMR has been used to characterize the chemical shifts of $^{133}Cs^+$ in salts that contain 18C6, 15C5 and C222 as complexants and the anions I^-, SCN^-, tetraphenylborate (TPB^-) and others. The structure of at least one salt with each of the three complexants has been determined and these structures can be used to

correlate the chemical shifts with structural features. Static powder and single crystal NMR spectra were used to evaluate the magnitude of each of the anisotropic broadening mechanisms.

V.A.2. Lineshape Functions for Static NMR Spectra of Powders and Single Crystals.

V.A.2a. Dipolar broadening. The powder lineshape due to dipolar broadening of equivalent nuclei of spin I by coupling with nuclei of spin S is approximately Gaussian. Van Vleck[19] calculated the second moment of the line to be

$$\langle \Delta\nu^2 \rangle = \frac{1}{15\pi^2} (\gamma_I \gamma_S h)^2 S(S+1) \left(\sum_k \frac{1}{r_k^6} \right) \qquad (5.1)$$

for each of the k nuclei of spin S, where γ_I and γ_S are the magnetogyric ratios for nuclei I and S respectively, and r_k is the distance between nucleus I and the kth nucleus S. If the line is assumed to be gaussian, the linewidth at half-height becomes

$$\Delta\nu_{1/2} = 2.35 \, (\langle \Delta\nu^2 \rangle)^{1/2} \text{ Hz.} \qquad (5.2)$$

MAS-NMR reduces dipolar broadening to zero[20] if the frequency of rotation is greater than $\Delta\nu_{1/2}$. Dipolar broadening may also be eliminated by using decoupling techniques in static spectroscopy, and in MAS experiments when the dipolar coupling can not be completely removed by spinning.

V.A.2.b. Chemical Shift Anisotropy. Inhomogeneous broadening of an NMR transition may arise from an anisotropic chemical shielding environment about a nucleus.[21] The orientation of the principal axes of a diagonalized chemical shift interaction tensor with respect to the applied field will shift the resonance position from the isotropic

value of the chemical shift. The chemical shift Hamiltonian for a nucleus i is

$$H = \gamma_i \sigma_{iZZ} H_o \ , \tag{5.3}$$

in which σ_{ZZ} is related to the contributions of the principal components σ_i of chemical shift tensor through

$$\sigma_{ZZ} = \lambda_1^2 \sigma_1 + \lambda_2^2 \sigma_2 + \lambda_3^2 \sigma_3 \tag{5.4}$$

where λ_i is the direction cosine of principal axis i. The isotropic chemical shift occurs at $\lambda_i^2 = 1/3$ for all i. That is,

$$\sigma_{iso} = (\sigma_1 + \sigma_2 + \sigma_3) / 3 \ . \tag{5.5}$$

Transforming the Eulerian angles, Θ_i', to the angles Θ and ϕ in spherical polar coordinates according to

$$\Theta_3' = \Theta, \ \cos\Theta_1' = \sin\Theta\sin\phi \text{ and } \cos\Theta_2' = \sin\Theta\cos\phi$$

gives

$$\sigma_{ZZ} = \sigma_{iso} + \frac{1}{2} \delta\eta\sin^2\Theta\cos 2\phi + \frac{1}{2} \delta(3\cos^2\Theta - 1) \ , \tag{5.6}$$

where the anisotropy parameter, δ, is $\delta \equiv \sigma_3 - \sigma_{iso}$, and the asymmetry parameter, η is

$$\eta = \frac{\sigma_2 - \sigma_1}{\sigma_3 - \sigma_{iso}} \ .$$

The shielding of the Cs^+ ion in the sandwiched cesium crown ether complexes studied in this work is generated by the coordinating oxygen lone pairs. There is a nearly cylindrical symmetry of the oxygens about the cation, so that two components of the chemical shift tensor,

σ_1 and σ_2, are equal. This axial symmetry further simplifies the anisotropic chemical shift. For an axially symmetric single crystal with random orientation of the principal axis σ_3 with respect to the applied field, the shift from σ_{iso} is

$$\sigma_{ZZ} = \sigma_{iso} + \frac{1}{2}\delta(3\cos^2\theta-1) \quad . \tag{5.7}$$

or re-expressed in frequency units, the shift from the isotropic Larmor frequency is

$$(\nu-\nu_L) = \frac{1}{2}\nu_L\delta(3\cos^2\theta-1) \quad . \tag{5.8}$$

The high field limit of the frequency shift occurs at $\theta = 0, 180°$ where $\nu-\nu_L = \nu_L\delta$, and the low field limit of the chemical shift at

$\theta = \pm 90°$ is $\nu - \nu = \frac{-\nu_L\delta}{2}$

The powder pattern for an axially symmetric material may be given as $g(\nu) = d\cos\theta/d\nu$.

$$g(\nu) = \frac{1}{(3\nu_L\delta)}\left[\frac{1}{3} + \frac{2}{3}\frac{(\nu-\nu_L)}{\nu_L\delta}\right]^{-1/2} \tag{5.9}$$

for

$$\frac{-\nu_L\delta}{2} < (\nu-\nu_L) < \nu_L\delta \quad .$$

Rotating the sample at an angle β from the applied field has been shown to introduce a factor $(3\cos^2\beta-1)$ into the time averaged chemical shift expression[20]

$$\overline{\sigma_{ZZ}} = \sigma_{iso} + \delta/2\ (3\cos^2\beta-1)\left[\frac{1}{2}\eta\sin^2\theta\cos2\varphi + \frac{1}{2}(3\cos^2\theta-1)\right]. \tag{5.10}$$

When β is the magic angle, 54.74°, $\overline{\sigma_{ZZ}} = \sigma_{iso}$, and the effect of chemical shift anisotropy broadening is removed.

V.A.2.c. Quadrupolar broadening. The NMR spectrum of a quadrupolar nucleus (I>1/2) in an axially symmetric anisotropic environment will show a powder pattern that reflects removal of the degeneracy of the 2I+1 spin transitions. The first order quadrupole effect, in the high field limit where the Zeeman splitting is large relative to the quadrupolar splitting, causes the resonance line to split into 2I+1 components.[22,23] To first order, the shift of an energy level in a spin state m is given by

$$\Delta E_m^1 = \frac{\nu_Q}{6} \left[\frac{1}{2} (3\cos^2\theta - 1) \right] \left[3m^2 - I(I+1) \right] . \qquad (5.11)$$

θ is the angle between the principal axis of the electric field gradient tensor and the applied magnetic field, and ν_Q is the nuclear quadrupole frequency obtained from the product of the electric field gradient, eq, and the quadrupole moment of the nucleus, eQ, as

$$\nu_Q = 3 \frac{e^2qQ}{2hI(2I-1)} \qquad (5.12)$$

Allowed NMR transitions have $\Delta m = \pm 1$, so the frequency shift of the transition

$m \rightarrow m-1$ is

$$\Delta\nu_m = \nu_Q \left[\frac{1}{2} (3\cos^2\theta - 1) (m - \frac{1}{2}) \right] \qquad (5.13)$$

To first order, there is no shift from the isotropic value in the case of the transition $m = 1/2 \rightarrow -1/2$; a single crystal will show a spectrum consisting of 2I+1 lines, equally spaced from the central

line at positions given by

$$\frac{\nu_Q}{2}(3\cos^2\theta-1)(m-1/2) .$$

The pattern that arises for a powder that contains crystallites at random orientations may be calculated as

$$g(\nu) = \frac{d\cos\theta}{d\nu} = \frac{1}{3\nu_Q(m-1/2)}\left[\frac{2}{3}\frac{\Delta\nu_m}{\nu_Q(m-1/2)}\right]^{-1/2} \qquad (5.14)$$

where $\Delta\nu_m$ lies between $\nu_Q(m-\frac{1}{2})$ (at $\theta = 0,180°$) to $\frac{-\nu_Q}{2}(m-\frac{1}{2})$ at $\theta = \pm 90°$.

Magic angle sample spinning is capable of averaging the first order quadrupole effect to zero,[24] but only in the limit that the spinning frequency is greater than the nuclear quadrupole frequency. In general this condition is seldom satisfied.

For nuclei with large quadrupole moments in strong electric field gradients, even the second order quadrupole effect is large. The second order effect shifts the center of gravity of the spectrum, broadens the central line, and can only be partially reduced by MAS. ^{133}Cs has a very small quadrupole moment and does not show significant second order effects.

The combined effects for a nucleus having both CSA and first order quadrupole effects can be calculated for the single crystal and powder cases. The simplest case is that which has both asymmetry parameters (η) equal to zero with colinear principal axes. The line that is shifted and broadened by CSA (equation 8) will be split into 2I lines by the first order quadrupole effect. The resonance position for each transition $m \rightarrow m-1$ will then be

$$\nu = \nu_L + (m - 1/2)\,\frac{\nu_Q}{2}\,(3\cos^2\theta - 1) \quad \text{so that}$$

$$\nu = \nu_L + \left[\, \nu_L\delta + (m - 1/2)\,\nu_Q \,\right] \left(\frac{3\cos^2\theta - 1}{2} \right) . \qquad (5.15)$$

The limits on the chemical shift are

$$-\frac{1}{2}\,|\nu_L\delta + (m - \tfrac{1}{2})\,\nu_Q| \leq |\nu - \nu_L| \leq |\nu_L\delta + (m - \tfrac{1}{2})\,\nu_Q|$$

The shape function of the powder pattern for each m can be derived as

$$g(\nu) = \frac{d\cos\theta}{d\nu} = \left| \frac{3^{1/2}}{(\nu_L\delta + (m - \frac{1}{2})\nu_Q \left(\frac{2\nu - \nu_L}{(\nu_L\delta + (m - \frac{1}{2})\,\nu_Q)} + 1 \right)^{1/2}} \right| \qquad (5.16)$$

The effect of CSA on the first order quadrupolar powder pattern is to extend both the high frequency and low frequency limits of nuclear transitions with $m > 1/2$ and to compress the breadth of the powder pattern for nuclear quadrupolar transitions with $m \leq -1/2$. The central line assumes the profile of a CSA broadened line in the absence of quadrupolar interactions.

V.A.3 EXPERIMENTAL

The synthesis of salts with complexed cesium cations used in this study followed the procedures of Metz *et al.*[9] for salts complexed with C222, and those of Pedersen[14] for salts complexed with crown ethers. A stoichiometric methanol solution containing reagent grade salt and vacuum-sublimed complexant was warmed gently until all components were dissolved. Butanol was added until the solution was saturated. The solution was placed in a flat crystallization dish in

a dust free area. Evaporation of the methanol left crystalline material in a butanol slurry. The crystals were first filter-dried and then oven-dried at ~70°C.

^{133}Cs NMR spectra were obtained at three frequencies: at 65.61 MHz with a home-built 11.75T spectrometer[25] (pulse length 4.5 ms and 10 s delay time); at 47.24 MHz with a Bruker 8.45T spectrometer (pulse length 6.0 ms and 10 s delay time); and at 23.62 MHz with a Bruker 4.23T spectrometer (pulse length 4 → 6 ms and 3 s delay time). Magic angle sample spinning with the two high frequency instruments used an Andrews-Beam spinning system. The rotors were made of either Delrin or d_8-polymethyl methacrylate. Spinning rates were between 2 and 4 KHz. Measurements at 23 MHz used a Doty dual bearing spinning system. The rotors were made of either sapphire or Delrin. Spinning rates were between 1.5 and 3 KHz. All measurements were made at room temperature. Static spectra were obtained with the same probes but with no spinning gas. Single crystal studies were done in the Doty probe by fixing a large single crystal (~2mm^3) onto a rotor wall with Apiezon N grease. All chemical shifts were measured with respect to a value of 0 ppm for Cs^+(aq) extrapolated to infinite dilution.

V.A.4.

RESULTS AND DISCUSSION

V.A.4.a. MAS-NMR of Simple Salts and Complexed Salts

The corrected chemical shifts and linewidths of several simple salts and complexed simple salts as determined by MAS-NMR are summarized in Table 21.

The simple cesium salts show a paramagnetic shift from the

Table 21: Chemical Shifts and Linewidths of Simple Cesium Salts With and Without Complexed Cations.

Compound	δ(ppm)[a]	$\Delta\nu_{1/2}$(Hertz)[b]
Cs^+SCN^-	+190	190
Cs^+Cl^-	+232	125
Cs^+Br^-	+264	
Cs^+I^-	+284	420
Cs^+TPB^-	undetected	---
$Cs^+(18C6)\cdot SCN^-$	+ 73	100
$Cs^+(18C6)\cdot I^-$	+171	280
$Cs^+(18C6)_2\cdot SCN^-$	- 59	70
$Cs^+(18C6)_2\cdot I^-$	- 59	47
$Cs^+(18C6)_2\cdot TPB^-$	- 43	80
$Cs^+(15C5)_2\cdot I^-$	+ 29	90
$Cs^+(15C5)_2\cdot SCN^-$	+ 32	108
$Cs^+C222\cdot SCN^-\cdot H_2O$	+50, +275	210, 420
$Cs^+C222\cdot SCN^-$	+238	140
$Cs^+C222\cdot I^-$	+232, 254	63, 135
$Cs^+C222\cdot Cl^-$	+167	860

[a] Chemical shift relative to a value of 0 ppm for $Cs^+_{(aq)}$ at infinite dilution.

[b] Full width at half height.

gaseous Cs° resonance position of ~550 ppm.[26] The chemical shift increases with increasing polarizability of the anion, ranging from +190 ppm relative to the chemical shift of $Cs^+(aq)$ for the thiocyanate salt to +284 ppm for the iodide. Ramsey[27] described the paramagnetic shift in terms of the change in the total angular momentum about the nucleus in one state relative to another. For the ionic cesium halides, for example, the magnitude of the shift is proportional to the energy gap between the ground state and an excited state that has electron density provided by an electron donor in Cs p or d orbitals. An anion which is a better electron donor provides stronger overlap and hence a larger chemical shift. Of the alkali halides Cs^+ is expected to show the greatest shifts, since the unoccupied p, d and f orbitals provide lower lying excited states than are available in the lighter alkali metals.

One-to-one complexes of simple salts with 18C6 were isolated for the iodide and thiocyanate. The large Cs^+ cation is not fully coordinated by the complexant molecule; thus, it still has a significant ability to interact with coordinating anions. The chemical shifts of these salts are upfield from the corresponding simple salts by some 110 ppm. The effect of interaction of the cation with the lone pairs on the crown ether oxygens is not as strong as that of any of the anions studied. There is, however, still a strong dependence on the counter-ion.

Compounds with a 2:1 mole ratio of complexant to cation were prepared from several simple salts with both 15C5 and 18C6. The 18C6 sandwich systems show a remarkably constant chemical shift as a function of the anion, δ = -59 ppm for the iodide and thiocyanate, and

δ = -43 ppm for the tetraphenyl borate. These shifts are close to the value of the chemical shift seen at high complexant concentrations in various solvents.[8] This invariance to the anionic environment indicates that the Cs^+ ion is well shielded by the crown ether sandwich from strong interactions with the anion. The paramagnetic Ramsey shift is thus due only to the interaction of Cs^+ with the twelve ether oxygens.

The chemical shifts of $Cs^+(15C5)_2 \cdot X^-$ salts are also upfield from the pure simple salts, and show only a weak dependence on the anion. The chemical shift range is +28±4 ppm for the iodide, bromide and thiocyanate salts; however, the previously established order for paramagnetic shift based on the anion donicity does not hold. Further, the chemical shift is about 90 ppm downfield from the $Cs^+(18C6)_2^-$ resonance. This suggests a stronger paramagnetic Ramsey interaction with the oxygens of 15C5 than with the oxygens of 18C6, and that the anion does not directly interact with Cs^+ in either case. In the structures of the two compounds, $Cs^+(15C5)_2 \cdot I^-$ [28] and $CS^+(18C6)_2 \cdot Na^-$ [29], the mean Cs-O distance in the 18C6 sandwich is significantly longer than that in the 15C5 sandwich

$$(\overline{Cs\text{-}O}_{18C6} = 3.35\text{Å}; \overline{Cs\text{-}O}_{15C5} = 3.15\text{Å})$$

This reduction in interatomic distances results in stronger electronic overlap of oxygen lone pairs with Cs orbitals in the case of the smaller complexing agent. The sensitivity to the Cs-O distance also implies that the small variations in the chemical shifts of the sandwiched cations from one salt to another may result from small changes in the mean Cs-O distances. For example, the +16 ppm shift

seen in $Cs^+(18C6)_2 \cdot TPB^-$ relative to $Cs^+(18C6)_2 \cdot I^-$ may be the result of shortened Cs-O distances in the TPB salt because of the conformational changes in the crown ether required to accommodate the bulky anion.

The three dimensional cryptand 222 (C222) is also able to form complexes with Cs^+, but only in a 1:1 ratio. Mei et al.[8] and Kauffmann et al.[9] studied the complexation of $Cs^+C222 \cdot X^-$ in several solvents for X^- = TPB^- and SCN^-. The temperature dependence of the resonance line of Cs^+C222 implied an equilibrium between an exclusive complex, stable at high temperatures, and an inclusive complex stable at low temperatures. With X^- = octanoate in a THF-H_2O mixture, a two line spectrum indicative of slow inclusive-exclusive exchange was observed.[9] The crystal structure of $Cs^+C222 \cdot SCN^- \cdot H_2O$ was solved[15] and consists of only the inclusive complex, in which the cation is completely encapsulated by the three polyether strands of the cryptand. In the exclusive complex, the cation interacts strongly with only two of the polyether strands of the cryptand, and not as strongly with the third. This leaves the cation exposed to its anionic environment on one face. The chemical shifts of inclusive complexes of Cs^+ with C222 in solution occur at ~240 ppm and are independent of the solution environment, whereas the exclusive complex displays a range of chemical shifts that are strongly dependent on the solvent, counter ion and temperature of the solution.

Solid state MAS-NMR results indicate that the inclusive complex may be seen either alone or in addition to the signal of an exclusive complex. The inclusive complexes of Cs^+C222 salts show a range of chemical shifts near 240 ppm. $Cs^+C222 \cdot SCN^- \cdot H_2O$ was the only sample to show only the signal of inclusive complex at 238 ppm, very close to

the value seen in solution. The mean Cs-O distance in this salt is 2.96 Å,[15] so the Ramsey shift is due to a strong interaction of Cs^+ with oxygen lone pairs. In those samples that show both inclusive and exclusive peaks, the range of chemical shifts is large for both peaks, indicating that ionic packing may place constraints on the available conformations of the C222 molecule.

The linewidths of the MAS-NMR spectra are, for the most part, between 50 and 400 Hz. Two trends are apparent in the comparison of linewidths. First, lines are broader at high frequency than at low frequency and, second, at any given frequency the more paramagnetic the chemical shift, the broader is the MAS-NMR line. These observations indicate that the broadening mechanisms are probably chemical shift anisotropy and dipolar broadening.

V.A.4.b. Static Spectra of Simple Salts and Complexed Salts

V.A.4.b.i. Cs_2SO_4. The importance of anisotropic chemical shift interactions in Cs salts can be seen in the Cs_2SO_4 spectra, at two resonance frequencies. The primary broadening mechanism in this salt was originally attributed to first order quadrupolar effects.[30] Figure 19 shows the static spectrum of Cs_2SO_4 at 52.48 MHz and at 23.62 MHz. The line is broadened by a factor of about 2.2 by increasing the applied magnetic field by the same factor. Chemical shift anisotropy broadening is proportional to the applied field, whereas quadrupolar effects are constant on a frequency scale and are a less significant effect at high fields. Therefore, the broadening mechanism in this non-cubic quadrupolar solid is due to chemical shift anisotropy rather than quadrupolar effects as was originally

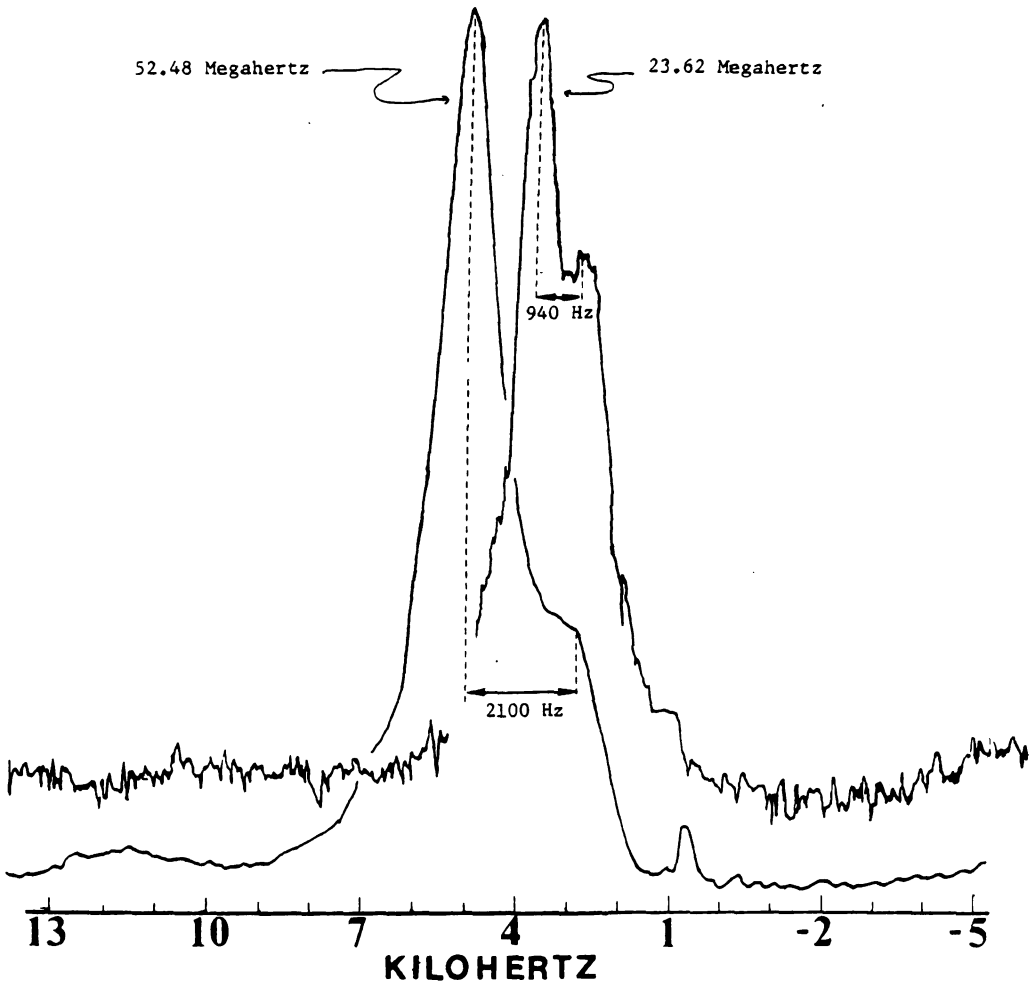


Figure 19. ^{133}Cs static NMR spectra, comparing linewidths of Cs_2SO_4 at 52.48 MHz and 23.62 MHz.

assumed.[30]

V.A.4.b.ii. Static spectra of $Cs^+(18C6)_2 \cdot I^-$ and $Cs^+(15C5)_2 \cdot I^-$. The static ^{133}Cs NMR spectra of $Cs^+(18C6)_2 \cdot I^-$ and $Cs^+(15C5)_2 \cdot I^-$ were studied to deduce the nature of the chemical shift and quadrupolar interactions. The parameters of these interactions give some insight into the local structure about the Cs cation. The static spectrum at 52.48 MHz for $Cs^+(18C6)_2 \cdot I^-$ is shown in Figure 20a. The spectrum consists of a broadened central component near the isotropic chemical shift and unsymmetrically spaced quadrupolar satellites. The same compound was studied at 23.62 MHz and the spectrum is shown in Figure 20b. The spectrum has an unstructured, broadened central line with symmetrically spaced quadrupolar satellites. This simple, low field spectrum reveals a nuclear quadrupolar coupling frequency, ν_Q = 6.4 KHz that corresponds to a quadrupolar coupling constant, e^2qQ/h = 89.6 KHz. The central line in the low field spectrum has a width at half height of 1200 Hz which is due to CSA broadening, and dipolar broadening. The strength of the chemical shift interaction is proportional to the field; the high field spectrum reflects the addition of a significant CSA contribution to the resonance. The central transition has a peak width at half height more than two times greater than the low field case, and has structure that reflects axial symmetry of the CSA tensor. The shape of the central peak is consistent with an asymmetry parameter (η) of zero. The width of the peak gives the anisotropy parameter $\delta \cong 32$ ppm. The anisotropic ($m \neq 1/2$) quadrupolar spin transitions are not equally spaced because of the CSA interaction. Equation 16 was used to generate the static powder

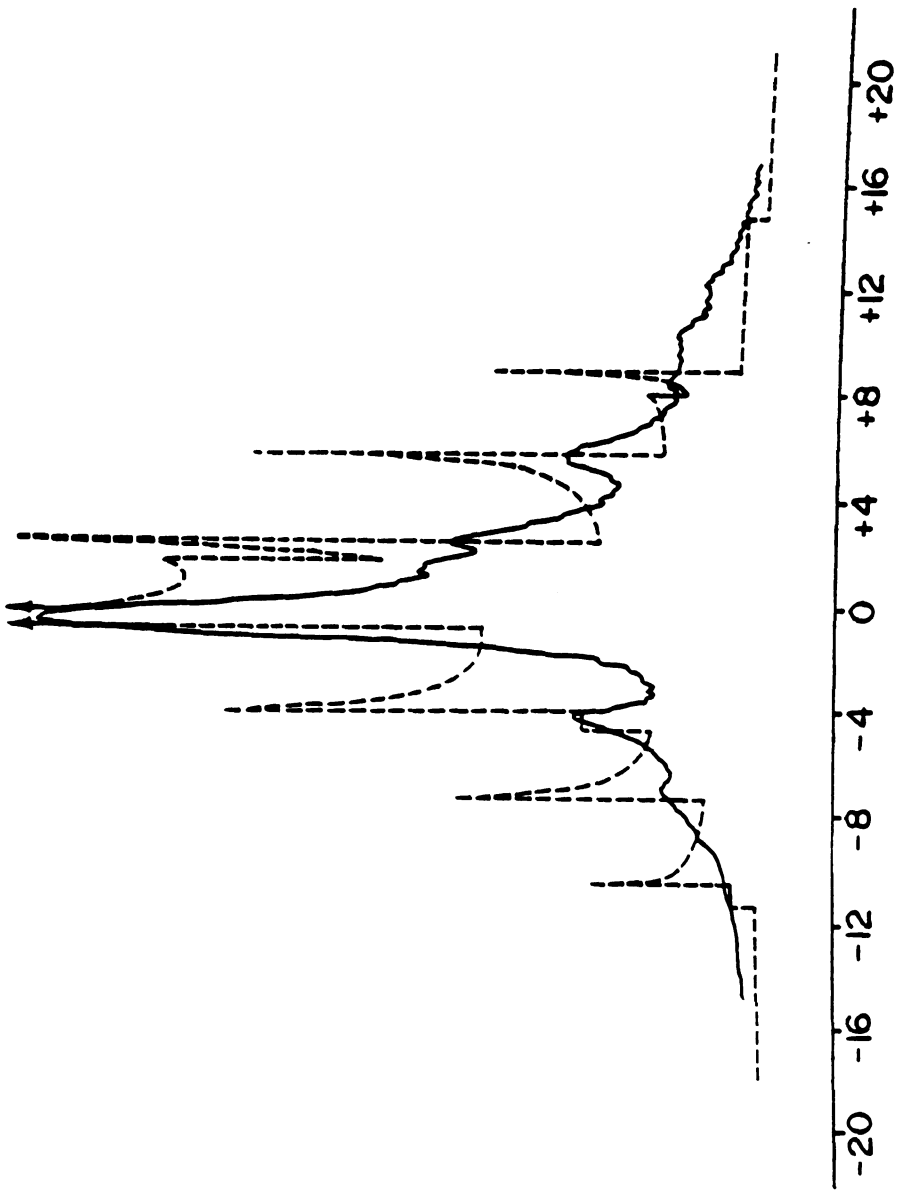


Figure 20a. Static ^{133}Cs NMR spectra of $Cs^{+}(18C6)_2 \cdot I^{-}$ at 52.48 MHz. The dashed lines are calculated spectra from equation 16 for $\nu_Q = 6.5$ KHz, $\delta = 32$ ppm and $\eta = 0$.

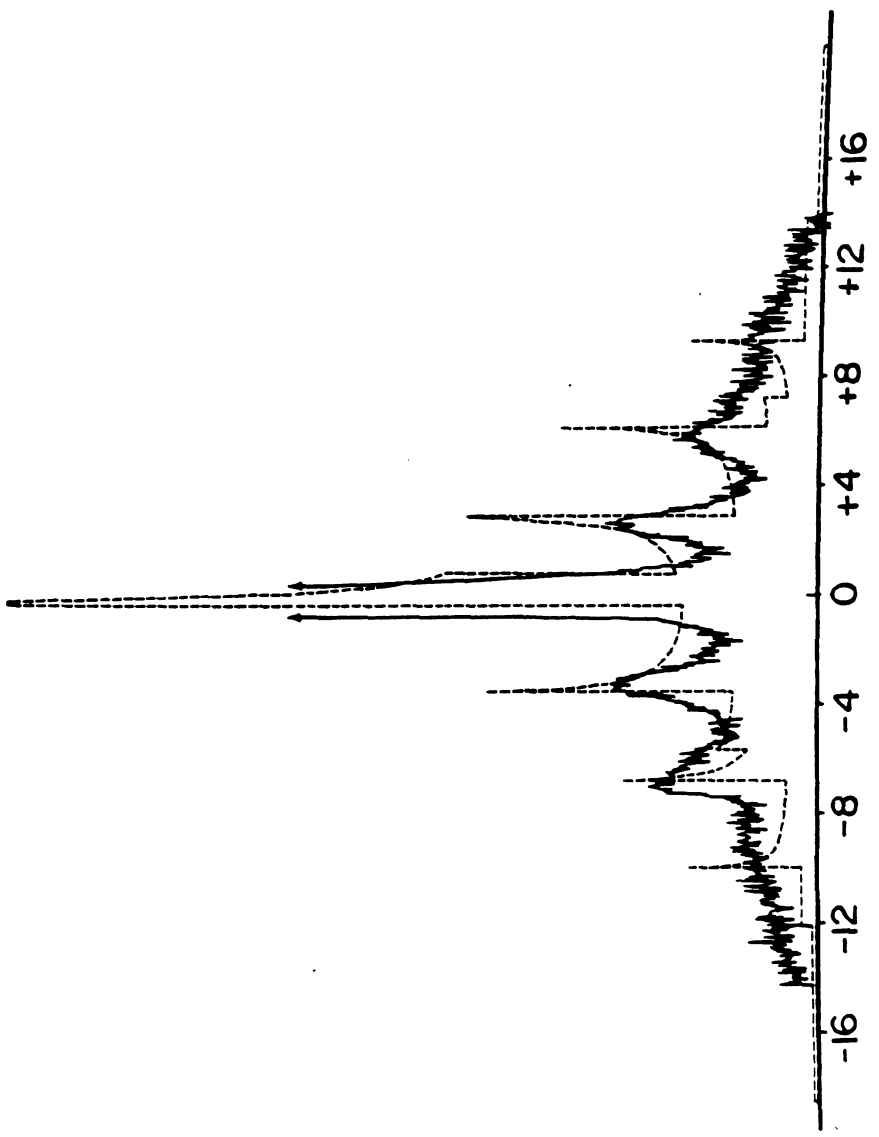


Figure 20b. Static ^{133}Cs NMR spectra of $Cs^{+}(18C6)_2 \cdot I^{-}$ at 23.62 MHz. The dashed lines are calculated spectra from equation 16 for $\nu_Q = 6.5$ KHz, $\delta = 32$ ppm and $\eta = 0$.

lineshape for the two Larmor frequencies with estimated values of ν_Q = 6.4 KHz, δ = 32 ppm and η = 0. The results are shown as dotted lines along with the actual spectra in Figure 20a & and 20b. The agreement is good in both cases although no refinement of the parameters was performed.

It has been assumed throughout this discussion that second order quadrupole effects are negligible in these salts. The second order quadrupole interaction shifts the center of gravity of the spectrum, the shift being given by[31]

$$\nu_L - \nu = \nu_Q^2/(\nu_L \cdot 30) \{ I(I+1) - 3/4 \} (1 + \eta^2/3) . \quad (5.17)$$

At ν_L = 23.62 MHz the calculated center of gravity is shifted by only 3.5 Hz and at ν_L = 52.48 MHz by only 1.56 Hz. Thus, second-order quadrupole effects can be neglected.

The static powder spectrum of $Cs^+(15C5)_2 \cdot I^-$ was measured only at 23.62 MHz. The spectrum is shown in Figure 21. The central line displays an asymmetric profile similar to that at high fields for $Cs^+(18C6)_2 \cdot I^-$, but without any of the non-central quadrupolar transitions apparent. A simulation of the central line yielded the chemical shift parameters δ = 52 ppm, η = 0. The calculated lineshape is shown as the dotted line in Figure 21. The absence of observable quadrupolar satellites indicates that the quadrupole coupling constant is large. The sweepwidth of this spectrum was 30 KHz.

The effect of the dipolar interaction of crown ether hydrogens with the ^{133}Cs nucleus on the static line of $Cs^+(15C5)_2 \cdot I^-$ may be calculated by equation (5.1). The cesium-hydrogen distances are obtained from the crystal structure of $Cs^+(15C5)_2 \cdot I^-$.[28] Interactions

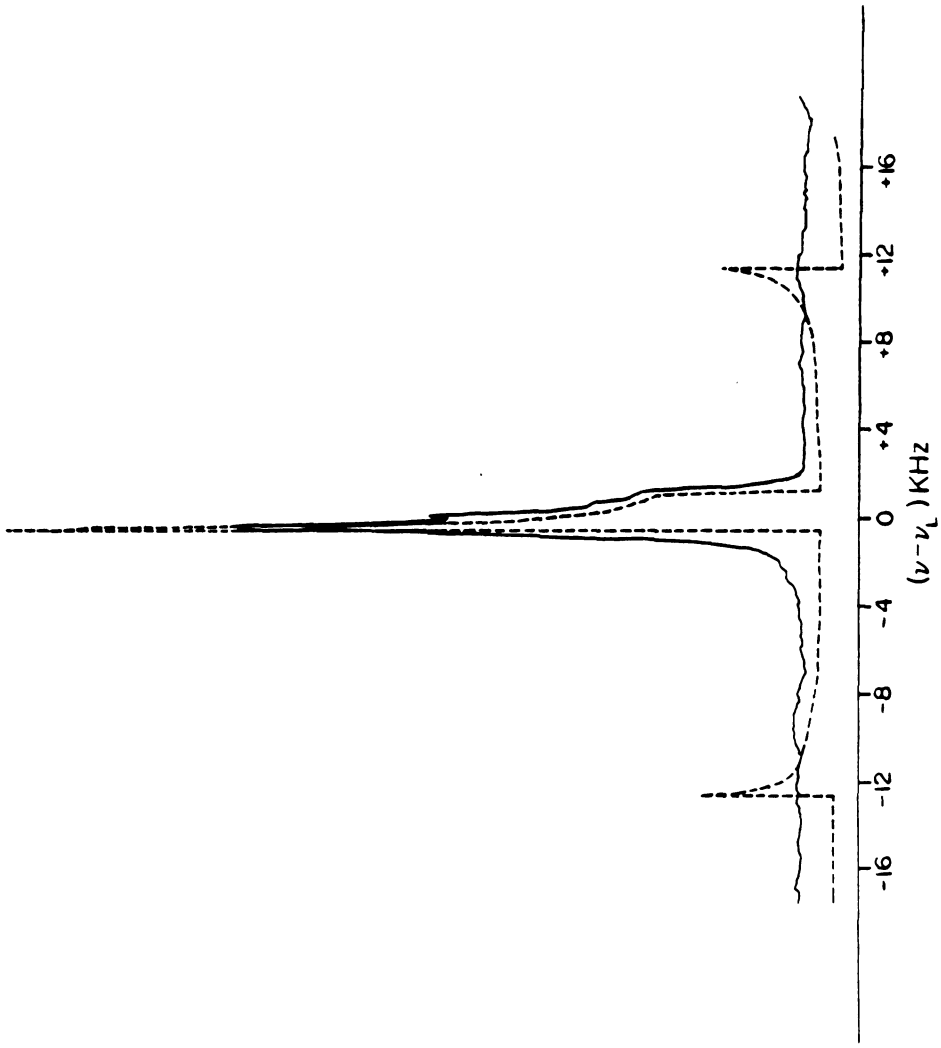


Figure 21. Static ^{133}Cs NMR spectrum of $Cs^+(15C5)_2 \cdot I^+$ at 23.62 MHz. The dashed line is the calculated spectrum from equation 16 for $\nu_Q = 30.5$ KHz, $\delta = 52$ ppm and $\eta = 0$.

with nuclei other than ^{1}H are small because of the low isotopic abundance of ^{13}C and ^{17}O, as well as the small magnetogyric ratios that they possess relative to ^{1}H. The nearest 83 hydrogen distances from Cs^{+} range from 3.054 A to 6.981 A. Given the magnetogyric ratios of ^{133}Cs and ^{1}H, $\gamma_{Cs} = 3.509 \times 10^{3}$ and $\gamma_{H} = 2.657 \times 10^{4}$, the Gaussian width at half height is calculated to be 1540 Hz. The dipolar broadening is superposed on the CSA width of the central line, which is ~1850 Hz at ν_{L} = 23.62 MHz. The breadth of the static peak is consistent with the magnitudes of the CSA and dipolar interactions.

The crystal structure of $Cs^{+}(18C6)_{2}\cdot I^{-}$ is not known, but the structure of another salt containing the sandwiched complexed cation, $Cs^{+}(18C6)_{2}\cdot Na^{-}$, was determined at 213 K. The compound includes 74 cesium-hydrogen distances between 3.848 A and 7 A. The Gaussian dipolar linewidth is calculated to be 1350 Hz; the width at half height of the static lines in both $Cs^{+}(18C6)_{2}\cdot I^{-}$ at room temperature and $Cs^{+}(18C6)_{2}\cdot Na^{-}$ at 250 K is 800 Hz. The static linewidth of $Cs^{+}(18C6)_{2}\cdot Na^{-}$ was measured at ~ 200 K to be 1300 Hz. The dipolar interactions of hydrogens with Cs^{+} in $Cs^{+}(18C6)_{2}$ are convoluted with CSA and quadrupolar interactions in the complexed cation; it is possible the reduced linewidth at high temperatures is due either to thermal motion of the hydrogens that partially averages their dipolar contribution to the width of the peak, or to a structural transition that increases Cs-H distances. The chemical shift of Cs^{+} in $Cs^{+}(18C6)_{2}\cdot Na^{-}$ is ~60 ± 2 ppm for all temperatures measured; the latter explanation may be ruled out since a significant increase in the Cs-H distances would require Cs-O distances to increase as well, a change that would affect the chemical shift. The static ^{23}Na NMR

spectrum of the Na^- ion more accurately reflects the reduced dipolar field at high temperatures, since the width of Na^- is primarily due to dipolar coupling with hydrogens. Figure 22 shows the static ^{23}Na NMR spectra of Na^- at 200 K and at 250 K, with widths at half height of 2300 Hz and 1350 Hz respectively. The calculated linewidth from equation 1, with $\gamma_{Na} = 7.076 \times 10^3$, is 2500 Hz, in good agreement with the low temperature linewidth.

In order to confirm the nature of the quadrupolar coupling in $Cs^+(15C5)_2 \cdot I^-$, a large single crystal was grown and studied in the MAS-probe. The experiment was done by fixing the crystal at a random orientation in the rotor and measuring the spectrum at several orientations. Two spectra are shown in Figures 23a and 23b for different orientations of the crystal with respect to the magnetic field. They consist of two closely spaced lines near the isotropic value of the chemical shift with quadrupolar satellites on either side of the central peaks. The isotropic chemical shift is indicated by the dashed line at +29 ppm. The two lines labelled A and B are the central transitions of chemically identical cations which have non-parallel principal axes. The crystal structure of $Cs^+(15C5)_2 \cdot I^-$ has been determined; the crown ether sandwich structure lies on a screw axis which requires successive complexed cations along the c-direction in the crystal to be rotated by 90° about $\underline{c}$. Thus, two orientations of the crown ethers about a Cs^+ do exist. Each central resonance line has associated with it a full quadrupolar spectrum, the components of central transitions A and B are labelled a and b respectively. The single crystal line pattern may be calculated as a function of the angle θ, between the principal axes of the quadrupolar and CSA

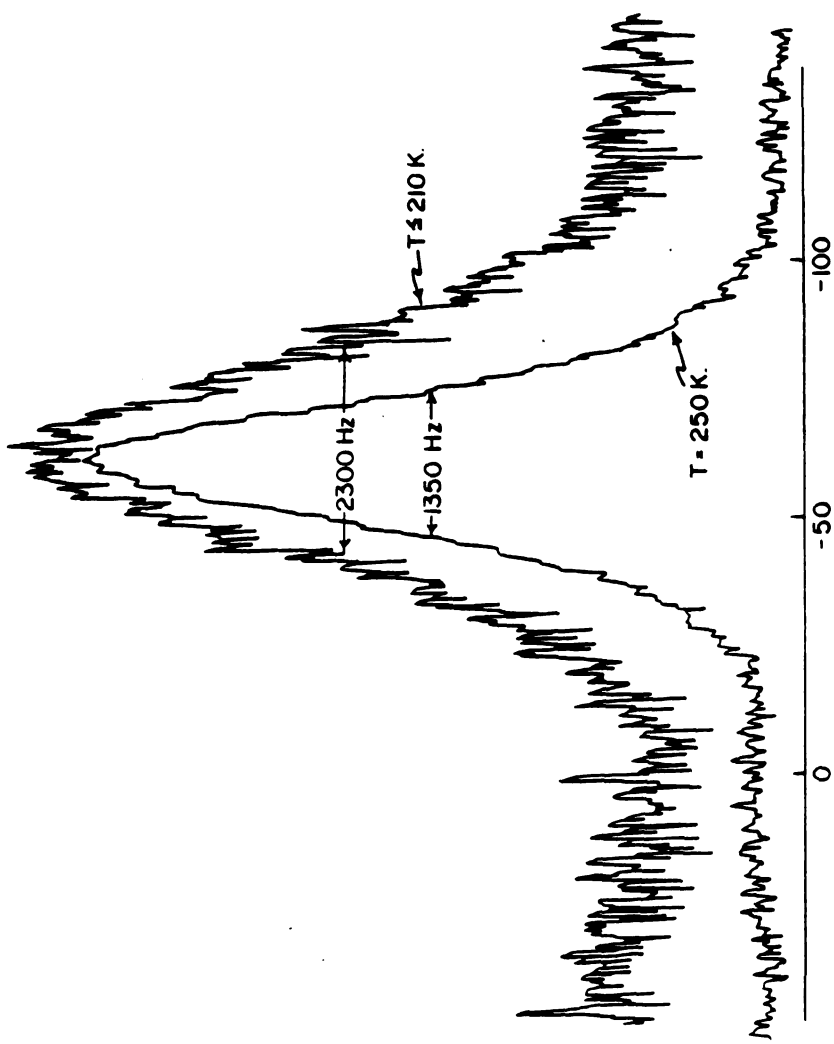


Figure 22. Static ^{23}Na NMR of $Cs^{+}(18C6)_2 \cdot Na^{-}$ at two temperatures, $T \leq 210$ and 250 K.

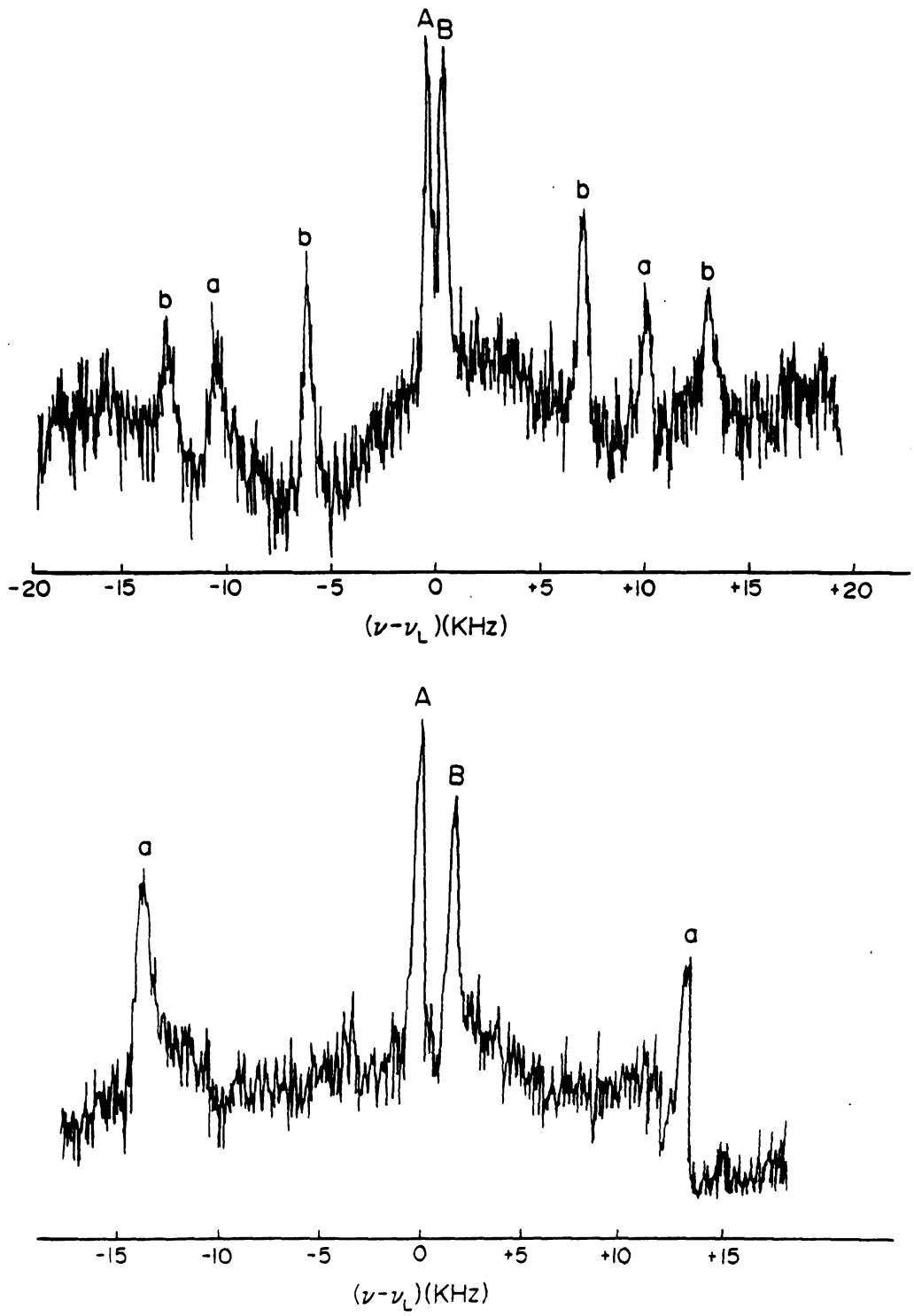


Figure 23. Single crystal ^{133}Cs NMR spectra of $Cs^{+}(15C5)_2 \cdot I^{-}$ at two random orientations. Lines labelled A and B are central $-^1/_2 \longleftrightarrow {}^1/_2$ transitions for two $Cs^{+}(15C5)_2$ orientations. Lines labelled a and b represent corresponding non-central quadrupolar transitions.

interactions if it is assumed that $\Theta_Q = \Theta_{CSA}$, and $\eta = 0$ by equation (5.15). For any one magnetically unique cation the unknown Θ and ν_Q may be calculated as follows. The shift of the central line from the isotropic chemical shift has no quadrupolar component, so Θ can be calculated with the value of δ obtained from the powder spectrum. ν_Q may then be calculated from the position of any of the satellites. The validity of the assumptions, and the value of δ, may be checked by comparison of the results for several central line positions. The results for the four lines of Figures 23a and 23b are given in Table 22. A quadrupole coupling frequency ν_Q = 30,500 Hz, which corresponds to a quadrupole coupling constant of 427 KHz, is obtained for $Cs^+(15C5)_2 \cdot I^-$, from each of the three observable lines. The fourth orientation predicts that the nearest quadrupolar satellites should occur beyond the sweep width of the spectrum. The results are consistent with the previously measured value of δ, and the assumption that $\Theta_Q = \Theta_{CSA}$ appears to be a good one.

A single crystal of $Cs^+(18C6)_2 \cdot I^-$ was studied in the same fashion as the 15C5 salt. The static single crystal spectrum (Figure 24) consists of only one line with quadrupolar satellites. While the structure of this compound is not known, crystal structures of the electride and sodide of $Cs^+(18C6)_2$ have been determined.[18,28] The packing in these salts indicates that only a single orientation of the two crown ethers about Cs^+ with respect to some axis in the crystal occurs. The NMR spectrum indicates that similar packing exists in the iodide.

Table 22. Parameters of Anisotropic Interactions in the NMR of Single Crystals of $Cs^{+}(15C5)_2 \cdot I^{-}$ at 23.62 MHz.

orientation	$\nu-\nu_L$(Hz)[b]	θ[c]	$3\cos^2\theta-1$	$\Delta\nu$(Hz)[d]	ν_QkHz[e]
A	-415	71°	-0.689	21,000	30,500
B	255	46.5°	0.424	13,010	30,679
A	1204	0°	2.00	unobserved[f]	---
B	-550	80.2°	-0.913	27,694	30,333

[a] Refers to spectra shown in Figure 23.

[b] The frequency shift due to CSA interactions of the central line from the isotropic chemical shift.

[c] θ is calculated from $\nu-\nu_L$ by equation 5.8.

[d] $\Delta\nu$ is twice the measured frequency difference between peaks corresponding to successive quadrupolar transitions; $\Delta\nu$ is the same as $\nu-\nu_L$ in equation 5.15.

[e] ν_Q is calculated from equation 5.15.

[f] Calculated to appear outside of the spectral width used.

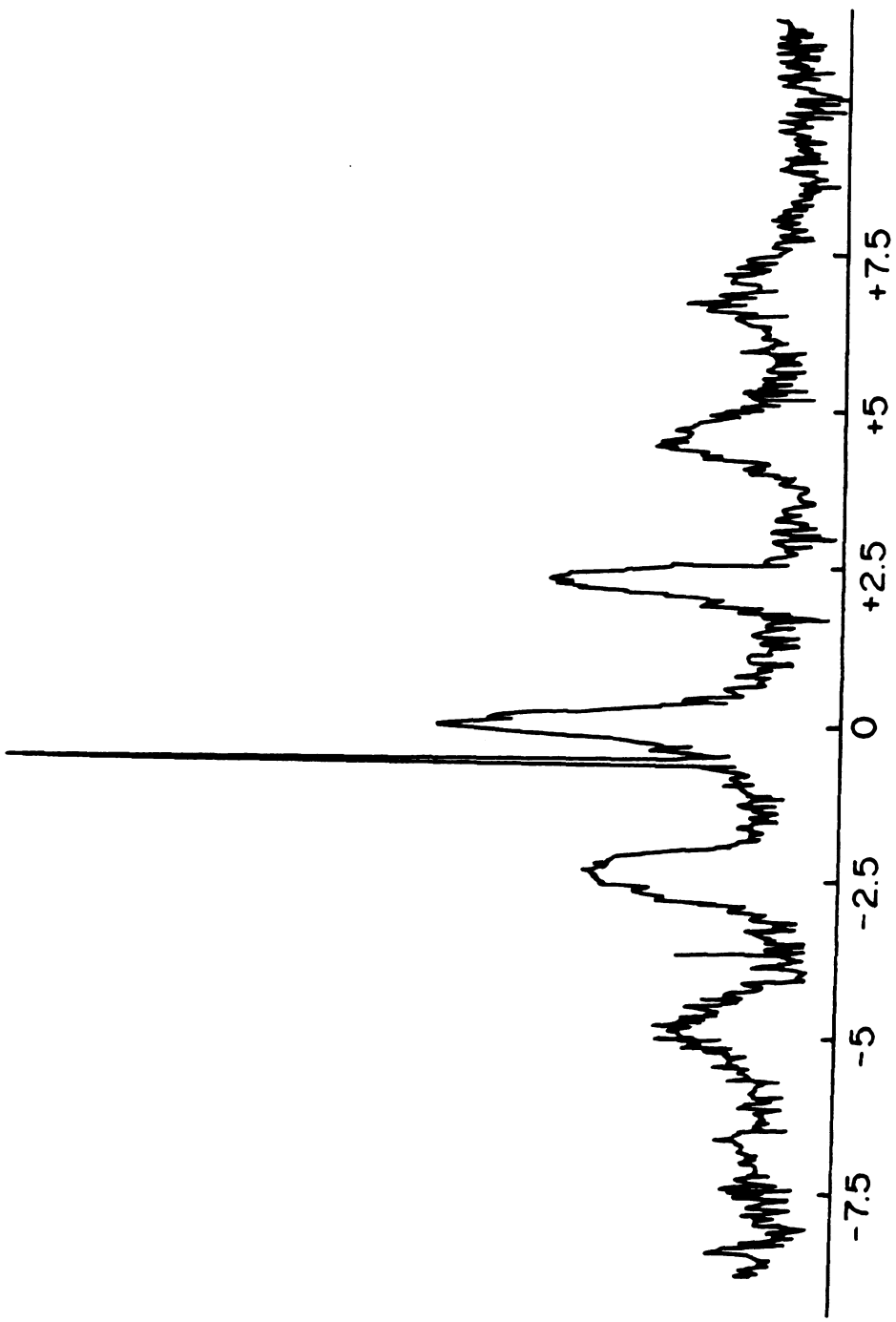


Figure 24. Single crystal ^{133}Cs NMR spectrum of $Cs^+(18C6)_2 \cdot I^-$ at a random orientation. The sharp spike is apparently due to residual solution.

V.A.5. CONCLUSIONS

It is clear that the local structure about a ^{133}Cs cation has a profound effect on its nuclear magnetic properties. Solid state NMR is sensitive to various anisotropic interactions; dipolar, CSA and quadrupolar interactions are usually significant. The isotropic chemical shift is an important property of a complexed Cs salt; it serves as a fingerprint for the nature of the complexation, inclusive or exclusive, and is even characteristic of the complexant. This information is typically accessible by MAS techniques.

Solid state spectra allow the parameters that characterize the strength and anisotropy of the line broadening mechanisms to be deduced; these are in turn strongly dependent on the local structure about the nucleus. The broadening characteristics of the iodides, $Cs^+(15C5)_2 \cdot I^-$ and $Cs^+(18C6)_2 \cdot I^-$, were determined by powder and single crystal static NMR methods. The spectra of other $Cs^+(18C6)_2$ salts have been measured, and have identical powder patterns, so that the anionic environment is relatively unimportant, just as was the case for the isotropic chemical shift. The iodide salts may serve as models for other salts with the complexed cesium cation, including the alkalides and electrides.[32] As new compounds are synthesized from more exotic complexants, NMR methods will remain as important probes, not only of the stoichiometry, but of local structural characteristics as well. Obviously, NMR does not add to the structural analysis of those compounds that can be studied by single crystal diffraction methods. There are, however, many compounds that contain complexed Cs^+, but which are not easily crystallized, so that a solid basis for structural information cannot be obtained. An understanding of how

known structural characteristics affect the isotropic and anisotropic magnetic interactions will provide a powerful tool for studies of ^{133}Cs containing compounds.

V.A.6. ACKNOWLEDGMENT

This research was supported by National Science Foundation - Solid State Chemistry Grants DMR 79-21979 and DMR 8414154. We are grateful to Dr. P. B. Smith of the Dow Chemical Company, and to Dr. E. Oldfield and Mr. B. Montez at the University of Illinois at Urbana-Champaign and Dr. Peter Edwards of Cambridge University, England for assistance in obtaining and interpreting NMR spectra.

V.A.7. REFERENCES:

1) Ellaboudy, A.; Tinkham, M. L.; VanEck, B.; Dye, J. L.; Smith, P. B.; **J. Phys. Chem.**, 1984, **88**, 3852.

2) Ellaboudy, A.; Dye, J. L.; **J. Am. Chem. Soc.**, 1983, **105**, 6490.

3) Dye, J. L.; Ellaboudy, A.; **Chem. Br.**, 1984, **20**, 21.

4) Tinkham, M. L.; Dye, J. L.; **J. Am. Chem. Soc.**, 1985, **107**, 6129.

5) Tinkham, M. L.; Ellaboudy, A.; Dye, J. L.; Smith, P. B.; **J. Phys. Chem.**, 1986, **90**, 14.

6) Ellaboudy, A. Dye, J. L.; **J. Mag. Res.**, 1986, **66**, 491.

7) IUPAC names: 18-Crown-6; 1,4,7,10,13,16 hexaoxa-cyclooctadecane, abbreviation 18C6. 15-Crown-5; 1,4,7,10,13 pentaoxa-cyclopentadecane, abbreviation 15C5. Cryptand (2.2.2); 4,7,13,16,21,24 hexaoxa-1,10 diaza-bicyclic (8,8,8) hexacosane, abbreviation C222.

8) Mei, E.; Popov. A. I.; Dye, J. L.; **J. Phys. Chem.**, 1977, **81**, 1677.

9) Kauffman, E.; Dye, J. L.; Lehn, J.-M.; Popov, A. I.; **J. Am. Chem. Soc.**, 1980, **102**, 2274.

10) Gutowsky, H. S.; McGarvey, B. R.; **J. Chem. Phys.**, 1953, **21**, 1423.

11) Andrew, E. R.; **Arch. Sci.** (Geneva), 1959, **12**, 103.

12) Andrew, E. R.; Bradbury, A.; Eades, R. G.; **Nature**, 1959, **183**, 1802.

13) Lowe, I. M.; **Phys. Rev. Lett.**, 1959, **12**, 285.

14) Pedersen, C. J.; **J. Am. Chem. Soc.**, 1967, **89**, 7017.

15) Moras, D.; Metz, B.; Weiss, R.; **Acta. Cryst.** 1973, **B29**, 388.

16) Poonia. N. S.; Bajaj, A. V.; **Chem. Rev.**, 1979, **79**, 389.

17) Dobler, M.; Phizackerly, R. P.; **Acta Cryst.**, 1974, **B30**, 2748.

18) Dawes, S. B.; Huang, R. H.; Ward. D. L.; Dye, J. L.; unpublished results, this laboratory.

19) Van Vleck, J. H.; **Phys. Rev.**, 1948, **74**, 1168.

20) Andrew, E. R.; **Intl. Rev. Phys. Chem.**, 1981, **1**, 195.

21) Bloembergen. N.; Rowland, T. J.; **Acta Metal.**, 1953, **1**, 733.

22) Abragam, A.; "The Principles of Nuclear Magnetism", Oxford University Press (London) 1961.

23) Cohen, M. H.; Reif, F.; **Solid State Physics**, 1957, **5**, 321.

24) Cunningham, A. C.; Day, S. M.; **Phys. Rev.**, 1966, **152**, 287.

25) Meadows, M. D.; Smith, K. A.; Kinsey, R. A.; Rothgreb, T. M.; Skarjune, S. P.; Oldfield, E.; **Proc. Nat'l. Acad. Sci., U.S.A.**, 1982, 79, 1351.

26) Beckmann, A.; Boklen, K. D.; Elke, D.; **Z. Phys. Chem.**, 1975, **79**, 173.

27) Ramsey, N. F.; **Phys. Rev.**, 1950, **77**, 567.

28) Dawes, S. B.; Ward, D. L.; Dye, J. L., unpublished results, this laboratory.

29) Dawes. S. B.; Fussa, O.; Ward, D. L.; Dye, J. L., unpublished results, this laboratory.

30) Tzalmona, A.; Andrew, E. R.; **Proceedings of the Congress of Magnetic Resonance and Related Phenomena**, 1974, **Ampere 18th**, 241.

31) Behrens, H.-J.; Schnabel, B.; **Physica**, 1982, **114B**, 185.

32) Dawes, S. B.; Ellaboudy, A.; Dye, J. L.; J. Am. Chem. Soc. (companion paper).

V.B. Cesium-133 Solid State Nuclear Magnetic Resonance Spectroscopy of Alkalides and Electrides

V.B.1. INTRODUCTION

Complexed cations, formed from simple alkali metal cations and crown ethers or cryptands, are sufficiently stable to reduction that salts with alkali metal anions ($M^+C \cdot N^-$, known as alkalides) or with electrons at the anionic sites ($M^+C \cdot e^-$, known as electrides) can be formed. The first alkalide, $Na^+C222 \cdot Na^-$, (C222 = cryptand[2.2.2]) was synthesized in 1974[1] and has been characterized by single crystal x-ray diffraction,[2] optical spectroscopy,[3,4] powder conductivity,[5] and more recently by photoelectron emission, and fluorescence spectroscopy.[6] The nature of the sodium anion was best characterized by NMR, first in solutions of $Na^+C222 \cdot Na^-$ in ethylamine,[7] THF and methylamine[8] and later in the solid state with polycrystalline $Na^+C222 \cdot Na^-$.[9] The chemical shift of the anion in each case was identical to the chemical shift calculated for Na^- in the gaseous state.[10] Thus, the sodium anion was shown to be a genuine spherical anion with a filled 3s orbital that is not strongly affected by its environment.

To date more than 40 alkalide and electride compounds have been synthesized, and Magic Angle Sample Spinning NMR (MAS-NMR) has become a primary technique for their characterization. The oxidation state if an ion or element in a compound is easily identified by the chemical shift of the resonance. The cationic and anionic species in an alkalide, which always contains two alkali metal nuclei, can often be properly identified by NMR. Signals have been detected for

$Li^+ \cdot C$ [23], $Na^+ \cdot C$ [9,11], Na^- [9-11], K^- [12,13], Rb^- [14], $Cs^+ \cdot C$ and Cs^- [15-17] in the solid state. In these expressions, C represents a cryptand such as C222 or a crown ether, such as 18-crown-6 (18C6) or 15-crown-5 (15C5). No signal was detected for either K^+C [13] or $Rb^+ \cdot C$ [14] due to extreme quadrupolar line broadening that could not be reduced by MAS.

In addition to the identification of alkali metal cations and anions in alkalides and electrides by measurement of the chemical shifts, analysis of the line shape, both in static and MAS narrowed spectra, can provide information about the interaction of the ions with their environments. The quadrupole coupling constants have been determined for $^{23}Na \cdot C222$ [11] ($e^2Qq\backslash h$= 1.2 MHz η = 0.1), $Cs^+(18C6)_2$ [17] ($e^2Qq\backslash h$= 89.6 KHz $\eta \approx 0$), and $Cs^+(15C5)_2$ [12] ($e^2Qq\backslash h$= 427 KHz $\eta \approx 0$), and upper limits for the quadrupole coupling constants have been established for Na^- ($e^2Qq\backslash h \leq 0.23$ MHz),[11] K^- ($e^2Qq\backslash h \leq 0.1$ MHz[12], and Rb^- ($e^2Qq\backslash h \leq 1.3$ MHz).[14] The relatively small value of the quadrupolar interaction in the anions testifies to their large, diffuse, spherical nature.

Some properties of ^{133}Cs NMR in alkalides and electrides have been previously reported.[15,16] The isolation of the electride, $Cs^+(18C6)_2 \cdot e^-$, was verified by ^{133}Cs NMR when the compound with a 1:2 ratio of Cs to 18C6 gave an NMR spectrum that consisted of a single paramagnetically shifted peak. The compound of stoichiometry Cs(18C6) was shown to be the ceside, $Cs^+(18C6)_2 \cdot Cs^-$, by virtue of a two peak spectrum: $Cs^+(18C6)_2$ resonated near the value seen for other diamagnetic $Cs^+(18C6)_2$ salts, and Cs^- was shifted upfield by about 160 ppm. One other cesium compound, $Cs^+(18C6)_2 \cdot Na^-$, has been characterized by ^{133}Cs NMR.[9]

V.B.2. EXPERIMENTAL

Alkalides and electrides are synthesized by anaerobically introducing stoichiometric amounts of the metal(s) and complexant into an evacuable vessel. The materials are dissolved in polar amines and/or ethers, and crystals are formed by first lowering the dielectric constant of the solution by adding less polar amines and/or ethers and then cooling the solution. The compounds are very reactive and must be handled under vacuum or in inert atmosphere at all times. Further, most compounds must be handled at temperatures below -20°C to avoid thermal decomposition. Details of the purification of materials and of the synthetic methods have been described elsewhere.[18,19]

NMR spectra were obtained at 47.24 MHz (at Dow Chemical Co., 8.4 Tesla, pulse length = 6.0 μs, 10s repetition time) and at 65.61 MHz (at the University of Illinois, 11.7 Tesla, pulse length = 4.5 μs, 10s repetition time) with Andrews Beam type MAS probes. The spinning gas was cooled by passing it through a copper coil immersed in an acetone/dry ice bath. Spinning rates were 2 to 4 KHz. The Andrews spinners were made of Delrin or d_8-polymethyl methacrylate. The spinners were loosely filled with the polycrystalline sample in an inert (dry N_2) atmosphere glove bag. Spectra were also obtained at 23.62 MHz (4.2 Tesla, pulse length = 4.5 μs, 2.5 s. repetition time) with a variable temperature Doty probe. Doty rotors were made of sapphire and were equipped with low temperature end caps. The rotors were firmly packed with the polycrystalline samples in inert atmosphere bags. Spinning rates were typically 1.5 to 3 KHz. The spinning gas was passed through a liquid nitrogen heat exchanger and

warmed to a set temperature with a feedback-controlled heater. Temperatures of the spinning gas were measured with a copper constantan thermocouple inserted in the gas line just before the stator. Further calibration of the temperature is described later. Chemical shifts were measured with respect to a value of 0 ppm for $Cs^+(aq)$ at infinite dilution. Observed linewidths are reported as $\Delta\nu_{1/2}$, the full width at half height.

V.B.3. RESULTS AND DISCUSSION

V.B.3.a. ^{133}Cs MAS-NMR of Alkalides

The chemical shifts and linewidths of ^{133}Cs ions in alkalide salts, determined by MAS-NMR are summarized in Table 23.

The chemical shifts of complexed cations in both the 18C6 and 15C5 sandwiched systems are nearly independent of the anion, and agree with the values found for halides and thiocyanates.[17] $Cs^+(18C6)_2$ resonates at -60±2 ppm for all salts except the ceside. The cesium cation is coordinated by 12 crown ether oxygens. The constant chemical shift implies that the structure of the complex does not differ significantly in the sodide, potasside and rubidide salts. The spectrum of $Cs^+(18C6)_2 \cdot Cs^-$ is discussed in detail below. $Cs^+(15C5)_2$ resonates at +25 ±1 ppm for both the sodide and potasside, and at 29 ppm[20] for the rubidide. $Cs^+(15C5)_2 \cdot Cs^-$ has not been isolated to date. The width of an MAS narrowed line may be due either to second order anisotropic effects (i.e., 2nd order quadrupolar broadening) or to incompletely narrowed first order effects. Insufficient spinning speeds, and/or slight deviations of the spinning angle could contribute to residual first order linewidths.[21] A trend in the MAS

Table 23. Chemical Shifts and Linewidths of ^{133}Cs MAS-NMR Lines in Alkalides and Electrides.

Compound	δ(ppm)[a]	$\Delta\nu_{1/2}$(Hz)[b]	Spectrometer[c]
$Cs^+(18C6)_2 \cdot Na^-$	-61	40	B
	-62	160	C
$Cs^+(18C6)_2 \cdot K^-$	-58	85	B
	-58	188	C
$Cs^+(18C6)_2 \cdot Rb^-$	-57	115	B
	-57	65	C
$\underline{Cs}^+(18C6)_2 \cdot Cs^-$	-41, -49		A
	-51	175	B
	-40, -50		C
$Cs^+(18C6)_2 \cdot \underline{Cs}^-$	-212		A
	-238	350	B
	-210	435	C
$Cs^+(15C5)_2 \cdot Na^-$	+24	130	A
$Cs^+(15C5)_2 \cdot K^-$	+24	270	A
$Cs^+(15C5)_2 \cdot Rb^-$	+29	250	A
$CsC222 \cdot e^-$	138,238	320,140	B
	134,240	500,356	C

a) Chemical shift relative to a value of 0 ppm for Cs^+(aq) at infinite dilution.

b) $\Delta\nu_{1/2}$ is the full width at half height.

c) The spectrum was observed at applied fields of
A) 4.2 T B) 8.4 T C) 11.7 T

linewidths of Cs complexes is apparent: cesium cations have a broader line for larger counter ions. Second order quadrupolar effects have been shown to be negligible in complexed Cs^+ salts, so a systematic residual linewidth must account for the trend in peakwidth. The dipolar linewidth of Cs^+ from coupling with surrounding hydrogen atoms has been shown to be temperature dependent in Cs^+ (crown ether)$_2$ salts.[17] Rapid motion of hydrogens on the crown ethers averages some of the dipolar anisotropy, and reduces the static linewidth. Larger anions would hinder rapid motion and increase the width of both the static spectrum and the imperfectly narrowed spectrum. No systematic decoupling experiments have been attempted.

The only ceside that has been synthesized and fully characterized is $Cs^+(18C6)_2 \cdot Cs^-$.[22] The structure of this compound has been determined,[23] and shows that Cs^- is an extremely large anion with a radius of 3.3-3.5 Å. Cs^- is a unique alkali metal anion because low energy d and f orbitals are available. Both the cation and anion are paramagnetically shifted from the pure ground state character of the gaseous ions, and both have temperature dependent values of the chemical shift. At low temperatures ($T < 225$ K) the resonance position of the cation is -40 ±1 ppm and the anion has a chemical shift of -213 ±2 ppm. Between 230 K and 285 K the cationic peak splits into two lines, one at -40 ppm, the other at -50 ppm. The relative intensities of the two lines are approximately 1:1 throughout this temperature range. The anion shifts downfield (from -212 to -205 ppm) with increasing temperature between 230 K and 285 K. Above 285 K the anion peak is at -240 ppm, and only the -50 ppm peak appears for the cation.

The chemical shift of Cs^+ in inclusive crown ether and cryptand complexes is due to the Cs-O overlap, and is inversely related to the mean Cs-O distance.[17] The change in paramagnetic shift of $Cs^+(18C6)_2 \cdot Cs^-$ from other $Cs^+(18C6)_2$ salts results from a different conformation of the 18C6 molecules in the ceside which shortens the mean Cs-O distance at T = 225 K from 3.35 A to 3.30A.[23] The temperature dependence of the cationic chemical shift indicates that two different environments exist for the complexed cation; between 230 and 285 K they co-exist, perhaps as dimers, and above 285 K only the 50 ppm environment is seen. No structural information exists to describe the -50 ppm resonance, but the complexed cation probably has a mean Cs-O contact distance shorter than those seen in salts of other anions, and longer than that of the low temperature phase.

The chemical shift for Cs^- is notable for the strong paramagnetic shift from that calculated for $Cs^-(g)$. The chemical shift of other alkali metal anions have been measured in solution and in the solid state; Table 24 shows these resonance positions and compares them to the calculated values for $M^-(g)$. It is clear that the paramagnetic deviation from the calculated values of the chemical shift as well as the range of observed shifts increases with increasing atomic weight. The paramagnetic Ramsey shift is inversely proportional to the energy required to promote an electron to excited states. Clearly Cs^- and Rb^- have low lying d and f orbitals available, whereas Na^- and K^- retain more nearly pure s^2 configurations.

The Cs^- shift with temperature suggests that the admixture of excited state character is very sensitive to the local structure about

Table 24. Summary of Calculated and Representative Observed Chemical Shifts of Alkali Metal Anions.

Compound	σ(M)	σ(M) observed		T(K)	Ref.
	Calculated	Solution	Solid		
^{133}Cs	-346.4				25
Cs/C222/THF		-292		202	8
$Cs^+(18C6)_2 \cdot Cs^-$			-213	220	This Work
$Cs^+(18C6)_2 \cdot Cs^-$			-240	285	This Work
^{87}Rb	-213.6				25
Rb/12/C4		-191			26
Rb/C222/EA		-185		233	8
Rb/C222/THF		-197		227	8
$Cs^+(15C5)_2 \cdot \underline{Rb}^-$			-189(2)		14
$Cs^+(18C6)_2 \cdot \underline{Rb}^-$			-194	~260	14
^{39}K	-103.4				25
K/Cs/12C4		-94.2			13
$K/15C5/Me_2O$		-101			12
$K^+(15C5)_2 \cdot K^-$			-105(1)		12
$Cs^+(18C6)_2 \cdot K^-$			-115(10)		12
^{23}Na	-63.4				25
Na/C222/THF		-62.8		269	8
Na/12C4		-61.8			26
$Na^+C222 \cdot Na^-$			-61	~260	9
$Cs^+(18C6)_2 \cdot Na^-$			-61	~260	9

the anion. The anion peak shifts gradually downfield by +10 ppm as the temperature is increased from 225 to 285 K. The small paramagnetic shift may be due to increased thermal motion of the crown ethers which reduces the effective radius of the anionic cavity. A smaller cavity favors the more confined electron density of 5d or 4f orbitals over the diffuse 6s orbital. The chemical shift changes by -35 ppm above 285 K, probably because of a phase change which increases the effective radius of the anionic cavity.

V.B.3.b. MAS-NMR of $Cs^+C222 \cdot e^-$

In contrast to the rich variety of alkalide and electride salts that contain sandwich complexes of Cs^+ with crown ethers, only two such compounds have been isolated with the Cs^+C222 cation. Indeed, until recently, when the structure of a crystal of the ceside, $Cs^+C222 \cdot Cs^-$, was determined by X-ray diffraction,[23] only the 1:1 compound of stoichiometry CsC222 had been isolated, regardless of the solution stoichiometry. Its ^{133}Cs MAS-NMR spectrum, shown in Figure 25, consists of two lines, whose relative intensities depend on the method of preparation of the sample. The two peak spectrum is similar to the inclusive/exclusive complex spectrum seen for $Cs^+C222 \cdot SCN^- \cdot H_2O$.[17] The absence of the Cs^- NMR peak was taken as evidence that the 1:1 salt is an electride.

Samples that were prepared from Cs rich mixtures of Cs and C222 tended to have both peaks, with nearly the same intensities (Figure 25a), while cryptand- rich starting mixtures and slowly grown crystals gave primarily the diamagnetic peak (Figure 25b). The two peaks are attributed to the presence of both inclusive and exclusive complexes of the cation. It is not clear whether a single crystallite is able

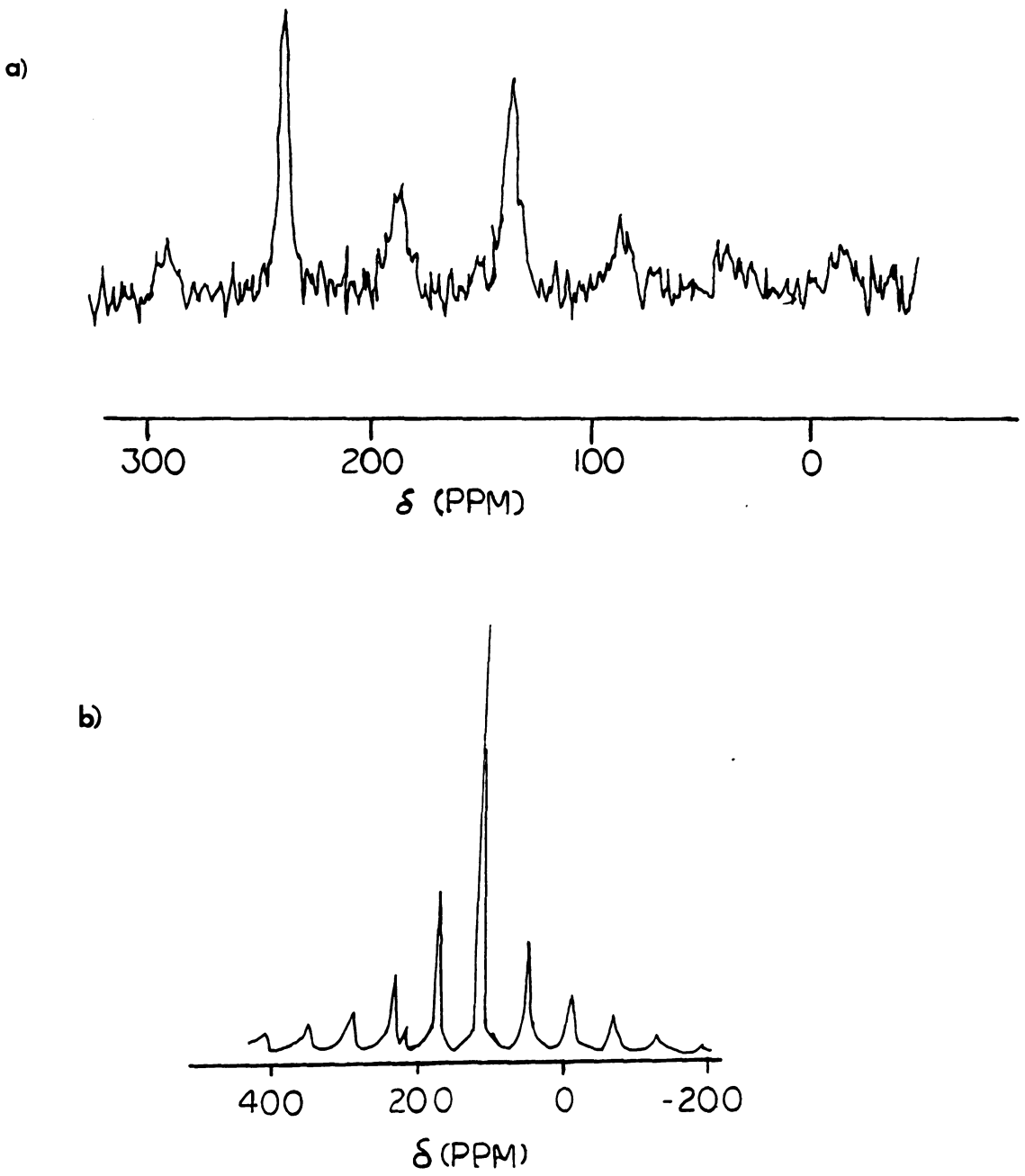


Figure 25. ^{133}Cs MAS-NMR spectrum of $Cs^{+}C222 \cdot e^{-}$, showing inclusive and exclusive complexed cations, prepared from solutions that contained excess quantities of a) cesium and b) C222. Other lines are spinning sidebands.

to support both types of complexed cations, or whether the polycrystalline sample contains a mixture of crystallites of pure inclusive complexed cations and of pure exclusive complexed cations.

Electron-electron interactions in the "electrides" are very strong. A sample taken from a batch with 1:1 stoichiometry was diamagnetic at all temperatures. Spin pairing is not uncommon in electrides; especially in compounds that contain cryptands as complexants. For example, LiC211 displays temperature dependent spin-pairing[27] below 50 K. $K^+C222 \cdot e^-$ and $Rb^+C222 \cdot e^-$ appear to have metallic character and the electronic susceptibility is dominated by a Pauli-type temperature-independent paramagnetism.[28]

The recent identification of ceside crystals in a preparation that was made in the same manner as the electrides[23] indicates the need for caution in interpreting the behavior of polycrystalline samples. The lack of an NMR signal due to Cs^- is not proof of its absence. For example, samples known to contain Rb^- showed no ^{87}Rb signal.[14] Thus, although the 1:1 stoichiometry and absence of a Cs^- NMR peak in CsC222 strongly suggest that it is an electride, final proof awaits determination of its crystal structure.

V.B.3.c. ^{133}Cs MAS-NMR of $Cs(18C6)_2 \cdot e^-$

The first reports of the synthesis and characterization of $Cs^+(18C6)_2 \cdot e^-$,[15] emphasized the electronic nature of the compound. $Cs^+(18C6)_2 \cdot e^-$ is a Curie-Weiss paramagnet which shows no magnetic ordering or spin pairing over the temperature range 1.5 to 250 K.[22] The d.c. conductivity indicates that the electride is a semiconductor with an intrinsic band-gap of 0.9 eV; however, the conductivity at X-band microwave frequencies gives an apparent band-gap of only ~0.1

eV.[22] The ^{133}Cs MAS-NMR was reported to consist of only one peak at +81 ppm. This paramagnetic shift from that of other $Cs^+(18C6)_2$ compounds could result from either a tighter coordination of the Cs^+ by the crown ethers, or from contact with the paramagnetic electron. NMR can be used to probe the interactions of the trapped electron with the complexed cations in the solid. Structural information now exists for $Cs^+(18C6)_2 \cdot e^-$;[29] the electride is nearly isostructural with $Cs^+(18C6)_2 \cdot Na^-$;[30] the mean Cs-O distance is 3.35 Å in each compound. The electride features a cavity at anionic sites in the lattice with a very low electron density.

The origin of the paramagnetic chemical shift in $Cs^+(18C6)_2 \cdot e^-$ is the Knight (or contact) shift. The Knight shift results from the strong local magnetic field generated at the nucleus of interest by paramagnetic electron density. The lowest energy unoccupied orbital in Cs^+ is the 6s orbital, which has a non-zero electron density at the nucleus, so that the cation should be very sensitive to any overlap with the paramagnetic trapped electron. The Knight shift is given by[31]

$$K(T) = \frac{8\pi}{3N_{AV}} < |\psi(0)|^2 > \chi(T) \qquad (1)$$

where $<|\psi(0)|^2>$ is the average electron density at the nucleus, and $\chi(T)$ is the magnetic susceptibility of the paramagnetic species. For a Curie-Weiss paramagnet, K(T) is proportional to 1/T, since $\chi(T)$ varies inversely with temperature. Preliminary attempts to measure the chemical shift as a function of temperature revealed a strong variation of the chemical shift with temperature that was approximately proportional to 1/T. Instrumental temperature control

and measurement were poor, however; resulting in inconsistent values from one determination to another.

Measurement of the temperature of the spinning gas prior to its entry into the stator suffers from poor contact of the thermocouple with the gas so that poorly controlled parameters (i.e. flow rate, heat leaks) affect the temperature reading. A different method, devised by English,[32] was therefore used. This method takes advantage of the known temperature dependence of the splitting of the chemical shifts of hydroxyl and methyl protons in methanol.[33] Over the range 220 K to 330 K the splitting, $\Delta\nu$, of the two peaks at 180 MHz may be used to calculate the temperature, T, by

$$T = 435.5 - 0.398\ \Delta\nu - 3.25 \times 10^{-4}\ \Delta\nu^2.$$

The method used to calculate the temperature of an electride sample was to alternately measure the proton splitting in methanol and the chemical shift of the electride at constant gas flow rates, and gas heater power. A value of the chemical shift of the electride was assumed to be at a known temperature if two alternate measurements of the proton splitting and the chemical shift remained constant. Four points measured in this way are shown in Figure 26. The chemical shift (in ppm) fits the equation

$$\delta(T) = \delta(\infty) + K(T) = -61 + \frac{4.06 \times 10^4}{T}\ .$$

The value of the chemical shift at infinite temperature [$\delta(\infty) = -61$ ppm] is nearly identical to the chemical shift of $Cs^+(18C6)_2$ seen in alkalides. This result correlates well with the structural data, since the complexed cations in $Cs^+(18C6)_2 \cdot e^-$ and $Cs^+(18C6)_2 \cdot Na^-$ have nearly identical structures.

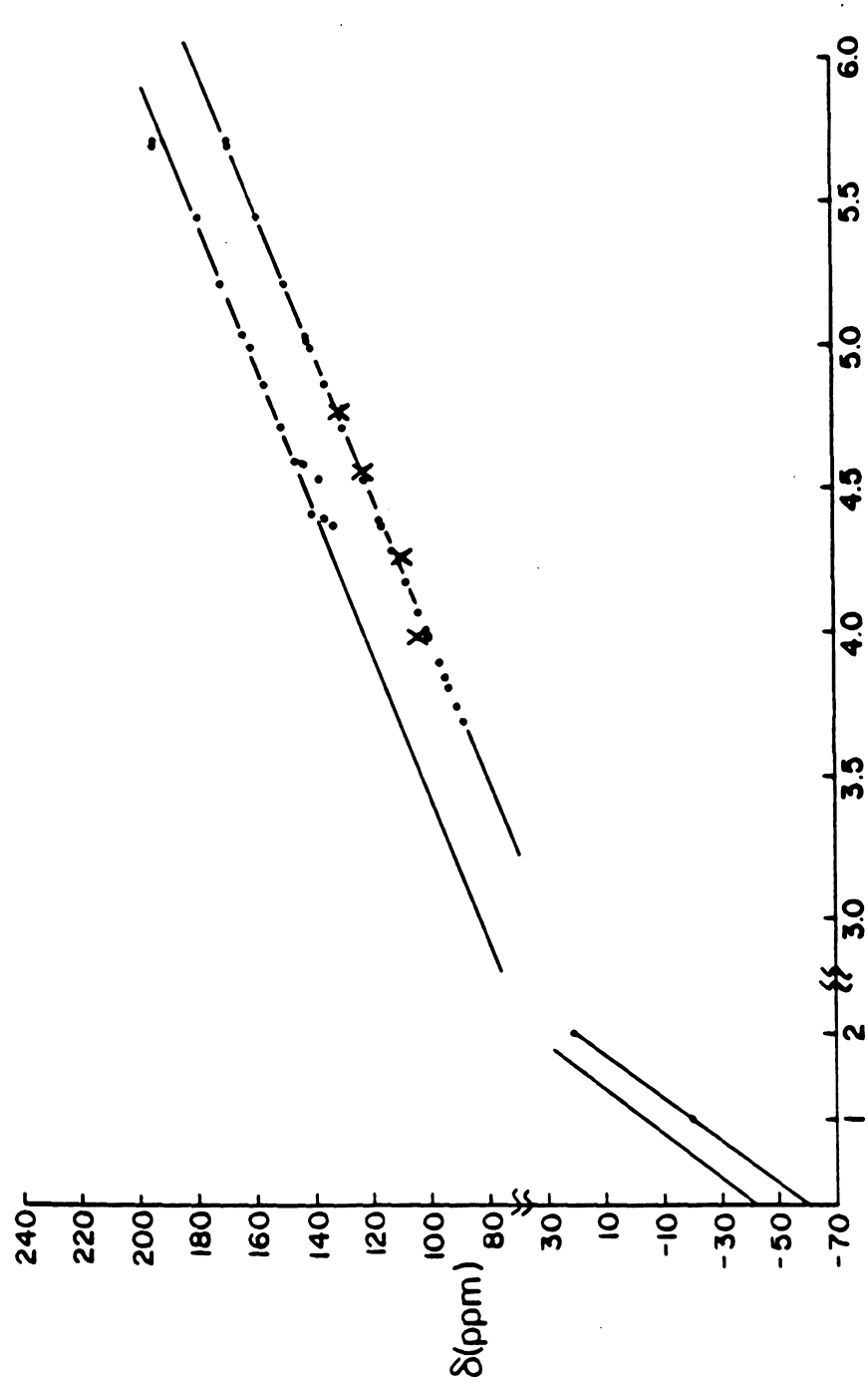


Figure 26. The chemical shift versus T^{-1} for $Cs^{+}(18C6)_2 \cdot e^{-}$. The temperatures of points marked by x were calibrated by comparison with the dipolar splitting of protons in methanol. Other points were constrained to lie on the best-fit line through the four calibrated points.

The fraction of atomic s-orbital character of the trapped electron may be calculated from the magnetic susceptibility and the slope of the Knight shift versus 1/T. The electronic part of the magnetic susceptibility of $Cs^{+}(18C6)_2 \cdot e^{-}$ at 250°K is $\chi_m^e = 1.37 \times 10^{-3}$ emu/mole. The fractional atomic character is defined as

$$F = \frac{\langle|\psi_o^2|\rangle}{\langle|\psi_o|^2\rangle_{atom}} , \qquad 5.19$$

where $\langle|\psi_o|^2\rangle_{atom}$, the electron density at the nucleus for an isolated gas atom, has been estimated to be 2.645×10^{25} $e^{-}cm^{-3}$.[34] The data given above yield $F = 3.3 \times 10^{-4}$ for $Cs^{+}(18C6)_2 \cdot e^{-}$. Table 25 compares this value with that of other paramagnetic cesium-containing systems. Lelieur and Rigny measured both the magnetic susceptibilities[35] and the Knight[36] shifts of ammonia solutions and found that solutions containing 2 to 20 mole percent Cs (MPM) had fractional atomic characters ranging from 0.04 to 0.60. The overall electron density in the electride is 1.1×10^{21} e^{-}/cm^3 at 216 K which is approximately the same as that of a 1.5 MPM solution of Cs in ammonia. Yet the contact density at the metal nucleus in the electride is much smaller than in cesium solutions in ammonia, amines and other solvents. Metal ions and solvated electrons in ammonia form loosely bound ion-aggregates in the intermediate range of metal concentrations betwen 10^{-2} MPM and 10^{-3} MPM, the majority of which are spin-paired and undetectable by magnetic resonance methods.[37] The paramagnetic species that do exist are probably 'solvent-shared' ion-pairs, which consist of a solvated electron and a cation, each with their complete solvation shells.[37] The spin density at the nucleus in metal ammonia solutions between 10^{-2} and 1 MPM is nearly constant[37] with $F \approx 2 \times 10^{-3}$, nearly an order

of magnitude higher than in the crystalline electride.

The effect of reducing the dielectric constant of the medium is to create stronger interionic interactions, mediated by weaker solvent interactions so that paramagnetic ion pairs have more excess electron density at the nucleus as indicated in Table 25 for solutions of cesium in methylamine (MA), ethylamine (EA) and isopropyl amine (iPA). The contact interaction in frozen solutions of Cs in the highly polar solvent HMPA indicates a different type of excess electron character.[39] Two EPR signals are detected in these solids, one with high contact density at the Cs nucleus ($F \approx 0.73$) attributed to solvated cesium atom and the other with a much lower contact density ($F \approx 0.01$).[34] The electron in the low atomic character species was presumed to occupy a large hydrogenic wavefunction centered on the screened solvated Cs cation, but having very little Cs orbital character.[34]

The trapped electron in $Cs^{+}(18C6)_2 \cdot e^{-}$ has exceptionally low cesium s-orbital character relative to other electron-cesium systems. The cesium cationic charge is apparently very well screened by its interaction with the crown ether oxygen lone pairs. A monomeric species, in a state similar to that described as the low s-orbital species of Cs/HMPA solutions,[34] might be invoked for the electride. The monomer in this case would have one electron in an extended orbital centered on each complexed cation. A major problem with this description of the crystal as a collection of "expanded atoms" is the observed weak electron-electron interactions. An alternative and better explanation of the low value of F is that the paramagnetic electron density is largely located in the anionic cavities, localized

Table 25. Fractional Atomic Character of Some Cs····e^- Solutions and Solids.

Compound	electron density	F	ref.
$Cs^o(g)$	2.645×10^{25}	1.00	34
Cs (metal)	1.56×10^{25}	0.59	b
Cs:NH_3			
15 MPM	2.12×10^{24}	0.08	36
5 MPM	7.94×10^{23}	0.03	36
Cs:HMPA			
Solvated Atom	1.93×10^{25}	0.73	34
Expanded orbital	6.08×10^{22}	2.3×10^{-3}	34
Cs:MA[a] 273 K	7.42×10^{24}	0.05	34
Cs:EA[a] 273 K	5.03×10^{24}	0.19	34
Cs:iPA[a] 273 K	7.14×10^{24}	0.27	34
$Cs(18C6)_2 \cdot e^-$	8.75×10^{21}	3.3×10^{-4}	this work

[a]Abbreviations used: HMPA - hexamethyl phosphoramide
MA - methylamine, EA - ethylamine, iPA - isopropylamine

[b]Chemical shift from Reference 36. Paramagnetic susceptibilities of Cs metal were calculated from $\chi_{metal} - \chi_{core}$, values from Reference 40.

by the coulombic attraction to eight nearest complexed cesium cations. The electron density at each cesium nucleus would then be the sum of the weak interactions with the eight nearest trapped electrons. Studies of electrides doped with sodium anions, described below, favor the latter interpretation of the electronic state in $Cs^{+}(18C6)_2 \cdot e^{-}$.

The chemical shift data shown in Figure 26 include a number of points at temperatures that were not calibrated as described above. Rather, the temperature corresponding to each data point was estimated from the peak position so that the plot of $\delta(T)$ vs $1/T$ was constrained to be linear. At temperatures below 225 K the spectrum became more complex, in that a second peak, paramagnetically shifted from the original, appeared as a shoulder at ~225 K and increased in relative intensity as the temperature was decreased. The two peaks are separated by about 20 ppm, and show a parallel temperature dependence. The increased paramagnetism does not necessarily signal increased electron density at the nucleus, but may instead be a measure of decreased Cs-O distances in the complexed cation. Extrapolation of the paramagnetic peak to infinite temperature gives a chemical shift f -40 ppm, the same as that seen in low temperature $Cs^{+}(18C6)_2 \cdot Cs^{-}$ salts. Apparently, at low temperatures, the complexed cation gradually shifts to a second conformation with a reduced mean Cs-O distance. The transition does not appear to be first order, and does not go to completion to the lowest temperatures measured.

V.B.3.d. ^{133}Cs MAS-NMR of Mixed Alkalide-Electride Salts.

The similar nature of the complexed cation in various electrides and alkalides suggests that crystals of mixed stoichiometry might be prepared. Reduction of the trapped electron density by

partial substitution of diamagnetic anions for anionic trapped electrons could significantly alter electron-electron interactions in these materials.

The preparation of mixed alkalide/electride materials was attempted by using two different alkali metal anions, Cs^- and Na^-, in the presence of $Cs^+(18C6)_2$ complexed cations, for several alkalide mole fractions, x. Figure 27 shows the ^{133}Cs MAS-NMR spectrum for a sample of overall stoichiometry $Cs^+(18C6)_2 \cdot Cs^-_{(.5)} \cdot e^-_{(.5)}$. The spectrum consists of three lines together with their spinning sidebands. The resonance positions are clearly those of the pure ceside (δ = -50 and -230 ppm) and the pure electride (δ = 77 ppm at 294 K). Several other samples resulted in similar spectra with only the relative intensities of the lines varying. These results demonstrate that doping electrons into the ceside lattice, or cesides into the electride lattice is clearly unfavorable. The anionic radius of each of these species has been determined,[29] the radius of the anionic cavity of the trapped electron in $Cs^+(18C6)_2 \cdot e^-$ is 2.2 Å whereas Cs^- has a radius of ~3.3 Å in $Cs^+(18C6)_2 \cdot Cs^-$. Lattices which are able to support each anion separately are, in this case, unable to co-exist. Mixtures of pure electrides and pure alkalides were useful for establishing the temperature characteristics of the alkalide based on the known temperature dependence of the electride peak.

The ^{133}Cs MAS-NMR spectra of samples with overall stoichiometry $Cs^+(18C6)_2 \cdot Na^-_x e^-_{1-x}$ are shown in Figure 28, for x = 0.2 and 0.8 respectively. These spectra consist of five lines at -61, +26, +42, +57 and +73 ppm. The extreme peaks are due to $Cs^+(18C6)_2$ in the pure sodide (-61 ppm) and in the pure electride (73 ppm). The three

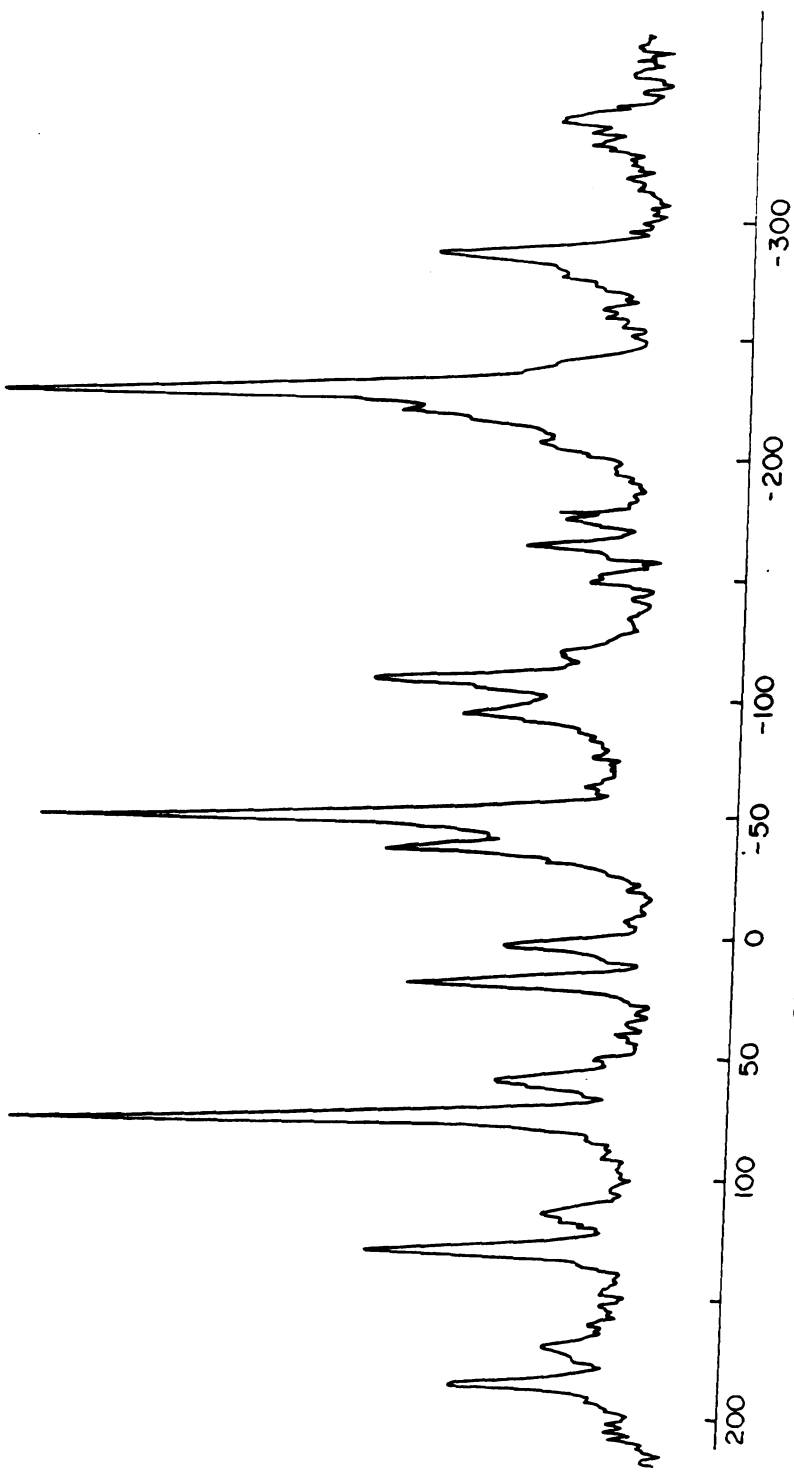


Figure 27. ^{133}Cs MAS-NMR spectrum of the product obtained from initial stoichiometry $Cs^{+}(18C6)_3$. Peaks at -50 ppm and -230 ppm are $Cs^{+}(18C6)_2$ resonances, the peak at 77 ppm is a $Cs^{+}(18C6)_2{\cdot}e^{-}$ resonance. Other features are spinning sidebands.

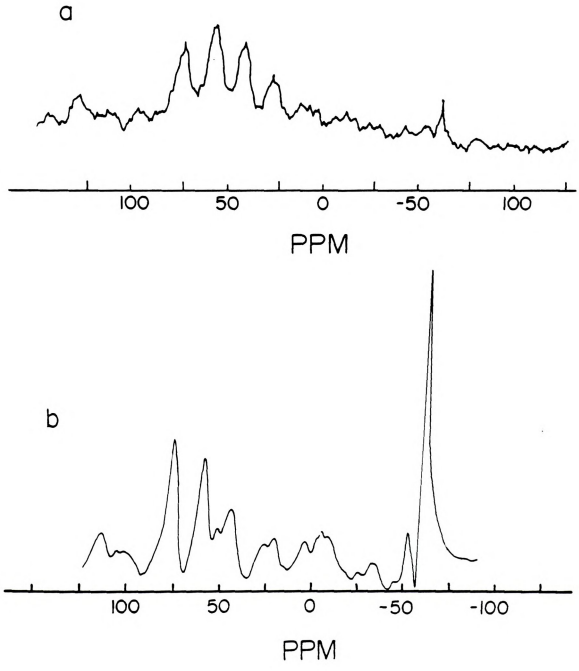


Figure 28. ^{133}Cs MAS-NMR spectra of compounds formed from initial stoichiometry $Cs^{+}(18C6)_2 \cdot Na_x \cdot e_{1-x}$ for a) $\chi = 0.2$ and b) $\chi = 0.8$. Peaks at 73, 57, 42 and 25 ppm are from a mixed compound with $\chi = 0.1$-0.2; the peak at -61 ppm is from excess $Cs^{+}(18C6)_2 \cdot Na^{-}$. Other features are spinning sidebands.

intermediate peaks are successively spaced by roughly 1/8 of the spectral breadth between the electride peak and the sodide positions. Structural determinations of $Cs^+(18C6)_2 \cdot e^-$ [29] and $Cs^+(18C6)_2 \cdot Na^-$ [30] indicate that each complexed cation has eight nearest neighbor anions. The four paramagnetically shifted peaks may thus be attributed to a complexed cation surrounded by eight, seven, six and five electrons in order of increasing field; the other anionic sites are occupied by diamagnetic Na^- ions. There does not appear to be any tendency for appreciable doping of the sodide lattice with electrons.

The relative intensities of the four paramagnetic peaks remains nearly constant as the overall mole fraction of Na^- is increased; only the pure sodide peak at -61 ppm increases markedly. The relative intensities of the four peaks are roughly 1:1:0.5:0.25. The constancy of the relative intensities suggests that a compound with an ordered structure may be formed, although random substitution of Na^- into the electride lattice up to saturation cannot be ruled out.

A superlattice that includes ordered substitution of sodium anions into anionic sites in $Cs^+(18C6)_2 \cdot e^-$ lattice can be postulated that is consistent with the known crystal structures of the pure compounds and gives approximate agreement with the mixed sodide/electride NMR spectra. The crystal structures of $Cs^+(18C6)_2 \cdot e^-$ and $Cs^+(18C6)_2 \cdot Na^-$ are nearly identical.[29,30] In the space group C2/c, the parameters of the unit cell of the electride are $\underline{a}$ = 13.075 Å, $\underline{b}$ = 15.840 Å, $\underline{c}$ = 17.359 Å, and β = 92.30°. The sodide has unit cell parameters $\underline{a}$ = 13.581, $\underline{b}$ = 15.684, and $\underline{c}$ = 17.429 Å, β = 93.16°. The anionic cavity in the sodide is larger in the $\underline{a}$-$\underline{b}$ plane than is the anionic cavity in the electride, resulting in interanionic

distances that are 0.1 A longer in a-b planes, (10.37 A in the sodide, 10.27 A in the electride). The cavities in each structure are separated by ~8.7 A in the c direction. The effect of inserting a sodium anion into the cavity in the electride lattice might be to distort the eight nearest complexed cations away from their equilibrium positions. The cavity sizes suggest that the distortion would have primarily an a-b component so that anionic sites along the c-direction from the first impurity center should be better able to include a sodium anion, leading to an infinite chain of Na^- ions along the c-direction. A third sodium anion may be substituted into only one of the two sets of equivalent neighboring anionic sites, either along the a-axis or the b-axis of the original unit cell, say at +a. In order to have cesium cations that are surrounded by three Na^- ions, neighboring cavities in the c direction must be empty, allowing occupation of only every other a-b plane. Then a Na^- ion will occupy a site at -a in those planes which have no Na^- sodide ion at +a. Additional substitution may be limited by strain in the crystal. The anions in one such superlattice unit cell are pictured in Figure 29. The volume of one mixed anion unit cell is equal to the volume of eight original unit cells, and requires that 4 of the 32 anionic sites be filled with sodium anions. In agreement with this, the intensity of the peaks in the sample with x = 0.2 showed that the sodium mole fraction in the mixed compound is less than 0.2. The model predicts relative ratios of complexed cations with 0, 1, 2, and 3 of the eight nearest anionic sites filled by Na^- to be 3:3:1:1, in good agreement with the observed line intensities. Regardless of the detailed structure of the mixed system, these results provide strong evidence

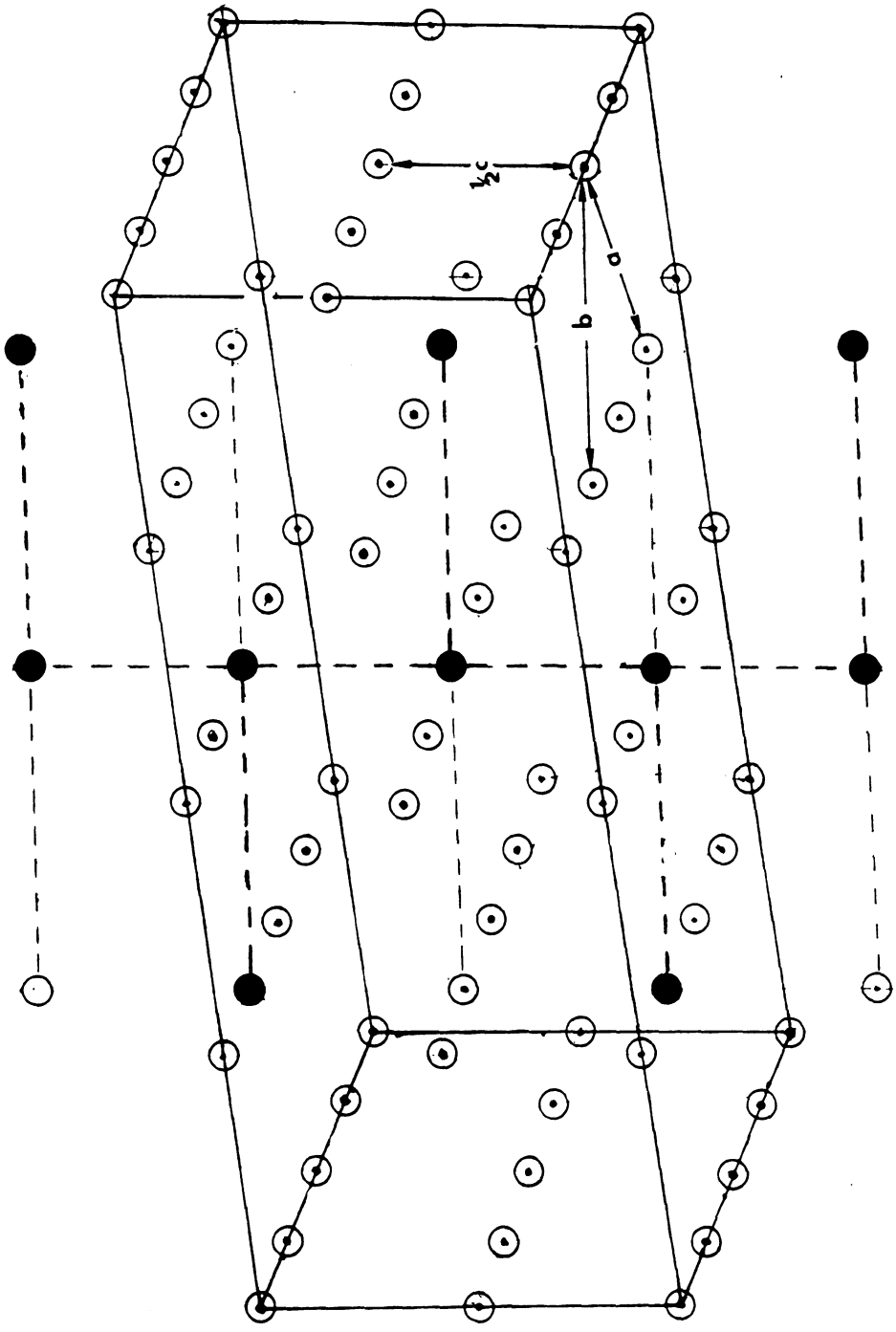


Figure 29. An anionic packing diagram showing a postulated mixed sodide/electride structure that could account for the observed mixed electride-sodide ^{133}Cs NMR spectra. Open circles are trapped electron sites, solid circles are sodium anions.

that each complexed Cs^+ interacts with eight nearest neighbor electrons, not just with one of them.

The temperature dependence of one sample of $Cs^+(18C6)_2 \cdot Na^-_x \cdot e^-_{1-x}$ was measured over a temperature range of 190 K to 255 K. The spectrum was very noisy so that uncertainties in the chemical shift are as large as ±5 ppm. The most paramagnetic peak was assumed to be the resonance of the complexed cation surrounded by eight trapped electrons (or the 'pure' electride). The temperature of the sample was calculated from the chemical shift of the pure electride peak by using the established Knight shift parameters. The temperature dependence of the peaks of $Cs^+(18C6)_2 \cdot Na^-_x \cdot e^-_{1-x}$ for x = 1/8, 2/8 and 3/8 appeared to be nearly linear, and were fit to a Knight shift equation $\delta(T) = \delta(\infty) + m/T$ for two cases: 1) $\delta(\infty) = -61$ppm, since the chemical shift of both the pure sodide and the pure electride at infinite temperature is -61 ppm, and 2) for a variable $\delta(\infty)$. The results are tabulated in Table 26. The slope is a measure of the paramagnetic electron density at the cesium nucleus. The peak that corresponds to the doped electride with x = 0.125 has a slope ~ 85% of that of the pure electride; the next peak, with x = 0.25 continues the trend with a slope ~70% of that of the pure electride. In the case of the least diamagnetic peak, with x = 0.375, it was difficult to determine accurate values of the chemical shift. This gave the least consistent values of the parameters of the temperature dependence of the chemical shift; the slope indicates that the electron density at

Table 26. Table of Least-Squares Best-Fit Parameters for the Temperature Dependence of the Knight Shift of Peaks in $Cs^{+}(18C6)_2 \cdot Na_x^{-} \cdot e_{1-x}$.

X	$\delta(\infty)$(ppm)[a]	m(10^4 ppm K)[b]	% electride character
0.000	-59 ± 1	4.05 ± 0.02	99
	-61 (Fixed)	4.091 ± 0.003	100
0.125	-66 ± 7	3.56 ± 0.16	87
	-61 (Fixed)	3.44 ± 0.01	84
0.250	-71 ± 11	2.85 ± 0.02	70
	-61 (Fixed)	2.63 ± 0.02	64
0.375[c]	-118 ± 13	3.05 ± 0.30	77
	-61 (Fixed)	1.74 ± 0.06	43

[a] $\delta(\infty)$ is the infinite temperature extrapolation of $\delta(T)$, i.e. where $K(T) \quad 0$.

[b] m is the slope of the best fit line for δ versus $1/T$.

[c] The peak corresponding to x 0.375 was very weak; the large spread in $\delta(\infty)$ and m is probably a result of large errors in measuring the chemical shift of the peak.

Cs^+ for x = 0.375 is between 45% and 75% of that of the pure electride.

V.B.4. CONCLUSIONS

^{133}Cs MAS-NMR is a powerful tool for the elucidation of cationic and anionic species in alkalide salts. The use of multinuclear metal NMR techniques can generally be used to fully characterize the stoichiometry of an electride or an alkalide.

Moreover, the resonance position in ^{133}Cs NMR may be used as a sensitive probe of local structure about the cesium ion, and for the study of interionic interactions. Changes in the Cs-O distances in cesium-crown ether or cryptand complexes brought about by phase transitions or by changes in the anionic constituent, or the temperature, can be monitored by the empirical observation that the paramagnetic Ramsey shift has an inverse relationship to r_{Cs-O}.

The Cs^- ion is also sensitive to the size of its anionic cavity. The presence of low lying excited states apparently causes the resonance position of Cs^- to be paramagnetically shifted from the pure s-state anion. This Ramsey shift is stronger for cavities which are smaller, or which favor a non-spherical anion.

Finally, the NMR data, in combination with structural data on $Cs^+(18C6)_2 \cdot e^-$, may be used to define the nature of the trapped electron. The structure clearly indicates that anionic cavities exist in the lattice, in a distribution that is nearly identical to the distribution of Na^- sites in the salt $Cs^+(18C6)_2 \cdot Na^-$, in which the electron could be localized by three dimensional coulombic attractions to the cations. The trapped electrons interact only very weakly with

each other, as evidenced by the absence of any spin pairing, or magnetic ordering. They also show only weak overlap with the complexed cations, as evidenced by the very small Knight shift. Further, the interaction of each electron with nearby cations is spread over all of the cations, and not just one of them, as shown by the mixed alkalide electride work. The electride described here is only one of a growing class of compounds which display rather diverse properties. The compound $Cs^{+}C222 \cdot e^{-}$, for example, is a spin-paired system that shows no paramagnetism at any temperature. The strength of electron-electron and electron cation interactions in other electride systems is of great interest. Undoubtedly solid state NMR will play a major role in measuring the nature of these interactions.

V.B.5. ACKNOWLEDGMENT

This research was supported by National Science Foundation—Solid State Chemistry Grants DMR 79-21979 and DMR 84-14154. We thank Dr. P. B. Smith of the Dow Chemical Company, and Dr. E. Oldfield and Mr. B. Montez at the University of Illinois at Urbana-Champaign for their assistance in obtaining some of the NMR spectra. We are grateful to Dr. M. Tinkham for help in preparing samples and measuring spectra.

V.B.6. REFERENCES

1. Dye, J. L.; Ceraso, J. M.; Lok, M. T.; Barnett, B. L.; Tehan, F. J.; **J. Am. Chem. Soc.** 1974, **96**, 608.

2. Tehan, F. J., Barnett, B. L.; Dye, J. L.; **J. Am. Chem. Soc.** 1974, **96**, 7203.

3. Dye, J. L.; Yemen, M. R.; DaGue, M. G.; Lehn, J.-M.; **J. Chem. Phys.** 1978, **68**, 1665.

4. Le, L. D.; Issa, D.; Van Eck, B.; Dye, J. L.; **J. Phys. Chem.** 1982, **86**, 7.

5. Dye, J. L.; **Angewante Chem., Intl. Eng. Ed.**, 1979, **18**, 587.

6. Jaenicke, S.; Dye, J. L.; **J. Solid State Chem.** 1984, **54**, 320.

7. Ceraso, J. M.; Dye, J. L.; **J. Chem. Phys.** 1974, **61**, 1985.

8. Dye, J. L.; Andrews, C. W.; Ceraso, J. M.; **J. Phys. Chem.** 1975, **97**, 3076.

9. Ellaboudy, A.; Tinkham, M. L.; Van Eck, B.; Dye, J. L.; Smith, P. B.;
J. Phys. Chem. 1984, **88**, 3852.

10. Dye, J. L.; **Prog. Inorg. Chem.** 1984, **32**, 327.

11. Ellaboudy, A.; Dye, J. L.; **J. Mag. Res.** 1986,

12. Tinkham, M. L.; Dye, J. L.; **J. Am. Chem. Soc.** 1985, **107**, 6129.

13. Edwards, P. P.; Ellaboudy, A. S.; Holton, D. M.; **Nature** (London) 1985, **317**, 242.

14. Tinkham, M. L.; Ellaboudy, A.; Dye, J. L.; Smith, P. B.; **J. Phys. Chem.** 1986, **90**, 14.

15. Ellaboudy, A.; Dye, J. L.; Smith, P. B.; **J. Am. Chem. Soc.** 1983, **105**, 6490.

16. Dye, J. L.; Ellaboudy, A.; **Chem. Brit.** 1984, **20**, 210.

17. Dawes, S. B., Ellaboudy, A., Dye, J. L.; This issue.

18. Van Eck, B.; Le, L. D.; Issa, D.; Dye, J. L.; **Inorg. Chem.** 1982, **21**, 1966.

19. Dye, J. L.; **J. Phys. Chem.** 1984, **88**, 3842.

20. Tinkham, M. L.; Ph. D. Dissertation, Michigan State University, 1986.

21. Andrew, E. R.; **Intl. Rev. Phys. Chem.** 1981, **1**, 195.

22. Issa, D.; Ellaboudy, A.; Janakiraman, R.; Dye, J. L.; **J. Phys. Chem.** 1984, **88**, 3847.

23. Huang, R. H.; Ward, D. L.; Dye, J. L.; unpublished results, this laboratory.

24. Beckmann, A.; Boklen, K. D.; Elbe, D.; **Z. Phys.** 1974, **270**, 173.

25. Pyper, N. C., Edwards, P. P.; **J. Am. Chem. Soc.** 1986, **108**, 78.

26. Holton, D. M.; Edwards, P. P.; Johnson, D. C.; Page, C. S.; McFarlane, W.; Wood, B.; **J. Chem. Soc.**, Chem. Commun. 1985, **740**.

27. Landers, J. S.; Dye, J. L.; Stacy, A.; Sienko, M. J.; J. Phys. Chem. 1981, **85**, 1096.

28. Faber, M. K.; Dye, J. L.; unpublished results, this laboratory.

29. Dawes, S. B.: Ward, D. L.; Huang, R. H.; Dye, J. L.; **J. Am. Chem. Soc.**,

30. Dawes, Fussa, Ward, Dye, unpublished results, this laboratory.

31. Knight, W. D.; **Phys. Rev.** 1944, **76**, 1259.

32. English, A. D.; **J. Mag. Res.** 1984, **57**, 491.

33. Van Geet, A. L.; **Anal. Chem.** 1968, **40**, 2227.

34. Edwards, P. P.; **Adv. Inorg. Chem. Rad.** 1982, **25**, 135.

35. Lelieur, J. P.; Rigny, P.; **J. Chem. Phys.** 1973, **59**, 1142.

36. Lelieur, J. P.; Rigny, P.; **J. Chem. Phys.** 1973, **59**, 1148.

37. Dye, J. L.; **Pure Appl. Chem.** 1977, **49**, 3.

38. O'Reilly, D. E.; **J. Chem. Phys.** 1964, **41**, 3729.

39. Catterall, R.; Edwards, P. P.; **Adv. Md. Relaxation Processes**, 1978, **13**, 123.

40. CRC Handbook of Chemistry and Physics, 60th edition, R. C. Weast ed., CRC Press, Boca Raton, Florida (1980).

V.C MAS-NMR of $Cs^+(15C5)_2 \cdot e^-$

^{133}Cs NMR spectra were measured for $Cs^+(15C5)_2 \cdot e^-$ over a temperature range of 170 K to 280 K. The chemical shift is temperature dependent and paramagnetically shifted from the chemical shifts of diamagnetic salts of $Cs^+(15C5)_2$. The temperature dependence of the chemical shift is a linear function of the reciprocal temperature below 230 K, but deviates from a linear Knight shift near the temperatures corresponding to phase transitions (238 K and 268 K). The sample temperatures in the NMR experiment were calibrated by two methods. The splitting of the chemical shifts of the hydroxyl and methyl protons in methanol, which has a known temperature dependence [91,92], was measured both prior to and after measurement of the cesium chemical shift at four different values of cooled gas flow rates and gas heater power settings. The chemical shifts of Cs^+ in $Cs^+(15C5)$, plotted as x's in Figure 30, were not entirely reliable however. The rotor that contained the electride was repeatedly removed from the stator and was subjected to temperature extremes that resulted in some decomposition. The ^{133}Cs spectra were very broad, even with good spinning rates, so that the error in the chemical shift was quite large. For example, the spectrum at 230 K

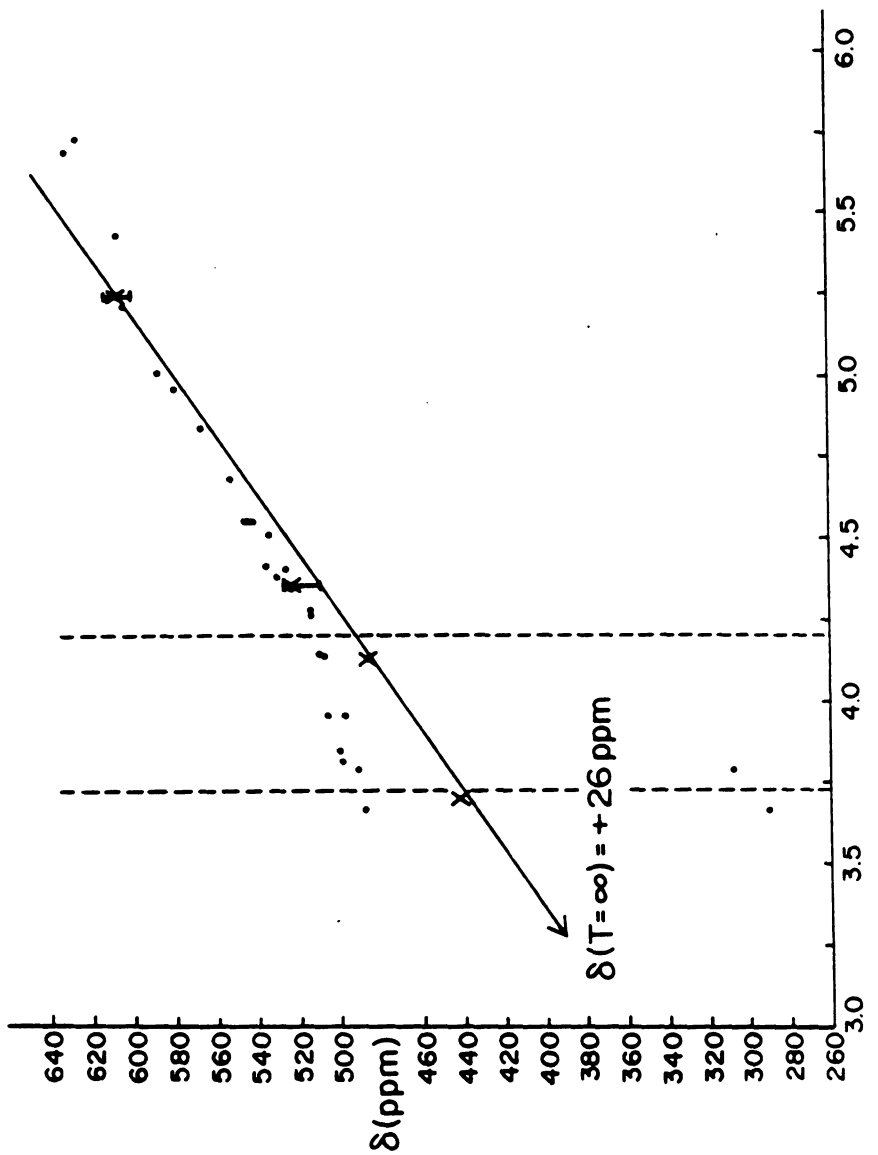


Figure 30. The chemical shift versus T^{-1} for $Cs^{+}(15C5)_2 \cdot e^{-}$. The temperatures of points marked by x were calibrated by comparison with the dipolar splitting of methanol. The temperatures of other points were calibrated by simultaneous measurement of the Knight shift of $Cs^{-}(18C6)_2 \cdot e^{-}$.

had a broad peak with a maximum that could lie between 524 ppm and 510 ppm; the shift was chosen to be 524 ppm. In addition, the two high temperature peaks displayed chemical shifts that have not otherwise been observed in $Cs^{+}(15C5)_2 \cdot e^{-}$. The spectra at 270 K ($\delta$ = 441 ppm) and at 242 K (δ = 487 ppm) had unique paramagnetic chemical shifts. In addition these two spectra had rather large peaks at +25 ppm, probably from decomposed electride. The chemical shifts of the four points that had consistent temperatures throughout two ^{1}H acquisitions and one ^{133}Cs acquisition are shown in Figure 30 as a function of 1/T, with their estimated errors. The best fit line gave an extrapolation for the chemical shift at infinite temperature at the y-intercept of $\delta(\infty)$ = 26.2 +/-65.4 ppm and a slope of 1.11 +/-0.15 x 10^{5} ppm K.

The temperature dependence of the ^{133}Cs NMR line of $Cs^{+}(15C5)_2 \cdot e^{-}$ was also measured by a second method. The spectrum of a sample that contained both $Cs^{+}(18C6)_2 \cdot e^{-}$ and $Cs^{+}(15C5)_2 \cdot e^{-}$ was measured at several gas flow and heater settings and the correct temperature was determined from the position of the $Cs^{+}(18C6)_2 \cdot e^{-}$ peak. The points measured in this way are represented by solid circles in Figure 30. The $Cs^{+}(15C5)_2 \cdot e^{-}$ chemical shifts between 190 K and 230 K agree well with the values of chemical shift calibrated by the methanol method. The parameters of the

best-fit lines include various combinations of the data calibrated by each of the two methods. A satisfactory fit was obtained with $\delta(\infty)$ = 25 ppm and slope = 1.1×10^5. Between 230 K and 270 K the shift deviates paramagnetically from the line. In addition, a peak that is shifted upfield by about 190 ppm appeared at 265 K; this peak rapidly became the major feature in the spectrum. It appears that the phase transitions at 238 K and 268 K affect the electron density at the nucleus and therefore affect the temperature dependence of the chemical shift. Data presented in Chapter VI, however, indicate that there is no significant change in the magnetic susceptibility of $Cs^+(15C5)_2 \cdot e^-$ in this range of temperatures. The phase transition at 238 K is weak, and may be similar in nature to the transition in $Cs^+(18C6)_2 \cdot Na^-$ that resulted in motionally averaged dipolar interactions in the static Na^- NMR spectrum. Hydrogen motion in the complexed cation may gradually allow more electron density to reside on the cesium nucleus. The phase transition at 268 K reduces the electron density at the nucleus dramatically. The transition from the downfield peak to the upfield peak is complete by about 275 K. This phase transition is also responsible for the shift of the maximum of the optical absorption spectrum to higher energies. Thus the interpretation of this phase transition is that the lattice softens

and the electron is able to reorient its environment to increase its localization energy. The interpretation is consistent with the observed NMR data; an electron that is more strongly localized at the cavity will have a smaller density on surrounding ions. Unfortunately, the sample also begins to decompose near these temperatures so that a complete temperature dependence of the spectrum of $Cs^{+}(15C5)_{2}\cdot e^{-}$ above 270 K could not be obtained.

The deviation of the chemical shifts above 230 K in the two temperature calibration methods may be caused by the partial decomposition of the sample that was calibrated by the methanol method. If the decomposition destroyed the crystallinity of the remaining electride it is possible that the phase transitions of the crystalline material might not be present. The cations that are observed at shifts greater than 400 ppm in the NMR spectrum do not appear to have lost any nearest neighbor trapped electrons to decomposition since there is no abrupt change in the paramagnetic shift.

The slope of the chemical shift versus 1/T plot below 230 K may be used to calculate the paramagnetic electron density at the nucleus via Equation 5.16. The magnetic susceptibility was measured as described in Chapter 6. The fractional atomic character is about 8.4×10^{-4}, which corresponds to an electron density at the cesium nucleus,

$\langle|\psi(o)|^2\rangle = 2.2 \times 10^{22}$ e^-/cm^3. An approximate fractional atomic character of the Cs^+ in the high temperature phase, F_{HT}, may be calculated if it is assumed that $\delta(\infty) = 25$ ppm for this peak. The Knight shift is 275 ppm at 270 K in the high temperature phase, compared to the 430 ppm shift calculated for the low temperature phase (calibration with methanol). If the magnetic susceptibility is linear in T^{-1} then $F_{HT} = (275/430) \cdot 8.4 \times 10^{-4} = 5.4 \times 10^{-4}$. This is still nearly two times greater than the value of F for $Cs^+(18C6)_2 \cdot e^-$. The electron density at the cesium nucleus is approximately three times greater in $Cs^+(15C5)_2 \cdot e^-$ than in $Cs^+(18C6)_2 \cdot e^-$, which may be attributed to the structure of the complexed cations. Whereas the crown ethers are in van der Waals contact with each other in $Cs^+(18C6)_2 \cdot e^-$, thus shielding the cesium cation from interactions with its environment, the cesium cation in $Cs^+(15C5)_2 \cdot e^-$ is less enclosed by the smaller hole of the two 15C5 molecules. The result is that the $Cs^+(15C5)_2 \cdot e^-$ exposes a "harder" charge to the trapped electrons and thus may attract electron density to the cation. The electronic wavefunction in $Cs^+(15C5)_2 \cdot e^-$ is probably more extended than is the trapped electron wavefunction in $Cs^+(18C6)_2 \cdot e^-$.

CHAPTER VI

MAGNETIC SUSCEPTIBILITY OF $Cs(18C6)_2 \cdot e^-$ and $Cs^+(15C5)_2 \cdot e^-$

The trapped electron in electride salts has a spin angular momentum which responds to an applied magnetic field in various detectable ways depending on its interactions with nearby electrons. The extent of electron-electron interactions in an electride salt can be measured by static magnetic susceptibility. Examples of metallic ($K^+C222 \cdot e^-$ [93]) electrides, localized spin paired electrides ($Cs^+C222 \cdot e^-$ [71]), and paramagnetic electrides have already been observed. This work will explore the electron-electron interaction of the two closely related electrides $Cs^+(18C6)_2 \cdot e^-$ and $Cs^+(15C5)_2 \cdot e^-$. The subtle structural differences in these two salts result in quite dramatic magnetic differences between them.

VI.A Background for Magnetic Susceptibility

VI.A.1 Metallic Paramagnetism

Since magnetic susceptibility is an important probe in the study of electrides, a brief description of the theory of magnetic susceptibility will be given. The discussion follows several sources, particularly the solid state physics texts by Kittel [94], and Ashcroft and Mermin [95], and the magnetism texts by Morrish [96], Smart [97], and Mattis [98].

If we neglect the contribution of nuclear angular momentum to the bulk magnetic susceptibility, the behavior of the material in question in an applied magnetic field, H, will depend on the quantum mechanical state of the electrons. (Neglect of the nuclear contribution is a good assumption in almost all cases since the nuclear magnetogyric ratio is nearly 2000 times smaller than that of the electron.) As is the case in almost any physical measurement, electrons which lie in a conduction band; that is, free or nearly free electrons behave much differently than do localized electrons.

The magnetic susceptibility displayed by conduction electrons is a feeble temperature independent paramagnetism which requires simple band theory to explain. In a macro-

scopic metal, those electrons that lie in a conduction band can be shown to have a density of electronic states g(E), at an energy E that is proportional to $E^{1/2}$. The Pauli exclusion principle states that each spatial energy level may be doubly occupied by electrons having opposing spin angular momentum. The population of these states as a function of the temperature is given by

$$N(E) = F(E)g(E)dE \tag{6.1}$$

where F(E) is the Fermi Dirac distribution function which may be derived from simple statistics of fermions and is given by

$$F(E) = \left[e^{+[(E-E_f)/kT)]}+1\right]^{-1} \tag{6.2}$$

The Fermi energy E_f is defined as the value of E for which $F(E) = 1/2$. At T = 0 K the Fermi function has a value of unity for all energies below E_f, and zero for all energies above E_f as depicted in Figure 31a. Increased temperature affects the distribution of states only slightly as E_f is typically on the order of several eVs and room temperature corresponds to a thermal energy of only 1/40 eV. Because each state is occupied by two electrons of opposing spins,

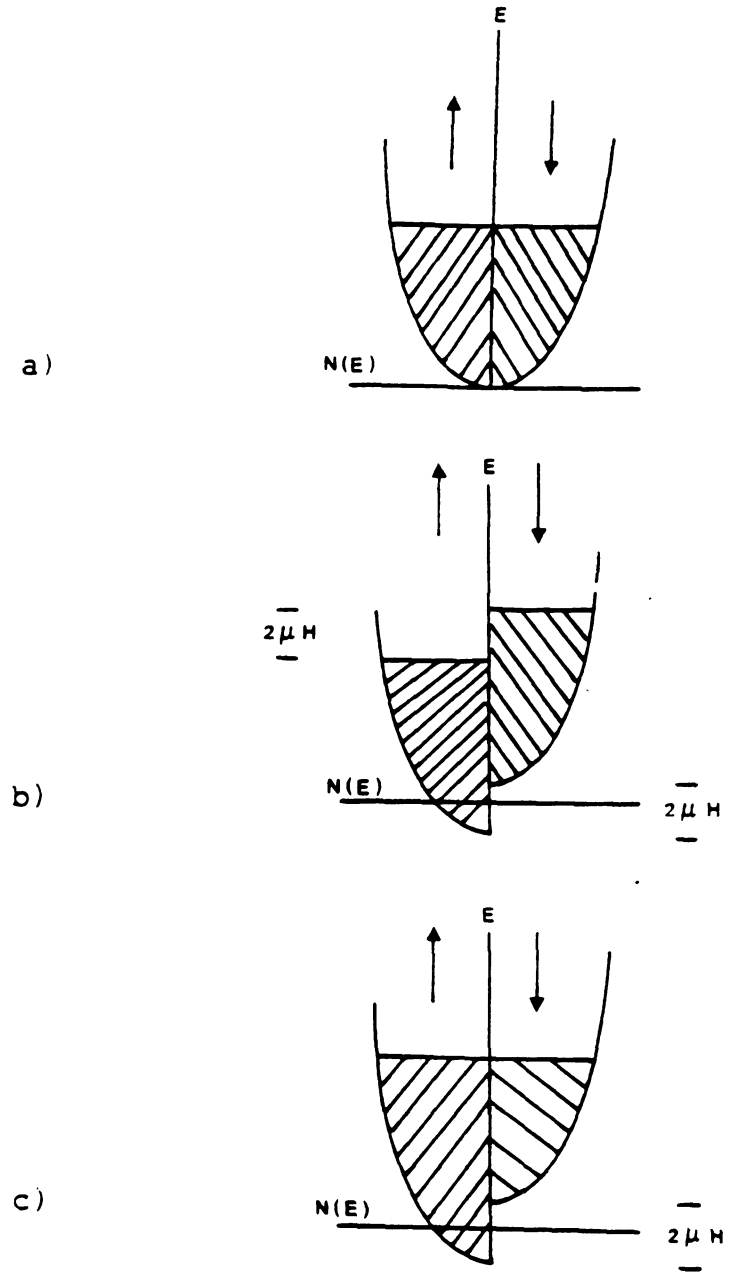


Figure 31. The density of states with spin up (↑) and spin down (↓) in a metal as a function of energy, E, a) at equilibrium in the absence of an external magnetic field, b) prior to equilibrium upon application of a field, H, and c) at equilibrium in the presence of the applied field [94].

it is possible to construct a density of states for separate spin states, arbitrarily assigned as parallel and antiparallel. The density of each spin state is one-half the full density of states in the absence of an applied magnetic field. Application of a magnetic field, H, lowers the energy of the distribution of electrons assigned as parallel to the field by $-g\mu_B m_s H$ where g is the electronic g factor, m_s is the electronic spin angular momentum quantum number, and μ_B is the electronic Bohr magneton. Typically $g = 2$ and $m_s = {}^1/_2$ so that $\Delta E = -\mu_B H$. Likewise the energies of the states antiparallel to the field direction are raised in energy by $\Delta E = \mu_B H$, so that before any equilibration is allowed the distribution of states might look like Figure 31b. The high energy states in the antiparallel states spill over (Figure 31c) to unoccupied parallel states to give a final distribution of spin states which has net spin angular momentum in the direction of the field. The magnetic moment of the metal is proportional to twice the number of electrons which spilled over from antiparallel states to parallel states, N, and is calculated by $M = 2\mu_B(\Delta N)$. ΔN is estimated by the number of electrons within $\mu_B H$ of the Fermi Energy at 0 K, and can be calculated to be

$$\Delta N = \{2(2m)^{3/2}/\hbar^3)\}\mu_B H(E_f(0))^{1/2} \qquad (6.3)$$

The magnetic susceptibility is given as

$$X = dM/dH = 3(N/V)\mu_B^2/2kT_F \qquad (6.4)$$

where $E_f(0)$ has been expressed in fundamental constants. The important points to notice are that there is virtually no temperature dependence, and that for typical conduction electron densities near $10^{22} e^-/cm^3$ the value of X = $\sim 10^{-6}/cm^3$.

In addition to the paramagnetism that arises from the orientation of electronic spin angular momentum, there is a diamagnetic contribution that arises from the induced translational or orbital motion of the free electron gas. The oscillations of the electron gas have a very complex dependence on the applied field, so that the Fermi Dirac statistics become very difficult to analyze for the theoretical value of conduction electron diamagnetism. The calculation will not be done here, only the remarkable result will be stated that the diamagnetic susceptibility is $-1/3$ of the Pauli spin susceptibility. Thus the total contribution to the bulk susceptibility of an electron gas is $2/3$ of the total spin susceptibility and is relatively temperature independent throughout the range of solid temperatures.

The situation is complicated when band structure arises from d or f orbitals and/or there is increased electron localization. Conduction electrons can interact with the metallic ions and mediate magnetic ordering. In addition, as the conduction electron density decreases, the electrons will follow Boltzmann statistics rather than the high density-low temperature Fermi Dirac statistics and magnetism of a stronger nature will occur. The predicted complexity of the magnetic susceptibility near the transition from the nearly free electron to non-metallic regimes has been seen in metal amine and methylamine compounds. For example $Li(MeNH_2)_4$ shows the behavior of a highly correlated metal with a magnetic moment which varies inversely with temperature [22]. As new electrides are synthesized with more nearly expanded metallic character, the discussion of conduction electron paramagnetism will become more important.

VI.A.2 Diamagnetism

For materials which have no conduction band electrons, the magnetic character of the material depends on how strongly the wave functions of the electrons overlap. The vast majority of electrons, those that are involved in covalent bonds, and those that fill nonvalence core

electronic shells do not display a spin angular momentum paramagnetism. Only orbitals that have degenerate levels that are not filled will show a paramagnetic response to an applied magnetic field. The Pauli exclusion principle favors filling the electronic spatial wave function with two electrons possessing antisymmetric spins. These states have no easily accessible excited states so the total spin and orbital angular momentum is zero. In order for electrons of this sort to show a net spin angular momentum as a result of an applied magnetic field, there would have to be a large population of electronic excited states; this excited state population is highly unstable at normal temperatures as typical excited state energies are of the order of eVs, much greater than normal thermal energies. These electrons do contribute to the bulk magnetic susceptibility however by induced orbital motion of the electrons by the applied field.

Classically, the Langevin diamagnetism is analogous to the effect that a magnetic field has on a current loop; a current is induced that generates a magnetic field opposing the applied field. If the motion of an atom's electrons is considered to be a current loop, then the electronic response and resultant field can be calculated. The motion that the electron follows is a precession about the axis of the applied magnetic field vector. Then the magnetic

moment is

$$\mu = (e/2mc) \cdot \omega_L \overline{\rho^2} \qquad (6.5)$$

where ω_L is the frequency of precession and is proportional to the applied field H, $\overline{\rho^2}$ is the mean square radius of the precession in a plane perpendicular to the applied field. Substituting $2\overline{r^2}/3$ for $\overline{\rho^2}$, where r is the mean square radius of the precession in general spherical coordinates, and differentiating with respect to H the magnetic susceptibility corrected for volume is

$$X = (Ne^2/6mc^2) \sum_{i=1}^{Z} \overline{r_i^2} \qquad (6.6)$$

for a system having Z paired electrons. The result predicts no explicit temperature dependence; only if increased thermal motion affects the mean electronic radius will the Langevin magnetic susceptibility vary with temperature. All electrons will precess and thus show weak diamagnetism with $X_{dia} = -10^{-6}$ per mole of diamagnetic electrons. The major problem in calculating the diamagnetic susceptibility is in evaluating $\overline{r^2}$. X_{dia} for atoms and ions may be evaluated from electronic distributions calculated with appropriate wave functions. The diamag-

netic susceptibility for molecules is somewhat more difficult to calculate from basic principles, but a set of values for various molecular fragments, known as Pascal's constants, have been generated by differential measurement of the susceptibilities of related materials and can be used to predict values of X_{dia} with fair accuracy.

VI.A.3 Curie Law Paramagnetism

In the opposite limit of electronic states, unpaired non-interacting localized electrons give an entirely different form of magnetism in the presence of applied fields. Electrons of this sort are found in organic radicals, transition metal salts, and, of particular importance to this study, electride salts. Application of the magnetic field lifts the degeneracy of the two electronic spin states of the isolated electron in the $S = {}^1/_2$ case. Electrons with spin parallel to the applied field have lower energies than electrons of antiparallel spin by an energy $\Delta E = -2\mu_B H$. This energy difference is comparable to thermal energies, so that there will be an appreciable population of electrons in the higher energy state; thus Boltzmann statistics apply. In the general case of an electron in an ionic orbital having both orbital and spin angular momentum (L and S respectively), with total angular

momentum (J) determined by Hund's rules, the problem may be set up as

$$e^{-F/kT} = \sum_{J_z=-J}^{J} e^{-\mu_B g H J_z/kT} \qquad (6.7)$$

where F is the Helmholtz free energy and the 2J+1 states that are thermally accessible arise from Zeeman splitting of the angular momenta. Now the magnetic moment is given by $\partial F/\partial H$ which may be calculated from the Boltzmann distribution. The summation and differentiation of eqn. 6.7 yields for the magnetization of N ions in a volume V

$$M = \frac{N}{V} g\mu_B J B_j\left[\frac{g\mu_B HJ}{kT}\right] \qquad (6.8)$$

where the Brillouin function, $B_J(x)$, is

$$B_J(x) = \frac{2J+1}{J} \coth\left[\frac{2J+1}{J}x\right] - \frac{1}{2J}\coth\left[\frac{x}{2J}\right] \qquad (6.9)$$

The magnetic susceptibility is given by M/H. In the limit that $kT >> g\mu_B H$ (i.e. $x<1$), the Brillouin function may be expanded to give

$$M = \frac{N}{V} \frac{J(J+1)}{3kT} (g\mu_B)^2 H \qquad (6.10)$$

and

$$\chi^M = \frac{C}{T} \qquad (6.11)$$

where C is the Curie constant, defined as

$$C \equiv \frac{N_{av}}{V} \frac{(g\mu_B)^2 J(J+1)}{3k} \qquad (6.12)$$

For $J = S = {}^1/_2$ the molar Curie constant, $C_m = 0.376$. The Curie Law assumes no magnetic interaction between the ions, and requires the high temperature and low field limits. It is good for rare earth and unfilled s and p orbital ions but does not give good agreement for transition metal (d shell ions). For these systems the orbital angular momentum (L) is quenched and the slope of 1/X vs. temperature corresponds with the J = S state. When either the temperature is very low (below 1 K) or the field is very high (H greater than 10 kG) saturation may occur and the susceptibility must be calculated from the unexpanded Brillouin function. In addition the result for the magnetization is general and is used as a starting point for various models such as the molecular field theory of

ordered magnetism.

VI.A.4 Magnetic Ordering and the Curie-Weiss Law

Ordered magnetism can arise when the condition that Curie type electrons be isolated and non-interacting is lifted. The overlap of two neighboring electrons affects the energy of the two electron system in a bonding or an antibonding fashion. The overlap then dictates the energetics of relative spin angular momenta of the two electrons based on the Pauli exclusion principle; bonding electrons tend to spin pair, antibonding electrons tend to maximize the total spin angular momentum. The three dimensional electron-electron interaction in a paramagnetic crystal results in an exchange energy which favors a particular orientation of the spin angular momentum of one electron relative to the orientation of the surrounding electrons. Ferromagnetism results when the repulsion between the electrons on neighboring ions is more important than the weak attraction to the screened charge on neighboring cations. The repulsive exchange energy causes the spins to align parallel to each other, thus the thermal distribution of states in the paramagnet is slightly altered at high temperatures. Below a critical temperature, known as the Curie temperature T_c, the exchange

energy overwhelms the thermal distribution of states, and the crystal displays a permanent magnetic moment even in the absence of an applied field. The case of ferromagnetic exchange is favored for ions with electrons having high angular momentum, i.e. d and f orbital ions where electron density tends to be far from the nucleus and near neighboring electrons.

The case of antiferromagnetism is more relevant to electrides and will be described in more detail. Here the electrons are attracted towards neighboring cation charge potentials. The attraction tends to pull paramagnetic electrons into the same space. The Pauli exclusion principle requires that no two electrons may have the same quantum numbers; if two electrons are to share space they must have antisymmetric spin wave functions. Thus an antiferromagnet below the critical temperature (called the Neél temperature T_N), where thermal effects are small relative to the exchange energy, consists of two interpenetrating sublattices having equal and opposite permanent magnetic moments. At zero applied field there is no net magnetic moment, but the sublattices may be detected by neutron diffraction experiments. The neutrons possess nuclear spin angular momentum, so that they scatter off the magnetic moments of the electrons via a magnetic dipole-dipole interaction. The diffraction pattern of an antiferromagnet

material above the Neél temperature is similar to that seen in x-ray crystallography, except that the scattering factors for various atoms are quite different for neutrons than the x-ray scattering factors. The diffraction pattern of an antiferromagnetic below the Neél temperature has enhanced intensity for the lines which correspond to a unit cell of twice the lattice parameter of the crystal above the critical temperature; exactly the period of a magnetic superlattice.

The magnetic susceptibility of an ordered magnet above the critical temperature is only slightly modified from the Curie law. The exchange interaction in antiferromagnetic materials favors the high temperature limit of an equal population of spins antiparallel and parallel to the applied field. In the case of a ferromagnet the low temperature limit of a saturated population of spins parallel to the applied field is favored by the exchange interaction. The Curie-Weiss Law may be derived from mean field theory to account for deviations from Curie Law paramagnetism in the presence of antiferromagnetic (ferromagnetic) exchange and is given by $X = C/(T-\theta)$ where θ is usually negative for antiferromagnets (positive for ferromagnets) and is known as the Weiss constant. θ is typically close to $-T_N$ and varies with the nature of the mean field. In general the stronger the interaction of one

spin on a sublattice with other spins on the same sublattice, the more θ deviates from T_N. Below T_N, at zero applied field, electron spins orient in their antiparallel superlattices. The direction of the spin angular momentum is not random but is determined by internal crystal fields generated by crystalline anisotropy forces which align the spins along an "easy" axis. These forces are most often the result of crystal field interactions, anisotropic exchange and anistropic magnetic dipole effects. The orientation of the magnetic moments in the low field limit is perturbed by thermal effects from the easy axis for $0<T<T_N$. The net magnetic moment may be calculated for situations where the easy axis is aligned perpendicular and/or parallel to the applied field. Figure 32a and b shows the perpendicular and parallel components of the magnetic susceptibility of a single crystal of an antiferromagnet as a function of temperature. $X_{\parallel}$ varies from the maximum at $T = T_N$ to 0 at $T = 0$ K, whereas $X_{\perp} = X(T_N)$ for all temperatures below T_N. The physical picture is that the susceptibility measures the torque applied on the spin/angular momentum by the applied field. For components of momentum parallel to the applied field the torque is zero. Perpendicular components may respond to the field, the angle between the angular momenta of the two spin lattices is reduced from 180° as the strength of the field

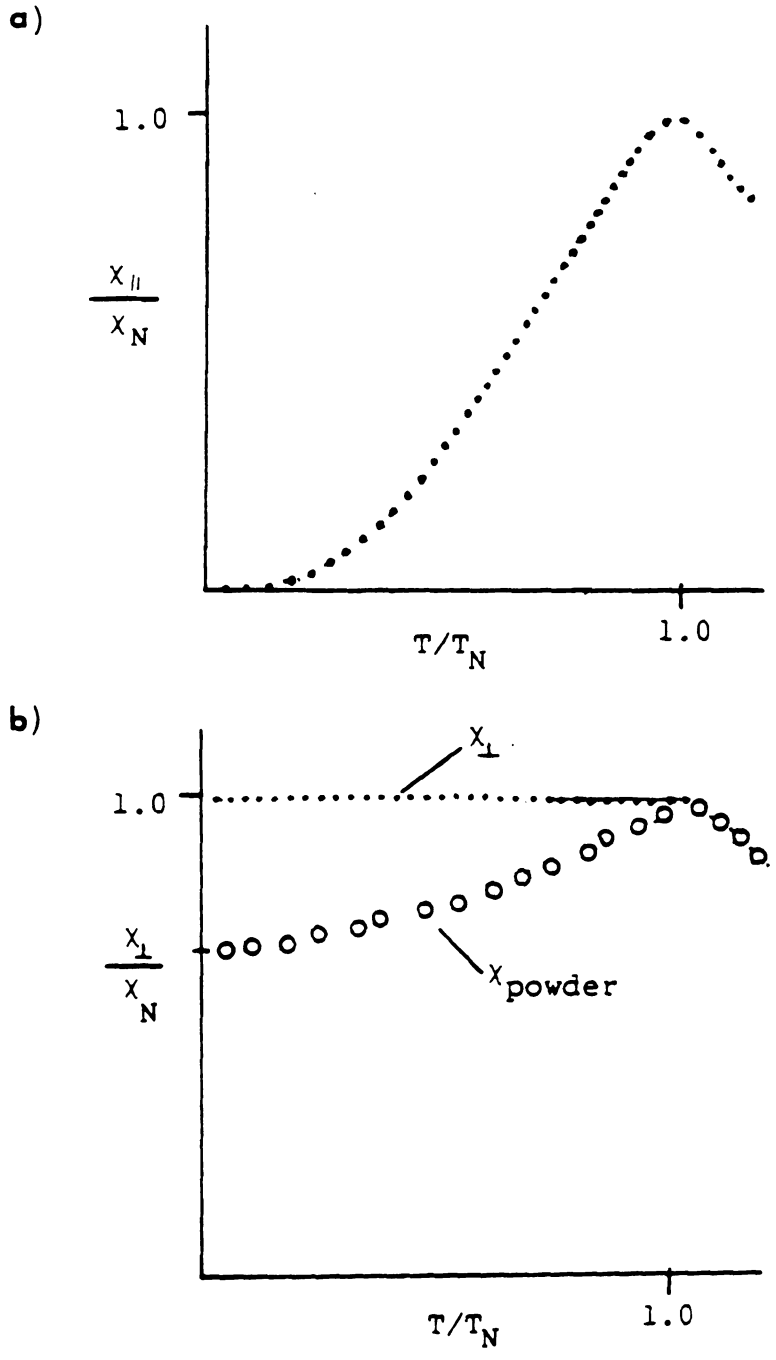


Figure 32. The susceptibility of an antiferromagnet as a function of temperature, normalized to the values at T_N; a) for a single crystal with easy axis $\parallel$ to the applied field, H, b) for a single crystal with easy axis $\perp$ to H and the powder average.

increases. At equilibrium the magnetic moment is proportional to the field, thus the change in the magnetic susceptibility is zero. Increasing the temperature from 0 K to the Neél point introduces no net change in the perpendicular component of the angular momentum. Since the perpendicular component is able to come to equilibrium with an applied field whereas the parallel component cannot, a crystal with its easy axis perpendicular to the applied field is in a lower energy state than when it is parallel to the field.

The magnetic susceptibility of a polycrystalline antiferromagnet below T_N may be expressed as

$$X_{powder} = (X_{\parallel} + 2X_{\perp})/3$$

since each crystallite may be reduced to 3 mutually perpendicular components, each equally populated in the limit of an infinite number of crystallites, one component parallel to H and two components perpendicular to H.

VI.B The Magnetic Susceptibility of Electrides

In most materials paramagnetism arises from a small minority of all of the electrons. Many measurements have been plagued by the problem of how to separate the various contributions to the bulk susceptibility so that accurate

values of one component might be obtained. Landers et al. [75] devised a method to procure the magnetic susceptibility due only to the paramagnetic electrons of a sample similar in nature to metal ammonia solutions and compounds and to electrides. The paramagnetic electrons in these systems decompose to form diamagnetic products. The diamagnetic susceptibility is measured after decomposition and is due to core electrons of the decomposition product and due to the diamagnetic bucket in which all of the measurements were made. This magnetic susceptibility is subtracted from the magnetic susceptibility of the original "live" sample. The decomposition that occurs in electrides is probably the reduction of the complexing agent by the trapped electron to liberate hydrogen gas. This reaction has not been studied in detail, but one simple observation points in favor of this reduction. $Cs^{+}(15C5)_{2}\cdot e^{-}$ melts at temperatures near 298 K. The slow decomposition that occurs in the liquid proceeds with liberation of a gas as evidenced by bubbles which grow on the surface of the melt. Assuming that the gas is H_2 then the decomposition process causes the sample to lose one diamagnetic electron in addition to losing the trapped paramagnetic electron. The correction is made by subtracting the measurement made with the decomposed sample and the bucket measurement seen from that of the "live" sample plus bucket. To very good

accuracy then, the result is the magnetic susceptibility of only the trapped electron. The loss of one diamagnetic electron is negligible due to the fact that the total diamagnetic susceptibility is due to some 300 core electrons in the Cs(15C5) system, in addition to the electrons in the bucket. This method would be valid independent of the mechanism of the decomposition reaction as long as the decomposed product is diamagnetic.

VI.B.1 Magnetic Susceptibility of $Cs^{+}(18C6)_2 \cdot e^{-}$

The electronic magnetic susceptibility of $Cs^{+}(18C6)_2 \cdot e^{-}$ has been reported previously [78] and has been verified since. The results are shown in Figure 33 in a plot of $1/X_e^M$ vs. T. The electride salt follows the Curie Weiss Law over a temperature range of 1.5 to 280 K. A good fit was obtained by using KINFIT, a least squares program with a modified Curie-Weiss equation

$$X_e^M = fC/(T-\theta) + B \qquad (6.13)$$

where X_e^M is the corrected electronic molar magnetic susceptibility at a temperature T, and the parameters f, θ, and B are the fraction of the full Curie constant, the Weiss constant and a temperature independent correction term respectively. The Curie constant, C, for a system with

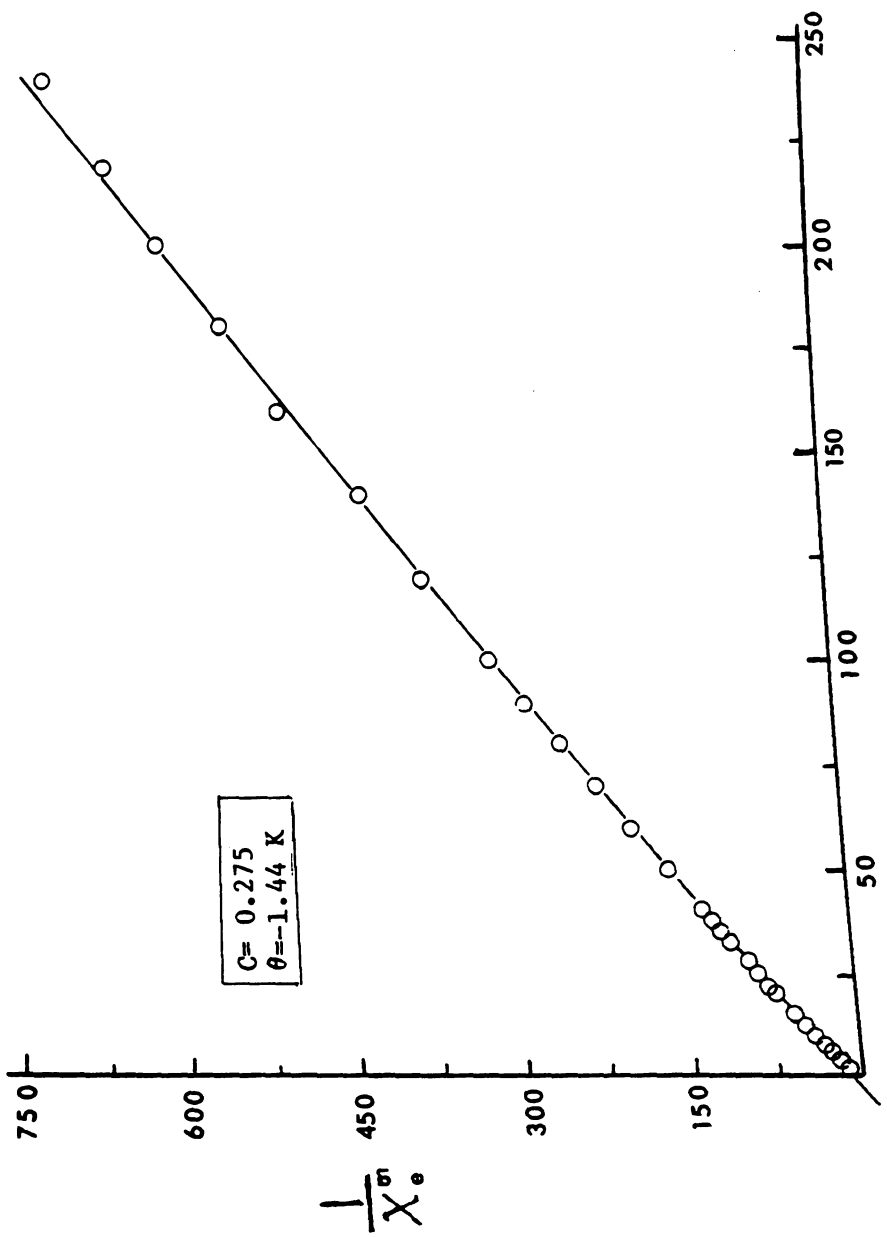


Figure 33. The reciprocal molar electronic susceptibility of $Cs^+(18C6)_2 \cdot e^-$ as a function of temperature [71].

$S = {}^1/_2$, $L = 0$, $J = {}^1/_2$ is 0.376. Ellaboudy [71] reported values of $f = 0.74$, and $\theta = -1.4$ K for $Cs^+(18C6)_2 \cdot e^-$. Other measurements have given rough quantitative agreement with the Curie constant being 0.6 to 0.8 times the $J = {}^1/_2$ value of 0.376, and $1 < -\theta < 2$ K. Better fits were obtained with a four parameter equation [71]

$$X_e^m = f_1 C/(T-\theta) + f_2 C/T + B \qquad (6.14)$$

but the interpretation of a system with partial Curie law and partial Curie-Weiss law paramagnetism is not clear. The fraction of the full Curie constant is only 74% of the value expected for a non-interacting trapped electron system. The fact that no sample shows a full $J = {}^1/_2$ paramagnetism is probably due to reduced electron content per unit mass of sample. If any non-electride impurity is present, i.e. $Cs^+(18C6)_2 \cdot Cs^-$ or decomposition product, the mass correction will overestimate the number of electrons present and reduce the value of the measured Curie constant. There seem to be no features which might indicate the onset of magnetic ordering or spin pairing as is seen in $Li^+C211 \cdot e^-$ [75]. The very small value of θ indicates that while there is a mean-field contribution to the magnetic field susceptibility, it corresponds to a very weak antiferromagnetic coupling. It may be that antiferromagnetic ordering would occur at temperatures below 1.5 K

but experiments of this kind would require better cooling than is available on the SQUID magnetometer. In light of the structure of the electron cavity and of the empty channels between the cavities as described in Chapter III, the lack of any extensive electron-electron interaction is not surprising. The cavity is highly constricted at the junctions of neighboring cavities by electron density of the crown ethers. In addition the distances to neighboring electrons is at least 8.68 Å (along the c axis of the crystal, the next nearest electrons are 10.27 Å away) so that overlap of the electronic wavefunctions is likely to be quite weak even with adequate channels of interaction. The Weiss constant may arise from an actual mean field which would require lower temperatures to order the magnetic moments, or it may arise from an anisotropic one dimensional electron-electron interaction with the electrons along the c axis in the crystal which would not result in antiferromagnetic ordering.

VI.B.2 The Magnetic Susceptibility of $Cs^+(15C5)_2 \cdot e^-$

The magnetic susceptibility of $Cs^+(15C5)_2 \cdot e^-$ has two very distinct types of behavior, depending on the thermal history of the sample. The behavior of a sample which is rapidly (10 seconds) cooled from approximately 270 K to 5 K

is displayed in a $1/X_e^M$ vs. T plot in Figure 34. This "quenched" sample follows a Curie-Weiss type behavior, especially at temperatures above 5 K. These data were fit to the modified Curie-Weiss equation, and the results are tabulated in Table 27. The Curie constant is .355 or about 95% of the expected value of 0.376. Other samples had fractional Curie constants in the range of 85% to 95%, so the deviation from pure $S = {}^1/_2$ $J = {}^1/_2$ behavior is small, and can be attributed to diamagnetic impurities or partial decomposition. The ceside of $Cs^+(15C5)_2$ is not as stable as that of $Cs^+(18C6)_2$, an observation that may account for the larger Curie constant in $Cs^+(15C5)_2 \cdot e^-$. The Weiss constant is -4.8 K, indicating a weakly antiferromagnetic mean field. In fact there is a slight systematic deviation from Curie-Weiss behavior at temperatures below 5 K in the direction of antiferromagnetic coupling as is seen in the low temperature detail in Figure 34. If the deviation is due to an antiferromagnetic coupling, it is either from a small population of coupled ions or the interaction is frustrated.

The second type of behavior appears when the $Cs^+(15C5)_2 \cdot e^-$ is gradually cooled from ~250 K to low temperatures. The magnetic susceptibility of the annealed sample is shown in Figure 35. The high temperature

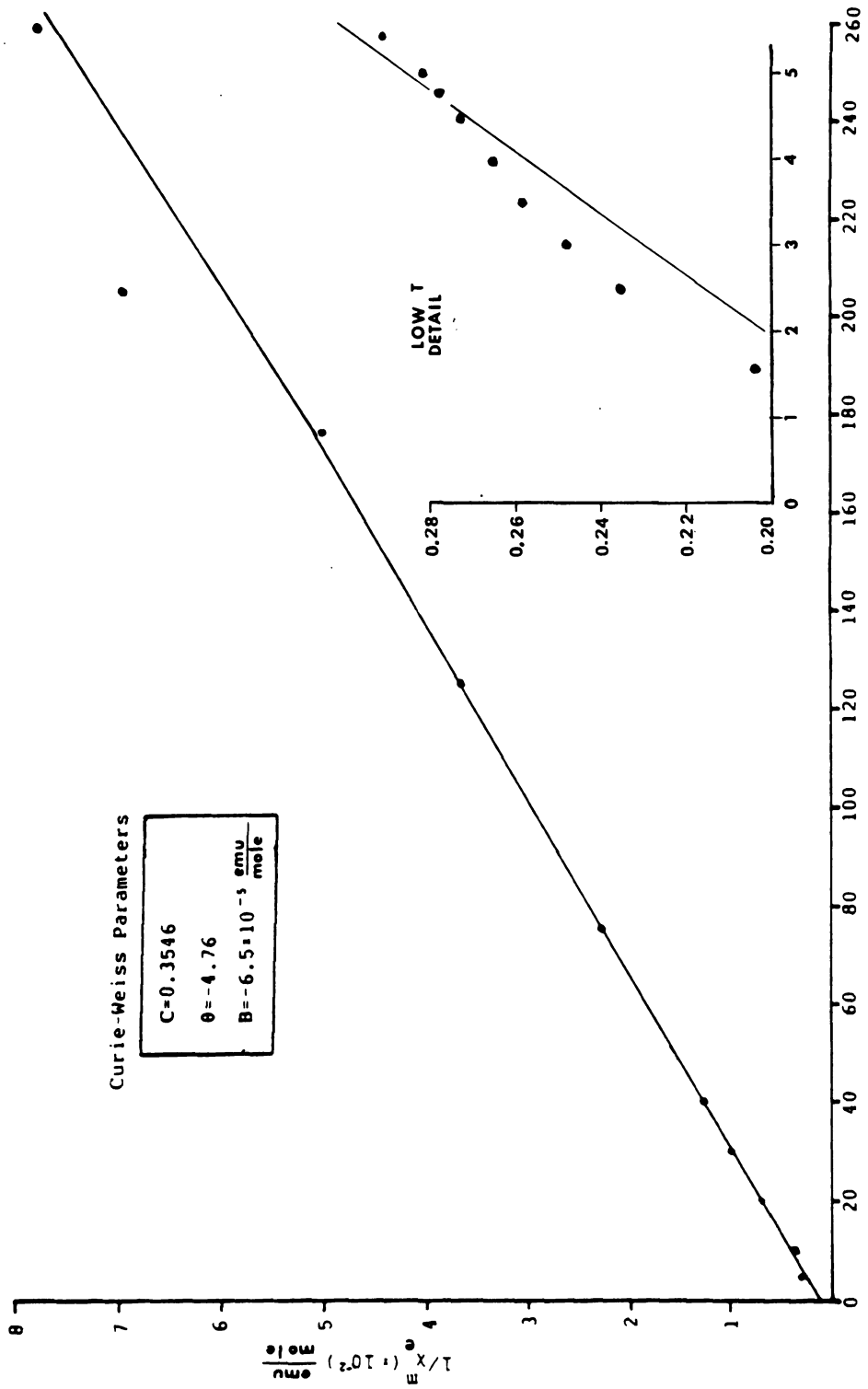


Figure 34. The reciprocal molar electronic susceptibility of a quenched sample of $Cs^+(15C5)_2 \cdot e^-$ as a function of temperature.

Table 27. Table of Parameters and Their Estimated Standard Deviations for the Modified Curie Weiss Law for $Cs^{+}(15C5)_2 \cdot e^{-}$.

	C	Fraction of C(molar) (%)	θ (°K)	B
Quenched 1.6-260 K	0.365	97	5.61	1.33×10^{-4}
est. std. dev.	0.049		0.21	0.35×10^{-4}
Quenched 5-260 K	0.355	94	4.76	$+6.54 \times 10^{-5}$
est. std. dev.	0.052		0.32	3.47×10^{-5}
Annealed 5-260 K	0.361	96	4.54	1.201×10^{-4}
est. std. dev.	0.014		1.08	0.61×10^{-5}
All data above 5 K	0.361	96	4.75	1.165×10^{-4}
est. std. dev.	0.006		0.53	0.314×10^{-4}

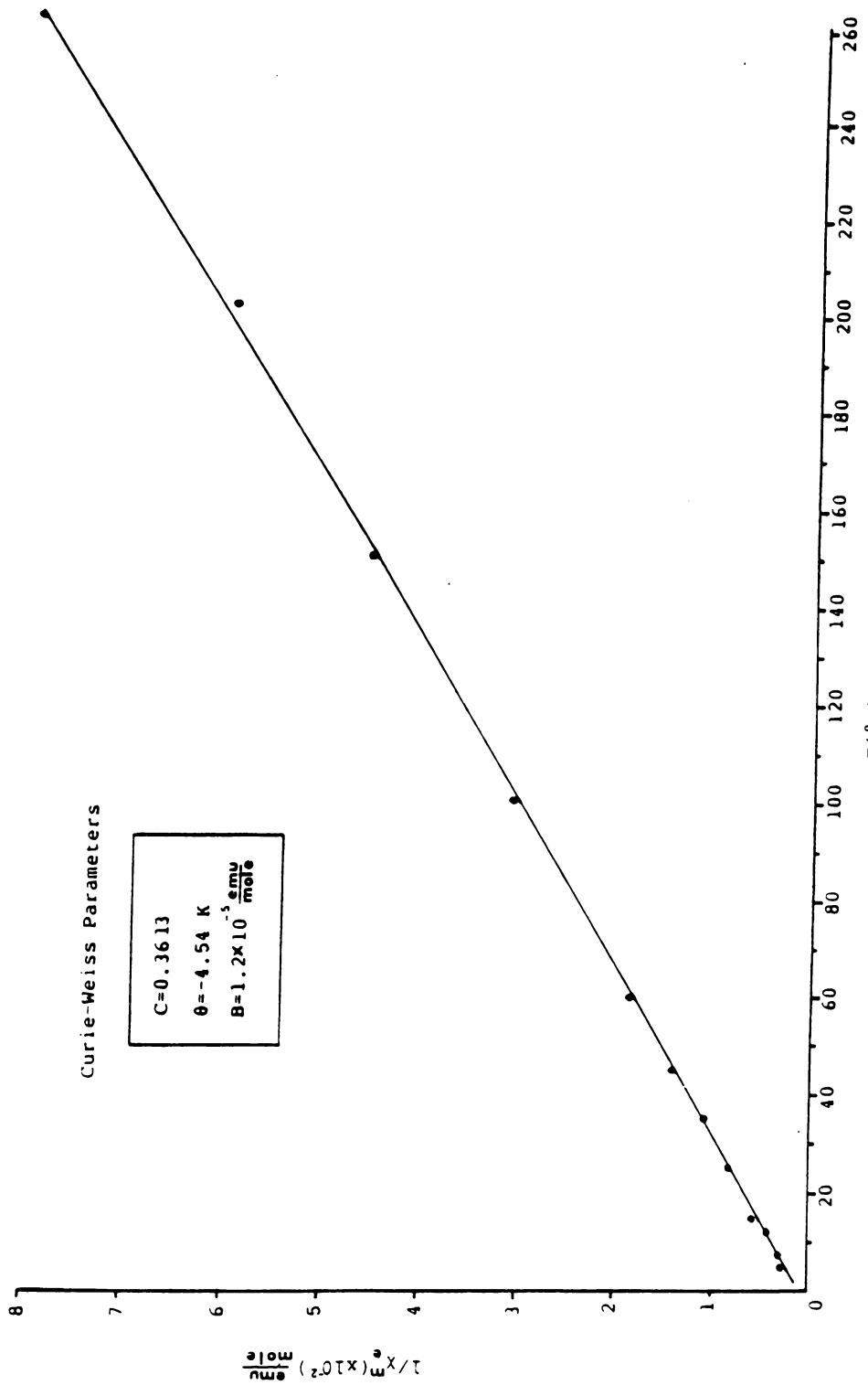


Figure 35. The reciprocal molar electronic susceptibility of an annealed sample of $\overline{Cs^{+}(15C5)_2}\cdot e^{-}$ as a function of temperature.

susceptibility follows Curie Weiss behavior with a fractional Curie constant of 97% and θ = -4.5 K, in accordance with the parameters obtained from the quenched sample. Below 5 K the behavior is much different. A plot of χ_e^M vs. T as a function of the applied field is shown in Figure 36. A maximum in the susceptibility occurs at ~4.2 K for all fields. The behavior below 4.2 K is field dependent, and indicative of antiferromagnetic coupling. At low fields (100 Gauss) the susceptibility falls off with decreasing temperature with an extrapolated value at 0 K of 69% of χ_e at 4.2 K. The susceptibility of a powdered antiferromagnet theoretically is expected to fall to $^2/_3$ of the value of the Neél point. Therefore at low fields the material acts as a classic antiferromagnet. As the field is increased to 7 kG the susceptibility falls with decreasing temperature to 3 K where it begins to rise with further decreases in temperature. Intermediate fields give intermediate behavior. For example the behavior at 1 kG falls with decreasing temperature to 2 K where it levels off at about 80 percent of the maximum susceptibility.

A plot of χ_e^M vs. H at a constant temperature of 1.6 K is shown in Figure 37. The susceptibility increases rapidly with the applied field until the field is ~4 kG.

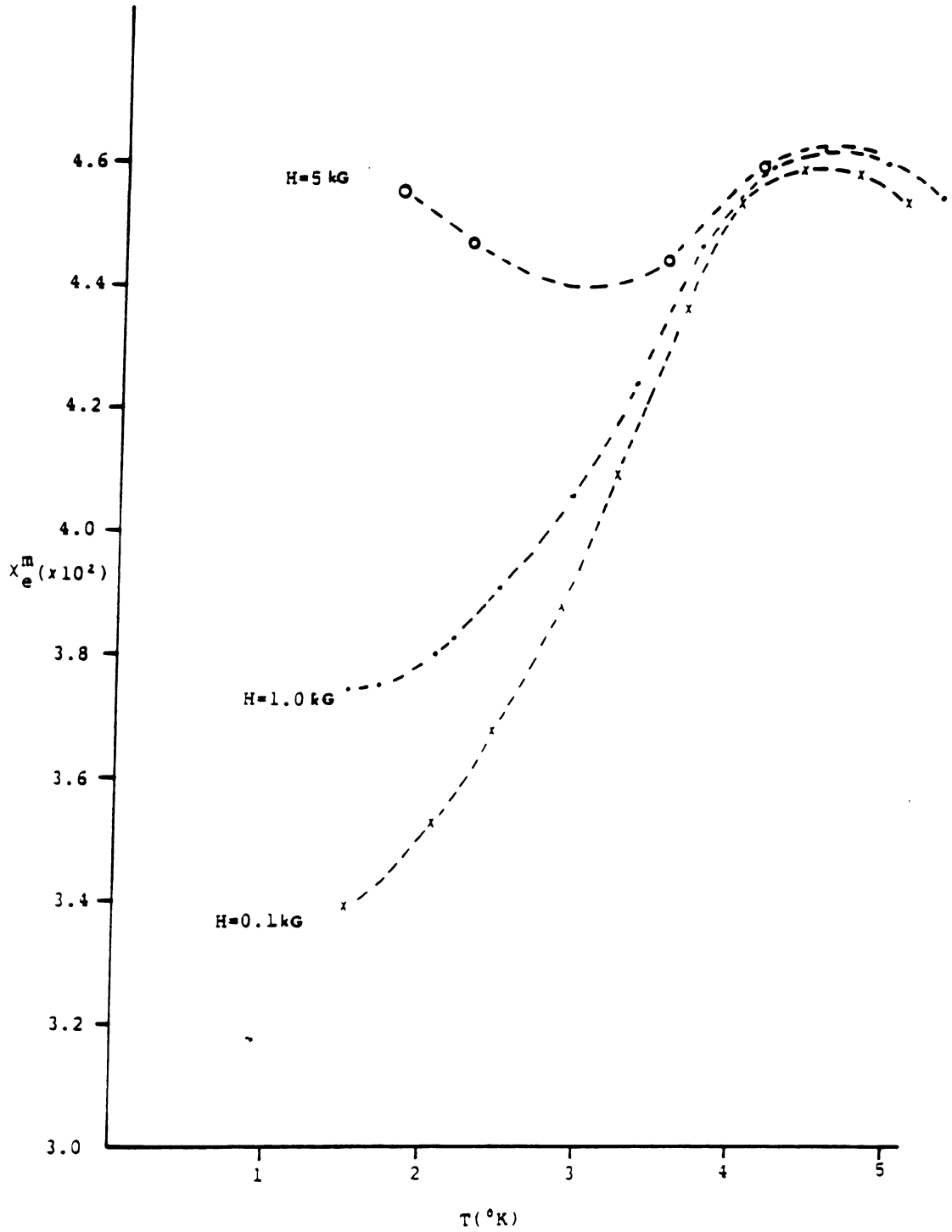


Figure 36. The temperature dependence of the molar electronic susceptibility an annealed sample of $Cs^+(15C5)_2 \cdot e^-$ as a function of the applied field.

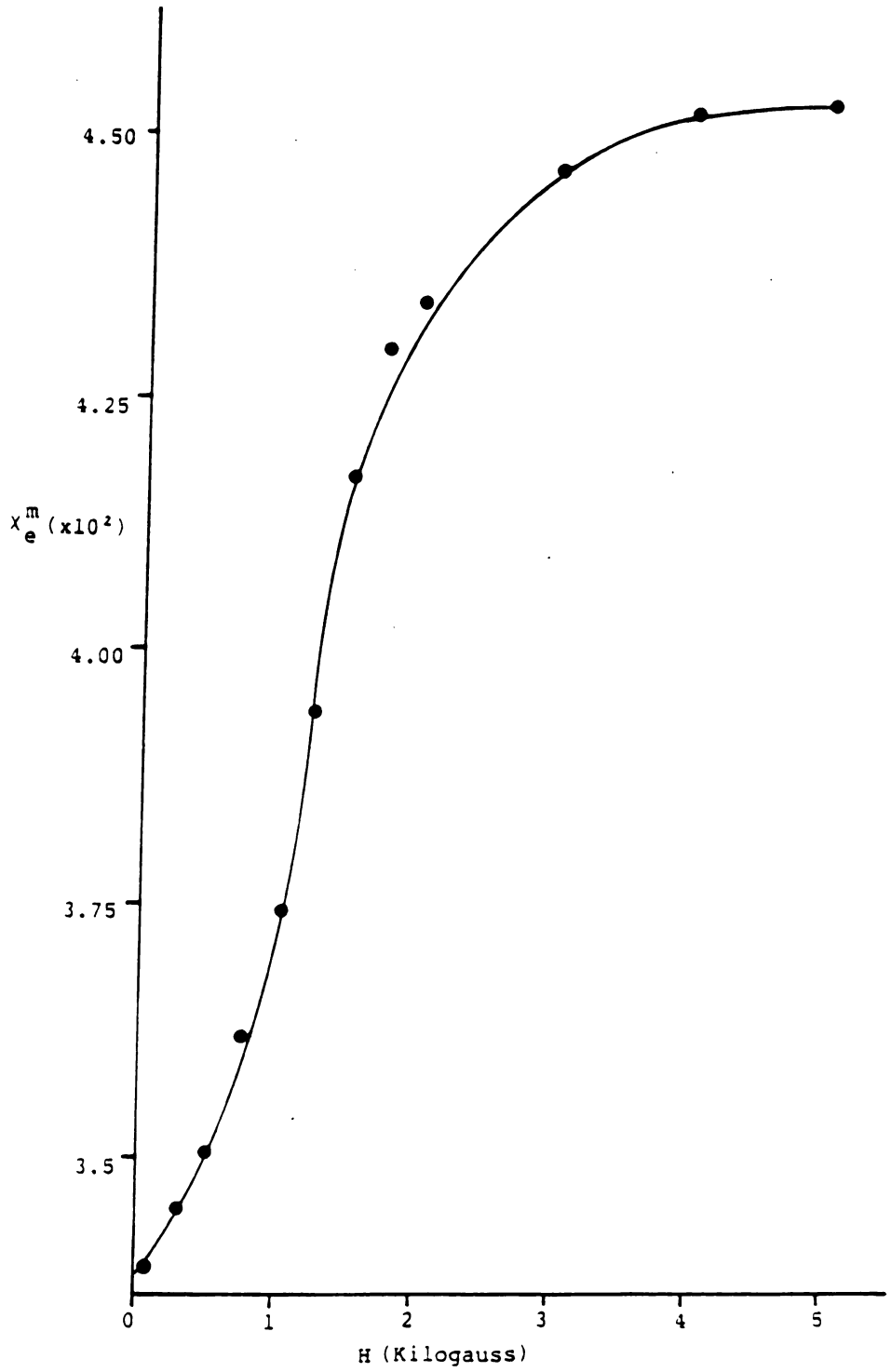


Figure 37. The molar electronic susceptibility of an annealed sample of $Cs^+(15C5)_2 \cdot e^-$ as a function of the applied field at 1.6 K.

At higher fields the susceptibility is approximately constant. An inflection in the curve occurs at ~1.5 kG.

The magnetic susceptibility of a non-metallic paramagnet is a probe of the electron-electron interactions. In the case of the electride the paramagnetic electrons are localized in cavities which are separated by 8.68 and 10.27 Å in the 18C6 salt and probably by a slightly shorter distance in the 15C5 salt. The $Cs^+(15C5)_2 \cdot I^-$ structure has interanionic distances of 8.32 and 9.31 Å. Since the iodide, sodide, and electride anions are nearly the same size a rough approximation of 8.5 and 9.5 Å from the iodide structure will be used for the nearest interelectron distance for comparative purposes. The shorter electron-electron distances in $Cs^+(15C5)_2 \cdot e^-$ with respect to $Cs^+(18C6)_2 \cdot e^-$ affects their respective interactions. The Weiss constant is ~-4.5 K for both quenched and annealed samples of $Cs^+(15C5)_2 \cdot e^-$ and is only -1.4 K for $Cs^+(18C6)_2 \cdot e^-$. The network of anionic nearest neighbors in each system gives an octahedral anionic nearest neighbor shell with four equivalent long interactions and two short axial distances. The short distances are very similar in the two electrides, 8.5 Å for the 15C5 salt, and 8.68 Å for the 18C6 salt, but the longer distances differ by ~1 Å. The 18C6 salt probably generates a mean field along the c direction with little interaction in the planes ∥ to the a-

b planes. The shorter distances in these planes in the 15C5 salt could allow a three dimensional magnetic lattice to exist. The Neél temperature of the annealed $Cs^+(15C5)_2 \cdot e^-$ is only ~4.2 K. Relative to other antiferromagnetic materials, $Cs^+(15C5)_2 \cdot e^-$ has several unique features. First the orbital angular momentum of the ground state of the trapped electron is zero, it is probably an s-state electron; typical antiferromagnets are composed of transition metal or rare earth ions where the magnetic electrons partially filled d or f orbitals. The distances between magnetic centers in $Cs^+(15C5)_2 \cdot e^-$ are very large on the scale of most antiferromagnets. Transition metal ions that are greater than 3 Å apart tend to have antiferromagnetic coupling that is mediated by a non-magnetic ion or conduction electrons. MnO [99] for example has Mn^{+2} separations of 4.3 Å -- too distant to have direct exchange. The material is antiferromagnetic (T_N = 122 K) by virtue of a super-exchange mechanism involving exchange interaction with filled oxygen orbitals. The closest magnetic ions in the electride salt are ~8.6 Å apart. It is possible but unlikely that a super-exchange mechanism is mediated by the Cs^+ cation. While NMR has shown electron density at the cesium nucleus due to interactions with eight nearest electrons, the orientation of cationic orbitals to mediate exchange for eight interacting

electrons would be difficult to arrange. Further, the interactions of the crown ether oxygen lone pairs with the Cs^+ ion would surely be a stronger influence on the p and d character of the cation than the diffuse electrons. Indeed, the paramagnetic Ramsey shift of the complexed cation is substantial and constant regardless of the anion, indicating that the excited state character of Cs^+ is a result of the Cs^+-O attraction. The extrapolations to infinite temperature of the paramagnetic Knight shift due to s orbital character of the trapped electron is equal to the Ramsey shift due to the complexed cation; there is no additional p or d character added by the trapped electron. The electron density at the nucleus might be better thought of as a measure of the diffuseness of the electron cloud, strengthening the possibility that the exchange is direct. The coupling is very weak although several antiferromagnets have lower Neél temperatures. Finally the field dependence below the Neél temperature is unusual, especially at such low fields. This field dependence is due to very weak coupling of the spin lattices to the easy axis in the crystal. The phenomenon is known as a 'spin flop' and is the result of weak crystalline anisotropy forces.

In a single antiferromagnetic crystal at temperatures below the Neél point, the magnetic moments of the two spin lattices in the absence of an applied field are opposed to

each other and parallel to the easy axis. As a weak field is applied, the crystal displays a susceptibility depending on the orientation of the easy axis with respect to the direction of the field. The energy of the crystal is lowered as the easy axis is rotated towards a 90° angle with the field. The perpendicular orientation of the easy axis is the lowest energy orientation because the magnetic moments are able to equilibrate with the externally applied magnetic field whereas there is no torque exerted on the spins that are aligned parallel to the applied field. The spin flop occurs when the applied field creates a difference in the energy of $\chi_\perp$ and $\chi_\parallel$ that is larger than the anisotropic force that is orienting the spins along the easy axis. Above this critical field all magnetic moments align perpendicular to the field regardless of the orientation of the easy axis, and a powder sample should have a similar susceptibility to that of the perpendicular single crystal as shown in Figure 32b. The critical field for the spin flop, H_f, is related to the anisotropy energy by

$$K = {}^1/_2(\chi_\perp - \chi_\parallel)H_f^2 \qquad (6.15)$$

Other antiferromagnets, with what are considered to be weak crystalline anisotropy energies, are $CuCl_2 \cdot 2H_2O$, with H_f = 7-8 kG [100], and Cr_2O_3, with H_f = 59 kG [101].

The crystalline anisotropy in $Cs^{+}(15C5)_2 \cdot e^{-}$ is very weak, but this is not a surprising result considering the origin of anisotropy fields. In general the anisotropy fields are due to crystal field quenching of the orbital angular momentum, anisotropic exchange mechanisms, and anisotropic dipole-dipole interactions. Since the postulated ground state of the electron has no angular momentum, and the exchange is expected to be direct, the only source of magnetic anisotropy in this system is dipole-dipole coupling. The trapped electron is expected, at least in the ground state, to occupy a spherical s-orbital in the trap, so that even dipole-dipole interactions should be weak. The nearly octahedral arrangement of the neighboring magnetic ions would be expected to generate only a small anisotropic field.

The nature of $Cs^{+}(15C5)_2 \cdot e^{-}$ includes long range magnetic ordering if the compound is cooled slowly from temperatures between 220 and 250 K, and does not show anti-ferromagnetism if it is rapidly cooled from above these temperatures. The DSC results indicate that there is a weak endothermic transition at 238 K. The exact nature of the transition cannot be deduced without structural information; however, a guess as to its nature might be made.

The electron-electron interaction in the $Cs^+(15C5)_2 \cdot e^-$ salt is probably similar to that of $Cs^+(18C6)_2 \cdot e^-$ where channels through the closest packed complexed cations serve as the least impeded means of communication. If none of the trapped electron density is considered to reside on proton, carbon, or oxygen orbitals then these saturated bonded atoms in the molecule would repel the electron density should they be near a channel between two adjacent electron traps. (This is probably a simplistic view since the hydrogen atoms nearest the electron center probably have some acidic character, hydrogens farther from the electron center are not as likely to have excess electron density however.) The channels in the $Cs^+(18C6)_2 \cdot e^-$ were described in Chapter III as being small in cross section with a significant amount of curvature at the most constricted point of the channel. The electrons in $Cs^+(18C6)_2 \cdot e^-$ do not communicate well through the lattice and thus do not show magnetic ordering.

To discuss the situation in $Cs^+(15C5)_2 \cdot e^-$ it will be assumed that the electride and iodide of $Cs^+(15C5)_2$ are isostructural. The structural features in $Cs^+(15C5)_2 \cdot e^-$ that would encourage stronger electron-electron overlap would be larger channels and shorter distances between cavities. The distances <u>are</u> on the average shorter in the 15C5 salt with a more isotropic arrangement of traps about

each cavity. The distance between electron centers is 8.68 Å along the c-axis and 9.6 Å in the x-y plane. The anionic cavity of $Cs^+(15C5)_2 \cdot I^-$ was studied on the Evans and Sutherland PS300 graphics system. The cavity in the 15C5 complex is considerably more spherical than the electron cavity in $Cs^+(18C6)_2 \cdot e^-$ (Figures 11 and 12), since the anion in the former compound sits on an inversion center and a four-fold rotation axis. There are only two unique channels between anionic cavities; anions along the c-axis are separated by a channel that is both longer and narrower than the interanionic channel in $Cs^+(18C6)_2 \cdot e^-$; however, the axial near neighbor anions in the iodide are separated by shorter, more open channels.

The endothermic transition at 238 K strongly affects the extent of the electron-electron interaction; it may also be related to the transitions seen in the static NMR of $Cs^+(18C6)_2 \cdot Na^-$ at similar temperatures. The linewidth of the static ^{23}Na resonance in this salt is primarily due to dipolar coupling of the protons to the sodium anion. At temperatures below 240 K the linewidth is ~2700 Hz in agreement with the linewidth calculated from the Van Vleck formula (eqn. 5.1) and the known proton-Na^- distances. Above 240 K the peak narrows to ~1300 Hz, a change that is far too dramatic to be the result of a phase transition between two static crystalline phases. The explanation for

the narrowing is that near 240 K there is an onset of rapid motion of the protons that line the anionic cavity such that the anisotropic dipolar coupling to ^{23}Na is partially averaged. It is clear that if this dynamic system were rapidly quenched the conformation of the crown ether would not necessarily be that of the lowest energy state. The electron-electron coupling in this compound is very weak so that a slight distortion, such as a hydrogen moved to further constrict a channel, could destroy the long range order necessary for magnetic ordering. The ^{133}Cs NMR in this temperature region does not show any splitting; however, the density at the cesium nucleus does deviate towards higher contact density at this point. It is unclear why there is a tendency for the electron to localize more strongly on the cesium with increased motion of the crown when at 270 K a second endothermic transition causes an abrupt decrease in the contact density. The increased density at the ^{133}Cs nucleus at temperatures above 240 K with the decrease in the magnetic order does indicate that a superexchange mechanism is not responsible for mediating the magnetic ordering in this salt.

The results of the magnetic susceptibility studies indicate that $Cs^{+}(15C5)_2 \cdot e^{-}$ and $Cs^{+}(18C6)_2 \cdot e^{-}$ have a very sensitive and unique form of electron interaction. The structures of the two electrides are quite similar, but

subtle changes in the trapped electron network are responsible for quite different behavior in the two compounds. $Cs^+(18C6)_2 \cdot e^-$ has essentially non-interacting trapped electrons, $Cs^+(15C5)_2 \cdot e^-$ shows a fragile magnetic ordering. Of the electrides isolated so far, only those with the complexed cations consisting of crown ether sandwiches show pure Curie-Weiss paramagnetism with or without magnetic ordering. In addition to the cesium compounds described here $K^+(15C5)_2 \cdot e^-$, and $Rb^+(15C5)_2 \cdot e^-$ have been isolated [72] and behave as Curie-Weiss paramagnets. Electrides with cryptand complexants tend to have much more strongly interacting electrons. $K^+C222 \cdot e^-$ and $Rb^+C222 \cdot e^-$ are metallic Pauli paramagnets [93]; $Cs^+C222 \cdot e^-$ is diamagnetically spin paired [93]; and $Li^+C211 \cdot e^-$ shows a temperature dependent spin pairing [74] which seems to be best described in terms of a dimerization of electrons at low temperatures. To date, no strong characterization of electrides containing 1:1 complexes with crown ethers exists. Only $Rb^+18C6 \cdot e^-$ has been reported [71] and the stoichiometry of this compound remains a puzzle. If it is an electride it too will fall into the category of electrides which show extensive spin pairing.

VI.C. Electron Paramagnetic Resonance of $Cs^+(15C5)_2 \cdot e^-$

The EPR spectra of $Cs^+(15C5)_2 \cdot e^-$ were measured over the temperature range 2-250 K for three different samples. The EPR line of the trapped electron of $Cs^+(15C5)_2 \cdot e^-$ might be expected to display hyperfine coupling to the eight cesium cations, since the NMR results show that there is a small but finite electron density at each cesium nucleus. The hyperfine constant, A, gives the splitting of each electron state due to interactions with the magnetic moment of the cesium nuclei. The strength of the hyperfine interaction is related to $\langle|\psi(o)|^2\rangle$, the electron density at the nucleus, by

$$A_{iso} = (8/3)\pi g \mu_B g_N \mu_N \langle|\psi(o)|^2\rangle \qquad (6.16)$$

where g and g_N are the electronic and nuclear g-values, and μ_B and μ_N are the electronic and nuclear magnetons. For $Cs^+(18C6)_2 \cdot e^-$ the density of one electron at each of eight nuclei is one-eighth of the total electron density at that nucleus if it is assumed that each anion-cation interaction is equal. The expected hyperfine spectrum for $Cs^+(15C5)_2 \cdot e^-$ at 200 K where $\langle|\psi(o)|^2\rangle = 2.2 \times 10^{22}$ e^-/cm^3 from Knight shift measurements, if it is assumed that eight equivalent nuclei interact with each trapped electron,

would consist of 57 lines arising from 2(7/2·8) + 1 different summations of the nuclear magnetic moments of the eight nearest cations. Each line would be separated by 0.10 G according to the value of $\langle|\psi(o)|^2\rangle$ from NMR measurements. Interactions with hydrogens on the crown ethers could further complicate the spectrum. In the absence of broadening interactions with the crown ether hydrogens, the spectral breadth would be about 6 G.

The observed spectrum at 200 K is a narrow single line. The peak to peak width of the line, ΔH_{p-p}, is 0.6 G, and the g-value of the line is 2.0022 +/- 1 × 10^{-4}, which is nearly identical to the free electron g value. Deviations in the g value are indicative of spin-orbit coupling to orbitals of non-zero angular momentum. The linewidth is about one order of magnitude smaller than the expected width of the hyperfine broadened spectrum. Therefore, it must be assumed that the line is narrowed by rapid exchange [94], in which electrons are able to exchange their spin angular momenta via a first order process. The large concentration of electrons in $Cs^+(15C5)_2 \cdot e^-$ and significant electron-electron interactions allow the exchange to proceed at a rate more rapid than the relaxation rate due to the hyperfine interaction so that the hyperfine coupling of electrons is averaged to a small value. Similar exchange narrowing occurs in $Cs^+(18C6)_2 \cdot e^-$, and in other

high electron density radicals, including DPPH.

The temperature dependence of the EPR spectrum of three samples of $Cs^{+}(15C5)_2 \cdot e^{-}$ was measured over a temperature range of 2.0 K to 240 K. Selected spectra at various temperatures for each sample are displayed in Figures 38, 39 and 40. In all cases the sample was rapidly quenched from 270 K to 2.5 K. The intensities of the spectra in general follow the 1/T dependence expected for Curie-Weiss paramagnets, and there is no significant g-shift. ΔH_{p-p} does vary with temperature, however. The temperature dependence of ΔH_{p-p} of sample 1, which maintained what appeared to be a single component peak at all temperatures, is shown in Figure 41. The increase in ΔH_{p-p} with decreasing temperature below 40 K empirically follows a $T^{-2/3}$ dependence. The low temperature spectra of the "quenched" sample in Figure 39 displays a partially structured, broadened line, the high field lobe of the first derivative of the resonance absorption is split into two peaks, while the low field absorbance shows no structure. Sample 3 displays the most complex behavior as a function of temperature. The spectra at 2.5 K and 6 K of the "quenched" sample are very narrow, ΔH_{p-p} = 1.1 gauss, but show some structure on the line. This sample was then

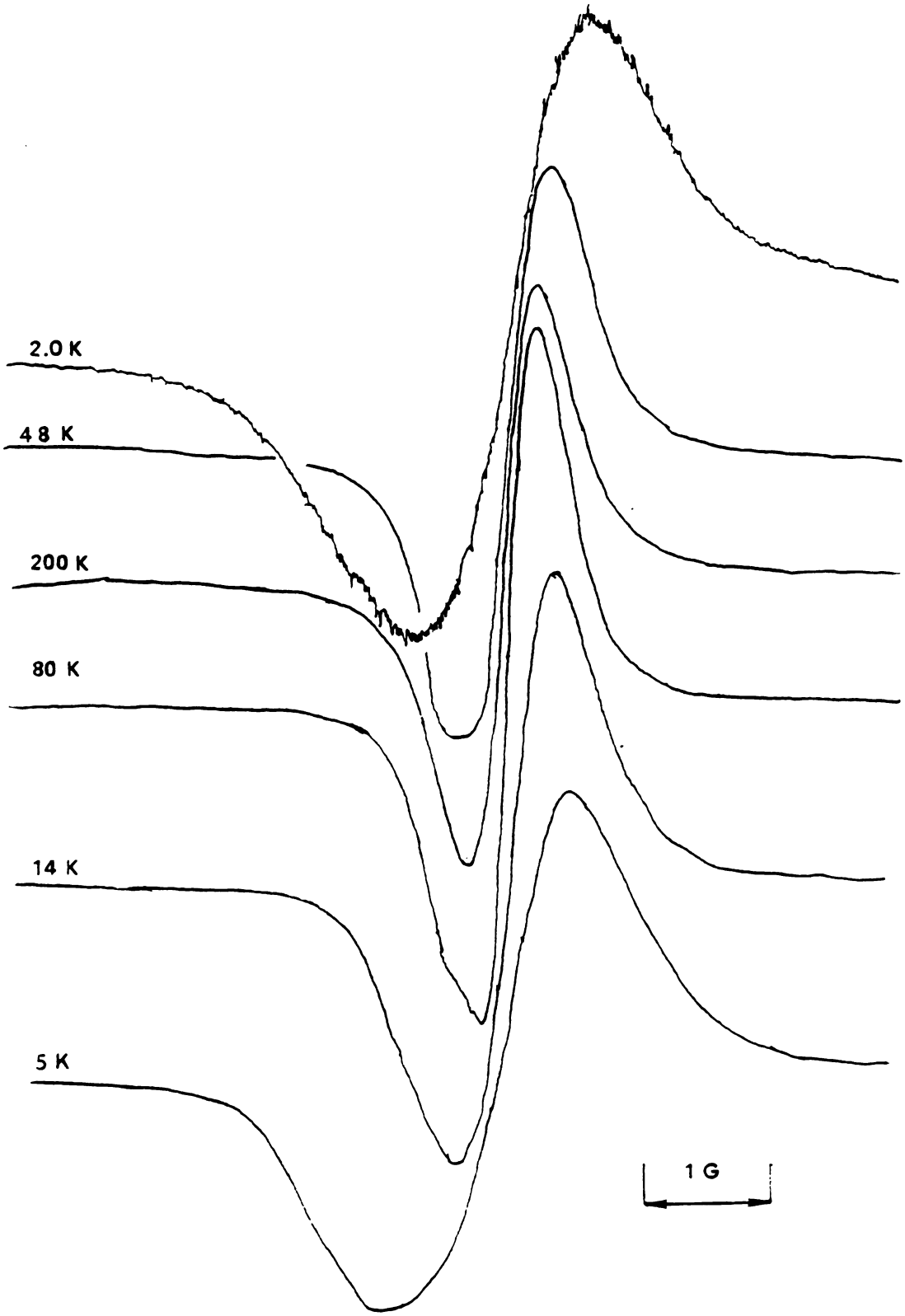


Figure 38. EPR spectra of $Cs^{+}(15C5)_2 \cdot e^{-}$, sample 1 at 2.0 K, 48 K, 200 K, 80 K, 14 K, and 5 K.

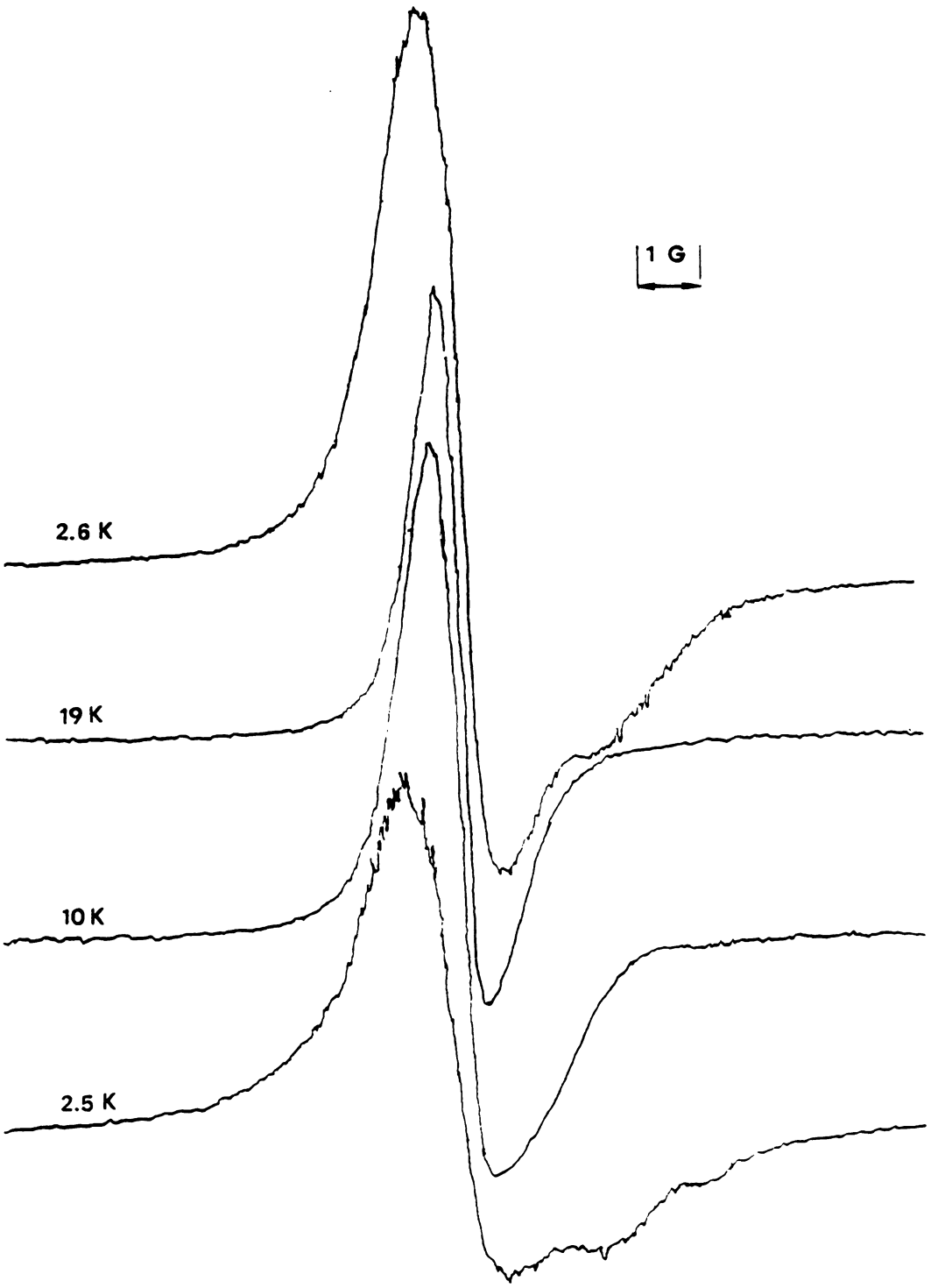


Figure 39. EPR spectra of $Cs^{+}(15C5)_2 \cdot e^{-}$, sample 2, at 2.8 K, 19 K, 10 K and 2.5 K.

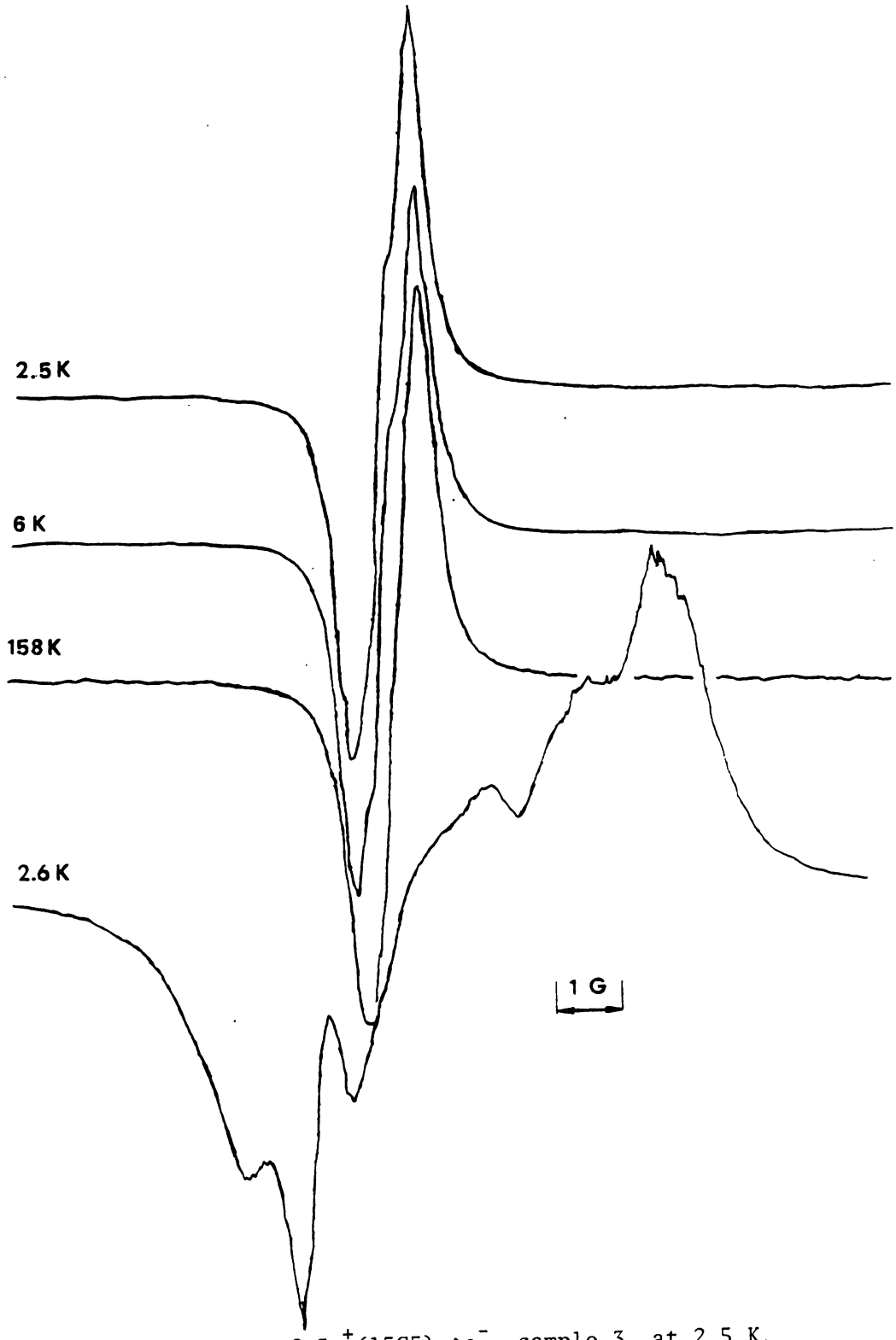


Figure 40a. EPR spectra of $Cs^{+}(15C5)_2 \cdot e^{-}$, sample 3, at 2.5 K, 6 K, 158 K, and 2.6 K.

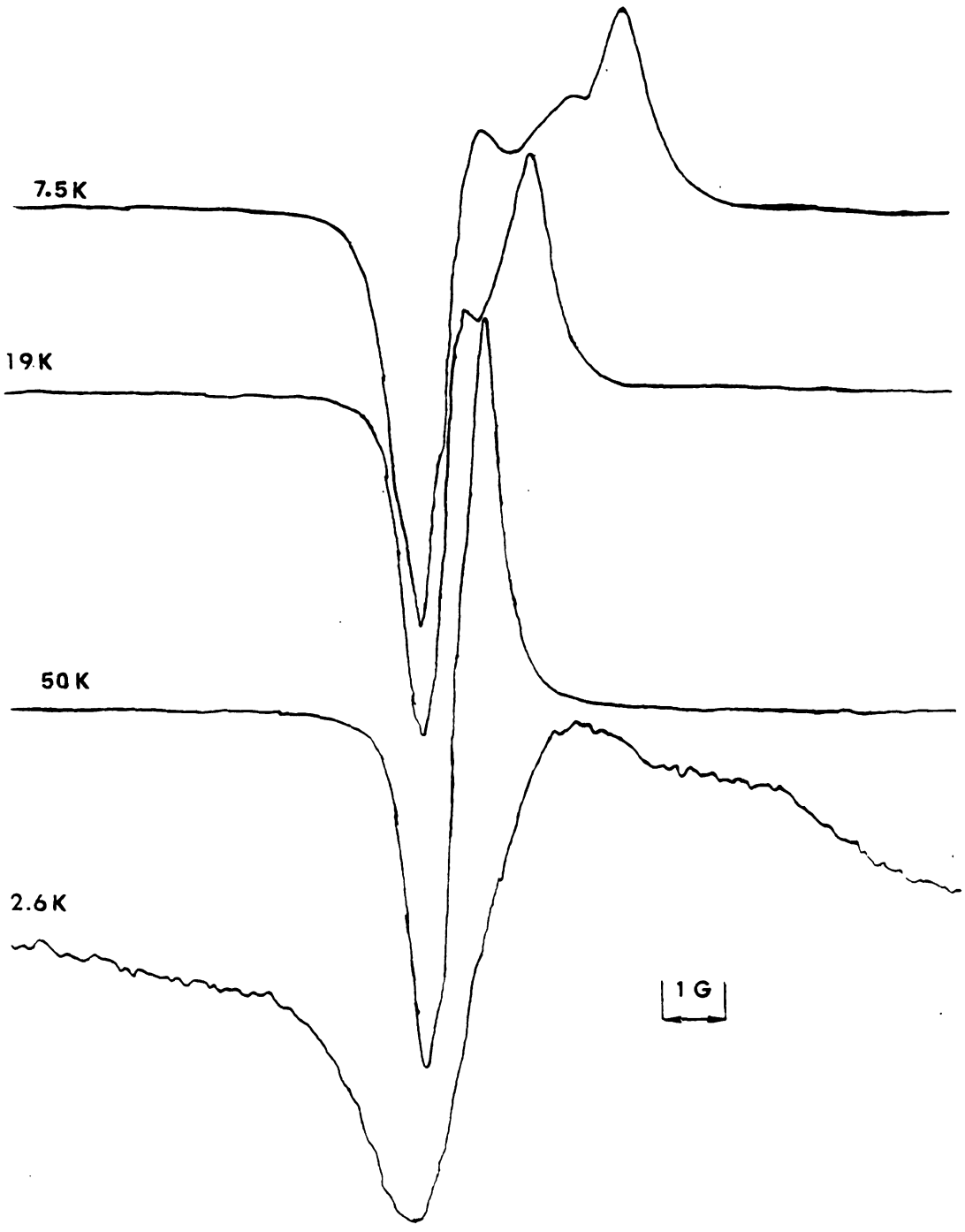


Figure 40b. EPR spectra of $Cs^{+}(15C5)_2 \cdot e^{-}$, sample 3, at 7.5 K, 19 K, 50 K, and 2.6 K.

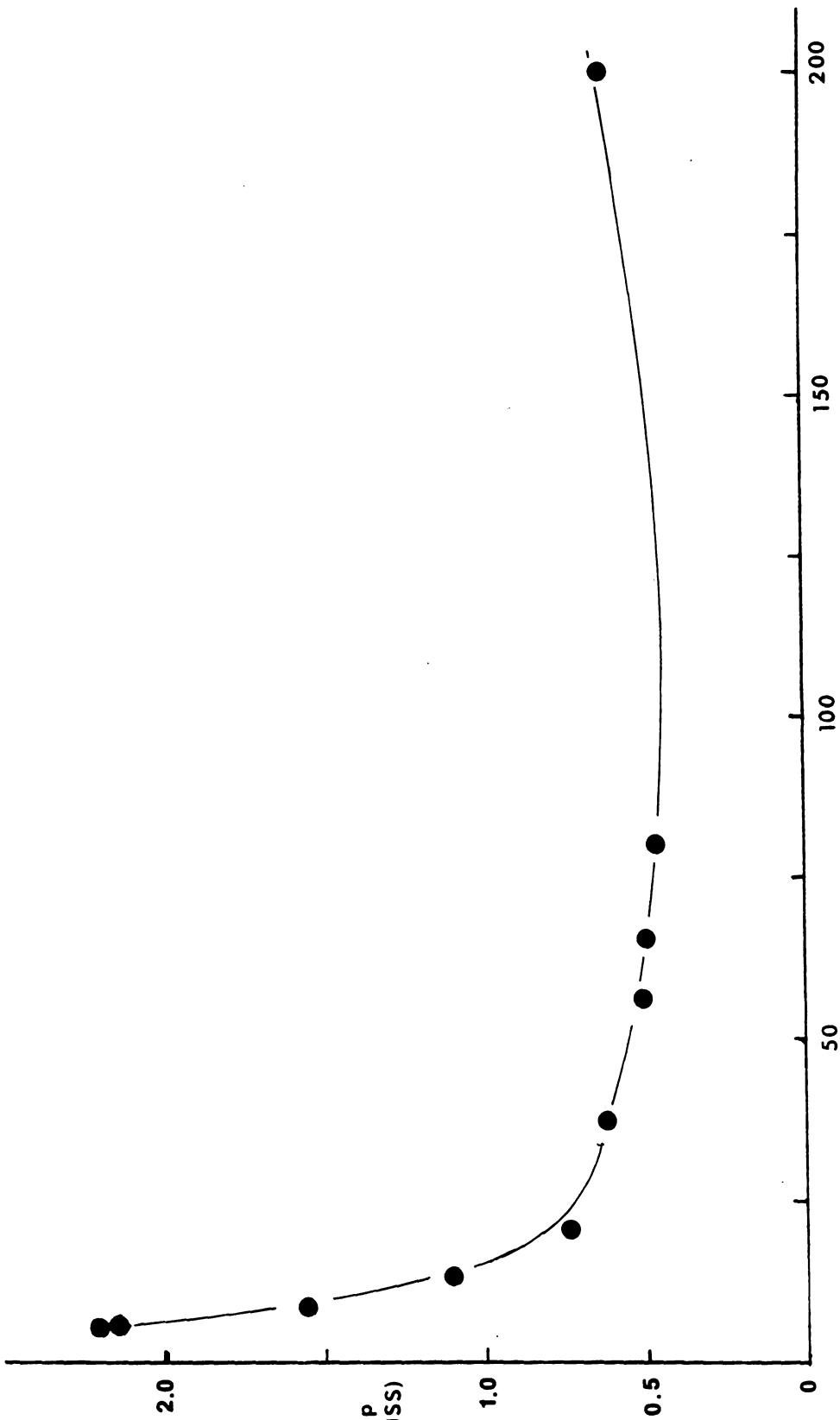


Figure 41. ΔH_{p-p} as a function of temperature for sample 1 of $Cs^{+}(15C5)_2 \cdot e^{-}$.

warmed to at least 160 K and then gradually recooled. The EPR spectrum of the "annealed" sample at 2.6 K, shows a remarkably broad, well-resolved six line structure. The splitting between peaks is roughly 1 G. As the sample was warmed to 7.5 K and then to 19 K the structure of the low field lobe of the line rapidly disappeared, while the structured high field absorption gradually narrowed. By 50 K the EPR line was indistinguishable from that of the other samples. The sample was then warmed to 220 K and rapidly cooled. The resulting spectrum at 2.6 K more closely resembled the low temperature spectra of Figure 39 with less resolved multi-line structure.

The increased breadth and onset of complicated structure of the EPR line of $Cs^{+}(15C5)_2 \cdot e^{-}$ at low temperatures appears to have a dependence on the thermal history of the sample, and, while the effect of thermal cycling is more profound in the temperature range of 5 K to 20 K, the similarity to the onset of quench/anneal behavior in the magnetic susceptibility is striking. The response of antiferromagnetically coupled spins to the EPR conditions requires consideration of crystalline anisotropy forces, and crystalline shape anisotropies in addition to the exchange and thermal energies. All measurements were made at x-band microwave frequencies, ν = 9.6 GHz, and at fields near 3400 gauss, well above the spin-flop critical field.

In order to investigate systematically the relative importance of the various influences on the EPR spectrum, single crystal experiments are required [96]. Single crystal EPR and zero-field or low-field antiferromagnetic resonance experiments [96] are capable of probing the strength of the sublattice magnetizations and the orientation and strength of the crystalline anisotropy forces.

While the low temperature spectra observed in $Cs^{+}(15C5)_{2}\cdot e^{-}$ are almost certainly affected by high temperature phase transitions that, in turn, affect bulk electron-electron interactions, the observed line broadening at low temperatures is not necessarily due to those electron-electron interactions, but may rather be the result of coincident changes in electron-nuclear interactions. The onset of low temperature broadening occurs at nearly 50 K, and the structure in the EPR lines appears at temperatures as high as 20 K, whereas the onset of magnetic ordering comes at only 4.2 K. Increased isotropic hyperfine coupling may result in a line that is not completely averaged by rapid exchange narrowing. Again the results from the three samples, while sharing general characteristics, are too varied to justify speculation about their interpretation. J. Kim, in Profesor James L. Dye's laboratory, is presently engaged in the design of an

EPR goniometer that could be used to further study the low temperature single crystal EPR spectra of $Cs^{+}(15C5)_2 \cdot e^{-}$.

CHAPTER VII

CONCLUSIONS AND SUGGESTIONS FOR FUTURE WORK

VII.A. Conclusions

A new electride, $Cs^+(15C5)_2 \cdot e^-$, was synthesized and characterized by DSC, solid state NMR, optical spectroscopy, and magnetic susceptibility. Analysis of the sample verified the stoichiometry.

A new method for mounting single crystals of the air and temperature sensitive alkalides and electrides for x-ray crystallography enabled the determination of the structure of $Cs^+(18C6)_2 \cdot Na^-$, the first crystal structure of an alkalide since 1974. The space group is the monoclinic C2/c, with lattice parameters $\underline{a}$ = 13.581 Å, $\underline{b}$ = 15.684 Å, c = 17.429 Å, β = 93.16. The first crystal structure of an electride, $Cs^+(18C5)_2 \cdot e^-$, was also determined. The electride is nearly isostructural to the sodide, with lattice parameters $\underline{a}$ = 13.075 Å, $\underline{b}$ = 15.840 Å, $\underline{c}$ = 17.359 Å, and β = 92.30 in C2/c. The structure consists of a lattice of tightly packed complexed cations with large (5 Å diameter) interstitial anionic cavities at the same location as the Na^- ions in the sodide. These cavities contain sub-noise

level electron density, and they do not contain any atomic species. The structure provides the first direct evidence of a site for the stoichiometric localized electrons.

The crystal structure of $Cs^+(15C5)_2 \cdot I^-$ was determined. The iodide anion has a similar anionic radius to the trapped electron and is expected to be similar in its packing to that of $Cs^+(15C5)_2 \cdot e^-$, whose structure has not been determined. The space group of the iodide is tetragonal I4, with lattice parameters $\underline{a}$ = 13.172 Å, and $\underline{c}$ = 16.645 Å. All three of the structures have similar packing of the ions, and similar anionic environments.

Solid state ^{133}Cs NMR was performed on a variety of simple and complexed Cs^+ salts, and on the one known compound that contains $Cs^+(18C6)_2 \cdot Cs^-$.

The chemical shift of simple cesium salts is dominated by a paramagnetic Ramsey shift that ranges from 284 ppm for CsI to 190 ppm for CsSCN; the shift is stronger for anions of greater polarizability. Exclusive complexes of Cs^+ with C222 as well as complexes of Cs^+ with 18C6 in a 1:1 ratio have a weaker, but anion dependent paramagnetic Ramsey shift.

The chemical shift of $Cs^+(18C6)_2$ sandwiched complexed cations is -60 +/-2 ppm for all anions except the ceside and the tetraphenylborate. The chemical shift of $Cs^+(15C5)_2$ salts is 28 +/-6 ppm, and the chemical shift of

inclusive Cs^+C222 salts is ~240 ppm. The chemical shift of inclusively complexed cations in the solid state, whether by C222 or by sandwiched crown ethers, is very sensitive to the overlap of oxygen lone pairs with empty Cs^+ orbitals, and is thus sensitive to the mean Cs-O distance in the complexed cation. Large anions in $Cs^+(18C6)_2$ salts apparently require a different conformation of the crown ethers about the cation in which the mean Cs-O distance is decreased.

Static and single crystal NMR studies revealed the anisotropic chemical shift and quadrupolar interaction parameters for $Cs^+(18C6)_2 \cdot I^-$ (δ = 32 ppm, η = 0, e^2Qq/h = 89.6 KHz) and $Cs^+(15C5)_2 \cdot I^-$ (δ = 52 ppm, η = 0, e^2Qq/h = 427 KHz).

Dipolar linewidths were measured for ^{133}Cs and ^{23}Na in $Cs^+(18C6)_2 \cdot Na^-$ at two temperatures, 200-210 K and 250 K. The low temperature linewidths correspond to the values calculated from structural parameters. The high temperature static spectra are substantially narrowed due to rapid motion of hydrogens on the crown ethers relative to Cs^+ and Na^- which averages their dipolar fields.

Cs^- in $Cs^+(18C6)_2 \cdot Cs^-$ is paramagnetically shifted from the chemical shift of the gaseous anions by ~135 ppm at 220 K. The anionic chemical shift approaches the gaseous anion value with increased temperature; a phase transition at 285 K shifts the resonance to -240 ppm. The phase

transitions in this material act to increase the anionic cavity size with increased temperature.

The chemical shift of electrides is strongly affected by a contact interaction of the paramagnetic trapped electrons. The temperature dependence of the chemical shift was carefully measured for both $Cs^+(18C6)_2 \cdot e^-$ and $Cs^+(15C5)_2 \cdot e^-$; both follow a 1/T dependence characteristic of the Curie Weiss paramagnetism of the electrons. The electron density at the Cs^+ nucleus was calculated from the magnitude of the slope of the chemical shift versus 1/T. The fractional atomic character of Cs^+ in $Cs^+(18C6)_2 \cdot e^-$ is 3.3×10^{-4}, and of Cs^+ in $Cs^+(15C5)_2 \cdot e^-$ is 8.4×10^{-4}.

A phase transition occurs at ~220 K for $Cs^+(18C6)_2 \cdot e^-$. The NMR spectrum indicates that a conformation of the complexed cation with shorter Cs-O distance is stable at low temperatures.

Two phase transitions at 238 K and 268 K affect the temperature dependence of the NMR spectrum of $Cs^+(15C5)_2 \cdot e^-$. The low temperature transition appears to increase the electron density at the nucleus as the temperature increases. The phase transition at 268 K appears to localize the electron in the cavity more strongly, in that the $Cs^+(15C5)_2 \cdot e^-$ resonance shifts abruptly upfield by 190 ppm.

The greater electron density at the cesium nucleus in $Cs^+(15C5)_2 \cdot e^-$ compared to $Cs^+(18C6)_2 \cdot e^-$ indicates that the cationic charge in the 15C5 salt is less effectively shielded by the crown ethers than is CS^+ in the 18C6 complex. The poorly shielded cations in $Cs^+(15C5)_2 \cdot e^-$ cause the electron density to be drawn into the lattice, resulting in relatively strong electron-cation interactions.

NMR spectra were measured for several samples of compounds of mixed anionic stoichiometry. Solid samples prepared from solutions of stoichiometry $Cs^+(18C6)_2 \cdot Cs^-_x e^-_{(1-x)}$ are separated into two phases, the pure electride and pure ceside, for all values of x between 0 and 1. Solid samples prepared from solutions of stoichiometry $Cs^+(18C6)_2 \cdot Na^-_x e^-_{(1-x)}$, for $0<x<1$, display a five line NMR spectrum which indicates that a solid compound, $Cs^+(18C6)_2 \cdot Na^-_{0.85}$, is formed that includes ~15% substitution of Na^- for trapped electrons. A superlattice based on the known structures of $Cs^+(18C6)_2 \cdot e^-$ and $Cs^+(18C6)_2 \cdot Na^-$ was proposed that gives good agreement with the spectral features. The results indicate that each Cs^+ interacts with each of the eight anions in its nearest neighbor shell.

The magnetic susceptibility of $Cs^+(15C5)_2 \cdot e^-$ was measured over the temperature range 1.5-280 K. $Cs^+(15C5)_2 \cdot e^-$ shows two types of behavior depending on the

thermal history of the sample. Quenched samples show Curie-Weiss paramagnetism over the full range of temperatures. Annealed samples display antiferromagnetism with a Neél temperature of 4.2 K. The exchange anisotropy is very weak in $Cs^{+}(15C5)_2 \cdot e'^{-}$ since a spin flop occurs at fields greater than 1.5 kG.

The thermal characteristics of $Cs^{+}(15C5)_2 \cdot e^{-}$ were measured by DSC and optical spectroscopy. Phase transitions occur at 238 K and 268 K. The optical spectrum shows a temperature dependent three peak absorbance in the near IR. In general the absorbance occurs at higher energies as the temperature is increased through the two phase transitions. The electron finds a deeper trap with increasing temperature. This stronger localization accounts for the lack of magnetic order in quenched samples of $Cs^{+}(15C5)_2 \cdot e^{-}$ as well as the decrease in electron density at the nucleus above 265 K.

The magnetic and structural information may be used to draw a clear picture of the trapped electron in the electrides $Cs^{+}(18C6)_2 \cdot e^{-}$ and $Cs^{+}(15C5)_2 \cdot e^{-}$. The electron is localized at the anionic sites in the crystal lattice by Coulombic attractions to eight complexed cations. The extent of localization is sensitive to the nature of the complexed cation, the less shielded positive charge in $Cs^{+}(15C5)_2 \cdot e^{-}$ attracts the electron density from the cavity so that interionic interactions are stronger than in the

well shielded $Cs^{+}(18C6)_2 \cdot e^{-}$.

VII.B. Suggestions for Future Work

While great strides have been made in improving the synthetic methods and increasing the number of known alkalides and electrides in the past five years, this work suggests several new synthetic directions.

Grey powders have been isolated from Cs/12C4 mixtures. There has, however, been no reproducible characterization of the compound. The electride of Cs/12C4 would complete the series of sandwiched crown ether electrides, and might be expected to show stronger interionic interactions. New complexants such as 21C7, C322, and nitrogen analogs of the crown ethers could be important for future syntheses of alkalides and electrides.

NMR studies of samples that contained both $Cs^{+}(15C5)_2 \cdot e^{-}$ and $Cs^{+}(18C6)_2 \cdot e^{-}$ gave a peak that was intermediate between the pure electride peaks, suggesting the possibility that a solid state reaction forms an electride with mixed complexants, $Cs^{+}15C5/18C6 \cdot e^{-}$. Stoichiometric compounds might be formed with mixed complexants, if they are more stable than those formed with a single complexant.

The successful preparation of a compound of mixed anionic stoichiometry, $Cs^{+}(18C6)_2 \cdot Na^{-}_{0.15}e^{-}_{0.85}$, may occur in other alkalide/electride salts. The effect of doping an electride that has strong electron-electron interactions with diamagnetic anions could strongly affect transitions to the metallic state or to an ordered magnetic state. Besides Na^{-}, other dopants might include K^{-}, Rb^{-}, I^{-}, and Br^{-}, since these spherical anions are closest in size to the trapped electron, depending on the size of the interstitial cavities in the particular salt.

Single crystal x-ray diffraction techniques have been established for alkalides and electrides, and should be used to determine crystal structures when possible in order to complete the physical characterization of these materials. Electride structures are especially important since the environments about the electron trap may be used to help explain the diversity of properties observed for compounds in this class of materials.

Powder diffraction methods should be initiated, with a focus on compounds that are not easily crystallized into large, high quality single crystals. Since salts that contain similar cations tend to be nearly isostructural, the use of single crystal structural information from similar salts, and other techniques that give some insight into structural features such as solid state NMR or EXAFS, in combination with the powder data, should enhance the

information obtainable from powder x-ray diffraction. In materials that display phase transitions, variable temperature powder diffraction should be used to discern the nature of the transition.

Differential Scanning Calorimetry should become a standard analytical technique. Phase transitions in electrides may have a large effect on the interionic interactions. DSC could be useful not only to explain results that have discontinuities, but also as a guide to those temperatures where interesting changes in magnetic or electrical behavior might occur.

NMR studies of ^{133}Cs may be used to obtain a great deal of structural information. For example, both static and MAS spectra can be used to study cation-anion interactions in paramagnetic electrides as a function of temperature. The temperature calibration of the chemical shift in $Cs^{+}(18C6)_{2}\cdot e^{-}$ makes this compound useful as a thermometer for further temperature studies involving salts that contain cesium.

The high temperatures narrowing of the static NMR line in $Cs^{+}(18C6)_{2}\cdot Na^{-}$ and $Cs^{+}(15C5)_{2}\cdot e^{-}$ implies that hydrogens on the crown ethers have sufficient thermal motion that their dipolar contributions to the magnetic field at the Cs^{+} ion is averaged to zero. It may be possible to detect ^{1}H NMR in these compounds. It would be interesting to measure the trapped electron density on the hydrogens to

better quantify the "location" of the trapped electron.

It appears that EPR spectra of electrides contain a great deal of information about electron interactions with other ions. However, a single crystal-multiple orientation spectra may be required to extract this information. The temperature dependence of the breadth of the EPR line in $Cs^{+}(15C5)_{2}\cdot e^{-}$ suggests that near the onset of magnetic ordering at 4.2 K, the exchange narrowed EPR line broadens, and becomes structured in some cases. This structure may give information about the relationship of the electron-electron interactions with crystal anisotropy and exchange forces.

The low temperature transition to an antiferromagnetic state and the onset from high temperatures of the magnetic ordering in $Cs^{+}(15C5)_{2}\cdot e^{-}$ could be explored by heat capacity measurements, and/or by neutron diffraction experiments.

Finally, now that the crystal structure of $Cs^{+}(18C6)_{2}\cdot e^{-}$ is known and can complement its physical characterization, the time is ripe for theoretical considerations of the localization of the trapped electron in this electride salt.

REFERENCES

REFERENCES

1. B. Henderson; "Defects in Crystalline Solids", Crane Russack & Co., New York, 1972.

2. H. Ivey; Phys. Rev. 72, 341 (1947).

3. W.B. Fowler in "The Physics of Color Centers", ed. W.B. Fowler, Academic Press, New York, 1968.

4. J.J. Markham; "F-Centers in Alkali Halides", Academic Press, New York, 1966.

5. H. Seidel and H.C. Wolf in "The Physics of Color Centers", ed. W.B. Fowler, Academic Press, New York, 1968.

6. W. Freyland, K. Garbade, H. Heyer and E. Pfeiffer; J. Phys. Chem. 88, 3745 (1984).

7. L. Kevan, Adv. Radiat. Chem. 4, 181 (1974).

8. W.J. Chase and J.W. Hunt, J. Phys. Chem. 79, 2835 (1975).

9. L. Kevan; J. Phys. Chem. 84, 1232 (1980).

10. L. Kevan, M.K. Bowman, P.A. Narayana, R.K. Boeckman, U.I. Yudanov and Yu.D. Tsvetkov, J. Chem. Phys. 63, 409 (1975).

11. L. Kevan, Acc. Chem. Res. 14, 138 (1981).

12. D.F. Feng and L. Kevan, Chem. Rev. 80, 1 (1980).

13. D.A. Copeland, N.R. Kestner, J. Jortner, J. Chem. Phys. 53, 1189 (1970).

14. K. Fueki, D.F. Feng, L. Kevan, J. Am. Chem. Soc. 95, 1398 (1973).

15. J. Jortner, Mol. Phys. 5, 257 (1962).

16. J.A. Morgan, R.L. Schroeder, and J.C. Thompson, J. Chem. Phys. 43, 4494 (1965).

17. N. Mammano and M.J. Sienko, J. Am. Chem. Soc. 90, 6322 (1968).

18. A.M. Stacy and M.J. Sienko, Inorg. Chem. 21, 2294 (1982).

19. W.S. Glaunsinger, S. Zolotov and M.J. Sienko, J. Chem. Phys. 56, 4756 (1972).

20. A.M. Stacy, D.C. Johnson and M.J. Sienko, J. Chem. Phys. 76, 4248 (1982).

21. M.J. Sienko, in "Metal Ammonia Solutions", eds. G. Lepoutre and M.J. Sienko, Benjamin, New York, (1974).

22. A.M. Stacy, P.P. Edwards and M.J. Sienko, J. Solid State Chem. 45, 63 (1982).

23. N.F. Mott, "Metal-Insulator Transitions", Taylor and Francis, London (1974).

24. P.P. Edwards and M.J. Sienko, Acc. Chem. Res. 15, 87 (1982).

25. W. Weyl, Annalen der Physik and Chemie 197, 601 (1864).

26. P.P. Edwards, Adv. Inorg. Chem. Radiochem. 25, 135 (1982).

27. C.A. Kraus, J. Am. Chem. Soc. 30, 653 (1908).

28. C.A. Kraus, J. Am. Chem. Soc. 43, 749 (1921).

29. J.C. Thompson, "Electrons in Liquid Ammonia", Claredon Press, Oxford, 1976.

30. J. Phys. Chem. 79, (1975).

31. J. Phys. Chem. 84, (1980).

32. J. Phys. Chem. 88, 3699 -3912(1984).

33. S. Freed and N. Sugarman, J. Phys. Chem. 11, 354 (1943).

34. A. DeMortier and G. LePoutre, C.r. hebd. Sceanc. Acad. Sci. Paris 268, 453 (1969).

35. J.L. Dye, Pure Appl. Chem. 44, 3 (1977).

36. J.L. Dye and L.R. Dalton, J. Phys. Chem. 71, 184 (1967).

37. D.E. O'Reilly, J. Chem. Phys. 41, 3729 (1964).

38. R. Catterall and P.P. Edwards, Adv. Mol. Relax. Int. Proc. 13, 123 (1978).

39. M.D. Newton, J. Phys. Chem. 79, 2795 (1975).

40. S.G. Bratsch and J.J. Lagowski, J. Phys. Chem. 88, 1086 (1984).

41. R.R. Dewald and J.L. Dye, J. Phys. Chem. 68, 121 (1964).

42. S. Matalon, S. Golden and M. Ottolenghi, J. Phys. Chem. 73, 3098 (1969).

43. C. Moore and B. C. Pressman, Biochem. Biophys. Res. Comm. 15, 562 (1964).

44. C.J. Pedersen, J. Am. Chem. Soc. 89, 7017 (1967).

45. J.D. Lamb, R.M. Izatt and J.J. Christensen, in "Progress in Macrocyclic Chemistry", eds. R.M. Izatt and J.J. Christensen, John Wiley and Sons, New York, 1981.

46. B. Dietrich, J.-M. Lehn and J.P. Sauvage, Tetrahedron 64, 2969, 2885, 2889 (1969).

47. J.-M. Lehn and J.P. Sauvage, J. Am. Chem. Soc. 97, 6700 (1975).

48. N.S. Poonia and M.R. Truter, J. Chem. Soc. Dalton, 2062 (1973).

49. H.K. Frensdorff, J. Am. Chem. Soc. 93, 600 (1971).

50. N.S. Poonia and A.V. Bajaj, Chem. Rev. 79, 389 (1979).

51. J.D. Dunitz, M. Dobler, P. Seiler and R.P. Phizackerley, Acta Cryst. B30, 2733 (1974).

52. F.P. Boer, M.A. Neuman, F.P. Van Remoortere and E.C. Steiner, Inorg. Chem. 13, 2826 (1974).

53. J.L. Dye, M. DeBacker and V.A. Nicely, J. Am. Chem. Soc. 92, 5226 (1970).

54. J.M. Ceraso and J.L. Dye, J. Chem. Phys. 61, 1585 (1974).

55. A. Beckmann, K.D. Böklen and D. Elke, Z. Phys. 270, 173 (1975).

56. J.L. Dye, C.W. Andrews and J.M. Ceraso, J. Phys. Chem. 79, 3076 (1975).

57. J.L. Dye, J.M. Ceraso, M.T. Lok, B.L. Barnett, F.J. Tehan, J. Am. Chem. Soc. 96, 608 (1974).

58. R.R. Dewald and J.L. Dye, J. Phys. Chem. 68, 128 (1964).

59. J. Pappaioannu, unpublished observations.

60. F.J. Tehan, B.L. Barnett and J.L. Dye, J. Am. Chem. Soc. 96, 7203 (1974).

61. U. Schindewolf, L.D. Le and J.L. Dye, J. Phys. Chem. 86, 2284 (1982).

62. S. Janicke and J.L. Dye, J. Solid State Chem. 54, 320 (1984).

63. A. Ellaboudy, M.L. Tinkham, B. Van Eck, P.B. Smith and J.L. Dye, J. Phys. Chem. 88, 3852 (1984).

64. B. Van Eck, L.D. Le, D. Issa and J.L. Dye, Inorg. Chem. 21, 1966 (1982).

65. F.N. Tientega, M.S. Dissertation, Michigan State University, 198 .

66. M.L. Tinkham, F.N. Tientega and J.L. Dye, unpublished results.

67. A.S. Ellaboudy, O. Fussá, Z. Li and J.L. Dye, unpublished results.

68. J.L. Dye, M.R. Yemen, M.G. DaGue and J.-M. Lehn, J. Chem. Phys. 68, 1665 (1978).

69. J.L. Dye, M.G. DaGue, M.R. Yemen, J.S. Landers and H.L. Lewis, J. Phys. Chem. 84, 1096 (1980).

70. J.L. Dye, Prog. Inorg. Chem. 32, 329 (1984).

71. A.S. Ellaboudy, Ph.D. Dissertation, Michigan State University, 1984.

72. M.L. Tinkham, Ph.D. Dissertation, Michigan State University, 1985.

73. J.S. Landers, Ph.D. Dissertation, Michigan State University, 1980.

74. M.G. DaGue, Ph.D. Dissertation, Michigan State University, 1978.

75. J.S. Landers, J.L. Dye, A. Stacy and M.J. Sienko, J. Phys. Chem. 85, 1096 (1981).

76. J.L. Dye, J. Phys. Chem. 88, 3842 (1984).

77. A. Ellaboudy, J.L. Dye, P.B. Smith, J. Am. Chem. Soc. 105, 6490 (1983).

78. D. Issa, A. Ellaboudy, R. Janakiraman and J.L. Dye, J. Phys. Chem. 88, 3847 (1984).

79. D. Issa, Ph.D. Dissertation, Michigan State University, 1982.

80. R.H. Huang, unpublished results.

81. "International Tables for X-Ray Crystallography", Volume 1, Kynoch Press, Birmingham, UK, 1965.

82. J. DeMeulenaeer and H. Tompa, Acta Cryst. 19, 1014 (1965).

83. H. Hope and P. Powers, private communication.

84. O. Fussá, S. Kauzlarich, J.L. Dye and B. Teo, J. Am. Chem. Soc. 107, 3727 (1985).

85. D. Moras, B. Metz and R. Weiss, Acta Cryst. B29, 388 (1973).

86. G.H. Stout and L.H. Jensen, "X-Ray Structure Determination", McMillan Co., New York, 1968.

87. A.J. Layton, P.R. Mallinson, D.G. Parsons and M.R. Truter, J. Chem. Soc. Chem. Comm., 694 (1973).

88. J.W.H.M. Uiterwijk, S. Harkema, B.W. Van den Waal, F. Gobel and H.T.M. Nibbeling, J. Chem. Soc. Perkin Trans. II, 1843 (1983).

89. A. Bondi, J. Phys. Chem. 68, 441 (1964).

90. C.K. Johnson, Program ORTEP, Report ORNL-3794, Oak Ridge National Laboratory, Oak Ridge, TN (1965).

91. A.L. Van Geet, Anal. Chem. 40, 2227 (1968).

92. A.D. English, J. Mag. Res. 57, 491 (1984).

93. M.K. Faber, Ph.D. Dissertation, Michigan State University, 1985.

94. C. Kittel, "Introduction to Solid State Physics", 5th ed., John Wiley & Sons, Inc., New York, 1976.

95. N.W. Ashcroft and N.D. Mermin, "Solid State Physics", Saunders College, Philadelphia, 1976.

96. A.H. Morrish, "The Physical Principles of Magnetism", John Wiley & Sons, Inc., New York, 1965.

97. J. Smart, "The Effective Field Theories of Magnetism", W.B. Saunders Co., Philadelphia, 1966.

98. D.C. Mattis, "The Theory of Magnetism; An Introduction to the Study of Cooperative Phenomena", Harper and Row, New York, 1965.

99. G.H. Bizette, C. Squire, B. Tsai, Compte. red. (Paris), 209, 1938.

100. N.J. Poulis, J. van den Handel, J. Ubbink, J.A. Poulis and C.J. Gorter, Phys. Rev. 82, 552 (1981).

101. S. Foner and S.-L. Hou, J. Appl. Phys. 33, 1289 (1962).

102. A. Currington and A.D. McLachlan, "Introduction to Magnetic Resonance", Harper and Row, New York, 1967.


MICHIGAN STATE UNIVERSITY LIBRARIES
3 1293 01750 7132